

ACTIVITY-BASED SENSORS FOR REACTIVE ALDEHYDES AND THEIR
CORRESPONDING ENZYMATIC MACHINERY

BY

THOMAS EDWARD BEARROOD

DISSERTATION

Submitted in partial fulfillment of the requirements
for the degree of Doctor of Philosophy in Chemistry
in the Graduate College of the
University of Illinois at Urbana-Champaign, 2020

Urbana, Illinois

Doctoral Committee:

Assistant Professor Jefferson Chan, Chair
Professor Martin D. Burke
Assistant Professor David Sarlah
Professor Steven C. Zimmerman

ABSTRACT

Molecular imaging agents are chemical tools that have become essential to the study of life. The field of molecular imaging encompasses a wide range of modalities and mechanism, but an exciting and growing subfield is that of activity-based sensing. Activity-based sensors provides new insights into biological processes since they report on the activity of biological species rather than just the presence. Naturally these are ideal probes for enzymes, affording multiple turnovers and higher signal from a single active enzyme. Activity-based sensors are also excellent sensors for reactive small molecules with unique chemical reactivity. Here, we report the development and/or progress on activity-based sensors for reactive biological aldehydes and the enzymatic machinery tasked with aldehyde metabolism.

We first developed AlDeSense, the first turn on fluorescent probe selective for aldehyde dehydrogenase (ALDH) 1A1. We pursued a probe for this enzyme since it's frequently cited as a cancer stem cell marker. AlDeSense had remarkable selectivity for ALDH1A1, producing a 20-fold increase in fluorescence signal upon oxidation by the enzyme. We confirmed ALDH1A1 activity, as measured by AlDeSense, was a reliable cancer stem cell marker in leukemia, melanoma, and breast cancer models. AlDeSense was then applied to image ALDH1A1 activity in aggressive and non-aggressive melanoma *ex vivo* and *in vivo*. We demonstrated that not only do the cancer stem cells have elevated ALDH1A1 activity in cell culture, but they maintain elevated activity through establishment of a tumor microenvironment.

We next sought to improve on certain limitations of AlDeSense, namely the green fluorescence and cell impermeability. Towards this goal, eleven possible Si-xanthene probes were synthesized. Each iteration provided new insights into the electronic and steric requirements for isoform selectivity and fluorescence turn on. In the end, the careful incorporation of two fluorine atoms on the reactive benzaldehyde moiety produced a selective molecule named red-AlDeSense. Red-AlDeSense was used to study ALDH1A1 activity in lung cancer models.

We also aimed to develop a selective probe for 4-hydroxynonenal (4HNE). It is one of the most reactive and abundant aldehydes produced during oxidative stresses (i.e. lipid peroxidation) and has been connected to many age-associated conditions including cancer and neurodegeneration. We hypothesized selectivity could be achieved against the other 10000-plus aldehydes reported in biological systems using an activity-based sensor. We are currently

investigating synthetic strategies to achieve a fluorophore capped by our hydrazinoacetate trigger. We anticipate this probe will be extremely useful to study the effects of 4HNE in living systems of many disease models. We are particularly interested in its connection to cancer stem cells.

ACKNOWLEDGMENTS

As I wrote this thesis, I frequently thought the permutations of gut decisions, chance encounters, and moments of good fortune that have brought me to where I am today. I am extremely fortunate that a lot of factors out of my control ended up positively. You don't choose your family, but I could not ask for a better one. I am sincerely grateful how supportive my parents, Doug and Teresa, have been my entire life. My sister, Anna, may have been annoying when we were young, but she unknowingly pushed me to excel more than anyone else. I appreciate the love from all my grandparents; they have always been people I look up to. My godmother, Marie Garbe, always challenged me to think about others when I set out to do things. My aunts and uncles, extended aunts and uncles, and cousins are each a unique source of positivity who have helped me along the way.

Continuing with the theme of 'factors out of my control,' I recognize and appreciate many of the privileges that I have been afforded as a straight, white, socioeconomically privileged male. (We all must continue to make the world a more equitable place.) I had access to excellent primary, secondary, and post-secondary education. I would like to explicitly thank Mrs. Gavin and Mr. Virgin for continuing to foster my passion for STEM. I had many more influential teachers (Ms. Carbone and others) that ought to be thanked, especially those who taught subjects and soft skills that I found unnecessary at the time. My first real control over my education came in my choice to attend St. Olaf College. It was an excellent four years with many talented and passionate professors. I am particularly grateful for Prof. Kalyani, Prof. Schweinefus, and the rest of the chemistry faculty for creating an inspiring space to explore my love of chemistry and supporting me both on and off the hill.

Though I will never know their name, I appreciate the person that turned down the RISE fellowship in 2013 so that I may work with (now Dr.) Ines Lüttnant. I was a very raw researcher, and her patience and mentorship were instrumental in putting me on the path I am currently walking. As I mentor younger students now, she is who I emulate. My second graduate mentor, (now Dr.) Greg Peterson was also a huge, positive influence. I appreciate that he let me make mistakes and explore my own day-to-day ideas even when doing so was not an efficient use of my time. In both experiences, I am very thankful for the support of the PIs in both cases, Prof. Dr. Bernhard Wünsch and Prof. AJ Boydston.

Graduate school has been quite the roller coaster, much more so than any previous experience. I am thankful for my advisor, Prof. Jeff Chan for the support through good times and bad. I have learned a lot about being a scientist in his lab, and I'm excited for where I go next. I would also like to thank my thesis committee members, Prof. Marty Burke, Prof. Dave Sarlah, and Prof. Steve Zimmerman. They all challenged me to be a better researcher and built the framework required for me to meet their challenges. I am also thankful for the other professionals around the department, especially Lori Johnson, Kara Metcalf, and Dr. Dean Olson for their support and smiles. I would be remiss if I also did not acknowledge the talented mentees who worked with me over the years: Daven Feng, Sami Steach, Sara Dibrell, Lupe Aguirre-Figueroa, and Arnab Dutta. Not only did they all become productive and reliable researchers, but they were also a unique source of energy and inspiration who helped through the tough times.

As my godmother says, "friends are the family you choose." I like to think I've chosen wisely. I had amazing friends growing up, especially Dylan Eike. I met many awesome friends in college, but I will limit myself to acknowledging my forever-roommate, (now Dr.) Andrew Hoisington, and my bff, Izzy Brandstetter. Finally, I have met many incredible friends in grad school. Many of my friends are/were awesome people in the Chan Lab, and many more could be found throughout the department. There were so many helpful conversations through the years, both scientific and personal. There were many good memories, including some fun nights that not everyone remembers. For the sake of space, I will just explicitly express my appreciation for my cohort, Dr. Hailey Knox, Dr. Chris Reinhardt, and Dr. Effie Zhou. We started together in 2015, and all defended during COVID-19. We've helped each other through milestones, and I know I am better off for knowing each and every one of you.

TABLE OF CONTENTS

CHAPTER 1. Molecular imaging.....	1
1.1 Introduction to molecular imaging.....	1
1.2 Imaging modalities.....	3
1.2.1 Fluorescence imaging	3
1.2.2 Photoacoustic imaging.....	6
1.2.3 Other modalities	9
1.3 Recognition modalities.....	9
1.3.1 Binding-responsive sensors.....	9
1.3.2 Activity-based sensors	11
CHAPTER 2. ALDH isoforms.....	14
2.1 Introduction to ALDH	14
2.1.1 ALDH1A1	15
2.1.2 ALDH1A3.....	15
2.2 Methods for measuring ALDH in live cells.....	15
2.2.1 Accumulation-based fluorescent probes.....	16
2.2.2 Accumulation-based PET probes	17
2.2.3 ICT-based fluorescent probes.....	17
2.2.4 d-PeT fluorescent probes	18
2.3 AlDeSense	20
2.3.1 Synthesis	20
2.3.2 Testing	22
2.3.3 Applications	30
2.4 red-AlDeSense and related molecules.....	31
2.4.1 Synthesis	32

2.4.2	Testing	33
2.4.3	Applications	40
2.5	Rhodols and rhodamines for ALDH1A3	41
2.5.1	Synthesis	41
2.5.2	Testing	42
2.6	Future directions and outlook	44
CHAPTER 3.	4HNE	45
3.1	Introduction of 4-hydroxy-2-alkenals.....	45
3.2	Design and synthesis	45
3.3	Future directions and outlook	48
3.4	Experimental	49
3.4.1	Materials and methods	49
3.4.2	Synthesis and characterization	49
CHAPTER 4.	Formaldehyde.....	54
4.1	Introduction.....	54
4.2	Synthesis	55
4.3	Future directions and outlook	57
4.4	Experimental	57
4.4.1	Materials and methods	57
4.4.2	Synthesis and characterization	57
Appendix A.	ALDH isoforms supporting information.....	60
A.1	AlDeSense supporting information.....	60
A.1.1	Experimental procedure	60
A.1.2	Synthesis and characterization	69
A.2	red-AlDeSense supporting information.....	74

A.2.1	Materials.....	74
A.2.2	Experimental procedure	75
A.2.3	Synthesis and characterization	77
A.3	Rhodamines and rhodols for ALDH1A3 supporting information	108
A.3.1	Experimental procedure	108
A.3.2	Synthesis and characterization	109
Appendix B.	Self-immolative ALDH probe	116
B.1	Introduction.....	116
B.2	Chemistry.....	117
B.2.1	<i>S</i> -formyl trigger.....	118
B.2.2	<i>N</i> -formyl trigger.....	118
B.3	In vitro testing	119
B.4	Future directions and outlook	122
B.5	Supporting information.....	122
B.5.1	Materials and methods	122
B.5.2	Synthesis and characterization.....	123
Appendix C.	Acoustogenic probe for calcium	128
C.1	Introduction.....	128
C.2	Design and synthesis of APCa.....	128
C.3	Preliminary results.....	131
C.4	Future directions and outlook	132
C.5	Supporting information.....	132
C.5.1	Materials and methods	132
C.5.2	Synthesis and characterization.....	133
Appendix D.	β -galactosidase.....	137

D.1	Introduction.....	137
D.2	Synthesis.....	137
D.3	Testing.....	138
D.4	Future directions and outlook	141
D.5	Supporting information.....	142
D.5.1	Materials and methods	142
D.5.2	Synthesis and characterization	142
	References.....	144

CHAPTER 1. Molecular imaging

1.1 Introduction to molecular imaging

In the continual pursuit to answer biological questions and improve human life, molecular imaging has made itself invaluable to everything from basic science to image-guided surgery. Broadly, molecular imaging agents are chemical tools which report on the levels of an analyte of interest. This analyte can range in size from a proton (i.e. pH sensitive probe) to a large protein. These molecular imaging agents allow researchers to peer into the chemical underpinnings of biological occurrences such as disease states. In cases where a correlation between disease state and an analyte of interest has been established, molecular imaging agents can be used for diagnosis, prognosis, or even image-guided surgery.

Molecular imaging agents come in all shapes and sizes, or more accurately, all analytes and modalities. The simplest molecular imaging agents are molecular imaging tags. (Figure 1.1.A) Imaging tags link an analyte recognition moiety to a reporter. Aside from the spatial constraints, the recognition and reporter systems remain functionally independent. Some of the most common examples of these systems are externally applied reporter-tagged antibodies and genetically encoded protein-fluorescent protein conjugates. The biggest advantage to these systems is the relative ease of their development for applications including protein imaging. These imaging tags suffer from a few major shortcomings, though. They rely on accumulation in areas of interest and washout of unbound tags which can lead to long incubation times and make them incompatible with more mobile species (e.g. membrane-permeable small molecules and ions).

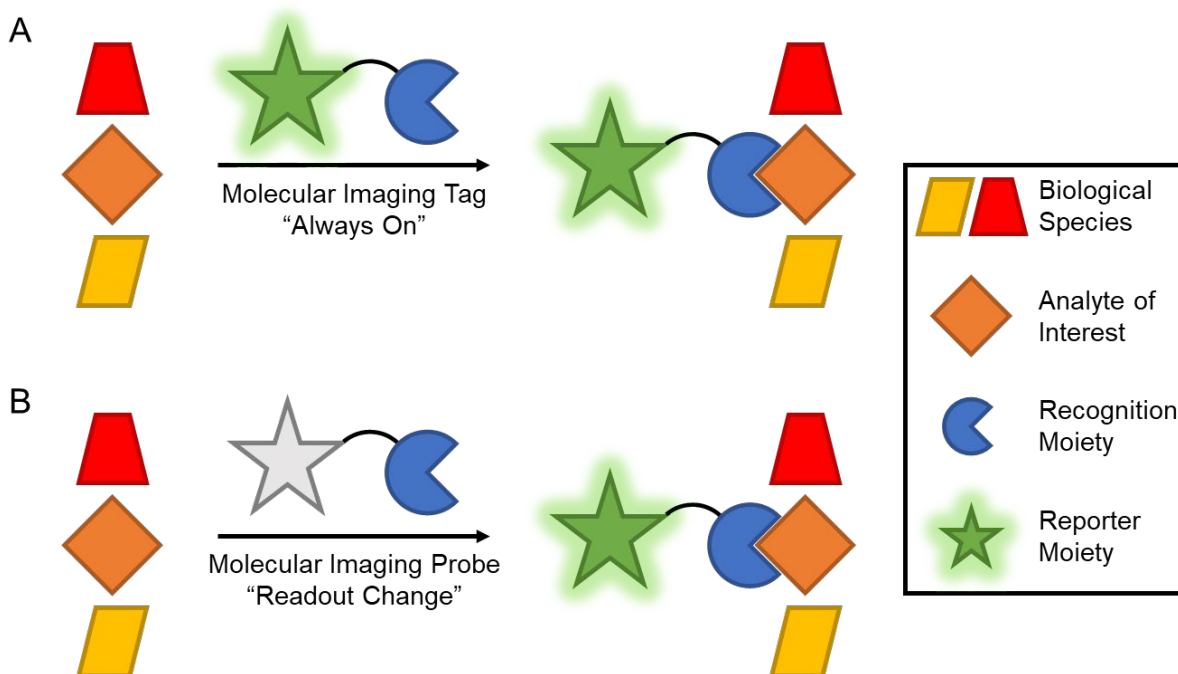


Figure 1.1. Comparison of the mechanisms of (A) molecular imaging tags and (B) molecular imaging probes.

More advanced molecular imaging agents are molecular imaging sensors and probes. (Figure 1.1.B) These combine an analyte recognition moiety and a reporter system wherein there is a change in the readout upon interaction with the analyte. Since the reporter and analyte are functionally linked, these can be much more challenging to design than the corresponding imaging tags. However, the opportunities to study new systems (e.g. small molecules), improve sensitivity, and increase dynamic range of the readout motivate the pursuit of new molecular imaging probes.

When a study does require the use of a molecular imaging agents, the first thing to consider before choosing a probe is the location of the analyte. Organelle specific imaging in 2D cell culture affords short imaging depths but requires greater resolution than tissue specific imaging centimeters deep in the body. Second, the concentration range of the analyte must be estimated. Together, these questions inform the options of imaging modalities (discussed in Section 1.2). The next question looks at the nature of the analyte. The recognition modality (discussed in Section 1.3) is thereby informed depending on the size, complexity, reactivity, and stability of the analyte.

Many molecular imaging agents are commercially available through reliable sources such as Fisher Scientific, MilliporeSigma, and StemCell Technologies. Many more have been reported in the literature by researchers eager to share their molecules. Still, scientific questions arise that

cannot be answered with current probes and technologies. These previously unanswerable questions are the motivation for the development of the molecular tools developed by our lab.

1.2 Imaging modalities

Molecular imaging is a broad field that has grown to incorporate many imaging modalities to suit the needs of the researcher. The main considerations when choosing an imaging modality to use, or on which to develop a new probe, are typically the required resolution and depth and the concentration of the analyte of interest. (Figure 1.2) Additional factors such as cost per analysis and concerns about radiation must also be considered.

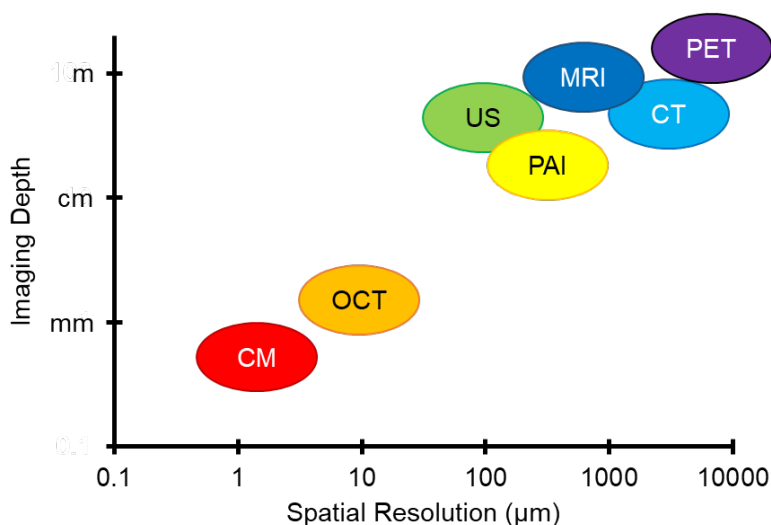


Figure 1.2. Molecular imaging technologies spatial resolution generally increases with imaging depth. CM = confocal microscopy. OCT = optical coherence tomography. US = ultrasonography. PAI = photoacoustic imaging. MRI = magnetic resonance imaging. CT = computed tomography. PET = positron emission tomography.

1.2.1 Fluorescence imaging

Fluorescence imaging is a powerful technique that offers some of the greatest resolution in the field of molecular imaging. Fluorescence relies on the principle of light in, light out. The process begins with absorption of a photon by the chromophore. (Figure 1.3) The photon's energy excites an electron from the ground state to an excited state. This electron then relaxes back to the ground state through a combination of radiative and non-radiative means. The radiative relaxation, consisting of only a fraction of the original absorbed energy, generates a photon of lower energy and longer wavelength than the excitation wavelength. The difference in wavelength allows filtering the excitatory light so only the longer wavelength emitted light is detected.

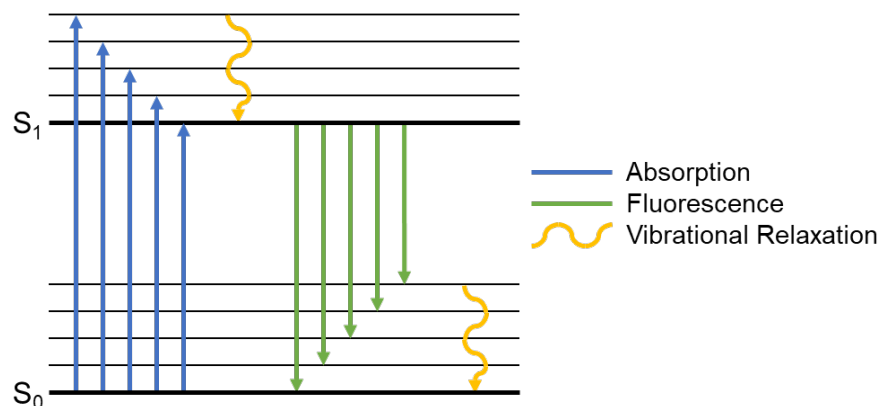


Figure 1.3. A simplified Jablonski diagram showing absorption of higher energy, shorter wavelength light and fluorescence of lower energy, longer wavelength light.

As a field, optical imaging using visible and near-infrared (NIR) light suffers from limited depth penetration. The light is readily scattered by biological tissue. This leads to a rapid decrease in localized intensity of the excitatory light and a degradation of spatial resolution of emitted light. Depending on the wavelength, it also is absorbed by many biomolecules including hemoglobin, deoxyhemoglobin, and water. Optimal wavelengths for excitation and emission generally lie in the biological imaging window wherein absorbance is minimized by endogenous species. (Figure 1.4) While no range has been fully agreed upon, the lower wavelength limit is generally between 650 and 700 nm, and the upper wavelength limit is between 900 and 1000 nm.

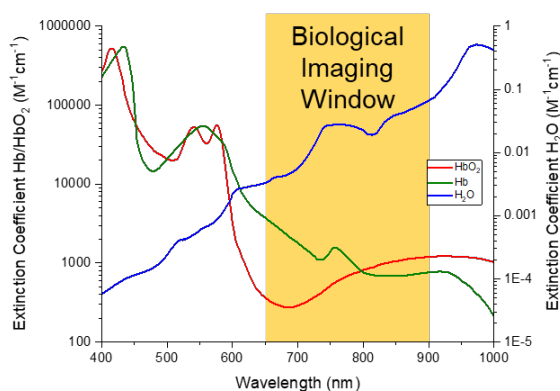


Figure 1.4. The biological imaging window exists where light absorbance from endogenous species is minimized. Raw data was acquired from the Oregon Medical Laser Center (omlc.org/spectra).

Fluorophores can become molecular imaging probes when interaction with an analyte of interest modulates the fluorescence signal read by the detector. In the broadest sense, this requires

a change in the signal at the wavelength being measured. The amount of emitted light is dependent upon two factors, the efficiency at which excitation light is absorbed (extinction coefficient) and the frequency at which the absorbed photon's energy is dissipated as light (quantum yield). An increase in either parameter will lead to an increase in the measurable signal.

Conceptually, the simplest molecular imaging probes are turn on probes. (Figure 1.5.A) Turn on imaging involves irradiating the fluorophore with a single excitation wavelength (or range of wavelengths) and measuring the signal from a single emission wavelength (or range of wavelengths). The simplicity allows the most rapid and inexpensive imaging since a single laser and filter set can be used for data collection. Turn on probes generate an increase in the fluorescent readout when interacting with an analyte of interest. Great care must be taken to account for other sources of signal increase, especially that of basal accumulation of unreacted probe. Turn off probes, which decrease signal output upon interaction with an analyte, use the same principle. These are less favorable since there are even more opportunities for false positives including dye washout and photobleaching.

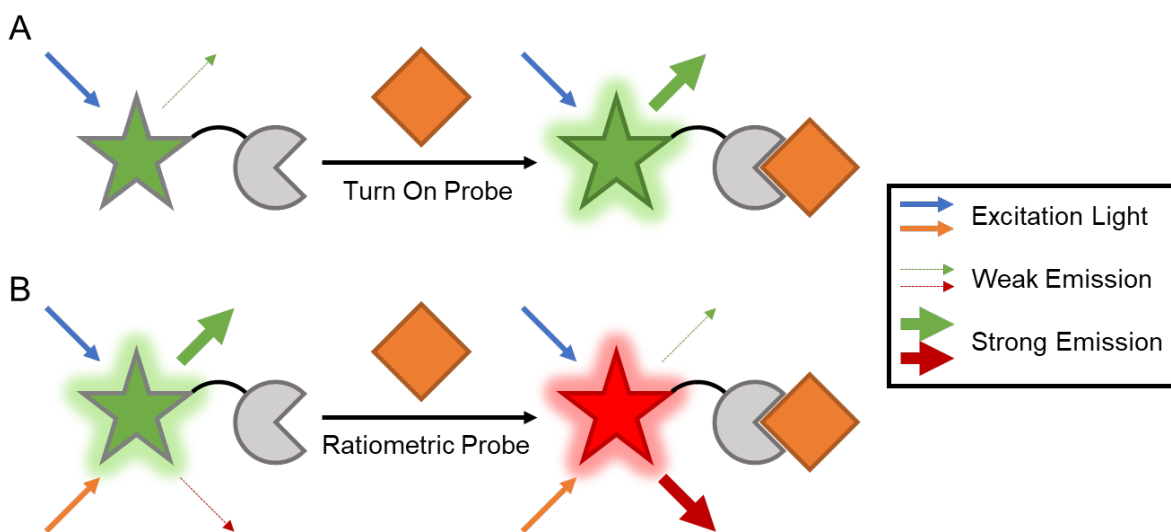


Figure 1.5. Comparison of (A) turn on and (B) ratiometric fluorescent probes.

A general approach to account for differences in dye levels is ratiometric imaging. (Figure 1.5.B) Ratiometric imaging requires all measurements be performed with two unique excitation/emission wavelength pairs. These may be one excitation laser with two emission wavelength filters, two lasers with one emission filter, or two unique laser and emission filter pairings. The basic requirement for ratiometric imaging is that the signals at each measurement

condition respond differently for the analyte-present state and analyte-absent state. In many systems, interaction with an analyte causes a decrease in the signal at one measurement and an increase at the other measurement as the absorption and emission spectra shift. Knowledge about the spectra for the analyte-present and analyte-absent states allows the user to determine the ratio of the two states present using basic algebra. A less common approach is to conjugate an unresponsive fluorescent dye as an internal standard. Here, the signal corresponding to the unreactive readout reports basal accumulation levels. The second signal is dynamic and accounts for the presence or absence of analyte. As above, basic algebra can be used to determine the ratio of the analyte-present state to analyte-absent state. Care must be chosen in dye selection to avoid photounstable probes which may lead to misreporting of the ratios. Additionally, the discrepancies in the absorption and scattering of different wavelengths of light by biological tissues can complicate analyses beyond surface level depths.

In principle, the resolution, D , of fluorescent systems is determined the Airy radius. Mathematically, this resolution is calculated using Equation 1.1.

$$D = \frac{0.61\lambda}{NA} \quad (1.1)$$

The term λ is the excitation wavelength while NA is the numerical aperture. The numerical aperture is dependent on the objective and the refractive index of the immersion medium. Most high-quality commercial setups feature numerical aperture values approaching 1.30. In such cases, the resolution limit is 0.47 times the excitation wavelength. For shorter wavelength violet excitation, this calculates to resolutions just below 200 nm. New technologies have enabled imaging at resolutions beyond the diffraction limit. This aptly named super-resolution imaging is afforded through a variety of technologies and techniques in fluorophore design and experimental setup.¹

In both normal and super-resolution imaging, the primary benefits fluorescence imaging is the excellent resolution and sensitivity. Analyte-responsive fluorescent probes are optimal for applications in isolated cells, and more red-shifted probes are being adapted for more *in vivo* imaging.

1.2.2 Photoacoustic imaging

Photoacoustic imaging is a relatively young imaging modality that relies an optical input to produce a measurable, acoustic output.² (Figure 1.6.A) The technology relies on the photoacoustic effect first described by Alexander Graham Bell way back when. Similar to

fluorescence imaging, the process of generating a photoacoustic signal is initiated by photoexcitation of an electron. Photoacoustic imaging relies on the generation of heat as the excited electron relaxes back to the ground state. This heat causes thermoelastic expansion in the local area. A subsequent phase of thermoelastic contraction can follow if the excitation light is removed. The cycle of expansion and contraction generates acoustic waves in the tissues. Therefore, pulsing the light source at ultrasonic frequencies can generate an ultrasound signal. (Figure 1.6.B) This signal is then detected using an array of ultrasound transducers, and the source of the signal can be located in a complex 3D system.

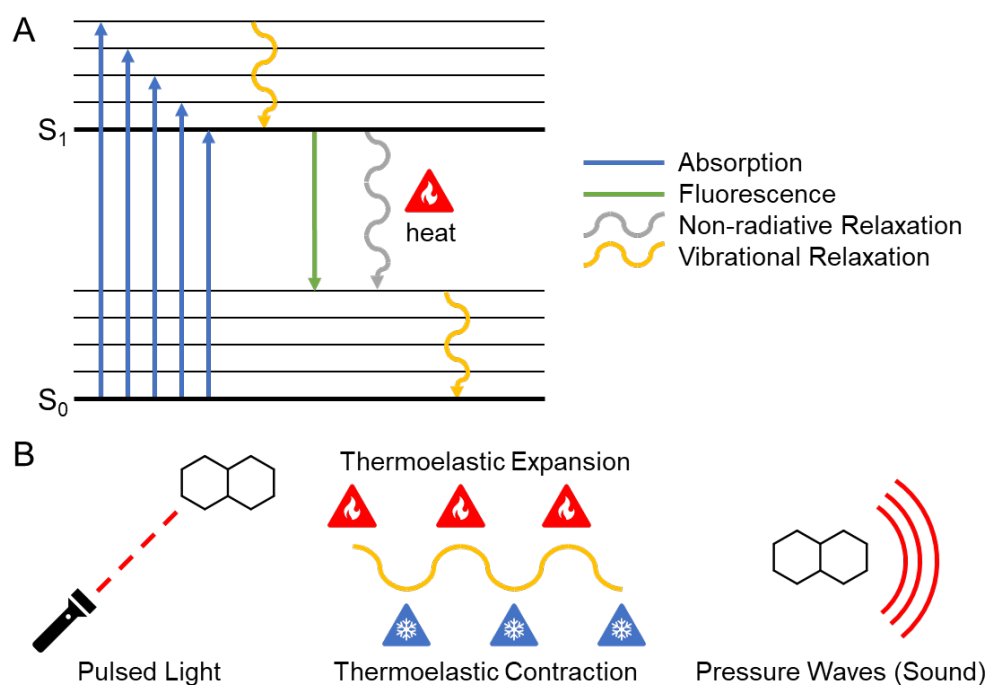


Figure 1.6. The fundamentals of photoacoustic imaging. (A) A Jablonski diagram comparing photoacoustic signal generation to that of fluorescence. (B) The basic components to generating an ultrasound signal using the photoacoustic effect.

The first activatable photoacoustic probe was reported by Gambhir and coworkers in 2010.³ The probe linked two chromophores, BHQ3 and Alexa750, by an MMP-2 cleavable linker. Upon proteolysis of the linker, the BHQ3 entered cells, since it was decorated with a cell penetrating peptide sequence. The Alexa750 dye diffuses away after linker cleavage. MMP-2 activity can therefore be detected by analyzing the signal at 675 nm (BHQ3) and 750 nm (Alexa750), where a decrease in the relative signal at 750 nm corresponds to enzyme activity. This is the same principle as the fluorescent ratiometric imaging discussed in section 1.2.1.

Gambhir and coworkers performed their work on a custom photoacoustic setup. The same year, Endra's Nexus 128 was released.⁴ The Nexus 128 was the first commercial photoacoustic tomographer capable of 3-dimensional photoacoustic imaging. This, along with other commercial setups, paved the way for the development of new activatable photoacoustic probes. The commercial tomographers generally feature an adjustable 680-950 nm laser. Though this incoming light can avoid absorbance with most endogenous molecules, it is scattered by tissue allowing illumination of larger regions of interest. This scattering would destroy the spatial resolution of the output light in fluorescence, but acoustic waves scatter around 3 orders of magnitude less than light.² With this technology, molecular imaging can be accomplished at depths up to 7 cm with resolutions on the order of 0.5 percent of the imaging depth.

While strategies like Gambhir's exist for using multiple chromophores in a single, large photoacoustic probe, our lab focuses on activatable probes using a single chromophore.⁵⁻⁷ The lower molecular weight of a single chromophore improves cellular penetrability for measuring intracellular analytes. These molecular probes for photoacoustic imaging rely on changes in the photophysical properties of the molecules upon interaction with a molecule of interest. A binding event or chemical reaction changes the electronics. Though not directly proportional, an increased photoacoustic signal generally correlates with an increase in absorbance.^{8,9} The most reliable way to measure this has been with ratiometric imaging. To maximize theoretical turn on, both absorption maxima should be within the 680-950 nm window corresponding to the commercial laser.

The strength of activatable photoacoustic imaging agents remains their good resolution at centimeter depths. Since few biomolecules are strongly photoacoustic, photoacoustic probes report on biological analytes with limited background signal. The most common biological species to contend with are hemoglobin and deoxyhemoglobin. Spectral unmixing allows one to account for any potential overlap between the probe and the biological species.¹⁰ The low background facilitates the dye and analyte levels in the micromolar range for small molecule organic dyes.¹¹ Overall, photoacoustic imaging tends to hit a happy medium of depth, resolution, and sensitivity, all while avoiding ionizing radiation. As technology and molecular imaging probes continue to improve, the field has tremendous potential in basic science, preclinical imaging, and clinical imaging.

1.2.3 Other modalities

Contrast agents relying on differential accumulation in the locations of interest have been developed for nearly all imaging technologies. The same cannot be said for activatable probes. It is true, some fields (e.g. MRI¹² and chemiluminescence¹³) have had tremendous work with OFF/ON probes in response to an analyte of interest. Others may remain unattainable for activatable probes. For instance, positron emission tomography (PET) relies on the decomposition of radioactive tags (e.g. ¹⁸F) in a process generally independent of its chemical surroundings. Clever approaches are being taken to develop analyte-responsive probes using other imaging techniques including ultrasound. All of these present their own design challenges and opportunities, but these imaging modalities exist beyond the scope of this thesis.

1.3 Recognition modalities

For clarity, this section focuses on recognition modalities of molecular imaging probes and sensors. The recognition modality describes how the probe interacts with the analyte of interest. There are two major classes: binding-responsive and activity-based. (Figure 1.7) Deciding to pursue a probe based on one or the other primarily depends on the stability of the analyte and secondarily on the reactivity of the analyte.

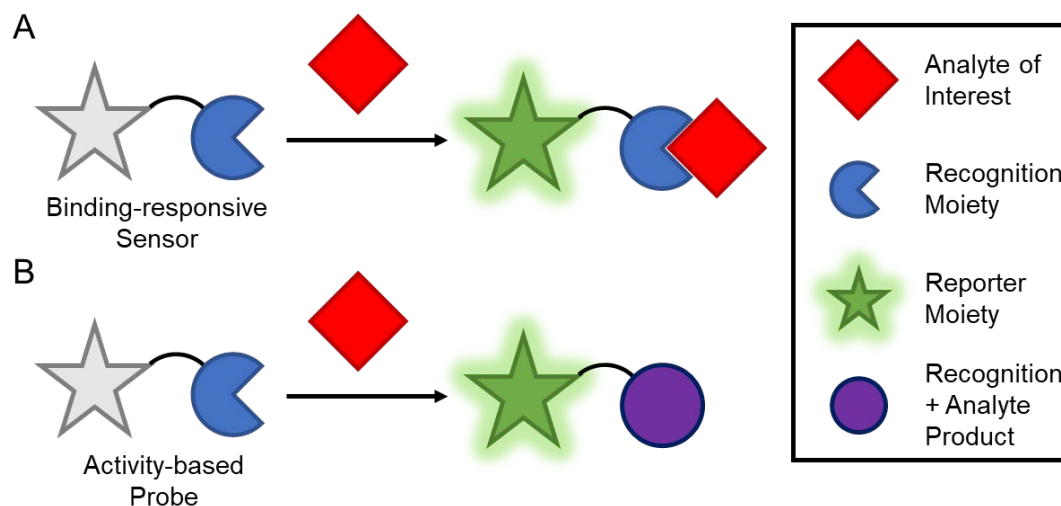


Figure 1.7. Comparison of (A) binding-responsive and (B) activity-based recognition modalities for molecular imaging probes.

1.3.1 Binding-responsive sensors

Binding-responsive sensors change a measurable output when the sensor binds to an analyte of interest. (Figure 1.7.A) The analyte does not produce a chemical change, but its binding

perturbs the electronic system to achieve a readout change. The binding event is typically reversible, producing readout 1 when unbound and readout 2 when bound. This makes these probes ideal for monitoring dynamic changes in the analyte of interest as it can account for the presence and subsequent absence of the analyte.

Some of the earliest small molecule binding-responsive sensors highlighting the power of this technology were Ca^{2+} sensors developed by Roger Tsien.¹⁴ Inspired by the selectivity of the chemical EGTA for Ca^{2+} over Mg^{2+} , Tsien designed the bis(o-aminophenoxy)ethane-N,N,N',N'-tetraacetic acid moiety known as BAPTA. In the absence of Ca^{2+} , the lone pair electrons on the aniline are free to delocalize into the aryl ring. Binding to Ca^{2+} occupies this lone pair, preventing electron donation into the aryl ring and modulating the photophysical properties.

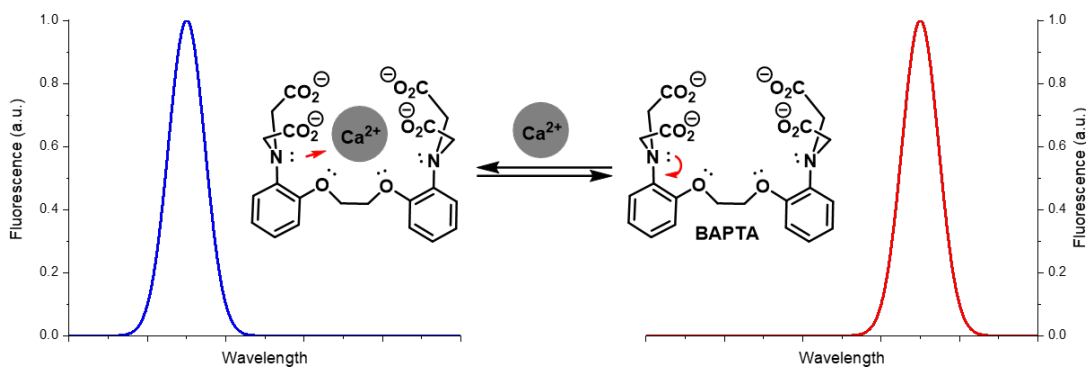


Figure 1.8. Mechanism of the fluorescence change from the reversible binding of Ca^{2+} to BAPTA. The fluorescence spectra are simplified representations demonstrating the bathochromic shift upon binding. Actual spectra can be found in the original publication.¹⁴

The analyte for binding-responsive sensors can be a metal ion; selective recognition moieties have been developed for a wide range of biologically relevant metals including K^+ ,¹⁵ Ca^{2+} ,¹⁴ Fe^{3+} ,¹⁶ and Zn^{2+} .¹⁷ The analyte can also be something larger and more complex like a protein. Binding-responsive sensors are ideal for proteins which are either non-enzymatic or have enzyme active sites that are highly conserved with other isoforms. This favorability stems from the ability of these probes to sense the proteins at unique surfaces. For instance, a binding responsive fluorescent probe for HER2 was recently reported.¹⁸ Binding to HER2 induces planarization of the probe, extending conjugation, and resulting in a fluorescent readout.

In summary, there are a few advantages to binding-responsive sensors. Foremost, they are inherently reversible and therefore report on the present location and concentration of an analyte

of interest. Depending on the application, the one-to-one binding ratio can be seen as an advantage as it offers a better opportunity for quantification. Finally, by being more concerned with steric and electronic requirements as opposed to reactivity, binding-responsive centers are more amenable to analytes such as metal ions, non-enzymatic proteins, and isozymes with highly conserved active sites.

1.3.2 Activity-based sensors

Activity-based sensors are distinct from binding-responsive sensors in that they experience a chemical change upon reacting with a molecule of interest. (Figure 1.7.B) The analyte-induced chemical change is accompanied by a change in the readout. Analytes with inherent chemical reactivity (e.g. reactive oxygen species, enzymes) are required for activity-based probes. Most activity-based sensors are effectively irreversible in a biological setting. This makes them optimal for unstable molecules whereby fleeting interactions would make some studies unfeasible. Activity-based sensors are also optimal for molecules that may not correlate between presence and activity.

1.3.2.1 Enzymes

Activity-based sensors are an ideal recognition modality for enzymes because presence does not equal reactivity.¹⁹ Post-translational modifications, small molecule inhibitors, and protein-protein interactions are among the many ways that proteins may switch from inactive to hyperactive states or anywhere in between. This is important since every active enzyme can catalyze the turn over of multiple activity-based probes, increasing the overall signal readout. In contrast, binding-responsive sensor turn on is limited to a one-to-one ratio with the enzyme regardless of activity, limiting theoretical turn on and losing important information on the system.

Even in cases where enzyme levels and activity may correlate, a second advantage is that activity-based sensors are capable of reporting on the enzyme activity with minimal perturbation to the native system. A binding-responsive sensor would require constant contact with the enzyme, possibly modifying its activity or other effects on the surrounding area. The minimal perturbation stems from the mode of action, namely that the sensor binds, undergoes a reaction, then leaves the protein unchanged. This is minimally perturbing when redox chemistry is involved (e.g. an NAD⁺ cofactor is reduced for each aldehyde dehydrogenase (ALDH)-catalyzed oxidation event), and it can be non-perturbing for non-redox reactions.

One of the biggest advantages of recognition modalities was that they could be used to report on the location of proteins of interest. Activity-based sensors localize based on their own physical properties and recognition moieties, not on where the protein-sensor interaction took place. Recent advancements have enabled researchers to acquire this localization information by making the turnover product highly reactive to a covalent modification to the nearby area. This work in the area of activity-based sensors was pioneered by Yao and coworkers using Quenched Activity-Based Probes (qABPs).²⁰ They simultaneously developed qABPs for both caspases and protein tyrosine phosphatases (PTPs), but for clarity I will only focus on the latter. The PTP hydrolyzes a phosphate group to uncap a phenol. This free phenol then undergoes 1,6-elimination to simultaneously displace a fluorescence quenching azobenzene and generate a para-quinone methide. The displacement of the azobenzene prevents Förster resonance energy transfer (FRET, aka fluorescence resonance energy transfer) from the fluorescein producing a fluorescence turn on. The para-quinone methide is highly susceptible to nucleophilic attack, including nucleophilic amino acids (i.e. cysteine) found on surrounding proteins. Combined, reaction with PTP leads to a fluorescence turn on and a covalent bond to the proximal biomolecules, marking the location of the active PTPs. More recent streamlined efforts have involved direct enzymatic uncapping of the fluorophore and subsequent generation of an ortho-quinone methide stemming from a benzyl fluoride derivative. This strategy is most commonly used for coumarin and xanthene scaffolds, but could theoretically be extended to HD dye and azo-BODIPY scaffolds as well. This strategy requires chemical removal of a protecting group to generate the quinoone methide, and is therefore optimal for hydrolyzing and other bond-cleaving enzymes. It has been used to develop probes for β -galactosidase,²¹ β -lactamase,²² phosphatase,²³ and sulfatase²⁴ enzymes.

1.3.2.2 Reactive small molecules

Transient species are difficult to measure with binding-responsive recognition moieties. If the off rate is rapid, the probe will just revert to an unactivated state. However, when a chemical change occurs in response to the molecule of interest, a persistent change can be measured reliably. Activity based sensors are therefore optimal for short-lived reactive species such as reactive oxygen, nitrogen, and sulfur species (ROS/RNS/RSS).²⁵

The key to analyte-selective activity-based sensors is to utilize unique properties of the analyte of interest to design a trigger which will only respond to the presence of said analyte. For instance, nitroxyl reacts with thiols to produce an *N*-hydroxysulfenamide. Our group used this

unique reactivity to selectively image nitroxyl amongst other ROS/RNS/RSS.²⁶ The unique properties are not limited to reactivity though; the unique properties extend to concentration and location. Glutathione exists at much higher concentrations than other biological thiols. This strategy was used by Urano and coworkers in a rare example of a reversible activity-based probe.²⁷

In contrast to enzymatic reactions, reaction between the activity-based probe and the small molecule analyte typically consume the analyte. This enables better quantification of the levels of the analyte, but it diverts an equivalent of analyte from its native function. To avoid disrupting the native environment, aptly named analyte replacement probes have been developed which release one equivalent of analyte for every equivalent that reacts. This was pioneered by Pluth and coworkers with an analyte replacement probe for H₂S, MeRho-TCA.²⁸ As part of its mechanism, MeRho-TCA releases an equivalent of carbonyl sulfide which, after reacting with carbonic anhydrase, releases a previously capped equivalent of H₂S. Lou, Wang, and coworkers build on this strategy with their probes NAP-FAP-1 and -2.²⁹ These react with formaldehyde and later release that same molecule without requiring an enzyme. Unlike binding-based probes, NAP-FAP-1 and -2 undergo an irreversible reaction so release of formaldehyde is accompanied by a permanent increase in fluorescence.

There are many strategies available in developing activity-based probes for small molecules. They can consume the analyte with or without replacement. Like activity-based probes for enzymes, reactivity can uncap a second group (e.g. quinone methide) to tag the location of reaction. In the end, activity-based probes expand the access of sensors to highly reactive small molecules previously inaccessible by binding-responsive sensors.

CHAPTER 2. ALDH isoforms

2.1 Introduction to ALDH

The aldehyde dehydrogenase (ALDH) family is a family of enzymes that catalyze the oxidation of aldehydes to their corresponding carboxylic acid products. The oxidation relies on a NAD(P)⁺ cofactor which acts as a stoichiometric oxidant. For most ALDH isoforms NAD⁺ is a better cofactor than NADP⁺.³⁰ The oxidation to the carboxylic acid is effectively irreversible in mammalian cells given the high NAD⁺-to-NADH ratio.³¹

The mechanism of catalysis begins with association of the aldehyde and the NAD⁺ cofactor.³² A deprotonated active site cysteine undergoes nucleophilic attack at the carbonyl carbon of the aldehyde to produce a deprotonated hemithioacetal. As the oxygen lone pair kicks back down, a hydride transfer occurs from the hemithioacetal to the NAD⁺ resulting in a thioester and NADH. The thioester is hydrolyzed by an activated equivalent of water to produce the carboxylic acid and restore the active site cysteine. Dissociation of NADH and the carboxylic acid return the enzyme to its original state, ready for the next round of catalysis. The rate limiting step of this process is isoform dependent.³³ For some isoforms, it is hydride transfer; for others, it is thioester hydrolysis; and for still others, the rate limiting step is dissociation of the NADH.

There are 19 known ALDH isoforms in humans, but not all have been fully characterized.³⁴ They vary in their preferred substrate and subcellular localization. However, there is significant overlap in the substrates. For the most part, their role is detoxification of both endogenous and xenobiotic aldehydes. For example, mitochondrial ALDH2 is one enzyme involved in the oxidation of ethanol to acetate. A partial-loss-of-function mutation in ALDH2 leads to the accumulation of toxic acetaldehyde after consumption of ethanol. This highly reactive aldehyde and others can form undesirable covalent adducts with protein and DNA.

Another important function of some isoforms is the production of important biomolecules. ALDH4A1, 5A1, and 18A1 are all involved in pathways of glutamate metabolism.³⁵ ALDH1L1 and 1L2 are involved in the oxidative deformylation of 10-formyltetrahydrofolate. This simultaneously restores the folate and NADPH pools in the cells. Other members of the ALDH1 subfamily and ALDH8A1 are involved in the synthesis of the retinoic acid.^{36,37} Retinoic acid is an important signaling molecule which initiates transcription of numerous genes binding to retinoic acid response elements. This retinoic acid signaling is important in cell fate determination.

2.1.1 ALDH1A1

ALDH1A1 is an important cytosolic enzyme that, as discussed in the previous section, serves to detoxify endogenous and xenobiotic aldehydes through its role as a catalyst oxidation. Likely due to these roles, elevated ALDH1A1 levels have been measured in a variety of cancers using immunohistochemistry.³⁴ Elevated ALDH1A1 corresponds to favorable prognosis in some cancers including hepatocellular carcinoma³⁸. But in most cases, elevated ALDH1A1 levels correlate with poor prognosis. Rocconi and coworkers attribute this in part to its role affecting proliferation and DNA repair via the retinoic acid signaling pathway in ovarian cancers.³⁹ Lai and coworkers correlate the elevated levels in ovarian cancer with drug resistance, possibly due to its metabolism of select chemotherapeutics.⁴⁰

Through a combination of these roles, ALDH1A1 is an important enzyme overexpressed in cancer stem cells (CSCs) of various cancer types. CSCs are a subpopulation of the tumor which demonstrate a combination of increased chemotherapeutic resistance, increased metastatic potential, and the ability to maintain or restore tumor heterogeneity.⁴¹ Due to its upregulation in these CSCs, ALDH1A1 has been used as a CSC marker in many cancers including breast,⁴² colorectal,⁴³ and esophageal cancers.⁴⁴

2.1.2 ALDH1A3

Since most of the early work in identifying CSCs by ALDH activity was completed using ALDEFLUOR™, and there was a misconception that ALDEFLUOR™ reported only on ALDH1A1 activity, most of the early work connected the two. It has since been shown that ALDEFLUOR™ reacts with numerous ALDH isoforms including ALDH1A3.⁴⁵ ALDH1A3 is a close relative to ALDH1A1 that is also involved in the detoxification of endogenous and xenobiotic aldehydes as well as the retinoic acid signaling pathway.³⁷ More recent studies using techniques such as siRNA knockdown have revealed that ALDH1A3 is a good CSC marker in a number of cancers including breast⁴⁶, colon⁴⁷, and lung⁴⁸ cancers.

2.2 Methods for measuring ALDH in live cells

Since all ALDH isoforms are intracellular enzymes, the development of methods to detect their activity in live cells as focused on cell permeable small molecule probes. Compared to large, non-permeable fluorescently tagged antibodies, these molecules are more difficult to make stable and selective.

2.2.1 Accumulation-based fluorescent probes

Accumulation-based probes are some of the most commonly developed probes for ALDH. These probes rely on the intrinsic carboxylate-producing enzymatic activity changing the charge of the molecule. This usually involves converting a neutral aldehyde-containing species to a mono anionic carboxylate-containing species. The newly formed negative charge can render molecules impermeable to the cell membrane. Thus, while the unaffected probe freely passes in to and out of each cell, only the cells with ALDH activity will begin to trap the molecule. (Figure 2.1)

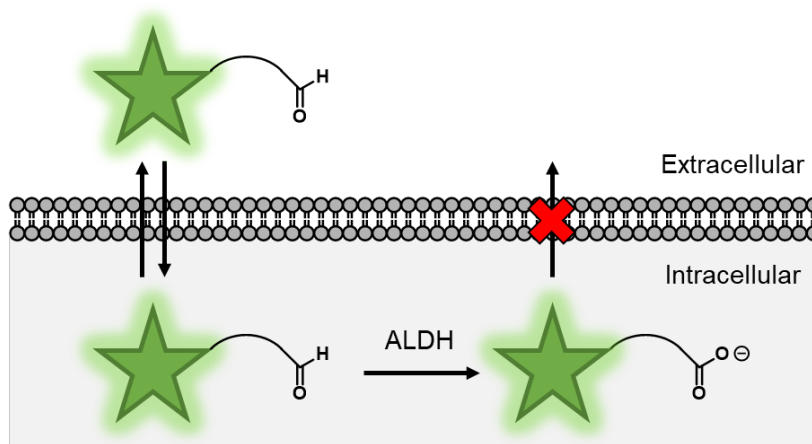


Figure 2.1. Mechanism of ALDH-responsive accumulation-based probes.

This strategy was pioneered by Jones and coworkers when they published Dansyl aminoacetaldehyde (DAAA), the first probe used to detect ALDH activity in live cells.⁴⁹ Citing issues of UV excitation and fluorescence spectral overlap with other common fluorophores, Smith and coworkers published BODIPY aminoacetaldehyde.⁵⁰ This molecule would go on to be commercialized as ALDEFLUOR™ by STEMCELL Technologies, and it remains the most common ALDH probe for basic science applications. In the literature, highly fluorescent cells tagged by ALDEFLUOR™ are reported as ALDH^{high} since it reports on broad spectrum ALDH activity. In other words, it is a substrate for many of the 19 ALDH isoforms. Using the same aminoacetaldehyde trigger, alternatives such as AldeRed™-588 have enabled studies at a different wavelength for use in multicolor imaging.⁵¹

This accumulation-based strategy was utilized by Urano and coworkers to develop selective fluorescent probes for ALDH1A1 and ALDH3A1. To achieve selectivity, the ALDH responsive aminoacetaldehyde was replaced with various benzaldehyde derivatives. ALDH1A1 selectivity was achieved with an *N*-(4-formylphenyl)amide trigger. Due to the trigger, the short

linker length, or a combination, no reactivity was observed from ALDH1A3 or ALDH3A1. On the other hand, attaching a fluorophore to one alkyl chain of *N,N*-diethylaminobenzaldehyde (DEAB) afforded selectivity for ALDH3A1. The probe has low μM affinity and high turnover rates for ALDH3A1. Similar to DEAB, the probe has high affinity for ALDH1A1 (high nM), but turns over very slowly, effectively acting as an inhibitor.³² In both cases, the change in trigger decreased the hydrophilicity to the point where the probes were leaking out after turnover. Switching the fluorophore and modifying the linker restored the required hydrophilicity of the carboxylate to enable labeling studies with the ALDH3A1 selective handle.

Overall, these probes are tremendously useful for flow cytometry analysis, fluorescence microscopy, and other isolated systems in which unconverted aldehyde forms of the probe can be readily removed to reduce background. These are also some of the easiest to achieve isoform selectivity for since the fluorescent readout and enzyme reactive moiety can be effectively separated for optimization. However, these molecules struggle in high throughput screening applications where washout is less feasible. They are all but useless in more complicated living systems (i.e. *in vivo*).

2.2.2 Accumulation-based PET probes

The accumulation strategy has also been applied to detect ALDH activity using other imaging modalities, predominantly positron emission tomography (PET) imaging. There are numerous patent claims for ALDH selective PET imaging agents, and Witney and coworkers recently reported the first isoform selective PET imaging agent.⁵² With this imaging agent, broad regions with high ALDH1A1 activity (e.g. the lungs) could be rapidly observed. However, it is not clear as to what extent the probe was accumulating since the PET tracers were quickly cleared through the bladder. No pathophysiological states were observed using ALDH-responsive PET imaging.

2.2.3 ICT-based fluorescent probes

Intramolecular charge transfer (ICT) is a process whereby a charge redistribution occurs within an excited molecule.⁵³ The precise mechanism by which ICT occurs is still being worked out, but the effect of ICT is a new, red-shifted emission band.⁵⁴ In general, a conformational change occurs in response to photoexcitation leading to a lower energy state. (Figure 2.2) This conformation may remain planar (planar ICT, PICT) or involve a new twist in one of the bonds

(twisted ICT, TICT). The electron in this previously inaccessible state is lower energy than before, and it can relax via radiative or nonradiative relaxation to ground state of the new conformation.

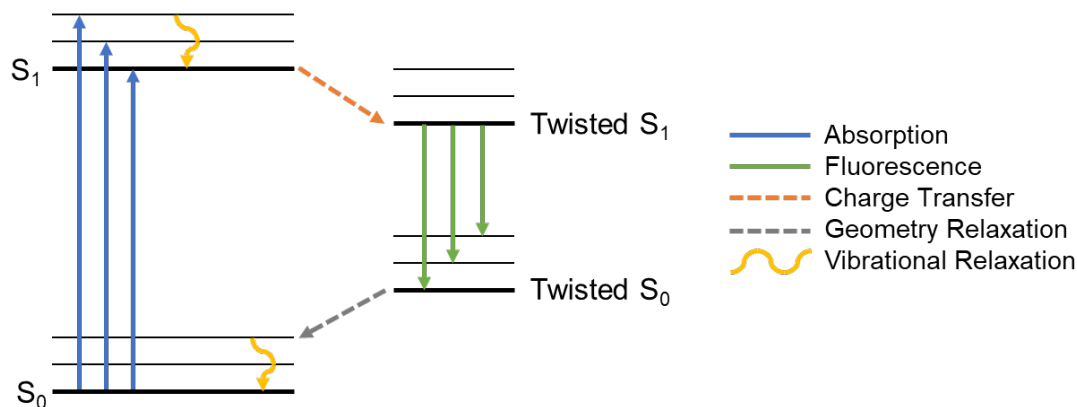


Figure 2.2. Simplified Jablonski diagram for fluorescence via the twisted intramolecular charge transfer mechanism.

The first ratiometric turn on fluorescent probes for ALDH activity were thiophene-bridged aldehydes (TBAs) reported by Murthy and coworkers.⁵⁵ These TBAs underwent a hypsochromic shifts after oxidation to thiophene-bridged carboxylates (TBCs). The shift was attributed to changes in the intramolecular charge transfer (ICT) properties of the TBAs and TBCs. Their lead compound, TBA2, showed activity against every recombinant ALDH isoform they tested. Thus, when applied to flow cytometry or fluorescence microscopy, broad spectrum ALDH activity is reported on. Though isozyme selectivity may be possible with a carefully decorated analogue, the biggest hindrance towards improvement of this ICT-based strategy is selectivity towards Lewis acids. For instance, similar probes featuring the TBA core have since been used to detect Cu^{2+} .⁵⁶

2.2.4 d-PeT fluorescent probes

Photoinduced electron transfer (PeT) is a fluorescence quenching mechanism involving excitation of a chromophore's photon and subsequent non-radiative relaxation of the excited electron to a proximal electronic system. (Figure 2.3) The proximal electronic system also transfers an electron to the ground state of the chromophore. Depending on the order of events, the quenching can be known either as acceptor-PeT (a-PeT) or donor-PeT (d-PeT) with naming being in relation to the chromophore. After photoexcitation of an electron, the chromophore in an a-PeT system accepts an electron from a proximal electron rich species. Conversely, the chromophore in a d-PeT system donates the photoexcited electron to a proximal electron poor species. In both cases, the original redox state is restored through a second electron transfer. The process nets the

same final ground state as traditional radiative relaxation in fluorescence, but it is known as quenching because the two electron transfers are nonradiative.

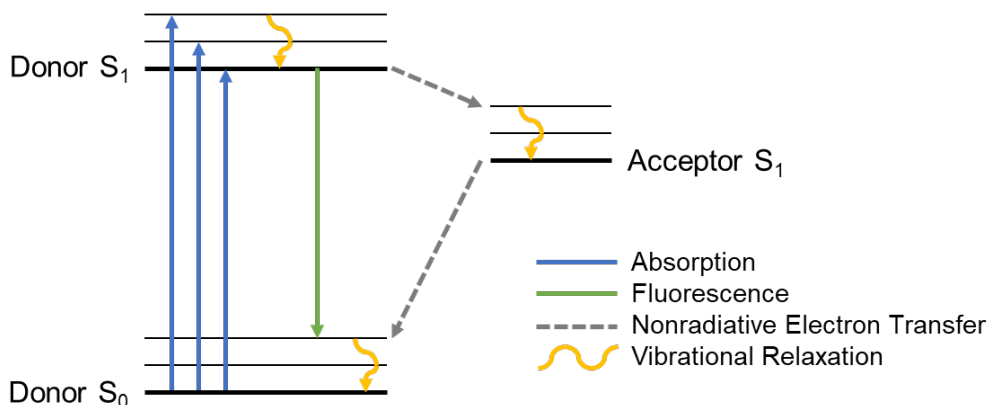


Figure 2.3. Simplified Jablonski diagram for donor-photoinduced electron transfer fluorescence quenching.

On a simple level, the LUMO of the proximal species must be lower than the LUMO of the chromophore for d-PeT quenching to take effect. Mathematically, favorability can be calculated using the Rehm-Weller equation (Equation 2.1)

$$\Delta G_{et} = E(D^+/D) - E(A/A^-) - \Delta E_{00} + w_p \quad (2.1)$$

The terms $E(D^+/D)$ and $E(A/A^-)$ are the reduction potentials of the oxidized donor and the acceptor, respectively. The term ΔE_{00} describes the energy difference between the lowest vibrational energy levels of the ground and first electronic energy states. This can be estimated by the intersecting wavelength of the normalized absorbance and emission profiles. Finally, w_p is the work term for charge separation.

No ALDH-responsive probes utilizing the d-PeT mechanism existed before our publication of AIDeSense. In fact, few d-PeT probes existed at all.⁵⁷[citations] However, we were inspired by the work of Nagano and coworkers demonstrating d-PeT quenching on xanthene-based dyes.⁵⁸ Fluorescence quantum yield generally fits a sigmoidal curve, where more readily reduced substrates (higher E_{red} (E vs. SCE)) facilitate d-PeT quenching. (Figure 2.4) We hypothesized that a benzaldehyde moiety appended to a xanthene dye would have a higher reduction potential than the corresponding aryl carboxylate. This is supported by electrochemical measurements performed on isolated aryl species. Namely, benzaldehyde has a reported reduction potential of -1.93 V while benzoic acid has a reduction potential of -2.29 V.⁵⁹ The reduction potential of the carboxylate present at physiological pH would be much lower given the species would be anionic. The asymptotic nature of the sigmoidal curve allows extended windows of reduction potentials in

which minimal change in the quantum yield is observed. Thus, we expect that perturbing the system through the potential coordination of metal ions (such as Cu^{2+} in the ICT example) will not be insufficient to dramatically change the quantum yield. Additionally, we intended to forego the traditional strategy of using chemical inhibitors as a control and instead use a non-responsive methyl ketone. At -2.11 V, the reduction potential for acetophenone is notably higher than that of benzaldehyde, but it should not be an issue if both are near the asymptote.

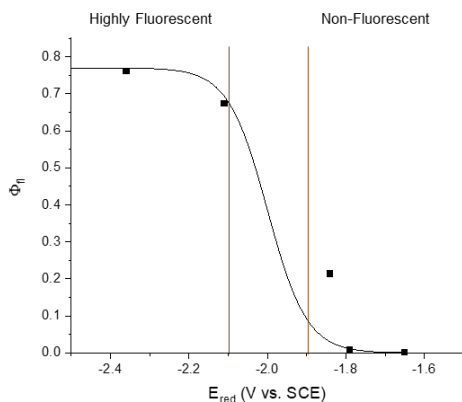


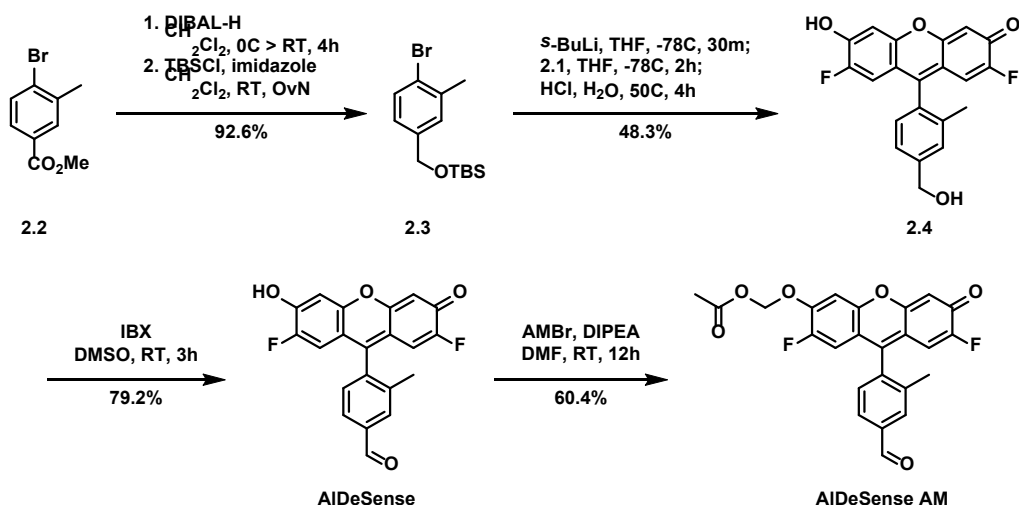
Figure 2.4. Fluorescence quantum yield as a function of reduction potential. Data points are replotted from Ueno, et al.c Line is representative of data. Mathematical fitting of sigmoidal curve, $f(x)=A/(1+e^{(k(x-x_c))})$ was not performed due to low quantity of data points.

2.3 AlDeSense

AlDeSense was the first turn on fluorescent probes selective for ALDH1A1. It's control compound, Ctrl-AlDeSense was the first matched control compound reported for ALDH activity which enabled accounting for basal accumulation without the use of a chemical inhibitor.

2.3.1 Synthesis

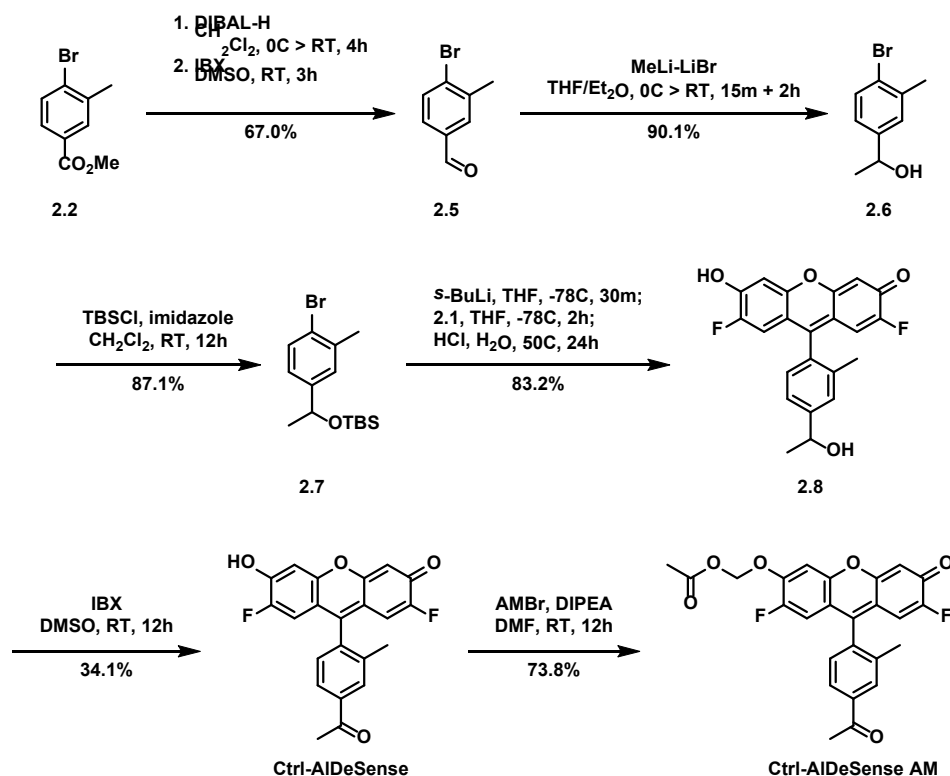
Just as they are electronically independent and modular, the benzaldehyde moiety and xanthene moiety come together in the synthesis of AlDeSense. (Scheme 2.1)



Scheme 2.1. Synthesis of AlDeSense and AlDeSense AM.

The difluoroxanthone is synthesized via a route first described by Peterson and coworkers.⁶⁰ Briefly, lithium-halogen exchange with 1-bromo-2,4,5-trifluorobenzene enables coupling with 2,4,5-trifluorobenzaldehyde to afford the symmetrical benzhydrol. This is oxidized under mild conditions with TEMPO and NaOCl. The resulting diaryl ketone then undergoes a series of $\text{S}_{\text{N}}\text{Ar}$ reactions in two sequential steps: the first converts the fluorines at the 2, 4, 2', and 4' positions to hydroxy groups, and the second closes the ring to form the xanthone. This difluoroxanthone is then protected with MEMCl to afford **2.1** which was used in the coupling.

The 4-bromobenzyl alcohol derivative starts as methyl 4-bromo-3-methylbenzoate **2.2**. This is reduced using a milder reducing agent, DIBAL-H, to afford the benzyl alcohol. Though cheaper and with better atom economy, LiAlH_4 caused partial debromination of the sample leading to an unproductive and poorly separable 3-methylbenzyl alcohol. The productive benzyl alcohol was protected with TBSCl as **2.3** before lithiation and coupling. For the synthesis of Ctrl-AlDeSense, the benzyl alcohol was reoxidized to benzaldehyde **2.5** with IBX, then methylated to secondary alcohol **2.6** with MeLi. (Scheme 2.2) As with the precursor to AlDeSense, the alcohol was protected with TBSCl to form **2.7** before coupling.



Scheme 2.2. Synthesis of Ctrl-AIDeSense and Ctrl-AIDeSense AM

Coupling proceeded via first performing lithium-halogen exchange with *tert*-butyllithium and the aryl bromide followed by nucleophilic attack onto the xanthone. Global TBS deprotection proceeded under acidic conditions to afford the benyl alcohol precursors **2.4** and **2.8**. Both the primary and secondary alcohols were oxidized with IBX to afford **AIDeSense** and **Ctrl-AIDeSense**, respectively. These molecules were alkylated with acetoxymethyl chloride to afford cell penetrable **AIDeSense AM** and **Ctrl-AIDeSense AM**.

2.3.2 Testing

AIDeSense and Ctrl-AIDeSense were used in all assays not requiring cell penetration; AIDeSense AM and Ctrl-AIDeSense AM were used for all assays in which cell penetration was required. To avoid confusion, the terms AIDeSense and Ctrl-AIDeSense is used to describe both.

2.3.2.1 In vitro

AIDeSense was first tested against purified recombinant ALDH1A1 and other purified recombinant ALDH isoforms. In the presence of ALDH1A1, a rapid 15- to 20-fold fluorescent turn on was observed. (Figure 2.5.A) One batch even managed to achieve a 40-fold turn on. This was reproducible with aliquots within the batch, but not from any other batches. This outlier was

never fully explained, as it was less pure, and improved purity was observed in later batches by ^1H and ^{19}F NMR. In any case, AlDeSense was found to react with $k_m = 1.2\ \mu\text{M}$ and $k_{cat} = 4.2\ \text{min}^{-1}$. (Figure 2.5.B)

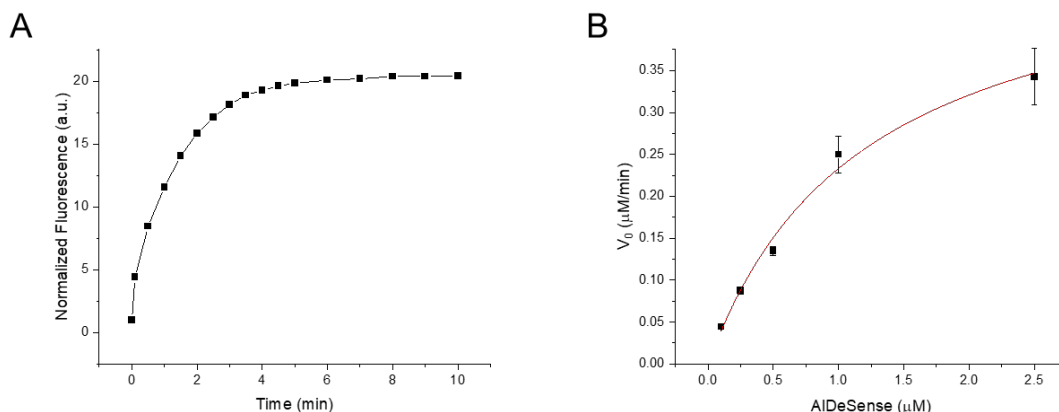


Figure 2.5. AlDeSense and ALDH1A1. (A) Normalized trace of fluorescence at 516 nm of 1 μM AlDeSense and 1 μM ALDH1A1 in TEA buffer. (B) Michaelis-Menten plot of AlDeSense and ALDH1A1.

To confirm any turn on in a biological setting was due to ALDH1A1 activity and not another analyte, AlDeSense was tested against other purified recombinant ALDH isoforms and biologically relevant reactive oxygen species (ROS), reactive nitrogen species (RNS), and reactive sulfur species (RSS). It displayed excellent ALDH isoform selectivity against all tested isoforms. (Figure 2.6.A) Isoforms tested were those that we could successfully express and purify from plasmids. Importantly, this set included ALDH1A1's closest relatives, ALDH1A2 and ALDH1A3, as well as one of the main aryl aldehyde oxidizing enzymes ALDH3A1. The ROS/RNS/RSS tested included those commonly tested against probes (H_2O_2 , GSH, $\bullet\text{OH}$, etc.) as well as some less common species that could be causes for concern for AlDeSense. (Figure 2.6.B) In particular, perturbing electronics of the aldehyde through reversible Schiff base formation could lead to a turn on, but none was observed in the presence of primary amine containing glycine, lysine, dopamine, or methylamine. Irreversible Pictet-Spengler chemistry could also replace the aldehyde with a substituted benzyl amine, perturbing electronics and leading to a fluorescent turn on. A low turn on (~ 3 -fold) was observed from 5-methoxytryptamine, a deacylated melatonin product, but these were at levels far above those found physiologically of tryptamine analogues. These data suggest that any observed turn on in cells would be from ALDH1A1 and not other analytes.

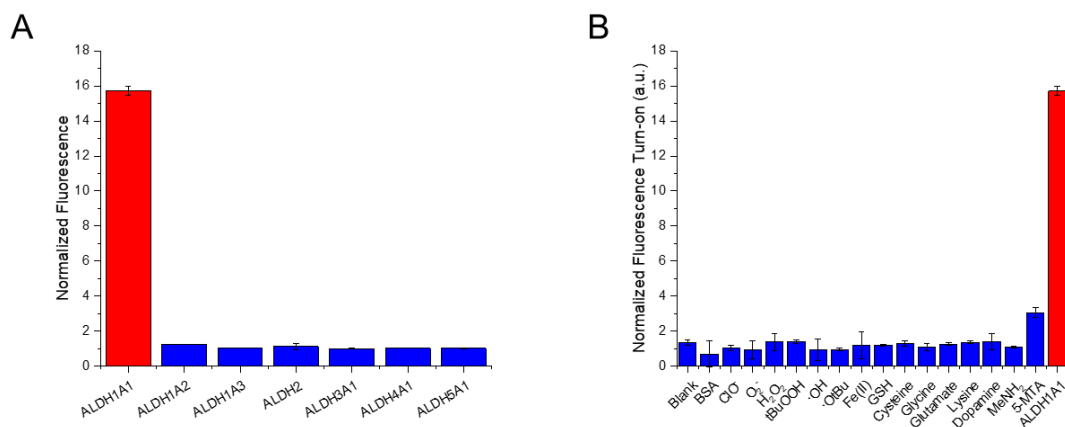


Figure 2.6. AlDeSense selectively turns on due to ALDH1A1 *in vitro*. Normalized fluorescent turn on of AlDeSense against ALDH1A1, (A) other ALDH isoforms, and (B) ROS/RNS/RSS. Each is performed in triplicate.

We set out to design a probe that would facilitate imaging CSCs while perturbing their native functions as little as possible. We still needed a way to account for background fluorescence. Historically, one of the most common ways is to use a chemical inhibitor. There are plenty of known inhibitors for ALDH,⁶¹ and one of the most common, DEAB, does prevent AlDeSense turnover. (Figure 2.7) But, inhibition perturbs the system. We therefore looked to synthesize a control compound which would have nearly identical physical and photophysical properties to match fluorescence and distribution, but which would be inactive towards ALDH1A1. We solved this with Ctrl-AlDeSense. Ctrl-AlDeSense features the same Pennsylvania Green dye platform but is decorated with a methyl ketone in place of the aldehyde from AlDeSense. This substitution renders Ctrl-AlDeSense inactive since a key step in the ALDH catalytic cycle is hydride transfer. Methanide transfer does not work. Thus, when screened against ALDH1A1, Ctrl-AlDeSense shows no turnover just like AlDeSense with the addition of inhibitor.

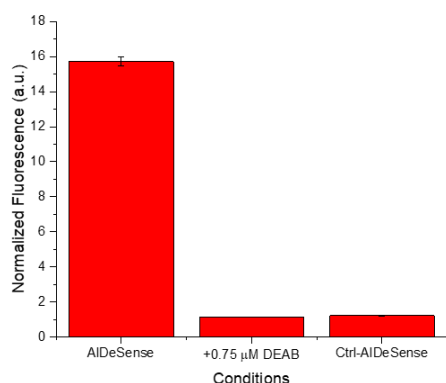


Figure 2.7. ALDH1A1 turn on of AlDeSense and Ctrl-AlDeSense. Normalized fluorescent turn on after 30 minutes of 1 μ M AlDeSense with or without 0.75 μ M DEAB, as well as 1 μ M Ctrl-AlDeSense in the presence of purified rhALDH1A1.

2.3.2.2 In silico

Unbiased enzymatic docking was performed with AlDeSense against published crystal structures of ALDH isoforms using the AutoDock Vina function in UCSF Chimera 1.12.

Protein crystal structures were imported into Chimera. When more than one crystal structure was available, the first choice was the protein bound to NAD⁺, then the apoprotein, then the protein bound to native substrate, and lastly protein bound to a chemical inhibitor. Mutant enzymes and non-human enzymes were not used in the analysis. After importing, the protein was simplified to a single monomer by deleting all duplicate strands in dimers, tetramers, etc. Next, water molecules, metal ions, organic substrates were deleted leaving only the protein and NAD⁺ cofactor. All atoms on the protein were hidden except for the active site cysteine(s). Finally, a surface was generated for the entire protein, excluding the NAD⁺.

The structure of deprotonated AlDeSense was optimized using Gaussian 03W over two iterations. The first iteration involved ground state optimization calculations using Hartree-Fock, default spin, 3-21G basis set, setting it with a charge of -1 and a singlet. The second iteration ground state optimization and frequency calculations using DFT B3LYP, default spin, 6-31g(+)d basis set, setting it with a charge of -1 and a singlet. The optimized structure was opened in Chimera along with the ALDH crystal structure from above.

Using AutoDock Vina, the protein was selected as the Receptor, and AlDeSense was selected as the Ligand. The receptor search volume was adjusted such that the entire protein was

encompassed. The options were left as default, except the number of binding modes was increased to the maximum. (Figure 2.8)

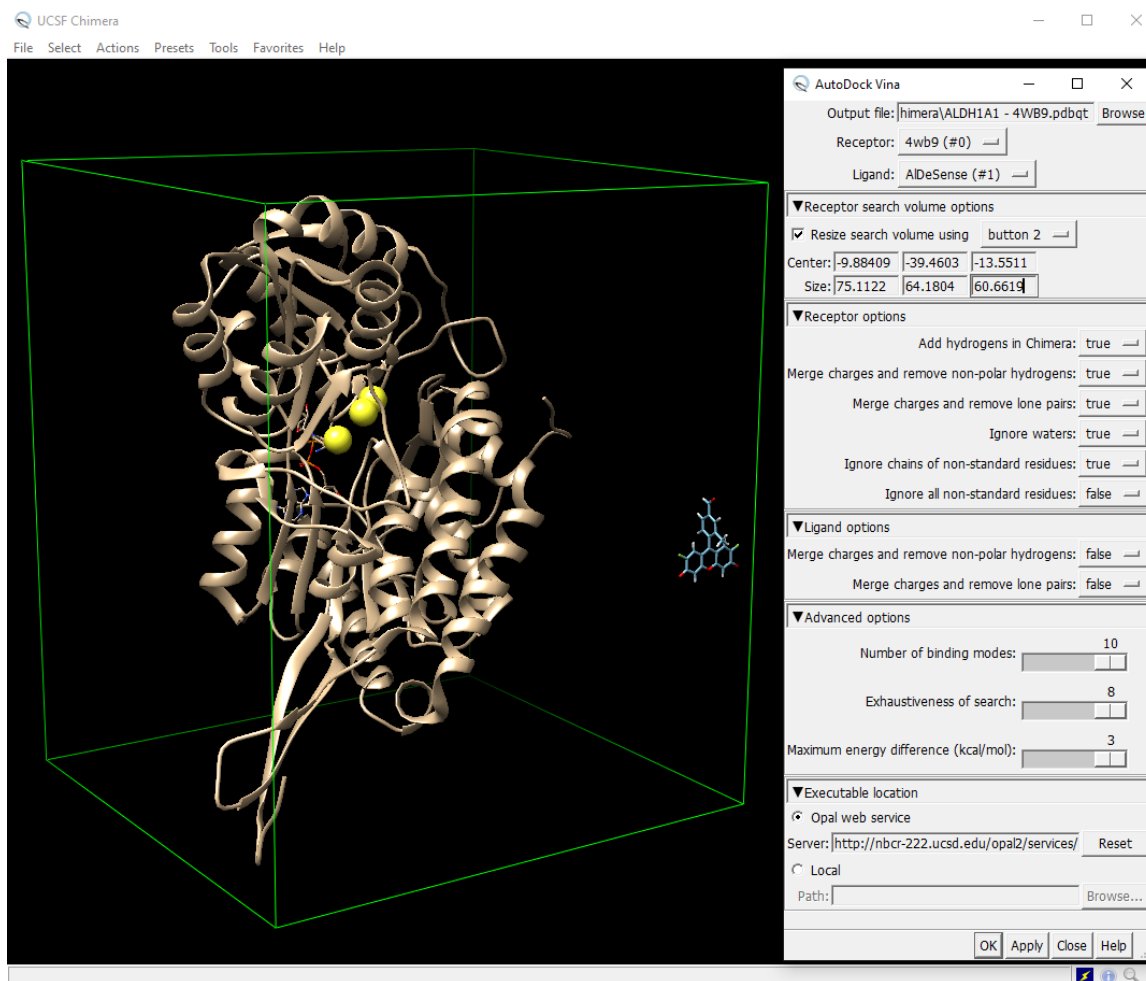


Figure 2.8. Example parameters for unbiased docking with AutoDock Vina. Shown is the parameters used to dock AlDeSense onto ALDH1A1 (PDB: 4WB9). Note: when the Opal web service is down, a copy of Vina can be downloaded to perform the calculations on your local computer.

After running the simulation, the top ten energetically favorable orientations were analyzed (only 5 orientations were output for ALDH1A1) for binding in the substrate binding pocket and whether the binding held the carbonyl carbon near the active site cysteine's sulfur. The top result, as determined by shortest length from carbonyl carbon to cysteine sulfur, was then recorded along with its reported energy. (Table 2.1) Analysis of the results shows AlDeSense only docks in a potentially productive geometry in ALDH1A1 and ALDH1A3. This suggests structurally, AlDeSense should be a substrate for both isoforms. However, AutoDock Vina does not include partial charges in its calculations, so the anionic nature of AlDeSense is ignored. This is important

since ALDH1A1 features cationic Lys128 near the entrance to the substrate binding pocket, likely providing a favorable interaction with anionic AlDeSense. Conversely, no such cationic residue exists near where the anionic phenol of AlDeSense is likely to be during productive binding with ALDH1A3. This provides evidence that while selectivity is provided over most isoforms by the steric restraints of the binding pockets, selectivity over ALDH1A3 is at least in part due to the low pKa of AlDeSense.

ALDH Isoform ^a	PDB	Docked in Binding Pocket ^b	Oriented Towards Active Site	C _{CHO} to S _{Cys} distance (Å)	Energy (kcal/mol)
1A1	4WB9	2	2	4.682	-10.1
1A2	6ALJ	2	0	9.538	-7.5
1A3	5FHZ	10	2	4.499	-10.1
2	1O02	1	0	15.623	-7.0
3A1	3SZA	5	0	6.061	-7.4
3A2	4QGK	3	0	7.279	-7.6
4A1	3V9G	0	0	- ^c	- ^c
5A1	2W8N	3	0	17.117	-7.9
7A1	4ZUK	1	0	8.074	-7.8

Table 2.1. Unbiased docking results of AlDeSense on ALDH isoforms. Simulations were performed in UCSF Chimera 1.12 using AutoDock Vina. ^aCrystal structures for ALDH isoforms 9A1 and 18A1 were omitted due to an incomplete assignment of the crystal near the active site. ^bALDH1A1 produced 5 docking events; all other isoforms produced 10 docking events. ^cThese measurements are omitted for ALDH4A1 since no docking event held AlDeSense in or near the binding pocket.

2.3.2.3 In cellulo

The low phenolic pKa of AlDeSense and Ctrl-AlDeSense leave them unable to diffuse across cell membranes. To address this, both were capped with an acetoxymethyl (AM) ether. This strategy is commonly used with other cell impenetrable molecules (e.g. calcium probes [citation]) since a broad range of esterases are capable of quickly uncapping the probe once in cells. It was not until later that we learned the concentrations of formaldehyde being released by the trigger are likely having an impact on the cells.⁶²

With AlDeSense AM and Ctrl-AlDeSense AM in hand, we continued testing to confirm cellular responses to AlDeSense were due selectively to ALDH1A1. Most commercially available

inhibitors are not selective for ALDH1A1 over other isoforms, DEAB included. Thus, we elected to perform siRNA knockdown experiments. Knockdown of ALDH1A1 using two unique siRNA sequences in K562 cells decreased the AlDeSense signal significantly using confocal microscopy. (Figure 2.9)

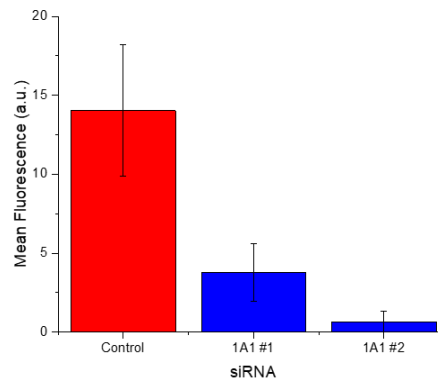


Figure 2.9. AlDeSense turn on is due to ALDH1A1 in cells. Mean fluorescence signal from K562 cells stained with AlDeSense after being treated with 50 μ M siRNA.

Having established in multiple forms that AlDeSense is selective for ALDH1A1, we next set to confirm that ALDH1A1 activity as measured by AlDeSense is a reliable CSC marker.

In one assay, K562 cells were co-stained with AlDeSense and fluorescently labeled antibodies for CD34, CD38, and CD133. A well-established CSC marker profile for chronic myeloid leukemia is CD34⁺/CD38⁻ [citation] with recent evidence indicating full CD34⁺/CD38⁻/CD133⁺ being a more refined marker set.⁶³ When viewed using confocal microscopy, the cells that were CD34⁺/CD38⁻/CD133⁺ were also ALDH1A1^{high}.

In another assay, MDA-MB-231 breast cancer cells were grown in ultralow adherent plates in low serum, high growth factor media to generate tumorspheres. It is well established that growing tumorspheres is a reliable way to increase the stem cell population. Differentiated cells either dedifferentiate or die under these conditions. Once the tumorspheres had grown to at least 50 μ m in diameter, they were transferred to standard adherent plates containing normal cell growth media. The tumorspheres were left under those conditions for time points ranging from 0 to 35 hours before staining with AlDeSense or Ctrl-AlDeSense for 1 hour. Imaging on a wide field fluorescence microscope demonstrated high ALDH1A1 activity of the tumorspheres immediately following the transfer. (Figure 2.10) This indicated that ALDH1A1 activity was upregulated in these cells. The longer the cells were allowed to grow under normal conditions, the lower the

ALDH1A1 activity became. After 36 hours, the ALDH1A1 activity had dropped to where there was little difference between the signals from AlDeSense and Ctrl-AlDeSense.

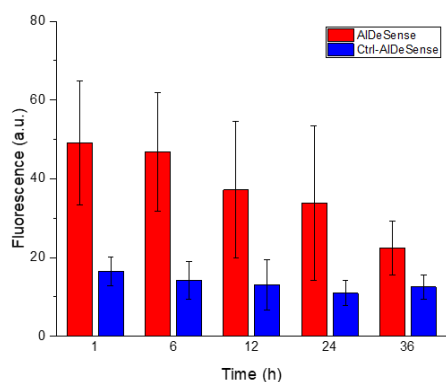


Figure 2.10. Decrease in ALDH1A1 activity over time as tumorspheres are grown in normal media. Mean fluorescence signal from MDA-MB-231 tumorspheres stained with AlDeSense or Ctrl-AlDeSense after being placed under regular cell culture conditions for the indicated amount of time. Time includes dye incubation period.

A more recent approach to increasing the stem cell population in cell culture is growing the cells on spiral patterned gels.⁶⁴ These cells have been shown to upregulate stem cell markers and exhibit increased tumorigenicity compared to cells grown on non-patterned gels or glass slides. B16F0 cells were grown on patterned and non-patterned gels. The cells were then stained with AlDeSense or Ctrl-AlDeSense. As before, Ctrl-AlDeSense was used to establish basal accumulation of dye. More cells from the patterned gel system were ALDH1A1^{high} compared to the non-patterned gel system. The performance of AlDeSense in these three model systems support that AlDeSense is identifying CSCs through its reporting on ALDH1A1 activity.

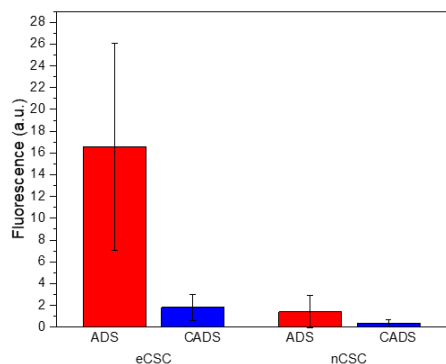


Figure 2.11. AlDeSense shows increased ALDH1A1 activity in enriched CSC (eCSC) patterned B16F0 melanoma cells compared to non-enriched CSC (nCSC) non-patterned B16F0 melanoma cells.

2.3.3 Applications

The primary goal in developing AlDeSense was to apply it to full animal systems. In particular, we were interested in whether the *in vitro* CSC marker ALDH1A1 was maintained in the tumor microenvironment.

Our first exploration of such applications used the B16F0 melanoma cells injected intravenously into immunocompetent mice. This injection simulated the entrance of cancerous cells into the blood stream whereby they are given the opportunity to metastasize in the lungs. Each mouse was injected with either a patterned, enriched CSC (eCSC) population or a non-patterned, non-enriched CSC (nCSC) population. After 11 days, the mice were sacrificed, and their lungs were excised. The freshly excised lungs were perfused with either AlDeSense or Ctrl-AlDeSense, washed with water until the fluorescence signal stabilized between washes, then imaged. The signal from AlDeSense in the eCSC lungs was higher than the Ctrl-AlDeSense signal in the comparable eCSC lungs indicating high ALDH1A1 activity. No such difference was observed between the AlDeSense and Ctrl-AlDeSense signals in the nCSC lungs, wherein the activity is thereby lower. Importantly, there was no difference in the Ctrl-AlDeSense signals between the eCSC and nCSC lungs indicating little difference in cellular uptake. The AlDeSense signal, however, was significantly higher in the eCSC lungs compared to the nCSC lungs. Taken together, high ALDH1A1 activity was observed in the eCSC-metastasized lungs compared to the nCSC-metastasized lungs. The high activity maintained over 11 days in a tumor microenvironment is in stark contrast to the rapid differentiation observed by CSCs in isolated systems.

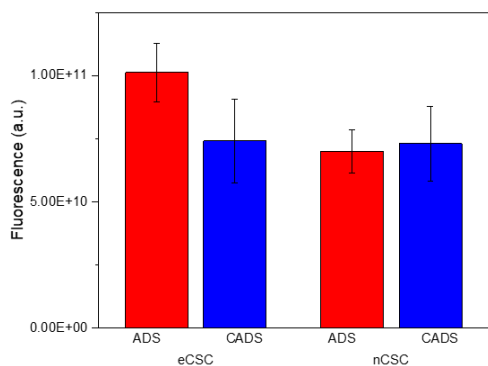


Figure 2.12. High ALDH1A1 activity is maintained in the metastases B16F0 melanoma cells enriched for CSCs.

The true test of the efficacy of AlDeSense was in live animal imaging. For this, B16F0 melanoma allografts were generated in BALB/c mice via subcutaneous injection. The eCSC and nCSC populations were injected in the right and left flanks, respectively, such that each mouse carried the tumors initiated from eCSC and nCSC populations. Tumors were injected with AlDeSense or Ctrl-AlDeSense after 14 days and imaged using a full body imager. The mice injected with Ctrl-AlDeSense consistently showed a lower signal in the nCSC tumors compared to the eCSC tumors. This is likely due to the increased melanin in the larger eCSC tumor absorbing some of the excitation or emission signal. The same low ratio was not observed in the AlDeSense-stained tumors. In fact, a higher signal was observed in the eCSC tumors compared to the nCSC tumors. The high ALDH1A1 activity after 14 days in the tumor allografts is consistent with high ALDH1A1 activity after 11 days in the lung metastases. In both cases, the tumor microenvironment facilitated the maintenance of elevated levels of CSCs as measured by ALDH1A1 activity. This demonstrates that AlDeSense is effective at imaging ALDH1A1 activity in living animals.

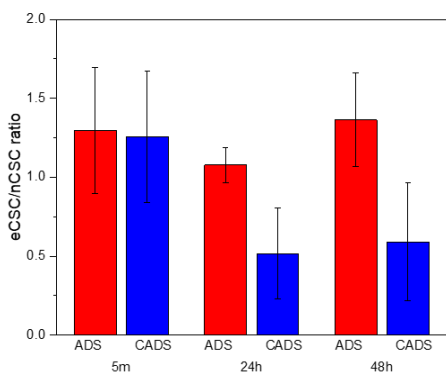


Figure 2.13. High ALDH1A1 activity is maintained in the B16F0 melanoma allografts originating from the eCSC population. Ratio of fluorescence signal from the eCSC tumor versus the nCSC tumor grown in different flanks of the same mouse. Time represents length of time staining the tumors with AlDeSense or Ctrl-AlDeSense. n=3.

2.4 red-AlDeSense and related molecules

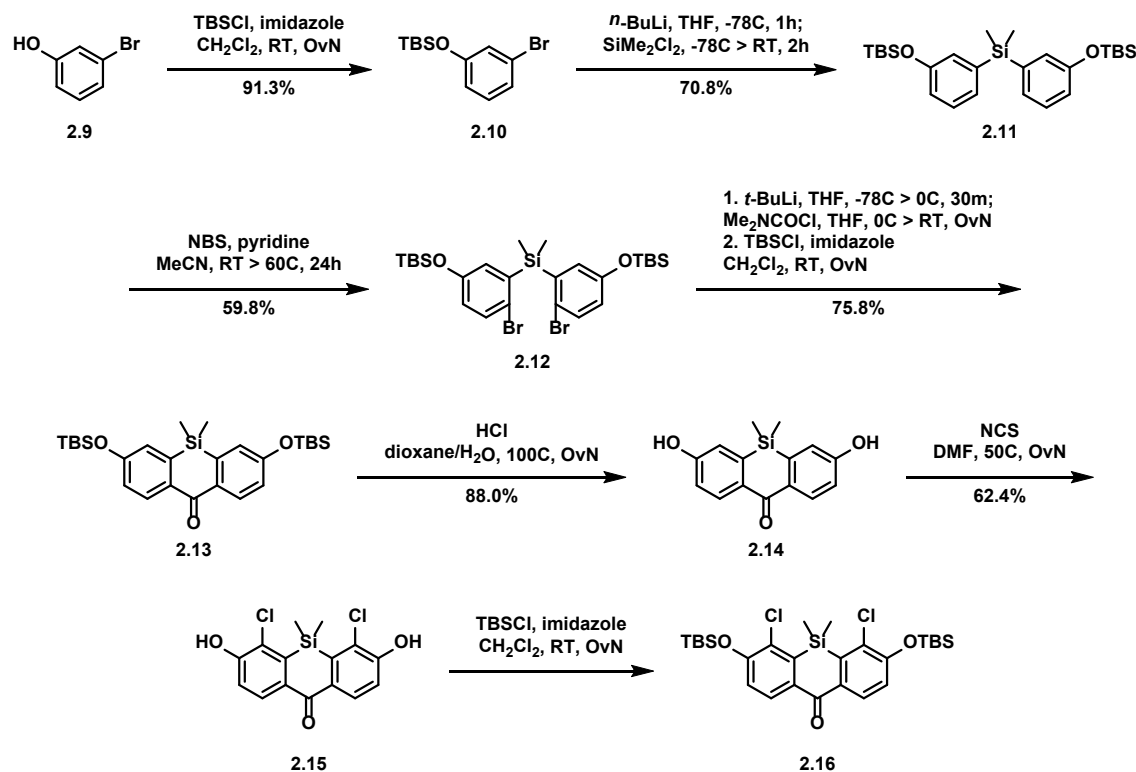
Despite the major advance AlDeSense represented, we aimed to improve two properties to broaden its general utility. First, AlDeSense is not cell permeable unless it is chemically modified with capping groups (i.e., acetoxymethyl ether) to mask the intrinsic negative charge character on the phenolic alcohol ($pK_a = 4.81$). Consequently, intracellular esterases are required for full activation. This process generates byproducts, namely acetate and formaldehyde, which are

released upon uncapping. Second, the absorbance and emission profiles of AlDeSense overlaps with that of FITC and GFP, small-molecule and protein handles, respectively, that are commonly used to visualize biological processes via molecular imaging.

2.4.1 Synthesis

The synthesis of the various probes on the way to red-AlDeSense was not the smoothest process. First attempts were made by synthesizing the xanthone and 4-bromobenzyl alcohols separately and stitching them together. These first attempts aimed at accessing the Si-xanthone through the route described by Nagano and coworkers.⁶⁵ In our hands, the route is robust for every step excluding the KMnO₄ oxidation of the benzhydryl moiety to the xanthone. Next, we attempted to use the recently published route developed by Lavis and coworkers.⁶⁶ This route resulted in inconsistent and poor yields in our hands. To be fair, this was optimized for more electron rich Si-rhodamine dyes with only limited examples of Si-fluoresceins, all of which used an anhydride rather than an ester for coupling.

Finally, we realized that the Lavis route to the dibromo species could be closed on dimethyl carbamoyl chloride to afford the desired xanthone.⁶⁷ Briefly, 3-bromophenol (**2.9**) was protected as TBS ether **2.10**. This then underwent lithium halogen exchange with *n*-butyllithium so that it could dimerize on dichlorodimethylsilane to form **2.11**. This was selectively brominated as **2.12** with *N*-bromosuccinimide, installing a bromine para to each of the silyl ethers. Notably, other conditions such as *N*-bromosuccinimide in DMF gave poor selectivity for the dibrominated species. The installed bromines underwent lithium halogen exchange with *sec*-butyllithium before closing on dimethylcarbamoyl chloride. Partial TBS deprotection under the reaction conditions necessitated reprotection with TBSCl to afford desired xanthone **2.13**. This route proved incompatible with more electron rich xanthenes such as the 3,6-dihydroxy-2,7-dimethoxyxanthone. 4,5-dichloro-3,6-dihydroxyxanthone could be accessed by first deprotecting the fully formed xanthone to compound **2.14**. Chlorination with *N*-chlorosuccinimide favored the 4 and 5 positions observed in **2.15**. Finally, reprotection of the poorly soluble substrate afforded dichloroxanthone **2.16**. Overall, the route to the regular xanthone, **2.13**, was consistently high yielding and easily scalable such that the burden of synthesis was placed on the bottom benzaldehyde precursors. The chlorination was more troublesome, but issues with the final dyes removed any motivation for optimizing the route to **2.16**.



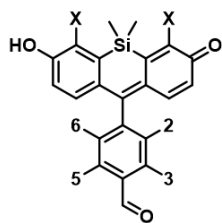
Scheme 2.3. Synthesis of Si-xanthenes.

The benzaldehyde precursors were synthesized from commercially available starting materials in 2-7 synthetic steps (detailed in Appendix A). Broadly, the desired functional groups were incorporated including a bromine for lithium halogen exchange, and the future aldehyde was reduced to the benzyl alcohol and TBS protected. These protected 4-bromobenzyl alcohols underwent lithium halogen exchange with *tert*-butyllithium and were added to the Si-xanthenes synthesized above. As before, the new xanthene dye was globally deprotected using mild heat and acid. The benzyl alcohol was then oxidized to the aldehyde using IBX. Oxidation using Swern conditions was required to generate Ctrl-red-AlDeSense.

2.4.2 Testing

As a baseline for selectivity and turn on, we first synthesized Probe 1. Probe 1 featured the same 3-methylbenzaldehyde reactive trigger as AlDeSense, but the Pennsylvania Green dye platform was replaced with a TokyoMagenta platform including an endocyclic dimethyl silicon and absent the two fluorine atoms. The change in dye platform facilitated a 90 nm red shift, but it decreased both the turn on and selectivity. The decrease in turn on was expected, since the quantum yield of unquenched TokyoMagenta is naturally lower than that of Pennsylvania Green. For

example, the benzyl alcohol precursor to Probe 1 is expected to show no d-PeT quenching similar to the carboxylate turn over product of Probe 1, and it has a quantum yield of 0.60. The d-PeT quenching is also expected to be less effective on red-shifted substrates based on the Rehm-Weller equation. This is observed with the higher quantum yield for Probe 1 (0.32) compared to that of AlDeSense (0.04). Raising the quantum yield of the probe and lowering the quantum yield of the turnover product produced a dismal 1.9-fold theoretical turn on and 1.7-fold enzymatic turn on. The sharp decrease in selectivity was less expected, but it was consistent with the hypothesis that the anionic nature of AlDeSense was important for isoform selectivity.



Probe	2	3	5	6	X
1	CH ₃	H	H	H	H
2	F	H	H	H	H
3	NO ₂	H	H	H	H
4	CF ₃	H	H	H	H
4-Cl ₂	CF ₃	H	H	H	Cl
5	F	H	H	F	H
6	OMe	H	H	OMe	H
7	CF ₃	H	CF ₃	H	H
8	CH ₃	H	F	H	H
9	CH ₃	F	H	F	H
RADS	CH ₃	H	F	F	H

Figure 2.14. Structure of all synthesized probes and red-AlDeSense (RADS).

We hypothesized that careful tuning of the xanthene and/or benzaldehyde would facilitate the desired red-shift without compromising on turn on and selectivity. Probes 2-4 were synthesized to begin to probe the effects of sterics and electronics on selectivity and turn on. The modifications on this first generation involved the replacement of the methyl group with other functional groups at the position meta to the benzaldehyde. The fluorine in Probe 2 was too small to prevent nucleophilic attack by alcohols, including water. This is consistent with previous observations that the analogous Si-rhodamines are highly susceptible to nucleophilic attack by glutathione.²⁷ The instability made relevant characterizations (e.g. quantum yield) in aqueous buffer unsuitable for quantitative measurement. Non-quantitative observations, however, indicated improved d-PeT quenching of Probe 2 compared to Probe 1. The nitro group in Probe 3 afforded an exceptionally quenched dye (quantum yield <0.001), but there was no observed turn-on in the presence of ALDH1A1. It was not determined whether this is due to the nitro remains an effective d-PeT quenching moiety despite the proximity of the carboxylate or a lack of substrate. Whether too large

or too withdrawing, the nitro functional group was not worth pursuing further. Probe 4, featuring a trifluoromethyl group, improved on the dynamic range achieving 2.7-fold enzyme turn on. The reactivity with ALDH1A3 decreased, but so too did the reactivity with ALDH1A1. Taken together, Probes 2-4 demonstrate a sweet spot in sterics lies somewhere between a fluorine atom (too small for stability) and trifluoromethyl group (approaching too large to fit). The electronic trends indicate that more electron withdrawing benzaldehydes improve the turn on, but a nitro group is too far.

With increasing evidence that AlDeSense's selectivity for ALDH1A1 was due in large part to its anionic nature, we looked to derivatives of TokyoMagenta with a decreased pKa. Installation of halogens on the xanthene chromophore should decrease the pKa. Additionally, Urano and coworkers demonstrated a 10 nm bathochromic shift and 0.10 increase in the fluorescence quantum yield after installation of two chlorines on 2-COOH TokyoMagenta.⁶⁸ After developing a synthetic approach to access the chlorinated Si-xanthone, Probe 4-Cl₂ was synthesized. Unfortunately, Probe 4-Cl₂ could not be used to test for isoform selectivity via a fluorescence readout since the probe demonstrated no d-PeT quenching in the benzaldehyde form compared to benzyl alcohol form.

We then set out to test synthetically accessible difunctionalized analogs (Probes 5-8) as we continued to hone in on optimized steric and electronic parameters. Adding an additional fluorine such that both fluorines were ortho to the xanthene core imparted stability in Probe 5. The electron withdrawing capacity of the fluorines improved the theoretical turn on to 4.2-fold and the measured enzymatic turn on to 3.9-fold. Unfortunately, the improved turn on was accompanied by a complete erosion of selectivity. Probe 5 turned over equally fast in the presence of ALDH1A1 and ALDH1A3. Probe 6, featuring two methoxy groups ortho to the xanthene, had a low turn on (1.2-fold enzymatic and 1.6-fold theoretical). This was expected from previous observations that electron withdrawing groups improve the d-PeT quenching, likely through increasing the reduction potential of the benzaldehyde. The less predicted phenomenon was the sharp decrease in ALDH1A1 activity. The two methoxy groups, though small and somewhat flexible, were bulky enough to hinder productive binding. An even more dramatic decrease in activity was seen in Probe 7, which featured trifluoromethyl groups at positions 2 and 5. The first trifluoromethyl group in Probe 3 had decreased activity, but the second shut it off completely. The 3.2-fold theoretical turn on of Probe 7 was an improvement over the 2.7-fold enzymatic turn on observed for Probe 3. This was consistent with our observations that electron withdrawing groups improved turn on.

Back closer to the sweet spot of selectivity, Probe 8 featured the methyl group of Probe 1 in addition to a fluorine atom para to the methyl. The addition of the fluorine improved turn on over Probe 1 from 1.7- to 2.6-fold enzymatic and 1.9- to 2.8-fold theoretical. The increased bulk at the 5 position also improved the selectivity by decreasing reactivity with ALDH1A3. No negative effects were observed on the reactivity with ALDH1A1 due to the increase in steric bulk. The five new probes developed continued to guide us towards an optimum structure balancing turn on and selectivity.

The plan for increasing to three substituents was to increase the number of small electron withdrawing groups, though not as electron withdrawing as the nitro group, and maintain the size somewhere between the single methyl and single trifluoromethyl groups. The latter was important because the reactivity with ALDH1A3 continues to decrease across that range, but somewhere within the range the reactivity with ALDH1A1 starts to decrease as well. We elected to synthesize the isomers containing one methyl group and two fluorine atoms, leaving the methyl group ortho to the xanthene. We did not pursue the isomer in which both fluorines are ortho to the aldehyde since 2,6-difluorobenzaldehyde was not a substrate of ALDH1A1 in *in vitro* testing. The first of the other two isomers, Probe 9, was based on 2,5-difluoro-3-methyl benzaldehyde. An improvement was seen over Probe 8 in the enzymatic turn on, from 2.6-fold to 3.1-fold. However, a decrease in the selectivity was also observed as it reacted with ALDH1A3 almost as fast as Probe 1. With the apparent importance of a fluorine para to the methyl group, red-AlDeSense was synthesized. Red-AlDeSense showed good selectivity over ALDH1A3 and a respectable 3.2-fold enzymatic turn on.

Red-AlDeSense achieves a nearly 100 nm red shift from AlDeSense. (Figure 2.15.A) The absorbance maximum (λ_{abs}) was at 594 nm, aligning with the commercially available HeNe-594 laser line. Meanwhile the emission maximum (λ_{em}) was at 614 nm, tailing off beyond 700 nm for effective red fluorescence. It is selective for ALDH1A1 over ALDH1A3 and all other tested isoforms. (Figure 2.15.B) Red-AlDeSense also demonstrate chemostability to a panel of common biological reactive oxygen, nitrogen, and sulfur species. (Figure 2.15.C) Surprisingly, red-AlDeSense ($k_{\text{cat}}/K_{\text{m}}$ of $7.91 \mu\text{M}^{-1} \text{min}^{-1}$) was also a better substrate for ALDH1A1 than AlDeSense ($k_{\text{cat}}/K_{\text{m}} = 3.46 \mu\text{M}^{-1} \text{min}^{-1}$) under identical conditions. (Figure 2.15.D)

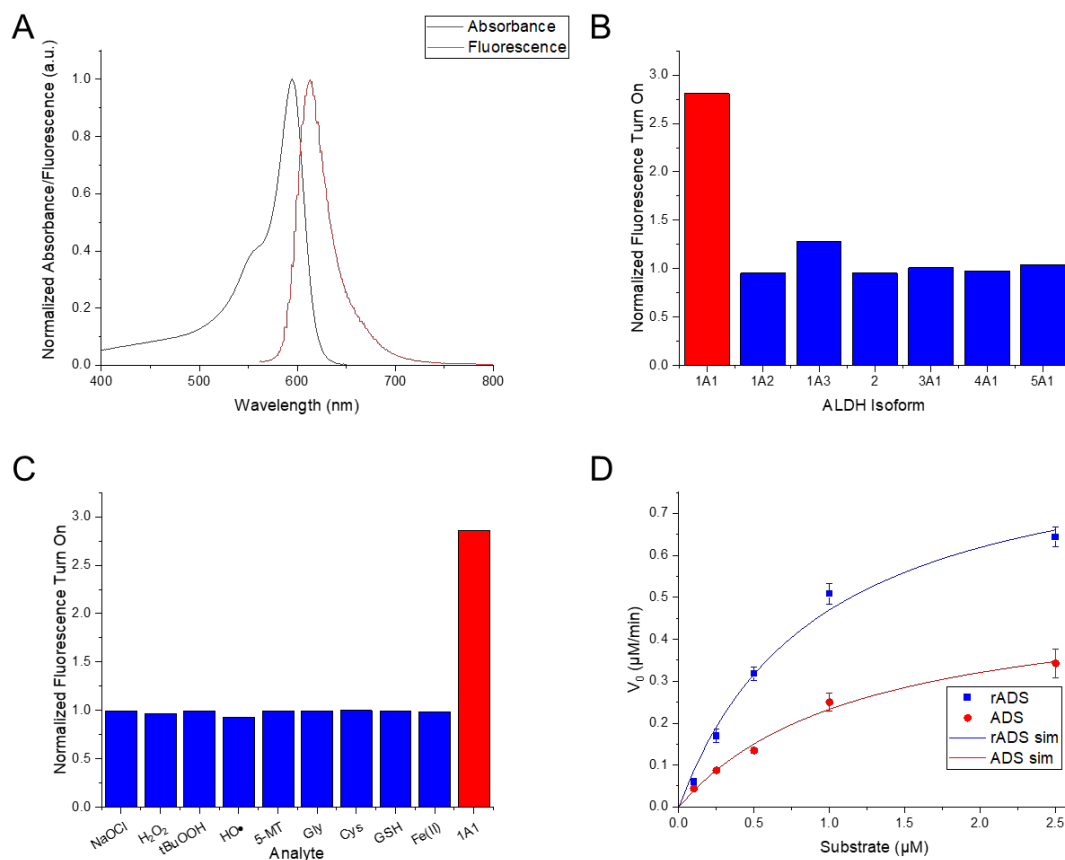


Figure 2.15. Selected properties of red-AIDeSense. (A) Normalized absorbance and fluorescence spectrum of red-AIDeSense. Selectivity of AIDeSense against (B) other ALDH isoforms and (C) other reactive biological species. (D) Michaelis-Menten plots for AIDeSense and red-AIDeSense against active ALDH1A1. Turnover was monitored by fluorescence.

The other goal in developing red-AIDeSense was to make the parent probe cell penetrant. Not only would this bypass the need for the formaldehyde releasing AM ether moiety, but it would also make it so that turn on and accumulation were due to ALDH1A1, increasing the dynamic range in cellular imaging. The switch to a TokyoMagenta dye platform afforded a pK_a of 6.68, significantly higher than that of AIDeSense (pK_a = 4.81). (Figure 2.16) The pK_a closer to physiological pH made red-AIDeSense cell permeable as desired as evidenced by a rapid increase in fluorescence upon staining. Unlike AIDeSense, this signal was not sustained. Further investigation pointed to active efflux by ABC transporters to be the culprit. Therefore, all cell imaging was performed with the addition of the ABC transporter inhibitors verapamil, probenecid, and novobiocin. With these inhibitors preventing active efflux, turn on and accumulation in cells was now due to ALDH1A1 alone.

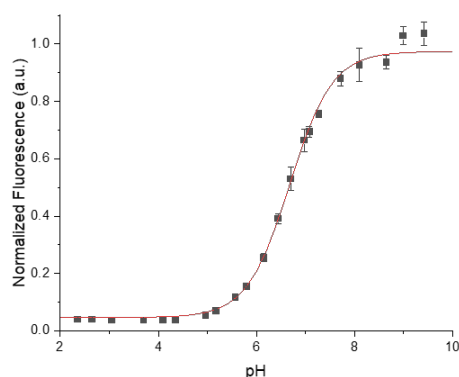


Figure 2.16. pKa determination of red-AIDeSense. All data was collected in triplicate. Data is shown in black. Fitted pKa curve is shown in red.

For the same reasons to develop Ctrl-AIDeSense in the previous project, Ctrl-red-AIDeSense was synthesized. (Figure 2.17.A) The quantum yields of AIDeSense (QY=0.041) and Ctrl-AIDeSense (QY=0.039) were nearly identical, but this did not translate to red-AIDeSense (0.21) and Ctrl-red-AIDeSense (0.54). We suspect this discrepancy is because we were still in the dynamic range of the d-PeT quenching curve described by Nagano and coworkers.⁵⁸ (Figure 2.4) The methyl ketone is less withdrawing than the corresponding aldehyde, and therefore shows less d-PeT quenching. Since Ctrl-red-AIDeSense was a good control in other aspects (e.g, pKa = 6.72), we carried on by modifying the concentrations to match initial fluorescent readouts. (Figure 2.17.B)

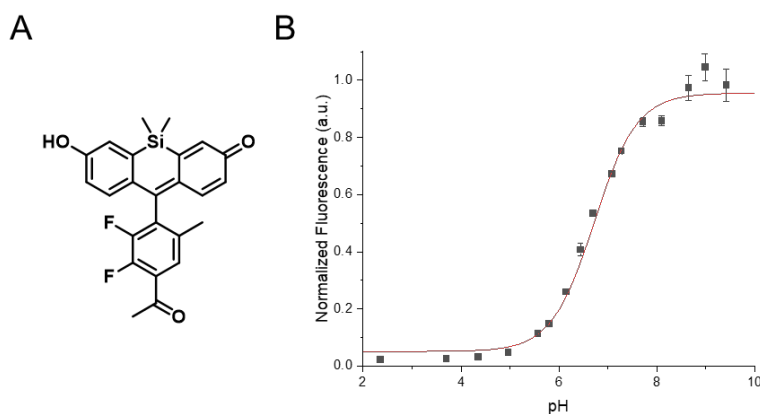


Figure 2.17. (A) Chemical structure and (B) pKa of Ctrl-red-AIDeSense

With a control compound in hand, we turned to testing red-AIDeSense in living cells. We started with A549 lung adenocarcinoma cells and K562 chronic myeloid leukemia cells. A549

cells are reported to have higher transcriptional levels of ALDH1A1 than K562 cells.⁶⁹ This transcriptional data correlates well with the higher percentage of ALDH1A1^{high} found via flow cytometry. Using Ctrl-red-AIDeSense to establish background fluorescence levels, $78.1 \pm 0.3\%$ of A549 cells displayed a high ALDH1A1 activity as measured by red-AIDeSense signal. (Figure 2.18.A-B) By comparison, only $39.0 \pm 8.3\%$ of K562 cells were measured to have high ALDH1A1 activity. (Figure 2.18.D) In both cell lines, preincubation with an ALDH inhibitor, DEAB, decreased the percentage of ALDH1A1^{high} cells. (Figure 2.18.C-D) To confirm translatability of the probe from flow cytometry to confocal microscopy applications, A549 cells were also stained with red-AIDeSense and imaged using confocal microscopy. Consistent with flow cytometry data, 77.6% of cells were determined to have high ALDH1A1 activity using Ctrl-red-AIDeSense as the baseline. (Figure 2.18.E)

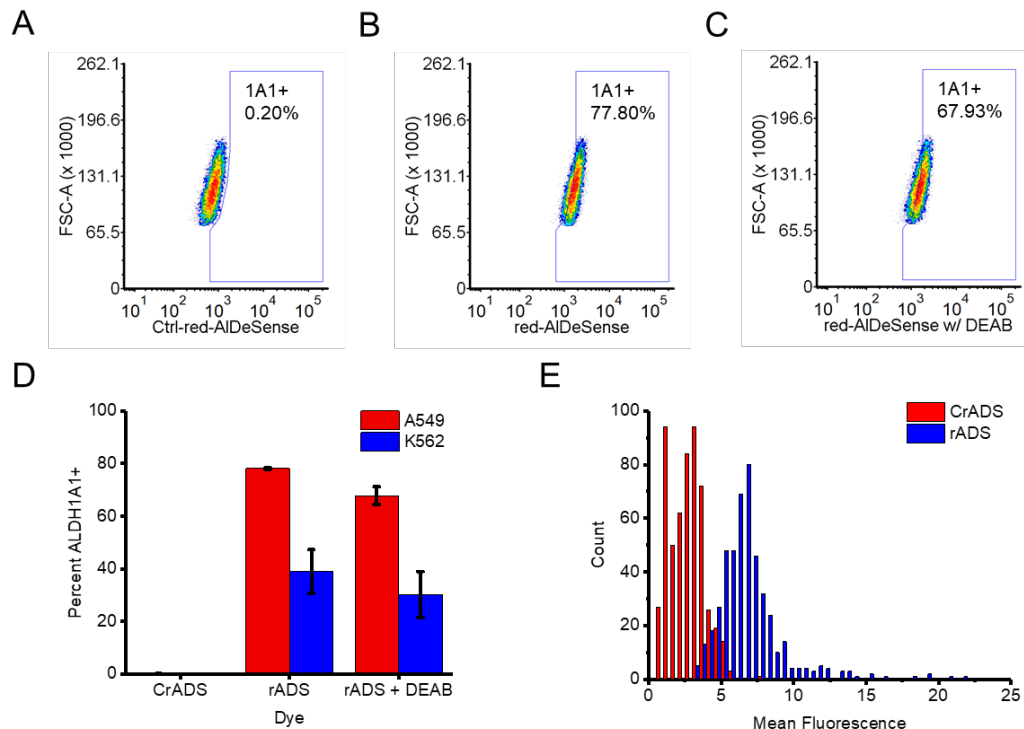


Figure 2.18. red-AIDeSense staining of A549 and K562 cells. Representative flow cytometry plots of A549 cells stained for 10 min at 0 °C with (A) Ctrl-red-AIDeSense, (B) redAIDeSense, and (C) red-AIDeSense plus 20 μ M DEAB. (D) Quantified data of each flow cytometry analysis with A549 and K562 cells. (E) Histogram of the mean fluorescence of cells stained for 10 min at room temperature with Ctrl-red-AIDeSense or red-AIDeSense. All assays were performed using 1 μ M Ctrl-red-AIDeSense or red-AIDeSense. Each flow cytometry analysis was performed in triplicate

2.4.3 Applications

The primary goal in developing red-AIDeSense was to enable costaining of cells with a probe for ALDH1A1 activity and a green fluorescent antibody or protein marking some other analyte of interest. To demonstrate this, we costained A549 cells with red-AIDeSense and a green FITC-labeled anti-CD44 antibody. (Figure 2.19.A-C) ALDH activity (as measured by ALDEFLUOR™) and expression of CD44 have independently been reported as CSC markers for lung cancers.⁷⁰ However, it is not clear whether these identify the same CSCs or different CSC populations as sometimes ALDH1A1 correlates with other markers⁷¹ and other times it does not⁷². Using confocal imaging, we found that CD44 staining and red-AIDeSense staining were independent of each other. (Figure 2.19.D-E) This suggests that either the ALDH1A1 and CD44 are independent markers for CSCs in A549 cells, or another ALDH isoform (e.g. ALDH1A3) is responsible for the CSCs marked by ALDEFLUOR™ in lung cancer.

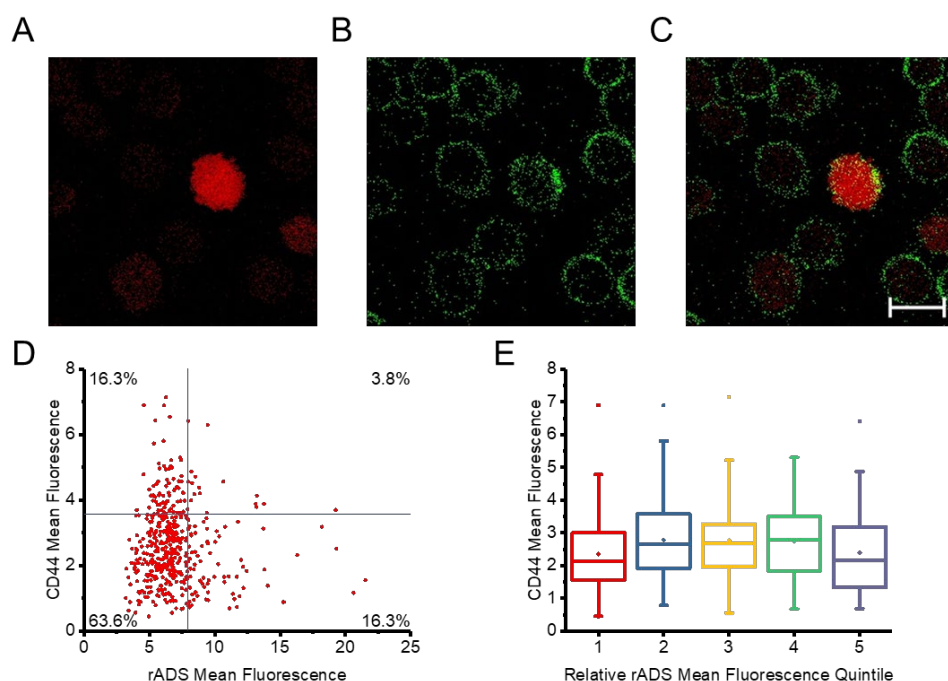


Figure 2.19. Confocal imaging of A549 cells stained with red-AIDeSense and a FITC-labeled anti-CD44 antibody. Representative confocal images of A549 cells costained with (A) redAIDeSense (red) and (B) a FITC-labeled anti-CD44 antibody (CD44, green) along with their overlays (C). Mean fluorescence (D) plotted every cell and (E) sorted into quintiles wherein the first quintile comprises the lowest red-AIDeSense mean fluorescence. All assays were performed using 1 μ M red-AIDeSense or Ctrl-AIDeSense.

2.5 Rhodols and rhodamines for ALDH1A3

With increasing evidence that some CSCs are better marked by ALDH1A3 activity rather than ALDH1A1 activity, we set out to develop a probe for ALDH1A3.⁴⁸

One important phenomena observed while developing red-ALDeSense was the elimination of isoform selectivity with the 2,6-difluoro species. This confirmed that, although the benzaldehyde binding pocket was slightly larger for ALDH1A1, it was not so different as to always bias activity for ALDH1A1. We hypothesized we could use the same xanthene platform to maintain selectivity over the 17 isoforms, while modifying it to afford selectivity for ALDH1A3 over ALDH1A1. The basis of this hypothesis was the larger xanthene-binding pocket observed in the crystal structures of ALDH1A3. (Figure 2.20) The more compact, Lys128-containing active site of ALDH1A1 would theoretically be too small to accommodate bulkier xanthenes. Given the struggles in developing a red-shifted probe for ALDH1A1, we elected to add steric bulk through non-conjugated means (e.g. bulky rhodols and rhodamines) rather than pi-expanded xanthenes (e.g. naphthofluoreceins⁷³).

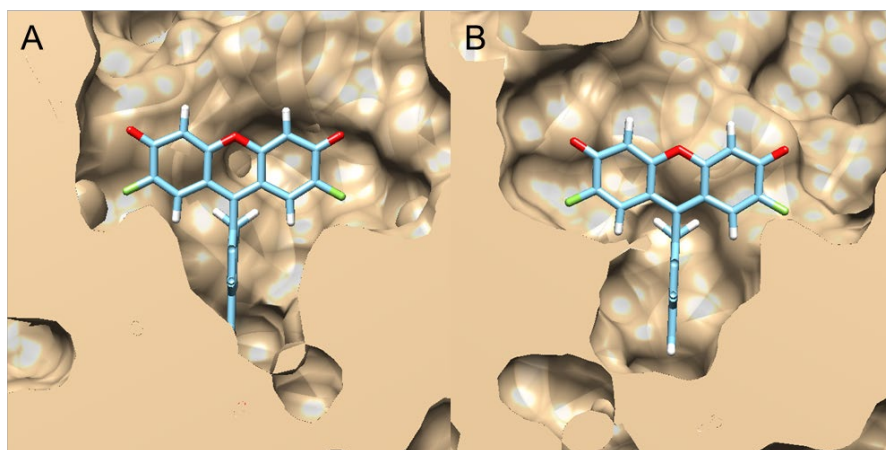
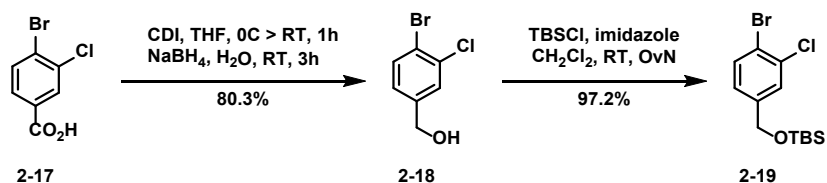


Figure 2.20. Side view of binding pockets of (A) ALDH1A1 (pdb:4WB9) and (B) ALDH1A3 (pdb:5FHZ). ALDeSense included for size comparison. No unbiased docking was performed for these visualizations.

2.5.1 Synthesis

A convergent xanthene synthetic route was chosen for rapid pursuit of an ALDH1A3 selective dye. Since our supplier of 4-bromo-3,5-difluorobenzaldehyde went out of business, and all other suppliers were expensive, we chose to screen xanthene selectivity using chlorinated benzaldehyde. Briefly, commercially available 4-bromo-3-chlorobenzoic acid, **2.17**, was reduced to benzyl alcohol **2.18** by treating with carbonyl diimidazole followed by sodium borohydride.

(Scheme 2.4) The TBS-protected benzyl alcohol **2-19** was subsequently produced under common TBS-protection conditions.



Scheme 2.4. Synthesis of chlorinated benzaldehyde precursor.

The xanthone coupling partners to the benzyl alcohol were synthesized by first forming 3,6-dihydroxyxanthone from the commercially available bis(2,4-dihydroxyphenyl)methanone using high temperature to affect the intramolecular S_NAr. The hydroxy groups were then activated with triflic anhydride before performing an intermolecular S_NAr with the appropriate secondary amine. Temperature and time could be adjusted to favor the mono- or di-substitutions of the amine nucleophile. Notably, bulkier amines (i.e. iPr₂NH) could not be effectively introduced. For the disubstituted rhodamine precursors, the xanthone was used as is. For the monosubstituted rhodol precursors, any remaining triflyl group was removed and replaced with a TBS protecting group.

The protected 4-bromo-benzyl alcohol underwent lithium halogen exchange with *tert*-butyllithium before introducing the xanthone to afford the coupled product. Deprotection with aq. HCl and oxidation of the alcohol to the aldehyde with IBX.

2.5.2 Testing

We concurrently synthesized a rhodol (AD84) and rhodamine (AD94) featuring the a morpholine group as the amine functional group. When tested against ALDH1A1 and 1A3, AD84 exhibited a rapid 5.7-fold turn on. (Figure 2.21.A) The kinetic trace was nearly identical between the two isoforms indicating no selectivity in either direction. AD94 produced no fluorescence turn on in the presence of ALDH1A1 or 1A3. (Figure 2.21.B) Upon further analysis, the benzaldehyde did not act as a d-PeT quencher on AD94. Its quantum yield was measured to be 0.09, and the quantum yield of its benzyl alcohol precursor was also 0.09. The absence of d-PeT quenching on this rhodamine is not surprising. Such a redox process would require the simultaneous generation of a radical anion on the benzaldehyde moiety and a radical cation on the xanthene to be more favorable than the basic excited state of the native rhodamine. This provided strong evidence that rhodamines would be incompatible with this strategy.

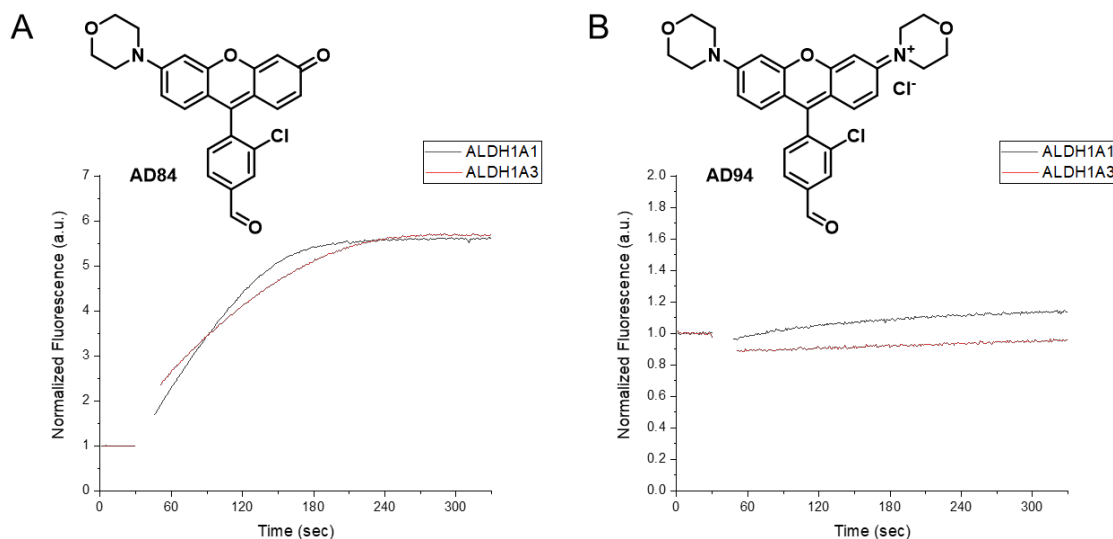


Figure 2.21. Kinetic traces of (A) AD84 and (B) AD94 against ALDH1A1 and ALDH1A3. Dye concentration was 1 μ M in both cases. ALDH1A1 and ALDH1A3 levels were normalized for activity against propionaldehyde. The first 30 seconds were dye alone to establish an initial fluorescence readout. Traces are normalized to this time. The gap in the trace corresponds to the opening of the fluorimeter for addition of the enzyme.

A second rhodol (AD52) was synthesized featuring a diethylamine group. We hypothesized a less rigid group might decrease the binding affinity for ALDH1A1. This was not observed in the kinetic traces. Instead, nearly identical initial rates were observed for both isoforms. (Figure 2.22) The traces differed after about 60 seconds, with ALDH1A1 continuing to catalyze the reaction as expected but ALDH1A3 experiencing a peculiar drop in reactivity. This drop may be due to self-inhibition, differing kinetics for differing atropisomers, or simply an artifact of the system (e.g. solubility). Regardless, AD52 underwent a 6.4-fold enzymatic turn on in the presence of ALDH1A1 and a 7.4-fold enzymatic turn on in the presence of ALDH1A3.

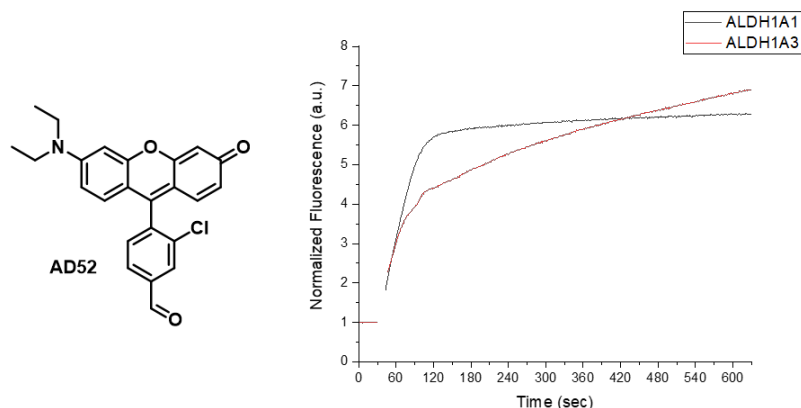


Figure 2.22. Kinetic traces of AD52 against ALDH1A1 and ALDH1A3. Dye concentration was 1 μ M in both cases. ALDH1A1 and ALDH1A3 levels were normalized for activity against propionaldehyde. The first 30 seconds were dye alone to establish an initial fluorescence readout. Traces are normalized to this time. The gap in the trace corresponds to the opening of the fluorimeter for addition of the enzyme.

2.6 Future directions and outlook

The further development of ALDH isoform selective probes is important for the continued identification of which isoforms are relevant for individual populations of CSCs. Additionally, as markers of CSCs, real time readouts for these cells should facilitate development and testing of new therapeutics that target CSCs. Probes that can be used from *in vitro* assays all the way through live animal imaging offer a consistent readout for the efficacy of drugs, guiding researchers to the sources of success and failure along the way.

The pursuit of a probe selective for ALDH1A3 had a healthy start, but we ended up hitting a wall. Continued screening of bulkier groups (e.g. julolidine) or pi-expanded xanthenes would be recommended as the next steps in exploring the hypothesis that selectivity can be afforded by the larger secondary binding pocket of ALDH1A3 compared to ALDH1A1.

The design of turn on probes selective for other isoforms, especially ALDH2 and ALDH3A1, should also continue. Such probes are likely to require a different platform than the xanthene dyes to find kinetically competent substrates.

CHAPTER 3. 4HNE

3.1 Introduction of 4-hydroxy-2-alkenals

4-hydroxynonenal (4HNE) is a lipid peroxidation product of polyunsaturated omega-6 fatty acids.⁷⁴ It was described as the most cytotoxic of the lipid peroxidation products,⁷⁵ and aberrant levels have since been linked to cancer,⁷⁶ metabolic diseases,⁷⁷ and neurodegenerative disorders.⁷⁸ Many methods have been developed to quantify free 4HNE and 4HNE adduct levels, but none are compatible with live cell imaging.⁷⁴ We aim to develop the first selective activity-based sensor for 4HNE and apply it to testing the ability of CSCs to respond to 4HNE stresses.

3.2 Design and synthesis

In pursuit of a probe that is selective for 4HNE over all other biologically relevant aldehydes, we aim to utilize 4HNE's unique chemical reactivity. Namely, there exists an α,β -unsaturated aldehyde and a hydroxy group at the γ carbon. The former is prime for electrophilic attack from soft nucleophiles in a Michael-type fashion or hard nucleophiles at the carbonyl carbon. The latter is a weak nucleophile that we hypothesize could be useful for an intramolecular cyclization. We hypothesize a hydrazinoacetyl ester will take advantage of the aforementioned groups to afford the desired selectivity. (Figure 3.1) Briefly, the hydrazine moiety can undergo hydrazone formation with the aldehyde followed by Michael addition to form a pyrazoline.⁷⁹ With the first ring closed, the hydroxy group is set up for a δ -lactonization, releasing the payload.

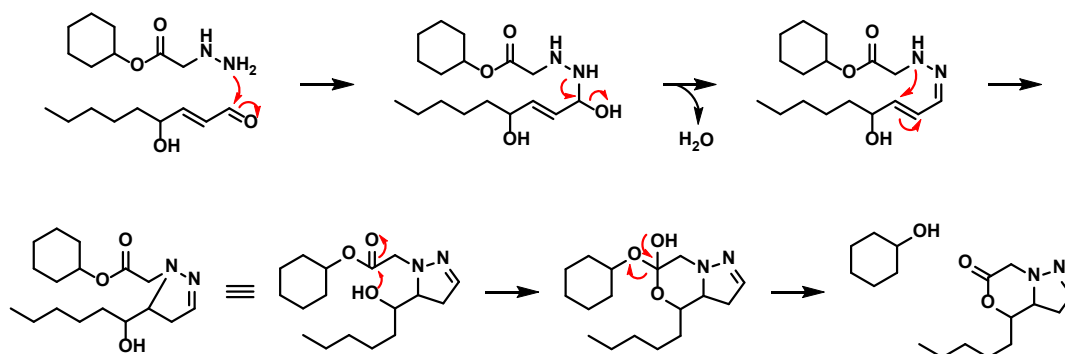
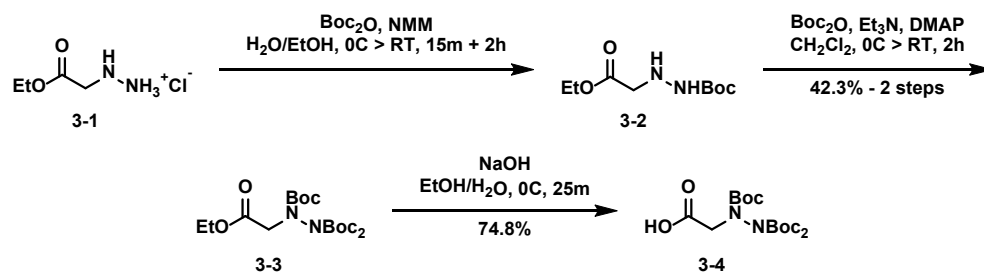


Figure 3.1. Proposed mechanism of 4HNE on a hydrazinoacetyl ester.

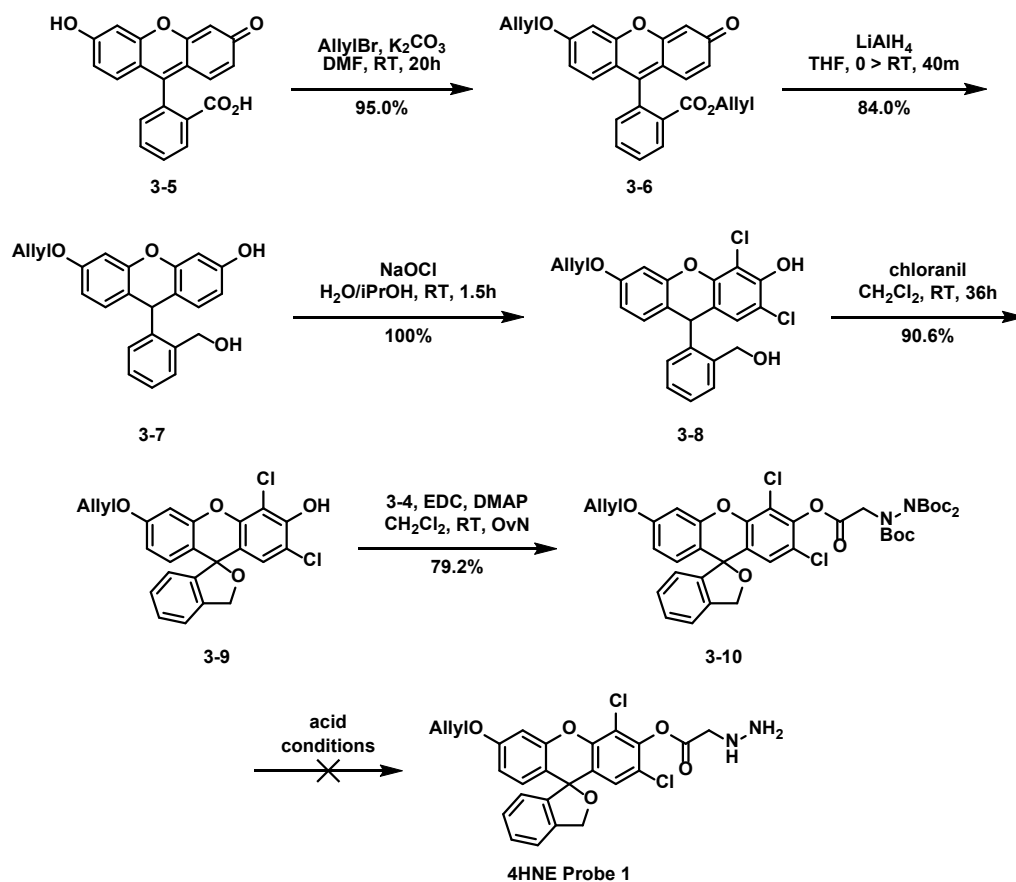
Our first synthetic pursuit involved attaching the trigger directly on to a xanthene dye. The strategy of cleaving an ester-capped dye to produce a fluorescence increase is well established.⁸⁰ Numerous synthetic routes and protecting group were pursued – building the trigger on the dye using both electrophilic and nucleophilic hydrazine equivalents, preforming a protected trigger before coupling with acid and base labile protecting groups, etc. The most successful strategy

began with ethyl hydrazinoacetate hydrochloride. (Scheme 3.1) This was mono-Boc-protected to **3-2**. Now soluble in organics, two more Boc groups were installed to afford tri-Boc-protected hydrazine **3-3**. The ester was carefully saponified to produce carboxylic acid **3-4**.



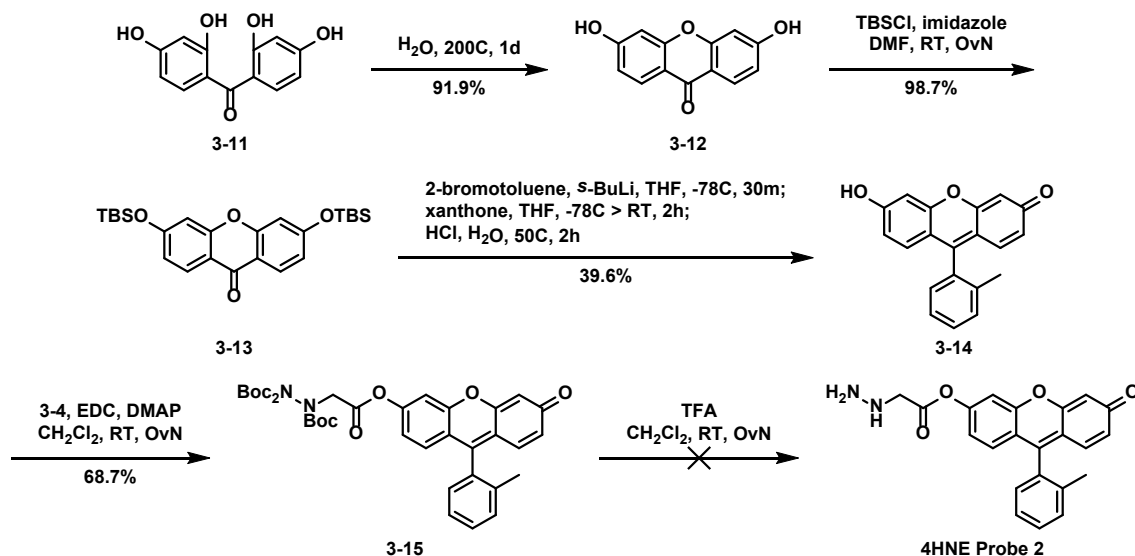
Scheme 3.1. Synthesis of tri-Boc protected hydrazinoacetic acid.

At the same time, a dichloro xanthene was synthesized. (Scheme 3.2) Chlorines positioned ortho to the ester are known to stabilize the carbonyl.⁸¹ This strategy has previously been used in our lab to stabilize a xanthene `ester against α -thiolactonization.²⁶ Here we aim to stabilize the ester against potential formation of a cyclic hydrazide. First, fluorescein was diallylated to yield ester **3-6**. The ester and xanthene were both reduced using LiAlH_4 to afford the deconjugated aryl system **3-7**. Treatment of **3-7** with excess NaOCl yield dechlorinated **3-8** which is readily reoxidized to xanthene **3-9** with chloranil. EDC coupling with **3-4** selectively installs the ester at the phenolic position. Unfortunately, acidic deprotection of the Boc groups did not produce the desired **4HNE Probe 1**, cleaving the ester group instead.



Scheme 3.2. Unsuccessful synthesis of 4HNE Probe 1.

I next pursued the synthesis of a probe based on the TokyoGreen dye platform since there would be no spirocyclic ring-opening upon ester cleavage. Synthesis of the Tokyo green started with closing to xanthone **3-12** at elevated temperatures. The was readily TBS protected to **3-12**. Lithium halogen exchange between *sec*-butyllithium and 2-bromotoluene produced an aryl nucleophile that could add to the protected xanthone. Acidic workup of this reaction removed the TBS groups to afford TokyoGreen **3-14**. This xanthene dye was esterified with the hydrazinoacetate using EDC coupling conditions to produce probe precursor **3-15**. Numerous acidic conditions were attempted to synthesize **4HNE Probe 2**, but none yielded the desired product.



Scheme 3.3. Unsuccessful synthesis of 4HNE Probe 2.

3.3 Future directions and outlook

Attempts to deprotect **3-15** to **4HNE Probe 2** under milder conditions resulted in no reaction. Once the reaction was acidic enough to initiate Boc deprotection, the reaction quickly turned from yellow to magenta. Analysis of the UV-Vis absorption spectra of the isolated material suggested a rhodol had formed upon Boc deprotection, likely the result of a Smiles rearrangement. (Figure 3.2) Based on these observations, synthetic routes are actively being pursued which involve the trigger and fluorophore being linked by a self-immolative linker.

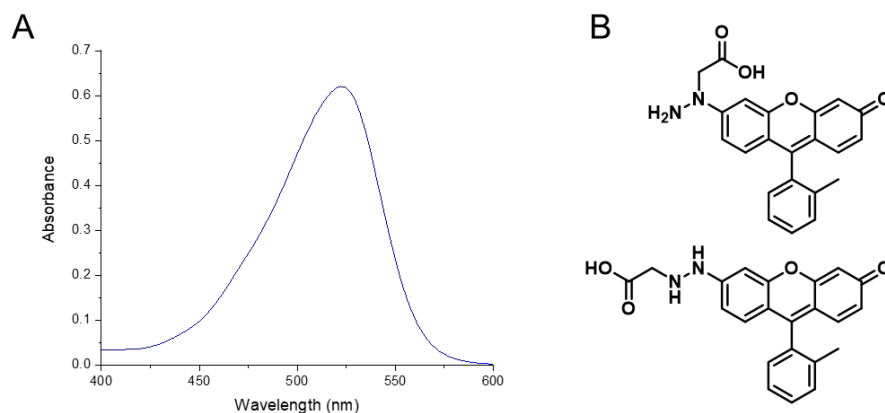


Figure 3.2. (A) Measured absorption spectra and (B) proposed structures of the product of 3-15 deprotection.

If a stable compound is possible with this trigger, the standard chemical selectivity and stability assays will be run. It will be especially important to perform an analyte competition assay between the probe and other biologically relevant aldehydes. Though we do not expect turn on due

to other aldehydes, other aldehydes may inactivate the probe through poorly-reversible hydrazone formation. The end goal in developing a probe for 4HNE is to study the interplay between 4HNE and ALDH1A1 in CSCs.

3.4 Experimental

3.4.1 Materials and methods

Bis(2,4-dihydroxyphenyl)methanone was purchased from 3B Scientific. Et₃N was purchased from Acros Organics. Allyl bromide was purchased from Alfa Aesar. Ethyl hydrazinoacetate HCl was purchased from AK Scientific. EtOH was purchased from Decon Labs. CH₂Cl₂, DMF, iPrOH, and THF were purchased from Fisher Scientific. 2-bromotoluene, Boc₂O, chloranil, DMAP, EDC HCl, NaOH, and *tert*-butyldimethylsilyl chloride were purchased from Oakwood Chemical. NaOCl (6% w/w in H₂O) was purchased from PureBleach. Anhydrous CH₂Cl₂, anhydrous DMF, anhydrous THF, fluorescein, LiAlH₄, *N*-methylimidazole, and 1.4 M *sec*-butyllithium in cyclohexane were purchased from Sigma Aldrich. Dry THF was prepared by drying THF on 4Å molecular sieves for a minimum of 24 hours, repeated 3x with freshly activated molecular sieves. All other chemicals were used without further purification.

3.4.2 Synthesis and characterization

***tert*-butyl 2-(2-ethoxy-2-oxoethyl)hydrazine-1-carboxylate (3-2)** A round bottom flask was charged with ethyl hydrazinoacetate HCl (3.09 g, 20.0 mmol, 1.00 eq.), Boc₂O (5.24 g, 24 mmol, 1.2 eq.), EtOH (10 mL) and H₂O (10 mL). After cooling to 0 °C, the mixture was treated with *N*-methylimidazole (3.8 mL, 48 mmol, 2.4 eq.). After 15 minutes, the reaction was warmed to room temperature. After stirring 2 hours at room temperature, the reaction was poured into saturated NaHCO₃ in H₂O. Product was extracted with Et₂O (2x). The organic layers were combined, washed with 0.5 M citric acid in H₂O, dried over Na₂SO₄, and concentrated to afford a crude yellow oil containing the title compound (3.93 g)

***tri-tert*-butyl 2-(2-ethoxy-2-oxoethyl)hydrazine-1,1,2-tricarboxylate (3-3)** A flame-dried round bottom flask was charged with Boc₂O (11.8 g, 54 mmol, 3.0 eq.), DMAP (0.660 g, 5.4 mmol, 0.3 eq.), and anhydrous CH₂Cl₂ (10 mL). This was cooled to 0 °C before being treated with a solution of crude **3-2** (3.93 g, 18 mmol, 1.0 eq.) and Et₃N (7.5 mL, 54 mmol, 3.0 eq.) in anhydrous CH₂Cl₂ (10 mL). The reaction came to room temperature with the melting ice bath overnight. After stirring overnight, the reaction was diluted with CH₂Cl₂, washed with KH₂PO₄ in H₂O, dried over Na₂SO₄, and concentrated. The crude residue was purified by flash chromatography on silica gel

(0:100 to 5:95 v/v EtOAc:CH₂Cl₂ gradient) to afford the title compound as a light yellow oil (3.54 g, 8.46 mmol, 42.3% 2-step yield). (1:3 ratio of diastereomers) ¹H NMR (400 MHz, Chloroform-*d*) δ 4.23 – 4.11 (m, 2H), 4.15 – 4.04 (m, 2H), 1.52 – 1.43 (m, 27H), 1.30 – 1.21 (m, 3H).

N-(bis(tert-butoxycarbonyl)amino)-N-(tert-butoxycarbonyl)glycine (3-4) A round bottom flask was charged with **3-3** (3.54 g, 8.46 mmol, 1.00 eq.) and EtOH (10 mL). After cooling to 0 °C, the solution was treated with cold 1.0 M NaOH in H₂O (10 mL). After stirring for 30 minutes, the reaction was acidified with 0.5 M citric acid in H₂O (12 mL). Product was extracted sequentially with CH₂Cl₂, Et₂O, CH₂Cl₂, and Et₂O. The organic fractions were combined, dried over Na₂SO₄, and concentrated to yield the title compound as an off-white crystalline solid (2.47 g, 6.33 mmol, 74.8% yield). ¹H NMR (500 MHz, DMSO-*d*₆) δ 4.03 (s, 2H), 1.69 – 1.20 (m, 27H).

allyl 2-(6-(allyloxy)-3-oxo-3H-xanthen-9-yl)benzoate (3-6) A round bottom was charged with fluorescein (6.6 g, 20 mmol, 1.0 eq.), K₂CO₃ (8.3 g, 60 mmol, 3.0 eq.), and DMF (40 mL). The mixture was treated with allyl bromide (5.2 mL, 60 mmol, 3.0 eq.). After stirring for 20 hours at room temperature, the reaction was poured in H₂O (200 mL), and the subsequent mixture was filtered. The precipitate was dissolved in CH₂Cl₂, washed with saturated NaHCO₃ in H₂O, dried over Na₂SO₄, and concentrated to afford the title compound as an orange solid (7.84 g, 19.0 mmol, 95.0% yield). ¹H NMR (400 MHz, Chloroform-*d*) δ 8.26 (dd, *J* = 7.7, 1.6 Hz, 1H), 7.74 (td, *J* = 7.5, 1.5 Hz, 1H), 7.67 (td, *J* = 7.6, 1.4 Hz, 1H), 7.31 (dd, *J* = 7.5, 1.2 Hz, 1H), 6.95 (d, *J* = 2.4 Hz, 1H), 6.89 (d, *J* = 8.9 Hz, 1H), 6.86 (d, *J* = 9.7 Hz, 1H), 6.75 (dd, *J* = 8.9, 2.5 Hz, 1H), 6.54 (dd, *J* = 9.7, 1.9 Hz, 1H), 6.44 (d, *J* = 1.9 Hz, 1H), 6.06 (ddt, *J* = 17.2, 10.6, 5.3 Hz, 1H), 5.59 (ddt, *J* = 17.4, 10.1, 6.0 Hz, 1H), 5.46 (dq, *J* = 17.3, 1.5 Hz, 1H), 5.36 (dq, *J* = 10.5, 1.3 Hz, 1H), 5.15 – 5.05 (m, 2H), 4.65 (dt, *J* = 5.3, 1.5 Hz, 2H), 4.52 – 4.47 (m, 1H), 4.47 – 4.41 (m, 1H).

6-(allyloxy)-9-(2-(hydroxymethyl)phenyl)-9H-xanthen-3-ol (3-7) A round bottom flask was charged with **3-6** (7.84 g, 19.0 mmol, 1.00 eq.) and anhydrous THF (130 mL). Once a solution had formed, the reaction was cooled to 0 °C and treated with LiAlH₄ (1.10 g, 28.5 mmol, 1.5 eq.) portionwise over 10 minutes. After stirring for 10 minutes at 0 °C, the reaction was warmed to room temperature. After an additional 40 minutes, the reaction was cooled back to 0 °C and quenched via the slow addition of H₂O. The mixture was acidified with 1.0 M HCl in H₂O to pH ~4. The organic layer was collected and concentrated under reduced pressure. The crude residue was purified via flash chromatography on silica gel (2:98 to 10:90 v/v MeOH:CH₂Cl₂ gradient) to afford the title compound as a light yellow solid (5.75 g, 16.0 mmol, 84.0% yield). ¹H NMR (500

MHz, Chloroform-*d*) δ 7.55 (s, 1H), 7.41 (dd, J = 6.4, 2.5 Hz, 1H), 7.28 – 7.19 (m, 2H), 7.20 – 7.14 (m, 1H), 6.77 (d, J = 8.5 Hz, 1H), 6.69 (d, J = 8.4 Hz, 1H), 6.65 (d, J = 2.5 Hz, 1H), 6.56 (d, J = 2.4 Hz, 1H), 6.52 (dd, J = 8.6, 2.6 Hz, 1H), 6.34 (dd, J = 8.4, 2.5 Hz, 1H), 6.05 (ddt, J = 16.1, 10.4, 5.3 Hz, 1H), 5.49 – 5.39 (m, 2H), 5.31 (d, J = 10.9 Hz, 1H), 4.64 (s, 2H).

6-(allyloxy)-2,4-dichloro-9-(2-(hydroxymethyl)phenyl)-9H-xanthen-3-ol (3-8) A round bottom flask was charged with **3-7** (2.4 g, 6.5 mmol, 1.0 eq.) and iPrOH (50 mL). Once a solution had formed, the reaction was treated with NaOCl (6% w/w in H₂O) (25 mL, 20 mmol, 3.0 eq.). After stirring for 1.5 hours, the reaction was acidified with 1.0 M HCl in H₂O (25 mL) and diluted with CH₂Cl₂ (100 mL). The organic layer was collected, dried over Na₂SO₄, and concentrated under reduced pressure. The crude residue was purified via flash chromatography on silica gel (2:98 v/v MeOH:CH₂Cl₂) to afford the title compound as an orange solid (2.91 g, 6.5 mmol, 100% yield). ¹H NMR (500 MHz, Chloroform-*d*) δ 7.41 (dd, J = 5.7, 3.5 Hz, 1H), 7.27 – 7.23 (m, 2H), 7.11 (dd, J = 5.6, 3.5 Hz, 1H), 6.86 (s, 1H), 6.80 (d, J = 8.5 Hz, 1H), 6.77 (d, J = 2.5 Hz, 1H), 6.57 (dd, J = 8.5, 2.6 Hz, 1H), 6.05 (ddt, J = 17.3, 10.4, 5.2 Hz, 1H), 5.53 (s, 1H), 5.42 (dd, J = 17.2, 1.7 Hz, 1H), 5.30 (dd, J = 10.5, 1.6 Hz, 1H), 4.74 (d, J = 12.6 Hz, 1H), 4.68 (d, J = 12.4 Hz, 1H), 4.53 (d, J = 5.0 Hz, 2H).

6'-(allyloxy)-2',4'-dichloro-3H-spiro[isobenzofuran-1,9'-xanthen]-3'-ol (3-9) A round bottom flask was charged with **3-8** (2.91 g, 6.9 mmol, 1.0 eq.), CH₂Cl₂ (100 mL), and chloranil (1.84 g, 7.5 mmol, 1.1 eq.). After stirring overnight at room temperature, the reaction was directly purified via flash chromatography on silica gel (0:100 to 5:95 v/v MeOH:CH₂Cl₂ gradient) to afford the title compound as a red solid (2.625 g, 6.14 mmol, 90.6% yield) ¹H NMR (500 MHz, Acetone-*d*₆) δ 7.50 (d, J = 7.6 Hz, 1H), 7.43 (t, J = 7.4 Hz, 1H), 7.32 (t, J = 7.5 Hz, 1H), 6.95 (d, J = 8.5 Hz, 2H), 6.92 (d, J = 7.6 Hz, 1H), 6.89 (d, J = 2.5 Hz, 1H), 6.76 (dd, J = 8.8, 2.6 Hz, 1H), 6.10 (ddt, J = 17.3, 10.4, 5.1 Hz, 1H), 5.45 (dq, J = 17.3, 1.7 Hz, 1H), 5.40 (d, J = 12.6 Hz, 1H), 5.35 (d, J = 12.6 Hz, 1H), 5.28 (dq, J = 10.6, 1.6 Hz, 1H), 4.67 (dt, J = 5.2, 1.7 Hz, 2H).

tri-tert-butyl 2-((6'-(allyloxy)-2',4'-dichloro-3H-spiro[isobenzofuran-1,9'-xanthen]-3'-yl)oxy)-2-oxoethyl)hydrazine-1,1,2-tricarboxylate (3-10) A round bottom flask was charged with **3-12** (0.042 g, 0.10 mmol, 1.0 eq.), **3-4** (0.08 g, 0.20 mmol, 2.0 eq.), EDC HCl (0.08 g, 0.40 mmol, 4.0 eq.), DMAP (0.02 g, 0.20 mmol, 2.0 eq.), and CH₂Cl₂ (5 mL). After stirring at room temperature overnight, the reaction was diluted with CH₂Cl₂, washed with 0.5 M citric acid in H₂O, dried over Na₂SO₄, and concentrated. The crude residue was purified by flash

chromatography on silica gel (20:80 v/v EtOAc:CH₂Cl₂) to afford the title compound as a yellow powder (0.0633 g, 0.0792 mmol, 79.2% yield). (1:1 ratio of diastereomers) ¹H NMR (500 MHz, Chloroform-*d*) δ 7.43 – 7.34 (m, 2H), 7.33 – 7.25 (m, 1H), 6.97 – 6.80 (m, 4H), 6.76 – 6.65 (m, 1H), 6.12 – 5.88 (m, 1H), 5.45 – 5.35 (m, 1H), 5.32 (s, 2H), 5.32 – 5.26 (m, 1H), 4.66 – 4.39 (m, 4H), 1.55 – 1.41 (m, 27H).

3,6-dihydroxy-9H-xanthen-9-one (3-12) A 25 mL autoclave chamber was charged with bis(2,4-dihydroxyphenyl)methanone (2.00 g, 8.12 mmol, 1.00 eq.) and H₂O (12 mL). The chamber was sealed and heated to 200 °C. After 1 day, the reaction was removed from the heat. Once at room temperature, the reaction was suspended in Et₂O and H₂O and filtered. The precipitate was washed with H₂O and vacuum dried to afford the title compound as a light brown solid (1.702 g, 7.46 mmol, 91.9% yield). ¹H NMR (500 MHz, DMSO-*d*₆) δ 10.82 (s, 2H), 7.98 (d, *J* = 8.6 Hz, 2H), 6.86 (dd, *J* = 8.7, 2.2 Hz, 2H), 6.82 (d, *J* = 2.2 Hz, 2H).

3,6-bis((tert-butyldimethylsilyl)oxy)-9H-xanthen-9-one (3-13) A round bottom flask was charged with **3-12** (2.28 g, 10.0 mmol, 1.00 mmol), imidazole (1.50 g, 22 mmol, 2.2 eq.), and anhydrous DMF (24 mL). Once a solution had formed, the reaction was treated with *tert*-butyldimethylsilyl chloride (3.32 g, 22 mmol, 2.2 eq.). After stirring overnight at room temperature, the reaction was diluted with saturated NaCl in H₂O (50 mL) and filtered. The precipitate was washed with H₂O and dried under reduced pressure to afford the title compound as a white solid (4.51 g, 9.87 mmol, 98.7% yield). ¹H NMR (500 MHz, Chloroform-*d*) δ 8.20 (d, *J* = 8.4 Hz, 2H), 6.89 – 6.80 (m, 4H), 1.01 (s, 18H), 0.29 (s, 12H).

6-hydroxy-9-(o-tolyl)-3H-xanthen-3-one (3-14) A flame-dried round bottom flask was charged with 2-bromotoluene (0.27 mL, 2.2 mmol, 2.0 eq.) and dry THF (10 mL). After cooling to -78 °C, the solution was treated with 1.4 M *sec*-butyllithium in cyclohexane (1.6 mL, 2.2 mmol, 2.0 eq.) dropwise over 1.5 minutes. After 30 minutes, the reaction was treated with a solution of **3-13** (0.500 g, 1.09 mmol, 1.00 eq.) in dry THF (5 mL) dropwise over 1 minute. The reaction was warmed to room temperature. After stirring for 2 hours, the reaction was treated with 1.0 M HCl in H₂O (6.5 mL, 6.5 mmol, 6.0 eq.) and heated to 50 °C. After heating for 2 hours, the reaction was cooled to room temperature, and solvent was removed under reduced pressure. The crude residue was dissolved in 33:67 v/v iPrOH:CH₂Cl₂ and H₂O. The organic layer was collected, dried over Na₂SO₄, and concentrated under reduced pressure. The crude residue was recrystallized from EtOH to afford the title compound as a dark orange solid (0.131 g, 0.433 mmol, 39.6% yield). ¹H

NMR (500 MHz, DMSO-*d*₆) δ 11.13 (s, 1H), 7.51 (t, *J* = 7.6 Hz, 1H), 7.48 (d, *J* = 7.3 Hz, 1H), 7.42 (t, *J* = 7.2 Hz, 1H), 7.27 (d, *J* = 7.5 Hz, 1H), 6.83 (d, *J* = 9.1 Hz, 2H), 6.59 (s, 4H), 2.02 (s, 3H).

tri-tert-butyl 2-(2-oxo-2-((3-oxo-9-(*o*-tolyl)-3H-xanthen-6-yl)oxy)ethyl)hydrazine-1,1,2-tricarboxylate (3-15) A round bottom flask was charged with **3-15** (0.030 g, 0.10 mmol, 1.0 eq.), **3-4** (0.080 g, 0.20 mmol, 2.0 eq.), EDC HCl (0.078 g, 0.40 mmol, 4.0 eq.), DMAP (0.024 g, 0.20 mmol, 2.0 eq.), and CH₂Cl₂ (5 mL). After stirring overnight at room temperature, the reaction was diluted with CH₂Cl₂, washed with 0.5 M citric acid in H₂O, dried over Na₂SO₄, and concentrated under reduced pressure. The crude residue was purified by flash chromatography on silica gel (50:50 v/v EtOAc:hexanes) to afford the title compound as a yellow solid (0.046 g, 0.0687 mmol, 68.7% yield). (4:1 ratio of diastereomers) ¹H NMR (500 MHz, Chloroform-*d*) δ 7.47 (td, *J* = 7.5, 1.3 Hz, 1H), 7.43 – 7.34 (m, 2H), 7.32 (d, *J* = 2.4 Hz, 1H), 7.19 – 7.13 (m, 1H), 7.04 (d, *J* = 8.7 Hz, 1H), 6.99 (dd, *J* = 8.7, 2.2 Hz, 1H), 6.95 (d, *J* = 9.8 Hz, 1H), 6.57 (dd, *J* = 9.8, 2.1 Hz, 1H), 6.44 (d, *J* = 2.0 Hz, 1H), 4.41 (s, 2H), 2.08 (s, 3H), 1.53 – 1.47 (m, 27H).

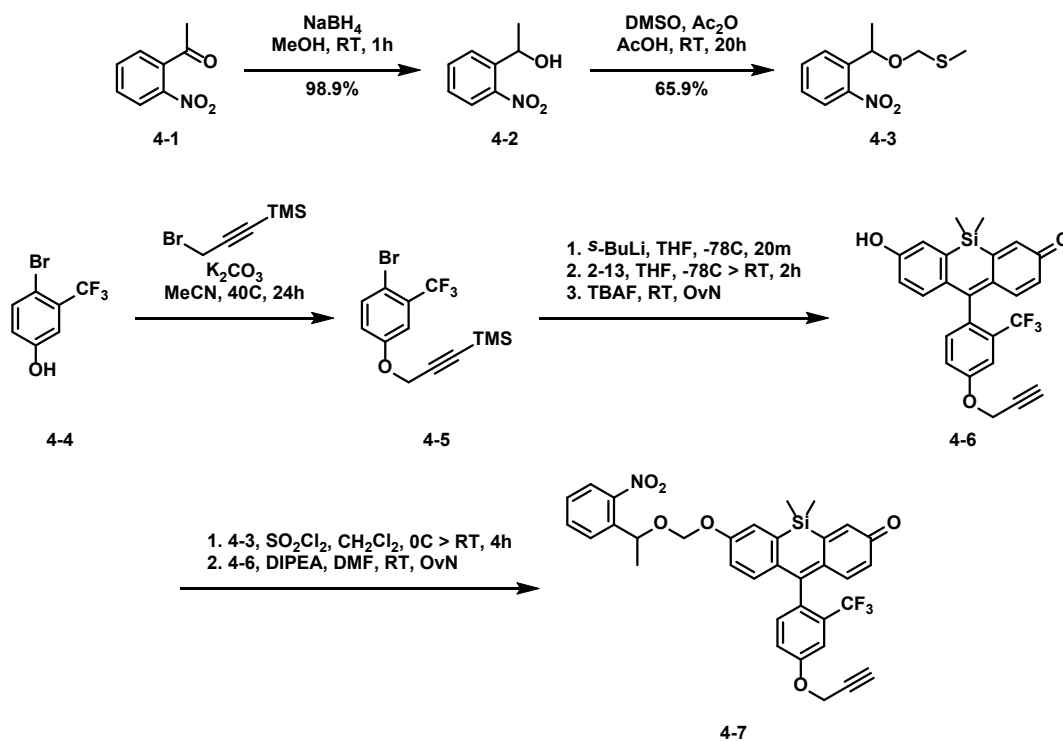
CHAPTER 4. Formaldehyde

4.1 Introduction

Formaldehyde is simple in structure but complex in function. The highly reactive aldehyde moiety plays many roles in biology ranging from beneficial (e.g. memory formation)⁸² to toxic (e.g. crosslinking biomolecules).⁸³ Numerous fluorescent probes have been published to aid in understanding how its cellular levels correlate with phenotypes.^{29,84} As talked about in Chapter 1.3.2.2, these can either consume an equivalent of formaldehyde or leave the formaldehyde levels unchanged. In order to study the effects of formaldehyde at abnormal concentrations, formaldehyde must be dosed in exogenously.

Recently, our lab reported photoFAD, the first ever photoactivatable formaldehyde donor which provided a quantitative output of small molecule release.⁶² The small molecule chemical tool features a photocleavable 2-nitrobenzyl moiety linked via a methylene ether bridge to a Si-xanthene fluorophore. Upon irradiation with a 395 nm LED array, the 2-nitrobenzyl moiety cleaves to generate a hemiacetal. This transiently stable species condenses to formaldehyde, expelling the now uncapped Si-xanthene fluorophore. Thus, formaldehyde release is coupled with a fluorescence increase to quantify the amount of formaldehyde donated to the area of interest.

PhotoFAD is a powerful tool for cellular studies, but the 395 nm light required for photoactivation precludes its use in deeper tissue. To effectively deliver formaldehyde in deep tissue, we need a red-shifted wavelength with which to induce the formaldehyde release. Improvements are continuously being made to small molecule red-shifted photocleavable protecting groups, but some issues (e.g. solubility and efficiency) remain. Up converting nanoparticles (UCNPs) are alternative strategy. When irradiated with longer wavelength, lower energy, deeper penetrating light, UCNPs can essentially sum the energies and reemit the higher energy, shorter wavelength light. Thus, ultraviolet light can be shone locally in deep tissue. Attaching a UV-photoactivatable formaldehyde donor to these UCNPs will allow formaldehyde release and quantification deep in the biological specimen.



Scheme 4.1. Synthesis of a clickable photoFAD.

We hoped we could use the red-AIDeSense benzyl alcohol precursor (or one of the other Si-xanthene probes' precursors) to difunctionalize with the formaldehyde and trigger at the phenol and an alkyne handle at the benzyl alcohol. The required order of functional group manipulation was impractical given the difficulty of controlling equivalents of the formaldehyde trigger incorporation. Thus, we proceeded with the expectation of coupling the prealkynylated bottom piece to the Si-xanthene. The Si-xanthone was prepared as described for red-AIDeSense.⁸⁵ Alkynylating conditions of benzyl alcohols from the red-AIDeSense project with TMS-protected propargyl bromide was incompatible with the TMS protecting group. Instead, 4-bromo-3-(trifluoromethyl) was alkylated with TMS-protected propargyl bromide under mild conditions in acetonitrile to afford TMS-protected propargyl phenol **4-5**. This was coupled on to the xanthone using common lithium-halogen exchange conditions. Workup of the reaction with TBAF removed all silyl groups to afford propargylated Si-xanthene **4-6**. This was alkylated with freshly generated 2-nitrobenzyl chloromethyl ether. The resulting dye, **4-7**, was given to our collaborator to attach on to a UCNP.

4.3 Future directions and outlook

There are many potential applications for a tool like photoFAD UCNP. Of particular interest to me would be to further investigate the role of exogenous formaldehyde in memory formation. It is known that formaldehyde levels increase with age and correlate with cognitive decline, especially in neurological disorders. However, past formaldehyde stresses have been released extracellularly. Presumably, much of this formaldehyde reacted before it could become in the intracellular DNA demethylation/remethylation (dMe/rMe) cycle. Intracellular, photoactivatable delivery would circumvent this and provide more direct access to the dMe/rMe cycle. With this we can explore whether localized release of formaldehyde can assist mice with memory related processes. Moreover, we can quantify the exogenous formaldehyde levels required to handicap cognitive processes.

4.4 Experimental

4.4.1 Materials and methods

Dry CH_2Cl_2 and THF were prepared by drying commercial solvent over activated 4Å molecular sieves 3 times for a minimum of 24 hours each time. Dry CHCl_3 and DMF were prepared by drying commercial solvent over activated 4Å molecular sieves 1 time for a minimum of 24 hours. 3-bromo-1-(trimethylsilyl)-1-propyne was purchased from AK Scientific. Acetic anhydride and 1.0 M sulfonyl chloride in CH_2Cl_2 were purchased from Alfa Aesar. Acetic acid and THF were purchased from Fisher Scientific. DMSO and methanol were purchased from Macron. 4-bromo-3-trifluoromethyl phenol, DIPEA, K_2CO_3 , NaBH_4 , and 2-nitroacetophenone were purchased from Oakwood Chemical. Anhydrous acetonitrile, 1.4 M *sec*-butyllithium in cyclohexane, and 1.0 M TBAF in THF were purchased from Sigma-Aldrich.

4.4.2 Synthesis and characterization

1-(2-nitrophenyl)ethan-1-ol (4-2). A flask was charged with 2-nitroacetophenone (1.65 g, 10 mmol, 1.0 eq.) and MeOH (15 mL). While stirring at room temperature, the solution was treated with NaBH_4 (0.372 g, 10 mmol, 1.0 eq.). After stirring for 1 hour, the reaction was quenched via the sequential addition of H_2O (5 mL) and 1.0 M NaOH in H_2O (5 mL). The MeOH was removed using a stream of air. The reaction was diluted with H_2O and extracted from with Et_2O (2x). The organic fractions were combined, dried over Na_2SO_4 , and concentrated to afford the title compound as a yellow oil (1.653 g, 9.89 mmol, 98.9% yield). ^1H NMR (500 MHz, Chloroform-*d*) δ 7.90 (dd, J = 8.1, 1.3 Hz, 1H), 7.84 (dd, J = 7.9, 1.4 Hz, 1H), 7.65 (td, J = 7.6,

1.3 Hz, 1H), 7.42 (ddd, $J = 8.5, 7.4, 1.5$ Hz, 1H), 5.42 (qd, $J = 6.3, 3.5$ Hz, 1H), 2.32 (d, $J = 4.1$ Hz, 1H), 1.58 (d, $J = 6.4$ Hz, 3H).

methyl((1-(2-nitrophenyl)ethoxy)methyl)sulfane (4-3). A flask was charged with **4-2** (0.337 g, 2.0 mmol, 1.0 eq.) and DMSO (10 mL). To this solution was added acetic acid (10 mL) and acetic anhydride (15 mL) simultaneously. After stirring for 20 hours at room temperature, the reaction was poured into ice (200 g) and saturated NaHCO_3 in H_2O (200 mL). Product was extracted with EtOAc (50 mL). The organic fraction was washed with saturated NaHCO_3 in H_2O , H_2O , and brine, then dried over saturated Na_2SO_4 and concentrated. The crude residue was partially purified via flash chromatography on silica gel (10:90 v/v EtOAc:hexanes) to afford the title compound as a light yellow oil. (0.300 g, 1.32 mmol, 65.9% yield). ^1H NMR (500 MHz, Chloroform- d) δ 7.91 (dd, $J = 8.3, 1.3$ Hz, 1H), 7.76 (dd, $J = 7.9, 1.5$ Hz, 1H), 7.64 (td, $J = 7.4, 1.2$ Hz, 1H), 7.42 (ddd, $J = 8.5, 7.6, 1.5$ Hz, 1H), 5.41 (q, $J = 6.4$ Hz, 1H), 4.61 (d, $J = 11.4$ Hz, 1H), 4.31 (d, $J = 11.5$ Hz, 1H), 2.12 (s, 3H), 1.55 (d, $J = 6.3$ Hz, 3H). ^1H NMR (500 MHz, Chloroform- d) δ 7.91 (dd, $J = 8.3, 1.3$ Hz, 1H), 7.76 (dd, $J = 7.9, 1.5$ Hz, 1H), 7.64 (td, $J = 7.4, 1.2$ Hz, 1H), 7.42 (ddd, $J = 8.5, 7.6, 1.5$ Hz, 1H), 5.41 (q, $J = 6.4$ Hz, 1H), 4.61 (d, $J = 11.4$ Hz, 1H), 4.31 (d, $J = 11.5$ Hz, 1H), 2.12 (s, 3H), 1.55 (d, $J = 6.3$ Hz, 3H).

(3-(4-bromo-3-(trifluoromethyl)phenoxy)prop-1-yn-1-yl)trimethylsilane (4-5). A flame-dried pressure flask was charged with 4-bromo-3-trifluoromethyl phenol (0.484 g, 2.0 mmol, 1.0 eq.), K_2CO_3 (0.556g, 4.0 mmol, 2.0 eq.), and acetonitrile (4 mL). The yellow mixture was treated with 3-bromo-1-(trimethylsilyl)-1-propyne (0.36 mL, 2.2 mmol, 1.1 eq.) and heated to 40 °C. After stirring for 24 hours, the reaction was cooled, and the acetonitrile was removed using a stream of air. The crude residue was suspended in CH_2Cl_2 , washed with H_2O , dried over Na_2SO_4 , and concentrated under reduced pressure to afford the title compound as a colorless oil. ^1H NMR (500 MHz, Chloroform- d) δ 7.59 (d, $J = 8.8$ Hz, 1H), 7.34 (d, $J = 3.0$ Hz, 1H), 7.00 (dd, $J = 8.9, 3.0$ Hz, 1H), 4.70 (s, 2H), 0.17 (s, 9H).

7-hydroxy-5,5-dimethyl-10-(4-(prop-2-yn-1-yloxy)-2-(trifluoromethyl)phenyl)dibenzo[b,e]silin-3(5H)-one (4-6) .A flame-dried flask was charged with **4-5** (0.206 g, 0.60 mmol, 3.0 eq.) and dry THF (5 mL). The solution was cooled to -78C and then treated with 1.4 M *sec*-butyllithium in cyclohexane (0.43 mL, 0.60 mmol, 3.0 eq.). After 20 minutes, the reaction was treated dropwise over 1 minute with a solution of **2-13** (0.099 g, 0.20 mmol, 1.0 eq.) in dry THF (3 mL). After addition, the reaction was allowed to come to room

temperature. After 2 hours, the reaction was treated with 1.0 M TBAF in THF (2.0 mL, 2.0 mmol, 10 eq.) and stirred overnight. The reaction was then treated with CaCO₃ and 0.5 M citric acid in H₂O. The mixture was diluted with Et₂O and THF. The organic layer was collected, dried over Na₂SO₄, and concentrated under reduced pressure. The crude residue was partially purified via flash chromatography on silica gel (3:97 v/v MeOH:CH₂Cl₂) to afford the title compound.

5,5-dimethyl-7-((1-(2-nitrophenyl)ethoxy)methoxy)-10-(4-(prop-2-yn-1-yloxy)-2-(trifluoromethyl)phenyl)dibenzo[b,e]silin-3(5H)-one (4-7). A flame-dried conical vial was charged with **4-3** (0.055 g, 0.24 mmol, 1.2 eq.) and dry CH₂Cl₂ (3 mL). The solution was cooled to 0 °C before treating with 1.0 M SO₂Cl₂ in CH₂Cl₂ (1.5 mL, 1.5 mmol, 7.5 eq.). The reaction was warmed to room temperature. After 4 hours, the reaction was concentrated under a stream of N₂. The crude material was resuspended in dry CHCl₃ and concentrated under a stream of N₂ three times to remove any remaining SO₂Cl₂. The crude material was dissolved in dry DMF (3 mL) and treated with a solution of **4-6** in dry THF (2 mL). The reaction was then treated with DIPEA (0.052 mL, 0.3 mmol, 1.5 eq.). After stirring at room temperature overnight, the reaction was concentrated under a stream of N₂. The crude material was purified via two rounds of flash chromatography on silica gel (first - 30:70 to 40:60 v/v EtOAc:hexanes gradient; second – 0:100 to 1:99 v/v MeOH:CH₂Cl₂ gradient) to afford the title compound as a red solid (0.01324 g, 0.0210 mmol, 10.5% over 2 steps). (1:1 mixture of diastereomers) ¹H NMR (500 MHz, Chloroform-*d*) δ 7.90 – 7.84 (m, 2H), 7.62 (dd, *J* = 7.9, 1.4 Hz, 1H), 7.59 (dd, *J* = 7.9, 1.4 Hz, 1H), 7.50 – 7.40 (m, 4H), 7.37 – 7.29 (m, 2H), 7.32 – 7.25 (m, 2H), 7.20 (d, *J* = 3.4 Hz, 1H), 7.18 (d, *J* = 2.9 Hz, 2H), 7.05 (d, *J* = 2.8 Hz, 1H), 6.87 – 6.80 (m, 5H), 6.72 (dd, *J* = 8.9, 2.8 Hz, 1H), 6.69 (d, *J* = 9.0 Hz, 1H), 6.65 (d, *J* = 9.0 Hz, 1H), 6.28 – 6.19 (m, 2H), 5.42 (q, *J* = 6.4 Hz, 1H), 5.42 (q, *J* = 6.4 Hz, 1H), 5.28 (d, *J* = 7.4 Hz, 1H), 5.27 (d, *J* = 7.4 Hz, 1H), 5.18 (d, *J* = 7.4 Hz, 1H), 5.17 (d, *J* = 7.4 Hz, 1H), 4.86 – 4.81 (m, 4H), 2.67 – 2.62 (m, 2H), 1.55 (d, *J* = 6.4 Hz, 3H), 1.54 (d, *J* = 6.4 Hz, 3H), 0.52 (s, 3H), 0.50 (s, 3H), 0.44 (s, 3H), 0.39 (s, 3H).

Appendix A. ALDH isoforms supporting information

A.1 AlDeSense supporting information

This section is adapted from with the permission from *Surveillance of Cancer Stem Cell Plasticity Using an Isoform-Selective Fluorescent Probe for Aldehyde Dehydrogenase 1A1*. ACS Cent. Sci. 2018, 4, 1045–1055. © 2018 American Chemical Society.

A.1.1 Experimental procedure

ALDH isoform activity assays

The activity of each isoform of ALDH was confirmed by monitoring the production of NADH at 340 nm when incubated with the most commonly used substrate for that enzyme (propionaldehyde for ALDH1A1, ALDH1A2, ALDH1A3, ALDH2 and ALDH4A1; benzaldehyde for ALDH3A1, and succinic semialdehyde for ALDH5A1). Each isoform was diluted with 50 mM triethanolamine (TEA, pH 7.4) to a final concentration of 1 μ M and placed in a 1 mL quartz cuvette. Directly before measurement, NAD⁺ was added to final concentration of 2.5 mM and the preferred substrate was added to a final concentration of 1 mM. Absorbance spectra were taken from 300 to 500 nm every half minute for 15 minutes. Units of activity for each enzyme were calculated from the slope of absorbance increase at 340 nm over time, (1 unit = 1 μ mol substrate turned over/ μ mol enzyme/ min).

AlDeSense isoform selectivity assay

Activation of AlDeSense was assessed using 20 units of each ALDH isoform. Activity was determined by activity measurements using each isoform's preferred substrate (1 unit = 1 μ mol substrate turned over / μ mol enzyme / min). Further details are in the supplementary information. All enzymatic reactions were performed in 50 mM triethanolamine buffer (pH 7.4, Thermo Fisher) with 2.5 mM NAD⁺ (Alfa Aesar) and 5% v/v DMSO (Thermo Fisher) in a 1 mL quartz cuvette at room temperature.

AlDeSense activation was determined using fluorescence. Immediately before measurement, AlDeSense (1 μ M) was added to a quartz cuvette. After vigorous mixing, the reaction was monitored at room temperature for 15 min. Fluorescence spectra were acquired according to following parameters: λ_{ex} = 498 nm, and emission range = 505-580 nm. All scans were normalized to the signal from AlDeSense in 50 mM TEA and 2.5 mM NAD⁺ (without

enzyme). Endpoint measurements at 15 min were performed in triplicate and reported as the averages \pm standard deviation.

Inhibition of ALDH1A1

ALDH1A1 (100 nM) in 50 mM TEA (pH 7.4) was incubated with 2.5 mM NAD⁺. Immediately before measurement, 4-diethylaminobenzaldehyde (DEAB) in 95% ethanol was added for a final concentration of 100 nM. The reaction was initiated with the addition of AlDeSense (1 μ M). The solution was mixed with vigorous pipetting and fluorescence spectra were acquired. Fluorescence spectra were acquired according to following parameters: λ_{ex} = 498 nm, and emission range = 505-580 nm. Scans were taken periodically for up to 30 min. The reaction proceeded at room temperature throughout the experiment. All scans were normalized to the peak of AlDeSense in 50 mM TEA and 2.5 mM NAD⁺ without the addition of enzyme.

siRNA knockdown of ALDH1A1

K562 cells were grown to ~70% confluency in a poly-L-lysine (Trevigen) coated Nunc™ Lab-Tek™ 8-well Chamber Slide™ system (Thermo Scientific) 1 day before treatment with siRNA. Both the negative control scrambled siRNA (Sigma-Aldrich, MISSION® siRNA Universal Negative Control #1) as well as the ALDH1A1 siRNA (Sigma-Aldrich, SASI_Hs01_00244056) was applied at 50 μ M concentrations following the Lipofectamine 3000 (Thermo Fisher) protocol for a 24-well plate. 0.75 μ L of the Lipofectamine 3000 reagent was used per sample. After treatment, cells incubated with the siRNA in Opti-MEM (Gibco) at 37°C, 5% CO₂ for 8 hours. At this point, the Opti-MEM was removed and replaced with full growth media (IMDM supplemented with 10% FBS). Cells were incubated further at 37°C, 5% CO₂ for 48 hours before imaging on the Zeiss LSM 700 confocal. To stain the cells with each imaging reagent, 1 μ L of 2 mM AlDeSense AM in DMSO was used per 1 mL of serum-free media (DMEM/F12 supplemented with 15 μ M HEPES). Growth media was removed from the cells and replaced with the premixed dye solution. Cell staining continued for 30 minutes at room temperature (25°C), after which the cells were immediately imaged. The optical configuration was optimized for the scrambled siRNA samples and the same optical settings were used for all images.

Mammosphere culture and imaging

Mammosphere formation from MDA-MB-231 breast cancer cells was performed as described previously with some modifications. Cells were resuspended and diluted to a density of 2000 cells/mL in DMEM/F12 (Sigma-Aldrich) supplemented with 2% B27 supplement (Thermo

Fisher), 40 ng/mL rhFGF-2 (Miltenyi Biotec), and 20 ng/mL rhEGF (Gibco®). They were plated in ultra-low attachment 6-well plates (Corning) and incubated at 37°C and 5% CO₂ for 5 days or until most mammospheres were between 60-100 nm. At this point, the mammospheres were transferred to a 4-well chamber slide coated with Poly-L-lysine as described previously. The mammospheres were then either immediately imaged with AlDeSense or Ctrl-AlDeSense, or the media was exchanged with full DMEM media supplement with 10% FBS and non-essential amino acids to allow differentiation over 36 hours.

At various time points, the mammospheres were stained with 2 μ M AlDeSense or Ctrl-AlDeSense as described above. Staining continued for 1 h at room temperature before imaging with a wide field fluorescence microscope (Zeiss Axiovert 200M). A GFP filter set was used to excite the fluorophores. Exposure times were set equally for all images taken within a data set and configured to give low signal in Ctrl-AlDeSense stained tumorspheres. Only mammospheres greater than 50 μ m in diameter were considered in the analysis.

B16F0 melanoma confocal imaging

B16F0 murine melanoma cells were cultured for 5 days on polyacrylamide hydrogels with or without spiral patterns as described previously. (18) The coverslips on which the hydrogels and cells were mounted were transferred to a glass-bottomed dish for confocal imaging, leaving the cells intact. Solutions of either 2 μ M AlDeSense AM or 2 μ M Ctrl-AlDeSense AM in PBS were added to the two types of cells. The cells were incubated at room temperature for 1 h and then immediately imaged. Confocal imaging was performed on a Zeiss LSM700 Confocal Microscope, utilizing the 488 nm laser line to excite AlDeSense AM and the 20X/0.8 objective. Three different coverslips of cells were imaged for each set of conditions and at least 6 images were taken for each coverslip. Using ImageJ, ROIs were drawn around areas covered with cells and mean fluorescence values were measured for each image.

***Ex vivo* lung metastases imaging**

Six to eight-week-old female C57BL/6J mice were purchased from Jackson Laboratory. Experimental metastases were established by injecting 2×10^5 melanoma cells via lateral tail vein injection. Mice were euthanized at either 7 or 11 days post injection. Immediately after euthanization, their lungs were excised and perfused with about 1 mL of either 15 μ M AlDeSense AM or 15 μ M Ctrl-AlDeSense AM in PBS. Outer portions of the lungs were rinsed in 15 mL of PBS to remove blood or excess dyes. After 2 hours incubation at room temperature (25°C), the

lungs were imaged on the IVIS spectrum imaging system (Perkin Elmer). Data was processed using Living Image software (Version 4.1).

***In vivo* melanoma tumor fluorescence imaging**

All *in vivo* imaging experiments were performed with the approval of the Institutional Animal Care and Use Committee of the University of Illinois at Urbana-Champaign. Six to eight-week-old female BALB/c mice were purchased from the Jackson Laboratory for the tumor imaging experiment. Primary localized tumors were established by subcutaneously injecting B16F0 cells (5×10^5 cells in 100 μ L of Hanks' balanced salt solution per injection). For each animal, cells that were grown on patterned gels were injected on the right lateral flank and cells grown on non-patterned gels were injected on the left lateral flank. At 1 and 2 weeks, mice were intravenously injected with either 15 μ M AlDeSense or Ctrl-AlDeSense. After 24 h, the mice were imaged using an IVIS spectrum imaging system for epifluorescence in conjunction with a CT scan. Data was processed using Living Image software (Version 4.1).

Photostability assay

2 μ M AlDeSense, Ctrl-AlDeSense, and AldeFluor were placed in triplicate in a 96-well plate. The plate was placed in an IVIS Spectrum imaging system and irradiated repeatedly using the FITC excitation filter for 30 minutes. Fluorescence of each sample was measured at various time points and normalized to the level of fluorescence emitted by each sample at time 0.

Expression and purification of ALDH1A1 and related isoforms

Expression constructs for recombinant human ALDH1A1, ALDH1A2, ALDH1A3, ALDH2, ALDH3A1, ALDH4A1, and ALDH5A1 were generously provided by Prof. Daria Mochly-Rosen (Stanford, Chemical and Systems Biology). *E. coli* BL21(DE3) cells were transformed with each of the above constructs. Colonies were selected from an agar plate containing 100 μ g/mL ampicillin and grown overnight (37°C, 220 rpm) with 100 μ g/mL ampicillin. The overnight culture (10 mL) was inoculated into 1000 mL LB supplemented with 100 μ g/mL ampicillin. At O.D. \sim 0.5, IPTG was added to a final concentration of 1 mM and incubated overnight (30°C, 200 rpm, 18 h or 25°C, 200 rpm, 24 h). The cells were then harvested by centrifugation (4°C, 4,000 rpm, 90 min) and cell pellets stored at -80°C until purification.

The bacterial pellets were resuspended in BugBuster® Master Mix (EMD Millipore, 15 mL for every 500 mL of cell culture collected) combined with protease inhibitor cocktail (1 tablet for every liter of cells collected, Pierce™ Protease Inhibitor Tablets, EDTA-free). They were then

lysed according to manufacturer instructions (30 min incubation, room temp, rocking). The extract was centrifuged (4°C, 4,000 rpm, 90 min) and the supernatant was filtered (0.22 µm syringe filter, EMD Millipore) and applied to a Ni-NTA column. The column was washed by the following binding buffer: 20 mM sodium phosphate pH 7.4, 0.5 M NaCl, 20 mM imidazole. Washing continued for 10 column volumes or until absorbance measurements at 280 nm were sufficiently low to ensure the removal of non-specific binders. Target proteins were then eluted by wash buffer (20 mM sodium phosphate pH 7.4, 0.5 M NaCl, 500 mM imidazole). Purity of eluted protein was determined to be $\geq 95\%$ by SDS-PAGE and concentration of protein was determined by bicinchoninic acid (BCA) assay. Protein was stored with 50% glycerol at -80°C.

BAAA isoform selectivity assay

BAAA activation was determined using UV/Vis spectroscopy. A 2 mM stock solution of BAAA was prepared in DMSO and activated with 2M HCL as described in the ALDEFLUOR™ Kit protocol (STEMCELL Technologies Inc.). Immediately before measurement, BAAA was added to the reaction mixture described above to a final concentration of 18 µM. The solution was mixed vigorously and the reaction proceeded at room temperature. UV/Vis absorbance spectra were taken from 300 to 500 nm every 30 seconds for 15 minutes. The rate of NADH produced per minute was calculated according to the absorbance at 340 nm ($\epsilon = 6,220 \text{ M}^{-1} \text{ cm}^{-1}$). All measurements were performed in triplicate and reported as the average \pm standard deviation. 20 units of enzyme and 18 µM of BAAA were necessary to detect a significant increase in absorbance at 340 nm for the ALDH1A1 isoform.

Cell culture

K562 cells were obtained from Prof. Paul Hergenrother (UIUC, Chemistry). K562 cells were cultured as a suspension in Iscove's Modified Dulbecco's Medium (IMDM, ATCC) supplemented with 10% fetal bovine serum (FBS, Sigma Aldrich) and 1% penicillin/streptomycin (Corning). MDA-MB-231 cells were purchased from the American Type Culture Collection (ATCC) and cultured in Dulbecco's Modified Eagle Medium (DMEM, ATCC) supplemented with 10% FBS, 1% pen-strep, and non-essential amino acids. B16F0 cells were obtained from the ATCC and cultured in Dulbecco's Modified Eagle Medium (DMEM, ATCC) supplemented with 10% fetal bovine serum (FBS, Sigma Aldrich) and 1% penicillin/streptomycin (Corning). All cells were grown at 37 °C in a humidified incubator with 5% CO₂ unless otherwise noted. For every cell line, media was changed or cells were passaged every three days.

Trypan Blue cytotoxicity assay

K562 cells were plated in a 96-well plate at a density of 500,000 cells/mL in full IMDM media supplemented with either 1 μ M or 5 μ M AlDeSense AM. Equivalent samples were supplemented with 1 μ M or 5 μ M DMSO as a vehicle control. At 6, 12, and 24 hours, a 10 μ L sample was removed from each of the samples and mixed 1:1 with a 0.4% wt/volume trypan blue solution in PBS. Samples were incubated for 1 minute at room temperature before being loaded onto a hemocytometer where live and dead cells were counted. Each sample was made in triplicate for each time point.

Analysis of AlDeSense AM de-esterification

To analyze the de-esterification of AlDeSense AM in cells, ~20 million K562 cells (grown in suspension using full IMDM media as described previously) were collected by centrifugation and resuspended in a 10 μ M solution of AlDeSense AM in PBS. The cells were incubated at room temperature with rocking for 15 min, then collected by centrifugation and washed with PBS. The cells were then resuspended by gentle pipetting into 5 mL of ice cold digitonin lysis buffer: 150 mM NaCl, 50 mM HEPES pH 7.4, and 25 μ g/mL digitonin (Sigma Aldrich). The cells were incubated on ice for 10 minutes and then centrifuged at 2000 RCF to pellet cell debris. The supernatant was collected as crude cytosolic lysate. Cell lysate was measured by mass spectrometry using a Thermo Scientific Orbitrap mass spectrometer (San Jose, CA, USA). Lysate samples were diluted 1:1000 in 50:25:25 methanol:acetonitrile:water with 0.1% formic acid and subsequently analyzed by chemical ionization in the positive mode.

Standard flow cytometry experiment with K562 cells

K562 cells were resuspended in PBS to a final concentration of 100,000 cells/mL. The suspension was divided into 0.5 mL aliquots and the cells were collected by centrifugation at 1000 rpm for 5 min at 4°C. Each sample was then resuspended in premixed AlDeSense AM or Ctrl-AlDeSense AM solutions (1.5 μ M, PBS). For each dye, triplicate samples were prepared. Cells were incubated with dye for 30 minutes at room temperature with rocking to prevent cell clumping and ensure even dye distribution. At the end of the incubation period, cells were again collected by centrifugation at 1000 rpm for 5 min at 4°C. The dye solution was removed by aspiration, and each sample of cells were resuspended in 0.5 mL of PBS. The samples were immediately placed on ice until analysis. The samples were analyzed by a BD LSR II Flow Cytometry Analyzer using a 488 nm laser and a FITC filter. Data analyzed on FCS Express 6.04.

Flow cytometry analysis of K562 cells grown under hypoxia

Using a hypoxic incubator, K562 cells were grown in full IMDM media at 1% O₂, 5% CO₂, and 94% N₂ for 48 hours. As a control, cells from the same passage were also grown in a standard cell culture incubator only supplied with 5% CO₂. At the end of the 48-hour period, the cells were collected by centrifugation and resuspended in either 1 μ M AlDeSense AM or 1 μ M Ctrl-AlDeSense AM (both in PBS) at a density of 1 million cells/mL. Cells were incubated in dye for 30 min at room temperature with rocking. At the end of the incubation period, the cells were spun down and resuspended as 100 μ L samples in PBS. CD34-VioBlue® and CD38-APC (Miltenyi Biotec) were added at 1:11 of the stock concentration and incubated for 10 minutes on ice, protected from light. At the end of this period, the cells were washed, resuspended in PBS, and kept on ice until analysis by flow cytometry. The samples were analyzed by a BD LSR II Flow Cytometry Analyzer using a 488 nm laser with a 530/30 bandpass filter for AlDeSense, a 403 nm laser with a 450/50 band pass filter for CD34-VioBlue®, and a 640 nm laser with a 660/20 bandpass filter for CD38-APC. Data analyzed on FCS Express 6.04.

Confocal imaging of K562 cells

The day before imaging, Nunc™ Lab-Tek™ Chamber Slide™ systems (Thermo Fisher) were coated with poly-L-lysine (Trevigen) according to manufacturer's instructions. Cells were added to the chamber slides at a concentration of 400,000 cells/mL, yielding 90% confluent cells after 24 h. To stain the cells with each imaging reagent (AlDeSense AM or Ctrl-AlDeSense AM), 1 μ L of 2 mM dye in DMSO was used per 1 mL of serum-free media (DMEM/F12 supplemented with 15 μ M HEPES). Growth media was removed from the cells and replaced with the premixed dye solution. Cells were incubated with dye for 30 minutes at room temperature (25°C), after which time the cells were immediately imaged. Live cell imaging was performed on a Zeiss LSM700 Confocal Microscope, utilizing the 488 nm laser and light filter settings for FITC dye. For each condition, three different wells of cells were imaged by taking at least three images each using the 20x/0.8 objective. The optical configuration was optimized by minimizing signal in samples stained with Ctrl-AlDeSense AM or in inhibited samples by adjusting gain. The same optical settings were used for images within each set of matched experiments. Images were analyzed using ImageJ software (Version 1.51n).

To inhibit ALDH1A1 before imaging, cells were pre-incubated with 10 μ M disulfiram in PBS for 60 min at 37°C in an incubator with 5% CO₂. Vehicle controls with PBS supplemented

with DMSO were subjected to preincubation conditions alongside the inhibited samples. At the end of the preincubation period, cells were stained with AlDeSense AM as described above.

Subcellular localization of AlDeSense and BAAA

To determine the subcellular localization of AlDeSense, K562 cells were plated and stained as described above with either 2 μ M AlDeSense AM or 2 μ M BAAA. BAAA was activated with 2M HCL as described in the ALDEFLUOR™ Kit protocol (STEMCELL Technologies Inc.). After 30 minutes of staining, about 5 μ L of 100x solutions of rhodamine 101 methyl ester (for mitochondrial staining), LysoTracker Red, or ER Tracker Red were added and allowed to stain for about 5 minutes before immediately imaging on a Zeiss LSM700 Confocal Microscope, utilizing the 488 nm laser for AlDeSense or BAAA signal and the 555 nm laser for each of the trackers. Pearson's R coefficients were calculated for 13 images using the Coloc 2 function of Fiji, a distribution of Image J optimized for biological image analysis.⁸⁶

Western blot of siRNA knockdown

K562 cell lysate's concentration was measured with an Epoch Microplate Spectrophotometer (BioTEK). Lysate was diluted to desired concentration and mixed with 2x Laemmli Sample Buffer (Bio-Rad) and heated at 95°C for 5 minutes. Samples were run on a 12% gel (12% Mini-PROTEAN TGX precast gel, Bio-Rad) and transferred to PVDF membrane (Mini format 0.2 μ m PVDF Trans-Blot Turbo™ Transfer pack, Bio-Rad) using a Trans-Blot Turbo™ Transfer System (Bio-Rad). The membrane was blocked in 5% bovine serum albumin (5% BSA) in TBS for one hour at room temperature. Then, the membrane was incubated in primary antibody (1:1000 in 5% BSA) (ALDH1A1 (B-5), sc-374149, lot #E1316, Santa Cruz Biotechnology) overnight at 4°C. The membrane was then washed three times for 5 minutes with TBS, then it was incubated in secondary antibody (1:500 in TBS) (m-IgG κ BP-CFL 680, sc-516180, lot #A0917, Santa Cruz Biotechnology) for 90 minutes. The membrane was washed twice with TBS for 5 minutes. The membrane was visualized with ChemiDoc™ XRS+ System (Bio-Rad).

Antibody colocalization

CD34-VioBlue®, CD38-APC, and CD133/1(AC133)-PE were purchased from Miltenyi Biotec (Auburn, CA, USA). K562 cells were grown on Poly-L-Lysine coated coverslips within 24-well dishes overnight at 37°C, 5% CO₂. The following day, the cells were treated with the antibodies at 1:25 concentration for 1 hour at room temperature. Following this, AlDeSense AM was added at a final concentration of 1 μ M and the cells were further incubated for 30 minutes at

room temperature. Once this was complete, the coverslips were removed and mounted onto glass slides for confocal imaging.

Live cell imaging was performed on a Zeiss LSM700 Confocal Microscope, utilizing the 488 nm laser to excite AlDeSense AM, the 405 nm laser to excite CD34-VioBlue®, the 639 nm laser to excite CD38-APC, and the 555 nm laser to excite CD133/1(AC133)-PE. Images were taken using the 63X/1.4 Oil objective.

Pearson's R coefficients were calculated for 13 images using the Coloc 2 function of Fiji.

Flow cytometry analysis of e-CSC versus non-CSC populations of B16F0 melanoma cells

B16F0 melanoma cells were grown on patterned or nonpatterned hydrogels as described previously.⁶⁴ Cells were trypsinized and resuspended at about 2 million cells/mL in PBS and kept on ice. Samples of cells were then spun down and resuspended in either 1 μ M AlDeSense AM or 1 μ M Ctrl-AlDeSense AM, maintaining the same cell density. The samples were then incubated with the dyes at room temperature for 30 minutes with rocking. Samples of unstained patterned and nonpatterned cells were also reserved on ice as a negative control. At the end of the 30-minute dye incubation period, the cells were pelleted by centrifugation and resuspended in 100 μ L of PBS buffer. The cells were then stained with CD271 (LNGFR)-APC, human and mouse (clone: REA648, Miltenyi Biotec). To achieve a 1:11 dilution, 10 μ L of antibody was added to each 100 μ L sample. The cells were incubated with antibody for 10 minutes at 4°C in the dark. Controls stained only with AlDeSense or Ctrl-AlDeSense were produced by incubating in PBS without antibody. At the end of the incubation period, all samples were spun down and resuspended in 500 μ L of PBS and kept on ice until analysis. The samples were analyzed by a BD LSR II Flow Cytometry Analyzer using a 488 nm laser with a 530/30 bandpass filter for AlDeSense or Ctrl-AlDeSense and a 640 nm laser with a 660/20 bandpass filter for CD38-APC. Data analyzed on FCS Express 6.04.

Statistical analyses

Statistical analyses were performed in GraphPad Prism version 7.03. Sample sizes in all experiments were of sufficient size to detect at least a p value < 0.05, which was considered to be significant. All data were analyzed using Student's t tests and were expressed as mean \pm SD, unless otherwise stated.

A.1.2 Synthesis and characterization

A.1.2.1 Synthesis of xanthone

2,7-Difluoro-3,6-bis((2-methoxyethoxy)methoxy)-9H-xanthen-9-one (2.1). The titled compound was prepared according the procedure published by Peterson and co-workers.⁶⁰

A.1.2.2 Synthesis of AlDeSense and AlDeSense AM

((4-Bromo-3-methylbenzyl)oxy)(tert-butyl)dimethylsilane (2.3). A flame-dried round-bottom flask was charged with methyl 4-bromo-3-methylbenzoate (11.5 g, 50.0 mmol, 1.00 eq.) and anhydrous CH₂Cl₂ (100 mL). A flame-dried addition funnel was attached to the flask and the system was flushed with nitrogen. The reaction was cooled to 0 °C and treated with 1.0 M DIBAL-H in CH₂Cl₂ (110 mL, 110 mmol, 2.2 eq.) via funnel addition over 23 minutes. The reaction was allowed to warm to room temperature. After stirring at room temperature for 4 hours, the reaction was cooled to 0 °C and quenched via the slow addition of H₂O (5 mL), 1 M NaOH (5 mL), and additional H₂O (30 mL). The resulting emulsion was poured over filter paper and washed with CH₂Cl₂. The organics were combined, dried over Na₂SO₄, and concentrated under reduced pressure. The crude residue containing **1** was eluted through a silica plug and concentrated to afford a light-yellow oil which was used without further purification. A solution of this intermediate in anhydrous CH₂Cl₂ (50 mL) was treated with imidazole (6.8 g, 100 mmol, 2.0 eq.) and *tert*-butyldimethylsilyl chloride (8.2 g, 55 mmol, 1.1 eq.). After overnight stirring, the reaction was filtered and washed with CH₂Cl₂. The filtrate was collected, washed with aqueous NH₄Cl, and concentrated under reduced pressure. The crude material was purified via flash chromatography on a silica column (2:98 v/v EtOAc:hexanes) to afford the title compound (14.6 g, 46.3 mmol, 92.6% yield over two-steps beginning from methyl 4-bromo-3-methylbenzoate). ¹H NMR (500 MHz, CDCl₃) δ 7.47 (d, *J* = 8.1 Hz, 1H), 7.18 (d, *J* = 1.6 Hz, 1H), 7.01 (dd, *J* = 8.2, 1.5 Hz, 1H), 4.66 (s, 2H), 2.39 (s, 3H), 0.94 (s, 9H), 0.10 (s, 6H). ¹³C NMR (125 MHz, CDCl₃) δ 140.82, 137.67, 132.22, 128.63, 125.20, 123.15, 64.48, 26.09, 23.09, 18.57, -5.10.

2,7-Difluoro-6-hydroxy-9-(4-(hydroxymethyl)-2-methylphenyl)-3H-xanthen-3-one (2.4). A flame-dried round-bottom flask was charged with **2** (0.348 g, 1.1 mmol, 1.1 eq.) and anhydrous THF (5 mL). The reaction was cooled to -78 °C and treated with 1.4 M *sec*-butyllithium in cyclohexane (0.9 mL, 1.1 mmol, 1.1 eq.). The reaction was stirred at the same temperature for 30 minutes and then treated with a solution of **3** (0.440 g, 1.0 mmol, 1.0 eq.) in anhydrous THF (5 mL). The reaction was stirred at the same temperature for 2 hours. The reaction was warmed to

room temperature and treated with 1.0 M aq. HCl (6.0 mL, 6.0 mmol, 6.0 eq.). The reaction was warmed to 50 °C and stirred for 4 hours. The reaction was concentrated under vacuum to remove the THF and cyclohexane. The remaining mixture was poured over filter paper, washed with H₂O (100 mL) and CH₂Cl₂ (100 mL), and vacuum dried to yield the title compound as a red-orange solid (0.176 g, 0.483 mmol, 48.3% yield). ¹H NMR (500 MHz, DMSO-*d*₆) δ 7.44 (s, 1H), 7.39 (d, *J* = 7.7 Hz, 1H), 7.23 (d, *J* = 7.7 Hz, 1H), 6.82 (d, *J* = 6.0 Hz, 2H), 6.59 (d, *J* = 11.3 Hz, 2H), 5.33 (s, 0H), 4.62 (s, 2H), 2.02 (s, 3H). ¹³C NMR (125 MHz, DMSO-*d*₆) δ 150.29 (t, *J* = 6.1 Hz), 144.31, 135.32, 129.86, 128.71, 128.50, 124.21, 114.00, 111.28 (d, *J* = 21.9 Hz), 105.06 (d, *J* = 4.3 Hz), 62.52, 19.11. HRMS-ESI (*m/z*): [M+H]⁺ Calc. mass for C₂₁H₁₅O₄F₂ = 369.0938; Found mass = 369.0930.

4-(2,7-difluoro-6-hydroxy-3-oxo-3H-xanthen-9-yl)-3-methylbenzaldehyde (AlDeSense). A round-bottom flask was charged with **4** (0.368 g, 1.0 mmol, 1.0 eq.), IBX (0.336 g, 1.2 mmol, 1.2 eq.), and DMSO (10 mL). After stirring for 3 hours at room temperature, the reaction was quenched via the addition of brine (100 mL). The resulting mixture was poured over filter paper and vacuum dried. The red solid was suspended in H₂O (200 mL) and heated to 80 °C. After stirring for 2 hours, the reaction was cooled to room temperature and poured over filter paper and vacuum dried to yield the title compound as a rust-orange solid (0.290 g, 0.792 mmol, 79.2% yield). AlDeSense used in biological assays was further purified via chromatography on a silica column (10:90 v/v MeOH:CH₂Cl₂). ¹H NMR (500 MHz, DMSO-*d*₆) δ 10.12 (s, 1H), 8.02 (s, 1H), 7.95 (d, *J* = 7.8 Hz, 1H), 7.52 (d, *J* = 7.6 Hz, 1H), 6.80 (d, *J* = 6.8 Hz, 1H), 6.60 (d, *J* = 11.4 Hz, 2H), 2.12 (s, 3H). ¹³C NMR (125 MHz, DMSO-*d*₆) δ 193.01, 154.48, 154.28, 152.48, 148.77 (t, *J* = 5.7 Hz), 138.57, 136.95, 136.83, 131.32, 129.88, 127.32, 110.11 (d, *J* = 21.7 Hz), 109.50 (d, *J* = 8.2 Hz), 104.93 (d, *J* = 5.4 Hz), 18.90. [M+H]⁺ Calc. mass for C₂₁H₁₃O₄F₂ = 367.0782; Found mass = 367.0784.

((2,7-difluoro-9-(4-formyl-2-methylphenyl)-3-oxo-3H-xanthen-6-yl)oxy)methyl acetate (AlDeSense AM). A flame-dried round-bottom flask was charged with AlDeSense (0.037 g, 0.10 mmol, 1.0 eq.), anhydrous DMF (2.0 mL), bromomethyl acetate (0.020 mL, 0.20 mmol, 2.0 eq.), and DIPEA (0.035 mL, 0.20 mmol, 2.0 eq.). After stirring for 12 hours at room temperature, all volatiles were removed under vacuum at room temperature. The crude material was purified via column chromatography on a silica column (20:80 v/v EtOAc:CH₂Cl₂) to afford the title compound as an orange solid (0.0265 g, 0.060 mmol, 60.4% yield). ¹H NMR (500 MHz,

DMSO-*d*₆) δ 10.14 (s, 1H), 8.03 (s, 1H), 7.98 (d, *J* = 7.8 Hz, 1H), 7.76 (d, *J* = 6.9 Hz, 1H), 7.52 (d, *J* = 7.7 Hz, 1H), 6.81 (d, *J* = 10.9 Hz, 1H), 6.63 (d, *J* = 11.1 Hz, 1H), 6.55 (d, *J* = 7.0 Hz, 1H), 6.01 (s, 2H), 2.14 (s, 3H), 2.13 (s, 3H). ¹³C NMR (125 MHz, DMSO-*d*₆) δ 193.51, 175.18 (d, *J* = 20.8 Hz), 169.80, 157.56 (t, d, *J* = 5.1 Hz), 155.16 (d, *J* = 265.5 Hz), 148.82 (d, *J* = 245.5 Hz), 149.12, 148.91 (d, *J* = 12.5 Hz), 147.81 (d, *J* = 9.8 Hz), 137.33, 137.23, 137.14, 131.55, 130.02, 127.44, 117.80 (d, *J* = 8.5 Hz), 113.98 (d, *J* = 7.7 Hz), 113.02 (d, *J* = 21.5 Hz), 109.73 (d, *J* = 21.8 Hz), 105.77 (d, *J* = 4.8 Hz), 104.62, 84.80, 20.58, 19.00. [M+H]⁺ Calc. mass for C₂₄H₁₇O₆F₂ = 439.0993; Found mass = 439.1008.

A.1.2.3 Synthesis of Ctrl-AIDeSense and Ctrl-AIDeSense AM

4-Bromo-3-methylbenzaldehyde (2.5). A flame-dried round-bottom flask was charged with methyl 4-bromo-3-methylbenzoate (2.29 g, 10 mmol, 1.0 eq.) and anhydrous CH₂Cl₂ (20 mL). A flame-dried addition funnel was attached to the flask and the system was flushed with nitrogen. The reaction was cooled to 0 °C and treated with 1.0 M DIBAL-H in CH₂Cl₂ (22 mL, 22 mmol, 2.2 eq.) via funnel addition over 10 minutes. The reaction was allowed to warm to room temperature. After stirring at room temperature for 4 hours, the reaction was cooled to 0 °C and quenched via the slow addition of H₂O (5 mL), 1 M NaOH (5 mL), and additional H₂O (20 mL). The resulting emulsion was poured over filter paper and washed with CH₂Cl₂. The organics were combined, dried over Na₂SO₄, and concentrated under reduced pressure to afford **1** as a crude residue which was used without further purification. A solution of this intermediate in DMSO (10 mL) was treated with IBX (3.36 g, 12 mmol, 1.2 eq.). After stirring for 3 hours at room temperature, the reaction was diluted with brine (100 mL), poured over filter paper, and washed through with Et₂O. The aqueous layer was extracted from with Et₂O (50 mL). The organics were combined, washed with brine, dried over Na₂SO₄, and concentrated. The crude material was purified by column chromatography (10:90 v/v EtOAc:Hexanes) to afford the title compound as a light red oil (1.333 g, 6.70 mmol, 67.0% yield). ¹H NMR (500 MHz, CDCl₃) δ 9.95 (s, 1H), 7.73 (d, *J* = 1.4 Hz, 1H), 7.71 (d, *J* = 8.1 Hz, 1H), 7.55 (dd, *J* = 8.1, 2.0 Hz, 1H), 2.48 (s, 3H). ¹³C NMR (125 MHz, CDCl₃) δ 191.52, 139.29, 135.57, 133.38, 132.35, 131.59, 128.40, 23.04.

1-(4-Bromo-3-methylphenyl)ethan-1-ol (2.6). A flame-dried round-bottom flask was charged with **5** (1.926 g, 9.68 mmol, 1.0 eq.) and anhydrous THF (25 mL). The reaction was cooled to 0 °C and treated with 1.5 M methyllithium lithium bromide in Et₂O (7.4 mL, 11.1 mmol, 1.15 eq.) dropwise via syringe addition. The reaction was stirred at the same temperature for 15 minutes

and then warmed to room temperature. After stirring 2 hours at room temperature, the reaction was quenched via addition of sat. NH_4Cl (50 mL). The organics were collected, dried over Na_2SO_4 , and concentrated to yield the title compound as a yellow oil (1.876 g, 8.72 mmol, 90.1% yield). ^1H NMR (500 MHz, CDCl_3) δ 7.49 (d, J = 8.2 Hz, 1H), 7.24 (d, J = 1.8 Hz, 1H), 7.05 (dd, J = 8.2, 1.8 Hz, 1H), 4.83 (q, J = 5.9 Hz, 1H), 2.40 (s, 3H), 1.93 (s, 1H), 1.46 (d, J = 6.5 Hz, 3H). ^{13}C NMR (125 MHz, CDCl_3) δ 145.17, 138.05, 132.48, 128.01, 124.51, 123.71, 69.93, 25.34, 23.08.

(1-(4-Bromo-3-methylphenyl)ethoxy)(*tert*-butyl)dimethylsilane (2.7). A round-bottom flask was charged with **6** (0.215 g, 1.0 mmol, 1.0 eq.), CH_2Cl_2 (5 mL), and imidazole (0.138 g, 2.0 mmol, 2.0 eq.). Once a solution had formed, the reaction was treated with *tert*-butyldimethylsilyl chloride (0.186 g, 1.2 mmol, 1.2 eq.). After stirring for 12 hours at room temperature, the reaction was concentrated. The crude residue was purified via flash chromatography on a silica column (5:95 v/v EtOAc:hexanes) to afford the title compound as a colorless oil (0.287 g, 0.871 mmol, 87.1% yield). ^1H NMR (500 MHz, CDCl_3) δ 7.47 (d, J = 8.2 Hz, 1H), 7.20 (d, J = 2.2 Hz, 1H), 7.04 (dd, J = 8.2, 2.2 Hz, 1H), 4.82 (q, J = 6.4 Hz, 1H), 2.41 (s, 3H), 1.39 (d, J = 6.4 Hz, 3H), 0.92 (s, 9H), 0.07 (s, 3H), 0.00 (s, 3H). ^{13}C NMR (125 MHz, CDCl_3) δ 146.44, 137.49, 132.16, 127.83, 124.41, 122.92, 70.40, 27.38, 26.01, 23.12, 18.40, -4.64, -4.68. $[\text{M}-\text{H}]^-$ Calc. mass for $\text{C}_{15}\text{H}_{24}\text{OBrSi}$ = 327.07798; Found mass = 327.07648.

2,7-Difluoro-6-hydroxy-9-(4-(1-hydroxyethyl)-2-methylphenyl)-3H-xanthen-3-one (2.8). A flame-dried round-bottom flask was charged with **7** (0.494 g, 1.5 mmol, 1.6 eq.) and anhydrous THF (5 mL). The reaction was cooled to $-78\text{ }^\circ\text{C}$ and treated with 1.4 M *sec*-butyllithium in cyclohexane (1.0 mL, 1.4 mmol, 1.4 eq.). The reaction was stirred at the same temperature for 30 minutes and then treated with a solution of **3** (0.441 g, 1.0 mmol, 1.0 eq.) in anhydrous THF (3 mL). The reaction was stirred at the same temperature for 2 hours. The reaction was warmed to room temperature and treated with 1.0 M HCl in H_2O (12 mL, 12 mmol, 12 eq.). The reaction was warmed to $50\text{ }^\circ\text{C}$ and stirred for 24 hours. The reaction was concentrated under reduced pressure. The crude residue was purified via chromatography on a silica column (10:90 v/v MeOH: CH_2Cl_2) to afford the title compound as a red-orange solid (0.318 g, 0.832 mmol, 83.2% yield). ^1H NMR (500 MHz, $\text{DMSO}-d_6$) δ 7.47 (s, 1H), 7.41 (d, J = 7.8 Hz, 1H), 7.21 (d, J = 7.8 Hz, 1H), 6.81 (d, J = 6.5 Hz, 2H), 6.58 (d, J = 11.3 Hz, 2H), 5.29 (s, 1H), 4.82 (q, J = 6.4 Hz, 1H), 2.02 (s, 3H), 1.42 (d, J = 6.5 Hz, 3H). ^{13}C NMR (125 MHz, $\text{DMSO}-d_6$) δ 153.48, 152.17 (d, J = 252.4 Hz), 150.32 (t, J = 5.8 Hz), 149.04, 135.22, 129.75, 128.66, 127.59 (d, J = 7.9 Hz), 123.30, 114.00, 111.27 (d,

$J = 21.5$ Hz), 105.03 (d, $J = 3.8$ Hz), 67.79, 25.71, 19.18. $[M+H]^+$ Calc. mass for $C_{22}H_{17}O_4F_2 = 383.1095$; Found mass = 383.1099.

9-(4-acetyl-2-methylphenyl)-2,7-difluoro-6-hydroxy-3H-xanthen-3-one (Ctrl-AlDeSense). A round-bottom flask was charged with **8** (0.191 g, 0.50 mmol, 1.0 eq.), IBX (0.168 g, 0.6 mmol, 1.2 eq.), and DMSO (5 mL). After stirring for 12 hours at room temperature, the reaction was quenched via the addition of brine (50 mL). The resulting mixture was poured over filter paper and vacuum dried. The crude residue was purified via chromatography on a silica column (5:95 v/v MeOH:CH₂Cl₂) to afford the title compound as a rust-orange solid (0.065 g, 0.171 mmol, 34.1% yield). ¹H NMR (500 MHz, DMSO-*d*₆) δ 8.05 (s, 1H), 7.99 (dd, $J = 7.9$, 1.8 Hz, 1H), 7.42 (d, $J = 7.9$ Hz, 1H), 6.67 (d, $J = 7.1$ Hz, 2H), 6.44 (d, $J = 11.2$ Hz, 2H), 2.67 (s, 3H), 2.11 (s, 3H). ¹³C NMR (125 MHz, DMSO-*d*₆) δ 197.73, 154.14 (t, $J = 5.9$ Hz), 138.17, 136.94, 130.75, 129.93, 126.59, 113.44 (d, $J = 7.8$ Hz), 111.46 (d, $J = 21.8$ Hz), 105.56 (d, $J = 4.4$ Hz), 27.37, 19.51. $[M+H]^+$ Calc. mass for $C_{22}H_{15}O_4F_2 = 381.0938$; Found mass = 381.0934.

((9-(4-acetyl-2-methylphenyl)-2,7-difluoro-3-oxo-3H-xanthen-6-yl)oxy)methyl acetate (Ctrl-AlDeSense AM). A flame-dried round-bottom flask was charged with **Ctrl-AlDeSense** (0.032 g, 0.084 mmol, 1.0 eq.), anhydrous DMF (2.0 mL), bromomethyl acetate (0.017 mL, 0.17 mmol, 2.0 eq.), and Hünig's base (0.029 mL, 0.17 mmol, 2.0 eq.). After stirring for 12 hours at room temperature, all volatiles were removed under vacuum at room temperature. The crude material was purified via column chromatography on a silica column (20:80 v/v EtOAc:CH₂Cl₂) to afford the title compound as an orange solid (0.0281 g, 0.062 mmol, 73.8% yield). ¹H NMR (500 MHz, CDCl₃) δ 7.86 (s, 1H), 7.82 (dd, $J = 7.9$, 1.6 Hz, 1H), 7.16 (d, $J = 6.7$ Hz, 1H), 7.12 (d, $J = 7.9$ Hz, 1H), 6.56 (d, $J = 10.6$ Hz, 1H), 6.44 (d, $J = 6.9$ Hz, 1H), 6.39 (d, $J = 10.4$ Hz, 1H), 5.73 (s, 2H), 2.54 (s, 3H), 2.02 (s, 3H), 1.99 (s, 3H). ¹³C NMR (125 MHz, CDCl₃) δ 197.26, 176.25 (d, $J = 20.8$ Hz), 169.33, 157.45 (d, $J = 1.8$ Hz), 156.82 (d, $J = 269.2$ Hz), 149.85 (d, $J = 249.1$ Hz), 149.65 (d, $J = 13.1$ Hz), 149.35, 147.28 (dd, $J = 10.0$, 2.9 Hz), 138.59, 137.18 – 136.51 (m), 136.50, 130.75, 129.52, 126.57, 118.94 (d, $J = 8.4$ Hz), 114.66 (d, $J = 7.5$ Hz), 113.41 (d, $J = 21.5$ Hz), 109.47 (d, $J = 22.4$ Hz), 107.09 (d, $J = 4.7$ Hz), 104.67, 85.03, 26.77, 20.77, 19.67. $[M+H]^+$ Calc. mass for $C_{25}H_{19}O_6F_2 = 453.1150$; Found mass = 453.1158.

A.2 red-ALDeSense supporting information

This section is adapted from with the permission from *Rational Design of a Red Fluorescent Sensor for ALDH1A1 Displaying Enhanced Cellular Uptake and Reactivity*. Bioconjugate Chem. 2020, 31, 224–228. © 2018 American Chemical Society.

A.2.1 Materials

Thin-layer chromatography (TLC) was performed on 0.25 mm silica-coated TLC plates containing an UV254 fluorescent indicator from Machery-Nagel. Compounds were visualized using a UVP UVGL-25 Compact UV Lamp. Flash chromatography was performed with 230-400 mesh silica gel P60 from SiliCycle Inc. Triethylamine was purchased from Acros Organics. Hydrogen gas was purchased from Airgas. 2-iodobenzoic acid, 4-bromo-3,5-dimethoxybenzaldehyde, and methylboronic acid were purchased from AK Scientific. 2,4-dinitrobenzenesulfonyl chloride and anhydrous pyridine were purchased from Alfa Aesar. 4-bromo-3,5-difluorobenzoic acid was purchased from Arctom. 3-methoxybenzyl alcohol was purchased from ArkPharm. All deuterated solvents were purchased from Cambridge Isotope Laboratories. 1,4-dibromo-2-fluoro-5-methylbenzene was purchased from Santa Cruz Biochemicals. 4-bromo-2,3-difluorobenzoic acid, 4-bromo-3-(trifluoromethyl)benzoic acid, 4-bromo-3-fluorotoluene, and methyl 4-bromo-3-methylbenzoate were purchased from Combi-Blocks. CH₂Cl₂, THF, Et₂O, EtOAc, hexanes, HNO₃, iPrOH, NaHCO₃, toluene, and the Pierce™ BCA Protein Assay Kit were purchased from Thermo Fisher Scientific. Cyclohexane, DMSO, H₂SO₄, MeOH, NaOH, and THF were purchased from Macron. CaCO₃ was purchased from Mallinckrodt Pharmaceuticals. 1,4-dioxane, 2,4,5-trifluorobenzoic acid, 3-bromophenol, Celite®, CuBr₂, dimethylcarbonyl chloride, imidazole, K₃PO₄, methyl iodide, N-bromosuccinimide, N-iodosuccinimide, Na₂S₂O₃, NaBH₄, Oxone®, Pd(dppf)Cl₂, *tert*-butyldimethylsilyl chloride, triethanolamine, and trifluoroacetic acid were purchased from Oakwood Chemical. 1.0 M BH₃-THF in THF, 1.0 M DIBAL-H in CH₂Cl₂, 1.0 M DIBAL-H in hexanes, 1.0 M LiHMDS in THF, 1.4 M *sec*-butyllithium in cyclohexane, 1.7 M *tert*-butyllithium in pentane, 10% w/w Pd/C, 2.5 M *n*-butyllithium in hexanes, 3.0 M methylmagnesium bromide in Et₂O, 4-bromobenzoic acid, AIBN, anhydrous MeCN, dichlorodimethylsilane, DMF, LiAlH₄, *tert*-butyl nitrite, and trypan blue were purchased from MilliporeSigma. 1,4-bis(trifluoromethyl)benzene was purchased from SynQuest Laboratories. Benzylamine was purchased from TCI America. HCl was purchased from

VWR. THF used for anhydrous reactions was dried over activated 4 Å molecular sieves for a minimum of 24 hours. All other chemicals were used as received.

A.2.2 Experimental procedure

pKa determination

Buffers used for pH titrations were glycine (pH = 2.3-3.7), NaOAc (pH = 4.0-5.6), MES (pH = 5.7-6.7), HEPES (pH = 6.9-8.1), and CHES (pH = 8.6-9.5). All buffers were prepared to a concentration of 50 mM in H₂O using aqueous NaOH and HCl to adjust pH. For each condition, 1 μM red-ALDeSense was excited at 594 nm, and an emission spectrum was collected from 600-650 nm. Each condition was performed in triplicate. Data was analyzed using Microsoft Excel.

Expression and purification of ALDH isoforms

Plasmids for ALDH1A1, ALDH1A2, ALDH1A3, ALDH2, ALDH3A1, ALDH4A1, and ALDH4A1 were generously provided by Professor Daria Mochly-Rosen (Stanford). Expression and purification of each isoform was performed as previously described.⁷¹

ALDH isoform selectivity

Each ALDH isoform was added to a 50 mM triethanolamine solution (pH 7.4) containing 2.0 mM NAD⁺ and 100 μM substrate at room temperature. Benzaldehyde was the substrate for ALDH3A1. Propanal was the substrate for all other isoforms. ALDH isoform activity was determined by monitoring the rate of NADH production through the increase in absorbance at 340 nm ($\epsilon = 6220 \text{ M}^{-1}\text{cm}^{-1}$). For these assays, 1 unit is defined as the amount of enzyme that catalyzes the conversion of 1 μM substrate per minute. For every combination of dye and enzyme, 2 μM dye was preincubated with 2.0 mM NAD⁺ in 50 mM triethanolamine solution (pH 7.4). The reaction was initiated by addition of 1 unit of ALDH. Dyes were excited at 590 nm, and fluorescence was measured continuously at 610 nm.

ALDH1A1 kinetics

Solutions were prepared of 2.0 mM NAD⁺ and 0.1-2.5 μM ALDeSense or red-ALDeSense in 50 mM triethanolamine solution (pH 7.4). For every concentration, 1 unit of enzyme (as defined and determined in ALDH Isoform Selectivity) was added. Fluorescence was monitored for 30 seconds to determine V_0 . ALDeSense was excited at 490 nm and monitored at 510 nm. Red-ALDeSense was excited at 590 nm and monitored at 610 nm. Each condition was performed in triplicate. Protein concentration was determined using the Pierce™ BCA Protein Assay Kit. Data was analyzed using Microsoft Excel.

Trypan Blue viability assay

K562 cells were plated in a 96-well plate with 50,000 cells per well. Each well was filled to a final volume of 100 μ L IMDM media with 0.25% DMSO. Wells were tested using red-AIDeSense or Ctrl- red-AIDeSense (1 μ M and 5 μ M each) or using a DMSO control. After 6-, 12-, and 24-hour incubation periods at 37 °C and 5% CO₂, a 10 μ L sample was removed from each condition and combined with 10 μ L 0.4% w/v trypan blue in PBS. Samples were incubated for 3 minutes at room temperature before being loaded on a hemocytometer where live and dead cells were counted. Conditions were tested in triplicate for each time point. Samples were analyzed on an EVOS digital inverted microscope using transmitted white light for brightfield imaging and the Cy5 filter cube for trypan blue visualization.

Cell culture

K562 cells were obtained from Prof. Paul Hergenrother (UIUC). K562 cells were cultured using Iscove's Modified Dulbecco's Medium (IMDM, ATCC) supplemented with 10% fetal bovine serum (FBS, Sigma) and 1% penicillin/streptomycin (pen-strep, Corning). A549 cells were purchased from the American Type Culture Collection (ATCC) and cultured in Dulbecco's Modified Eagle Medium (DMEM, ATCC) supplemented with 10% FBS, 1% pen-strep, and non-essential amino acids. All cells were grown at 37 °C in a humidified incubator with 5% CO₂. For each cell line, media was changed or cells were passaged every 3 days. Passage numbers were kept below 20 for all experiments.

Flow cytometry

For all cell lines, 200,000 cells in a single-cell suspension were transferred into 1.5 mL Eppendorf tubes. Cells were pelleted by centrifugation at 400g for 5 minutes at room temperature. After removing the supernatant by aspiration, cells were resuspended in 300 μ L premixed PBS supplemented with verapamil, probenecid, and novobiocin. For the indicated samples, DEAB (final concentration 20 μ M) was added. Samples were immediately stored on ice. Cells were stained with red-AIDeSense or Ctrl- red-AIDeSense (100 μ L of 4 μ M dye solution; dyes were normalized by fluorescence spectroscopy). Samples were analyzed on a BD LSR II Flow Cytometry Analyzer using a 488 nm laser and a 550 LP and 610/30 filter set. Samples were analyzed every 5 minutes for 15 minutes, with the samples being placed back on ice between data collection. Data were analyzed on FCS Express 6.04.

Confocal imaging

Nunc™ Lab-Tek™ 8-well Chamber Coverglass (Thermo Fisher) were coated with poly-L-lysine (Trevigen). For cells that were also stained with an antibody, 2,000,000 cells were transferred to an Eppendorf tube. The cells were resuspended in 200 μ L of antibody buffer (5% BSA and 1 mg/mL NaN₃ in PBS) and treated with 2 μ L FITC-labeled anti-CD44 antibody (10 mg/mL, Sino Biological) and left on ice for 20 minutes. In all cases, cells were added at 150,000 cells/well to the coated slides 1 hour prior to imaging. Before imaging, the media was aspirated and each chamber was refilled with 300 μ L premixed imaging buffer (100 μ M verapamil, 2.5 mM probenecid, and 200 μ M novobiocin in PBS plus 5% BSA and 1 mg/mL NaN₃ for antibody-stained cells) at room temperature. Cells were treated with 100 μ L red-AIDeSense or Ctrl- red-AIDeSense solution (4 μ M dye in imaging buffer; dyes were normalized by fluorescence spectroscopy) and 0.8 μ L Hoescht 33342 (5 mg/mL in PBS) for 10 minutes. Live cell imaging was performed on a Multiphoton Confocal Microscope Zeiss 710. Hoescht 33342 was excited with a 405 nm laser and detected with a 415-502 filter set. FITC was excited with a 488 nm laser and detected with a 502-561 filter set. Hoescht 33342 was excited with a 594 nm laser and detected with a 600-735 filter set. For each condition, three images were taken for each of four different wells using the 40x objective. The same optical settings were used for images within each set of matched experiments. Images were analyzed using ZEN 3.0 (blue edition) software. Mean fluorescence for the FITC-labeled anti-CD44 antibody was multiplied by the cell diameter to account for its 1-dimensional cell membrane staining, as opposed to 2-dimensional intracellular staining of (Ctrl-)red-AIDeSense. Cells were considered to have high ALDH activity when they had a mean red-AIDeSense fluorescence signal greater than 99% of Ctrl-red-AIDeSense-stained cells.

A.2.3 Synthesis and characterization

A.2.3.1 Synthesis of Si-xanthenes

(3-Bromophenoxy)(*tert*-butyl)dimethylsilane (2-10) A round-bottom flask was charged with 3-bromophenol (8.65 g, 50.0 mmol, 1.0 eq.), *tert*-butyldimethylsilyl chloride (7.9 g, 52 mmol, 1.05 eq.), imidazole (3.6 g, 52 mmol, 1.05 eq.), and CH₂Cl₂ (70 mL). After stirring overnight at room temperature, the reaction was washed sequentially with 1.0 M HCl in H₂O (50 mL) and 1.0 M NaOH in H₂O (50 mL). The organics were collected, dried over Na₂SO₄, and concentrated under reduced pressure to afford the title compound as a colorless oil (13.12 g, 45.7 mmol, 91.3%). ¹H NMR (500 MHz, CDCl₃) δ 7.12 – 7.04 (m, 2H), 7.03 – 6.98 (m, 1H), 6.76 (ddq, *J* = 6.5, 4.2, 2.2

Hz, 1H), 0.98 (s, 9H), 0.20 (s, 6H). ^{13}C NMR (126 MHz, CDCl_3) δ 156.68, 130.55, 124.61, 123.67, 122.61, 118.96, 25.76, 18.33, -4.31.

Bis(3-((*tert*-butyldimethylsilyl)oxy)phenyl)dimethylsilane (2-11) A flame-dried round-bottom flask was charged with **2-10** (13.12 g, 45.7 mmol, 2.0 eq.) and anhydrous THF (25 mL). The reaction was cooled to $-78\text{ }^\circ\text{C}$ and then treated dropwise with 2.5 M *n*-butyllithium in hexanes (18 mL, 45.7 mmol, 2.0 eq.) over 25 minutes. After stirring for an additional hour at $-78\text{ }^\circ\text{C}$, the reaction was treated dropwise with a solution of dimethyldichlorosilane (2.75 mL, 22.8 mmol, 1.0 eq.) in anhydrous THF (15 mL) over 5 minutes via syringe addition. After addition, the reaction was warmed to room temperature and stirred for 2 hours, then poured over sat. NaHCO_3 (50 mL) and diluted with H_2O (50 mL). The organics were collected, dried over Na_2SO_4 , and concentrated. The crude material was purified via flash chromatography on a silica column (0:100 to 2:98 v/v EtOAc:hexanes gradient) to afford the title compound as a colorless oil (7.65 g, 16.2 mmol, 70.8% yield). ^1H NMR (500 MHz, CDCl_3) δ 7.22 (t, $J = 7.6\text{ Hz}$, 2H), 7.09 (dt, $J = 7.3, 1.1\text{ Hz}$, 2H), 6.97 (dd, $J = 2.5, 1.1\text{ Hz}$, 2H), 6.83 (ddd, $J = 8.1, 2.6, 1.1\text{ Hz}$, 2H), 0.97 (s, 18H), 0.51 (s, 6H), 0.16 (s, 12H). ^{13}C NMR (126 MHz, CDCl_3) δ 155.25, 139.87, 129.09, 127.09, 125.71, 120.92, 25.88, 18.39, -2.32, -4.23.

Bis(2-bromo-5-((*tert*-butyldimethylsilyl)oxy)phenyl)dimethylsilane (2-12) A round-bottom flask was charged with **2-11** (1.42 g, 3.0 mmol, 1.0 eq.), anhydrous MeCN (20 mL), and anhydrous pyridine (2.0 mL, 24 mmol, 8.0 eq.). The reaction was treated with *N*-bromosuccinimide (2.35 g, 13 mmol, 4.4 eq.). The reaction was heated to $60\text{ }^\circ\text{C}$ for 24 hours. After cooling to room temperature, the reaction was diluted with Et_2O and EtOAc, then washed sequentially with 1.0 M HCl in H_2O , 1.0 M NaOH in H_2O , and brine. The organics were collected, dried over Na_2SO_4 , and concentrated. The crude material was purified via flash chromatography on a silica column (2:98 v/v EtOAc:hexanes) to afford the title compound as a white solid (1.13 g, 1.79 mmol, 59.8% yield). ^1H NMR (500 MHz, CDCl_3) δ 7.35 (d, $J = 8.5\text{ Hz}$, 2H), 6.91 (d, $J = 3.0\text{ Hz}$, 2H), 6.71 (dd, $J = 8.6, 3.0\text{ Hz}$, 2H), 0.95 (s, 18H), 0.72 (s, 6H), 0.14 (s, 12H). ^{13}C NMR (126 MHz, CDCl_3) δ 154.59, 140.03, 133.90, 128.76, 123.17, 121.41, 25.83, 18.39, -1.07, -4.27.

3,7-Bis((*tert*-butyldimethylsilyl)oxy)-5,5-dimethyldibenzo[b,e]silin-10(5H)-one (2-13) A flame-dried round-bottom flask was charged with **2-12** (3.60 g, 5.7 mmol, 1.0 eq.) and anhydrous THF (50 mL). The reaction was cooled to $-78\text{ }^\circ\text{C}$ and then treated dropwise with 1.7 M *t*-butyllithium in pentane (14 mL, 23.4 mmol, 4.1 eq.) over 10 minutes. After stirring for 30

minutes, the reaction was warmed to 0 °C and treated dropwise with 1.0 M dimethylcarbonyl chloride in THF (11.5 mL, 11.5 mmol, 2.0 eq.) over 40 minutes. The reaction was slowly warmed to room temperature with the melting ice bath. After stirring overnight, the THF was removed *in vacuo*. The crude residue was suspended in CH₂Cl₂ and treated with imidazole (0.82 g, 12 mmol, 2.1 eq.) and *tert*-butyldimethylsilyl chloride (1.9 g, 13 mmol, 2.2 eq.). After stirring overnight, the reaction was washed with H₂O and concentrated. The crude material was purified via flash chromatography on a silica column (0:100 to 2:98 v/v EtOAc:hexanes gradient) to afford the title compound. This was further dissolved in EtOH and triturated with H₂O to afford a white solid (2.16 g, 1.33 mmol, 75.8% yield). ¹H NMR (500 MHz, CDCl₃) δ 8.37 (d, *J* = 8.7 Hz, 2H), 7.04 (d, *J* = 2.5 Hz, 2H), 6.99 (dd, *J* = 8.7, 2.5 Hz, 2H), 1.01 (s, 18H), 0.46 (s, 6H), 0.26 (s, 12H). ¹³C NMR (126 MHz, CDCl₃) δ 186.11, 158.87, 141.31, 134.71, 132.42, 123.85, 121.92, 25.82, 18.47, -1.39, -4.13.

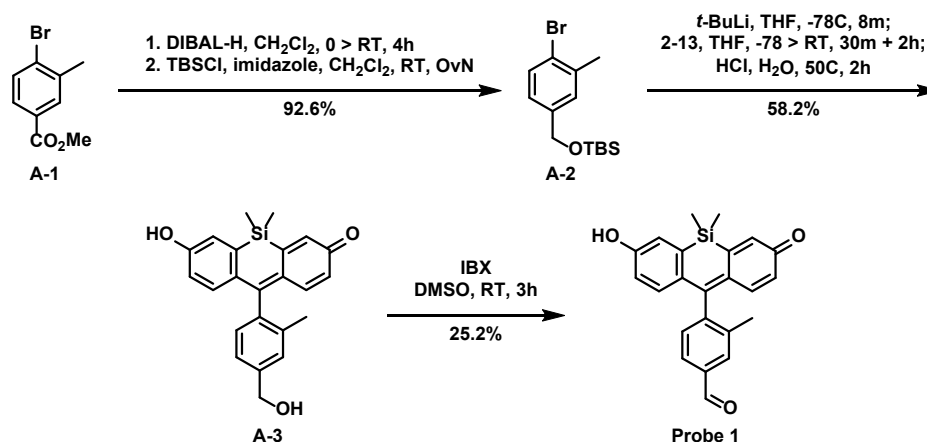
3,7-dihydroxy-5,5-dimethyldibenzo[b,e]silin-10(5H)-one (2-14). A flask was charged with **2-13** (0.950 g, 1.90 mmol, 1.0 eq.), dioxane (10 mL), and 1.0 M HCl in H₂O (2.0 mL). The reaction was heated to 100 °C and stirred overnight. After cooling to room temperature, the product was extracted with 33:67 v/v iPrOH:CH₂Cl₂. The organic layer was collected, washed with H₂O, and concentrated. The crude material was purified via flash chromatography on a silica column (2:98 v/v MeOH:CH₂Cl₂) to afford the title compound (0.456 g, 1.67 mmol, 88.0% yield). ¹H NMR (400 MHz, DMSO-*d*₆) δ 10.32 (s, 2H), 8.17 (d, *J* = 8.8 Hz, 2H), 7.08 (d, *J* = 2.7 Hz, 2H), 6.96 (dd, *J* = 8.7, 2.6 Hz, 2H), 0.41 (s, 6H).

4,6-dichloro-3,7-dihydroxy-5,5-dimethyldibenzo[b,e]silin-10(5H)-one (2-15). A flask was charged with **2-14** (0.106 g, 0.393 mmol, 1.0 eq.), DMF (5 mL), and *N*-chlorosuccinimide (0.131 g, 0.973 mmol, 2.5 eq.). The reaction was heated to 50 °C and stirred overnight. After cooling to room temperature, the product was extracted with 33:67 v/v iPrOH:CH₂Cl₂. The organic layer was collected, washed with H₂O, and concentrated. The crude material was purified via flash chromatography on a silica column (20:80 v/v EtOAc:hexanes) to afford the title compound (0.083 g, 1.67 mmol, 0.245 mmol, 62.4% yield). ¹H NMR (400 MHz, DMSO-*d*₆) δ 8.21 (d, *J* = 8.8 Hz, 2H), 7.22 (d, *J* = 8.7 Hz, 2H), 0.74 (s, 6H).

3,7-bis((*tert*-butyldimethylsilyl)oxy)-4,6-dichloro-5,5-dimethyldibenzo[b,e]silin-10(5H)-one (2-16). A vial was charged with **2-15** (0.022 g, 0.065 mmol, 1.0 eq.), imidazole (0.022 g, 0.324 mmol, 5.0 eq.), and CH₂Cl₂ (3 mL). Once a solution formed, the reaction was treated

with TBSCl (0.049 g, 0.324 mmol, 5.0 eq.). After stirring overnight at room temperature, the reaction was concentrated. The crude material was purified via flash chromatography on a silica column (5:95 to 10:90 v/v EtOAc:hexanes gradient) to afford the title compound. ¹H NMR (500 MHz, Chloroform-*d*) δ 8.35 (d, *J* = 8.7 Hz, 2H), 7.06 (d, *J* = 8.7 Hz, 2H), 1.06 (s, 18H), 0.81 (s, 6H), 0.30 (s, 12H). ¹³C NMR (126 MHz, Chloroform-*d*) δ 185.11, 155.22, 140.68, 134.36, 131.16, 130.80, 121.71, 25.77, 18.57, -1.85, -4.08.

A.2.3.2 Synthesis of Probe 1



Scheme A.1. Synthesis of Probe 1.

((4-Bromo-3-methylbenzyl)oxy)(tert-butyl)dimethylsilane (A-2) A flame-dried round-bottom flask was charged with methyl 4-bromo-3-methylbenzoate (22.9g, 50 mmol, 1.0 eq.) and anhydrous CH₂Cl₂ (100 mL). The reaction was cooled to 0 °C before treating dropwise with 1.0 M DIBAL-H in CH₂Cl₂ (110 mL, 110 mmol, 2.2 eq.) over 23 minutes. After stirring for 30 minutes, the reaction was warmed to room temperature. After 4 hours, the reaction was cooled back to 0 °C before quenching with the sequential addition of H₂O, 1.0 M NaOH in H₂O, and more H₂O. The mixture was filtered. The organics were collected, washed with brine, and concentrated. The crude material was treated with imidazole (6.8 g, 100 mmol, 2.0 eq.) and CH₂Cl₂ (50 mL). Once a solution had formed, *tert*-butyldimethylsilyl chloride (8.2 g, 50 mmol, 1.1 eq.) was added. After stirring overnight at room temperature, the reaction was filtered. The filtrate was washed with aqueous NH₄Cl and concentrated under reduced pressure. The crude material was purified via flash chromatography on a silica column (2:98 v/v EtOAc:hexanes) to afford the title compound as a colorless oil (14.6 g, 46.3 mmol, 92.6% yield). ¹H NMR (500 MHz, CDCl₃) δ 7.47 (d, *J* = 8.1 Hz, 1H), 7.18 (d, *J* = 1.4 Hz, 1H), 7.01 (dd, *J* = 8.2, 2.1 Hz, 1H), 4.66 (s, 2H), 2.39 (s,

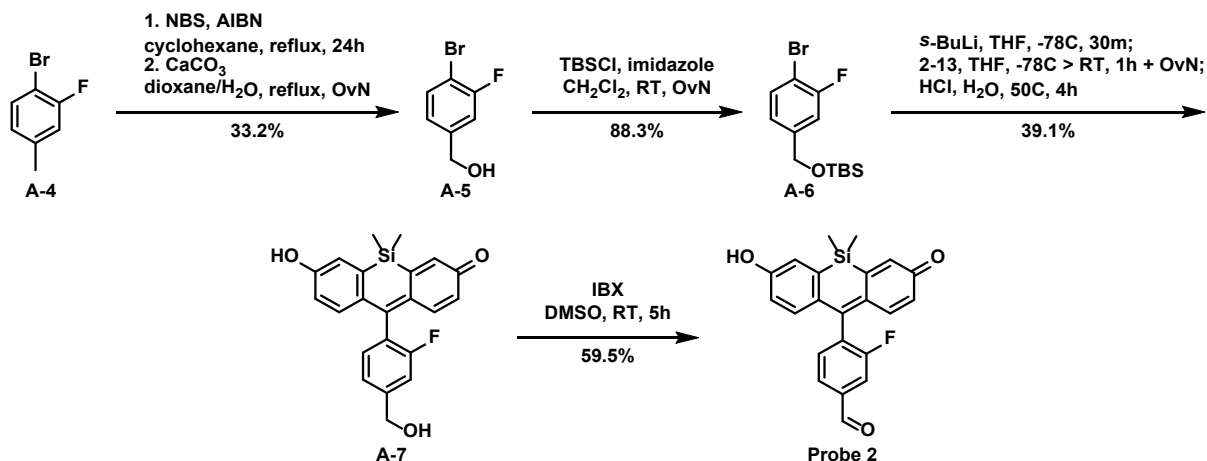
3H), 0.94 (s, 9H), 0.10 (s, 6H). ^{13}C NMR (126 MHz, CDCl_3) δ 140.83, 137.67, 132.23, 128.64, 125.21, 123.16, 64.49, 26.09, 23.08, 18.57, -5.10.

7-Hydroxy-10-(4-(hydroxymethyl)-2-methylphenyl)-5,5-dimethyldibenzo[b,e]silin-3(5H)-one (A-3) A flame-dried round-bottom flask was charged with **A-2** (0.325 g, 1.0 mmol, 10 eq.) and anhydrous THF (5 mL). The reaction was cooled to $-78\text{ }^\circ\text{C}$ and then treated dropwise with 1.7 M *t*-butyllithium in pentane (0.59 mL, 1.0 mmol, 10 eq.) over 1 minute. After stirring for an additional 8 minutes at $-78\text{ }^\circ\text{C}$, the reaction was treated dropwise with a solution of **2-13** (0.051 g, 0.10 mmol, 1.0 eq.) in anhydrous THF (2 mL) over 2 minutes. 30 minutes after addition, the reaction was warmed to room temperature and stirred for 2 hours. The reaction was treated with 1.0 M HCl in H_2O (3 mL, 3.0 mmol, 30 eq.) and heated to $50\text{ }^\circ\text{C}$. After stirring for 2 hours, the reaction was cooled to room temperature. The reaction was diluted with Et_2O and THF and washed with brine. The organics were collected, dried over Na_2SO_4 , and concentrated. The crude material was purified via flash chromatography on a silica column (5:95 v/v $\text{MeOH}:\text{CH}_2\text{Cl}_2$). The crude material was washed with Et_2O to afford the title compound as a red solid (0.0218 g, 0.0582 mmol, 58.2% yield). ^1H NMR (500 MHz, $\text{DMSO}-d_6$) δ 7.33 (d, $J = 1.5\text{ Hz}$, 1H), 7.29 (dd, $J = 7.8, 1.6\text{ Hz}$, 1H), 7.07 (d, $J = 7.7\text{ Hz}$, 1H), 7.00 (s, 2H), 6.76 (d, $J = 9.5\text{ Hz}$, 2H), 6.43 (d, $J = 7.8\text{ Hz}$, 2H), 5.29 (s, 1H), 4.57 (s, 2H), 1.98 (s, 3H), 0.46 (s, 3H), 0.44 (s, 3H). ^{13}C NMR (126 MHz, $\text{DMSO}-d_6$) δ 156.30, 143.67, 142.55, 138.07, 137.45, 134.98, 129.14, 128.84, 128.09, 123.98, 122.02, 62.66, 19.08, -1.28, -1.61. HRMS (ESI $^+$): m/z calculated for $[\text{M}+\text{H}]^+ = 375.1411$; found = 375.1411.

4-(7-Hydroxy-5,5-dimethyl-3-oxo-3,5-dihydrodibenzo[b,e]silin-10-yl)-3-methylbenzaldehyde (Probe 1) A round-bottom flask was charged with **A-3** (0.0187 g, 0.050 mmol, 1.0 eq.), 2-iodoxybenzoic acid (0.0169 g, 0.060 mmol, 1.2 eq.), and DMSO (1 mL). After stirring 3 hours at room temperature, the reaction was quenched with brine and filtered. The filtrate was extracted from with 33:67 v/v $i\text{PrOH}:\text{CH}_2\text{Cl}_2$. The organics were combined with the precipitate and purified via flash chromatography on a silica column (0:100 to 5:95 v/v $i\text{PrOH}:\text{CH}_2\text{Cl}_2$ gradient). The resultant solid purified via flash chromatography on a silica column (Et_2O) to afford the title compound as a red solid (0.0047 g, 0.0126 mmol, 25.2% yield). ^1H NMR (500 MHz, CDCl_3) δ 10.09 (s, 1H), 7.86 (s, 1H), 7.85 (dd, $J = 7.6, 1.5\text{ Hz}$, 1H), 7.31 (d, $J = 7.7\text{ Hz}$, 1H), 7.06 (d, $J = 2.4\text{ Hz}$, 2H), 6.81 (d, $J = 9.5\text{ Hz}$, 2H), 6.52 (dd, $J = 9.4, 2.4\text{ Hz}$, 2H), 2.15 (s, 3H), 0.48 (s, 3H), 0.47 (s, 3H). ^{13}C NMR (126 MHz, CDCl_3) δ 191.92, 146.01, 145.13, 138.97,

137.63, 136.51, 131.37, 130.31, 130.15, 129.51, 127.46, 122.56, 19.60, -1.12, -1.34. HRMS (ESI⁺): m/z calculated for $[M+H]^+ = 373.1254$; found = 373.1259.

A.2.3.3 Synthesis of Probe 2



Scheme A.2. Synthesis of Probe 2.

(4-Bromo-3-fluorophenyl)methanol (A-5) A flame-dried round-bottom flask was charged with 4-bromo-3-fluorotoluene (0.67 mL, 5.3 mmol, 1.0 eq.), *N*-bromosuccinimide (1.04 g, 5.8 mmol, 1.1 eq.), AIBN (0.086 g, 0.53 mmol, 0.1 eq.), and cyclohexane (20 mL). The reaction was heated to reflux. After stirring for 24 hours, the reaction was cooled to RT and concentrated *in vacuo*. The crude material treated with dioxane (10 mL), H₂O (10 mL), and CaCO₃ (1.59 g, 16 mmol, 3.0 eq.). The reaction was heated to reflux. After stirring overnight, the reaction was cooled to room temperature and concentrated *in vacuo*. The crude material was purified via flash chromatography on a silica column (5:95 to 30:70 v/v EtOAc:hexanes gradient) to afford the title compound as a colorless oil (0.360 g, 1.76 mmol, 33.2% yield). ¹H NMR (500 MHz, CDCl₃) δ 7.46 (t, *J* = 7.5 Hz, 1H), 7.08 (d, *J* = 9.1 Hz, 1H), 6.94 (d, *J* = 7.7 Hz, 1H), 4.57 (s, 2H). ¹³C NMR (126 MHz, CDCl₃) δ 159.12 (d, *J* = 247.4 Hz), 142.75 (d, *J* = 6.8 Hz), 133.47, 123.34 (d, *J* = 3.4 Hz), 114.71 (d, *J* = 22.6 Hz), 107.62 (d, *J* = 20.9 Hz), 63.74. ¹⁹F NMR (471 MHz, CDCl₃) δ -107.22 (dd, *J* = 9.2, 7.4 Hz).

((4-Bromo-3-fluorobenzyl)oxy)(tert-butyl)dimethylsilane (A-6) A round-bottom flask was charged with **A-5** (0.360 g, 1.76 mmol, 1.0 eq.), imidazole (0.135 g, 1.9 mmol, 1.1 eq.), and CH₂Cl₂ (20 mL). Once a solution had formed, *tert*-butyldimethylsilyl chloride (0.35 g, 2.3 mmol, 1.3 eq.) was added. After stirring overnight at room temperature, the reaction was poured through filter paper. The filtrate was purified via flash chromatography on a silica column (0:100 to 5:95

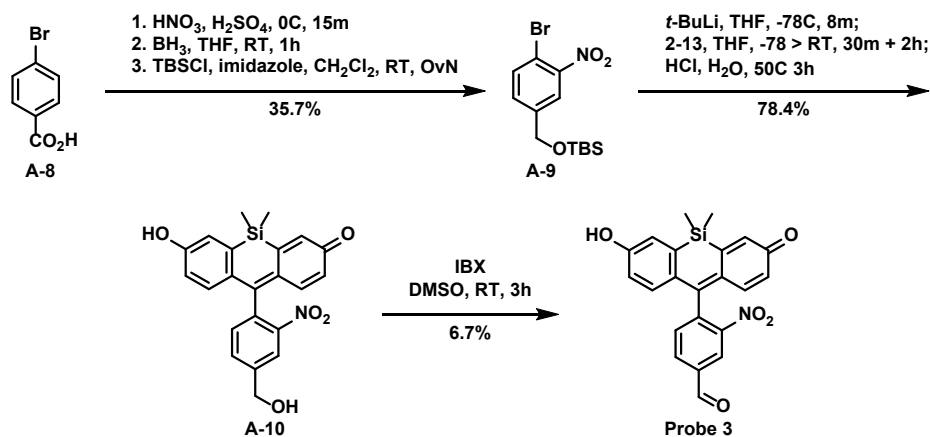
v/v EtOAc:hexanes gradient) to afford the title compound as a colorless oil (0.490 g, 1.55 mmol, 88.3% yield). ¹H NMR (500 MHz, CDCl₃) δ 7.48 (dd, *J* = 8.2, 7.0 Hz, 1H), 7.12 (d, *J* = 9.6 Hz, 1H), 6.96 (d, *J* = 8.2 Hz, 1H), 4.68 (s, 2H), 0.94 (s, 9H), 0.10 (s, 6H). ¹³C NMR (126 MHz, CDCl₃) δ 159.25 (d, *J* = 247.1 Hz), 143.72 (d, *J* = 6.3 Hz), 133.27, 122.61 (d, *J* = 3.6 Hz), 114.17 (d, *J* = 22.7 Hz), 106.95 (d, *J* = 21.1 Hz), 63.93 (d, *J* = 1.7 Hz), 26.04, 18.52, -5.16 ¹⁹F NMR (471 MHz, CDCl₃) δ -107.75 (dd, *J* = 9.5, 7.0 Hz).

10-(2-Fluoro-4-(hydroxymethyl)phenyl)-7-hydroxy-5,5-dimethyldibenzo[b,e]silin-3(5H)-one (A-7) A flame-dried round-bottom flask was charged with **A-6** (0.095 g, 0.60 mmol, 6.0 eq.) and anhydrous THF (10 mL). The reaction was cooled to -78 °C and then treated dropwise with 1.4 M *s*-butyllithium in cyclohexane (0.46 mL, 0.60 mmol, 6.0 eq.) over 1 minute. After stirring for an additional 30 minutes at -78 °C, the reaction was treated dropwise with a solution of **2-13** (0.052 g, 0.10 mmol, 1.0 eq.) in anhydrous THF (3 mL) over 3 minutes. 1 hour after addition, the reaction was transferred to an ice bath. The reaction was stirred overnight in the melting ice bath before being treated with 1.0 M HCl in H₂O (4.0 mL, 4.0 mmol, 40 eq.) and heated to 50 °C. After stirring for 4 hours, the reaction was cooled to room temperature and quenched with H₂O. The THF was removed *in vacuo*. The resulting mixture was extracted from with 33:67 v/v iPrOH:CH₂Cl₂. The organics were collected, dried over Na₂SO₄, and concentrated. The crude material was purified via flash chromatography on a silica column (0:100 to 5:95 v/v MeOH:CH₂Cl₂ gradient). The resulting solid was washed with CH₂Cl₂ to afford the title compound as a red solid (0.0148 g, 0.0391 mmol, 39.1% yield). ¹H NMR (500 MHz, DMSO-*d*₆) δ 10.54 (s, 1H), 7.32 (d, *J* = 9.0 Hz, 2H), 7.28 (t, *J* = 7.5 Hz, 1H), 7.03 (s, 2H), 6.85 (d, *J* = 8.4 Hz, 2H), 6.49 (s, 2H), 5.45 (s, 1H), 4.63 (s, 2H), 0.46 (s, 3H), 0.45 (s, 3H). ¹³C NMR (126 MHz, DMSO-*d*₆) δ 158.76 (d, *J* = 243.1 Hz), 149.83, 146.30 (d, *J* = 6.8 Hz), 131.99 – 129.79 (m), 124.70 (d, *J* = 17.3 Hz), 122.26 (d, *J* = 2.5 Hz), 113.20 (d, *J* = 21.8 Hz), 62.01, -1.29, -1.55. ¹⁹F NMR (471 MHz, DMSO-*d*₆) δ -115.72 (dd, *J* = 9.4, 7.7 Hz). HRMS (ESI⁺): *m/z* calculated for [M+H]⁺ = 379.1160; found = 379.1162.

3-Fluoro-4-(7-hydroxy-5,5-dimethyl-3-oxo-3,5-dihydrodibenzo[b,e]silin-10-yl)benzaldehyde (Probe 2) A round-bottom flask was charged with **A-7** (0.0078 g, 0.021 mmol, 1.0 eq.), 2-iodoxybenzoic acid (0.0068 g, 0.025 mmol, 1.2 eq.), and DMSO (0.5 mL). After stirring 5 hours at room temperature, the reaction was quenched with brine. The mixture was chilled and filtered. The filtrate was extracted from with 33:67 iPrOH:CH₂Cl₂. + organics were combined with

the precipitate and concentrated. The crude material was purified via flash chromatography on a silica column (0:100 to 2:98 v/v iPrOH:CH₂Cl₂ gradient) to afford the title compound as a red solid (0.0046 g, 0.012 mmol, 59.5% yield). ¹H NMR (400 MHz, DMSO-*d*₆) δ 10.62 (s, 1H), 10.12 (s, 1H), 7.95 (dd, *J* = 7.7, 1.3 Hz, 1H), 7.93 (d, *J* = 8.9 Hz, 1H), 7.63 (t, *J* = 7.3 Hz, 1H), 7.27 – 7.19 (m, 1H), 6.93 – 6.79 (m, 2H), 6.79 – 6.68 (m, 2H), 6.25 – 6.07 (m, 1H), 0.47 (s, 3H), 0.46 (s, 3H). ¹⁹F NMR (376 MHz, DMSO-*d*₆) δ -114.38 (t, *J* = 8.2 Hz). HRMS (ESI⁺): *m/z* calculated for [M+H]⁺ = 377.1004; found = 377.1025.

A.2.3.4 Synthesis of Probe 3



Scheme A.3. Synthesis of Probe 3.

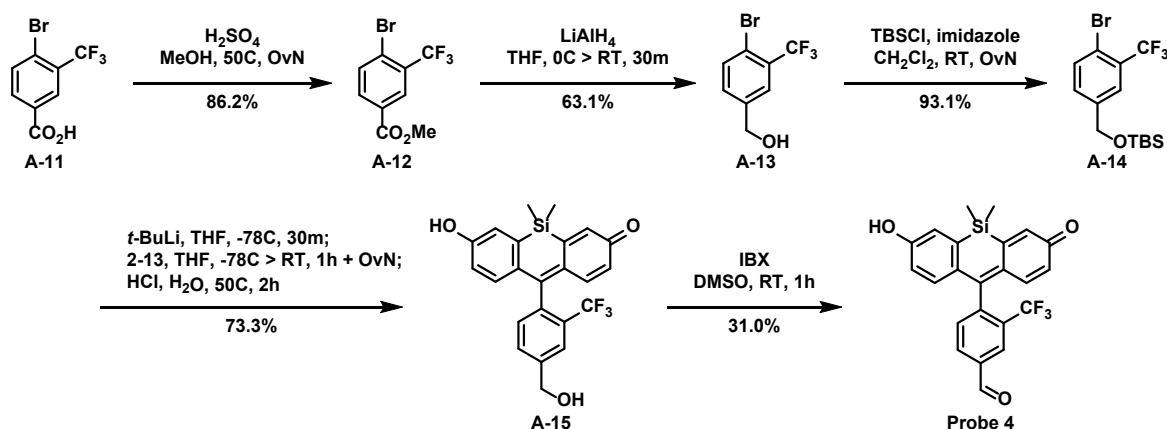
((4-Bromo-3-nitrobenzyl)oxy)(tert-butyl)dimethylsilane (A-9) A round-bottom flask was charged with 4-bromobenzoic acid (1.04 g, 5.62 mmol, 1.0 eq.) and H₂SO₄ (20 mL). The reaction was cooled to 0 °C and the treated dropwise with a solution of HNO₃ (0.25 mL, 5.9 mmol, 1.05 eq.) in H₂SO₄ (3 mL) over 4 minutes. After stirring for 15 minutes at 0 °C, the reaction poured over ice. Product was extracted with EtOAc, dried over Na₂SO₄, and concentrated. The white solid was dissolved in anhydrous THF. While stirring at room temperature, the reaction was treated dropwise with 1.0 M BH₃·THF in THF (17 mL, 17 mmol, 3.3 eq.) over 30 seconds. After stirring for 1 hour, the reaction was quenched by slow addition of 1.0 M NaOH in H₂O. The mixture was diluted with Et₂O. The organics were collected, dried over Na₂SO₄, and concentrated. The crude residue was treated with imidazole (0.36 g, 5.4 mmol, 1.0 eq.), and CH₂Cl₂ (10 mL). Once a solution had formed, *tert*-butyldimethylsilyl chloride (0.82 g, 5.4 mmol, 1.0 eq.) was added. After stirring overnight at room temperature, the reaction was filtered. The crude filtrate was purified via flash chromatography on a silica column (2:98 to 5:95 v/v EtOAc:hexanes gradient) to afford

the title compound as a yellow oil (0.695 g, 2.01 mmol, 35.7% yield). ^1H NMR (500 MHz, CDCl_3) δ 7.81 (dd, $J = 2.0, 0.9$ Hz, 1H), 7.68 (d, $J = 8.2$ Hz, 1H), 7.37 (ddd, $J = 8.2, 2.0, 0.9$ Hz, 1H), 4.74 (s, 2H), 0.94 (s, 9H), 0.12 (s, 6H). ^{13}C NMR (126 MHz, CDCl_3) δ 149.91, 143.04, 134.88, 130.51, 123.02, 112.39, 63.44, 26.00, 18.49, -5.19.

7-Hydroxy-10-(4-(hydroxymethyl)-2-nitrophenyl)-5,5-dimethyldibenzo[b,e]silin-3(5H)-one (A-10) A flame-dried round-bottom flask was charged with **A-9** (0.345 g, 1.0 mmol, 10 eq.) and anhydrous THF (5 mL). The reaction was cooled to -78°C and then treated dropwise with 1.7 M *t*-butyllithium in pentane (0.60 mL, 1.0 mmol, 10 eq.) over 1 minute. After stirring for an additional 8 minutes at -78°C , the reaction was treated dropwise with a solution of **2-13** (0.050 g, 0.10 mmol, 1.0 eq.) in anhydrous THF (2 mL) over 30 seconds. 30 minutes after addition, the reaction was warmed to room temperature and stirred for 2 hours. The reaction was treated with 1.0 M HCl in H_2O (3 mL, 3.0 mmol, 30 eq.) and heated to 50°C . After stirring for 3 hours, the reaction was cooled to room temperature. The reaction was diluted with CH_2Cl_2 and THF and washed with brine. The organics were collected, dried over Na_2SO_4 , and concentrated. The crude material was purified via flash chromatography on a silica column 5:95 to 10:90 v/v iPrOH: CH_2Cl_2 gradient). The crude material was washed with CH_2Cl_2 to afford the title compound as a red solid (0.0318 g, 0.0784 mmol, 78.4% yield). ^1H NMR (500 MHz, $\text{DMSO}-d_6$) δ 10.51 (s, 1H), 8.28 (s, 1H), 7.85 (d, $J = 8.5$ Hz, 1H), 7.48 (d, $J = 7.8$ Hz, 1H), 7.02 (s, 2H), 6.69 (d, $J = 9.3$ Hz, 2H), 6.43 (s, 2H), 5.65 (s, 1H), 4.74 (s, 2H), 0.50 (s, 3H), 0.44 (s, 3H). ^{13}C NMR (126 MHz, $\text{DMSO}-d_6$) δ 152.56, 147.71, 145.49, 132.72, 131.93, 131.80, 122.20, 61.58, -1.05, -2.19.

4-(7-Hydroxy-5,5-dimethyl-3-oxo-3,5-dihydrodibenzo[b,e]silin-10-yl)-3-nitrobenzaldehyde (Probe 3) A round-bottom flask was charged with **A-10** (0.0164 g, 0.040 mmol, 1.0 eq.), 2-iodoxybenzoic acid (0.0138 g, 0.049 mmol, 1.2 eq.), and DMSO (1 mL). After stirring 3 hours at room temperature, the reaction was concentrated under reduced pressure. The crude material was purified via flash chromatography on a silica column (5:95 v/v iPrOH: CH_2Cl_2). The resultant solid was washed with CH_2Cl_2 to afford the title compound as a red solid (0.0011 g, 0.0027 mmol, 6.7% yield). ^1H NMR (500 MHz, $\text{DMSO}-d_6$) δ 10.60 (s, 1H), 8.72 (s, 1H), 8.37 (d, $J = 7.9$ Hz, 1H), 7.63 (d, $J = 7.9$ Hz, 1H), 7.23 (s, 1H), 6.71 (s, 4H), 6.14 (s, 1H), 0.49 (s, 3H), 0.44 (s, 3H). HRMS (ESI^+): m/z calculated for $[\text{M}+\text{H}]^+ = 404.0949$; found = 404.0963.

A.2.3.5 Synthesis of Probe 4



Scheme A.4. Synthesis of Probe 4.

Methyl 4-bromo-3-(trifluoromethyl)benzoate (A-12) A round-bottom flask was charged with 4-bromo-3-(trifluoromethyl)benzoic acid (1.35 g, 5.0 mmol, 1.0 eq.), MeOH (10 mL), and conc. H_2SO_4 (0.5 mL). The reaction was heated to 50 °C. After stirring overnight, the reaction was neutralized with saturated NaHCO_3 . The resulting mixture was poured through filter paper. The precipitate was further washed with H_2O and dried to afford the title compound as an off-white solid (1.22 g, 4.3 mmol, 86.2% yield). ^1H NMR (500 MHz, CDCl_3) δ 8.34 (d, $J = 2.1$ Hz, 1H), 8.03 (dd, $J = 8.3, 2.1$ Hz, 1H), 7.80 (d, $J = 8.3$ Hz, 1H), 3.95 (s, 3H). ^{13}C NMR (126 MHz, CDCl_3) δ 165.32, 135.47, 133.75, 130.78 (q, $J = 32.1$ Hz), 129.72, 129.06 (q, $J = 5.4$ Hz), 125.58 (q, $J = 2.0$ Hz), 122.64 (q, $J = 273.7$ Hz), 52.83. ^{19}F NMR (471 MHz, CDCl_3) δ -62.94.

(4-Bromo-3-(trifluoromethyl)phenyl)methanol (A-13) A flame-dried round-bottom flask was charged with A-12 (0.283 g, 1.0 mmol, 1.0 eq.) and anhydrous THF (10 mL). The reaction was cooled to 0 °C before treating with LiAlH_4 (0.038 g, 1.0 mmol, 1.0 eq.) portionwise over 1 minute. After effervescence ceased, the reaction was warmed to room temperature. After 30 minutes, the reaction was cooled to 0 °C and quenched via the sequential addition of H_2O (2 mL), 1.0 M NaOH in H_2O (2 mL), and more H_2O (2 mL). The mixture was diluted with CH_2Cl_2 and filtered. The organics were collected, dried over Na_2SO_4 , and concentrated. The crude residue was recrystallized in hexanes to afford the title compound as a white crystalline solid (0.161 g, 0.631 mmol, 63.1% yield). ^1H NMR (500 MHz, CDCl_3) δ 7.69 (s, 1H), 7.68 (d, $J = 7.5$ Hz, 1H), 7.38 (d, $J = 7.4$ Hz, 1H), 4.71 (s, 2H), 1.96 (s, 1H). ^{13}C NMR (126 MHz, CDCl_3) δ 140.55, 135.16, 131.22, 130.37 (q, $J = 31.2$ Hz), 126.22 (q, $J = 5.4$ Hz), 123.01 (q, $J = 273.4$ Hz), 118.88 (q, $J = 2.0$ Hz), 64.02. ^{19}F NMR (471 MHz, CDCl_3) δ -62.66.

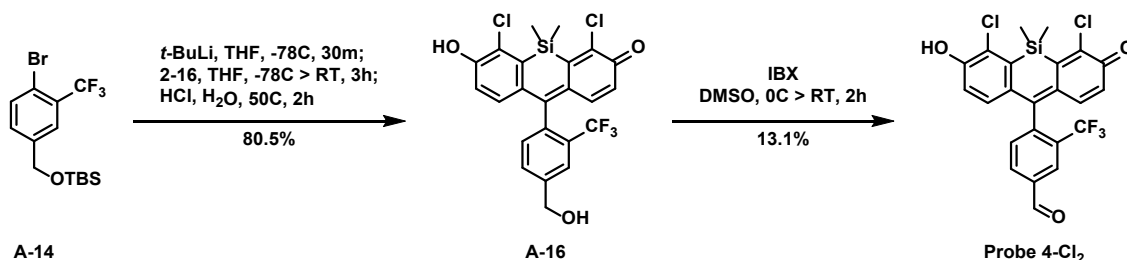
((4-Bromo-3-(trifluoromethyl)benzyl)oxy)(*tert*-butyl)dimethylsilane (A-14) A round-bottom flask was charged with **A-13** (0.161 g, 0.63 mmol, 1.0 eq.), imidazole (0.055 g, 0.77 mmol, 1.2 eq.), and CH₂Cl₂ (10mL). Once a solution had formed, *tert*-butyldimethylsilyl chloride (0.134 g, 0.89 mmol, 1.4 eq.) was added. After stirring overnight at room temperature, the reaction was washed with H₂O. The organics were collected and concentrated under reduced pressure. The crude material was purified via flash chromatography on a silica column (2:98 v/v EtOAc:hexanes) to afford the title compound as a colorless oil (0.217 g, 0.588 mmol, 93.1% yield). ¹H NMR (500 MHz, CDCl₃) δ 7.66 (d, *J* = 7.8 Hz, 1H), 7.66 (s, 1H), 7.34 (d, *J* = 8.3 Hz, 1H), 4.72 (s, 2H), 0.95 (s, 9H), 0.11 (s, 6H). ¹³C NMR (126 MHz, CDCl₃) δ 141.44, 134.86, 130.42, 130.05 (q, *J* = 31.0 Hz), 125.44 (q, *J* = 5.5 Hz), 123.13 (q, *J* = 273.3 Hz), 118.04 (q, *J* = 1.9 Hz), 63.87, 26.00, 18.50, -5.18. ¹⁹F NMR (471 MHz, CDCl₃) δ -62.64.

7-Hydroxy-10-(4-(hydroxymethyl)-2-(trifluoromethyl)phenyl)-5,5-dimethyldibenzo[b,e]silin-3(5H)-one (A-15) A flame-dried round-bottom flask was charged with **A-14** (.367 g, 1.0 mmol, 10 eq.) and anhydrous THF (5 mL). The reaction was cooled to -78 °C and then treated dropwise with 1.7 M *t*-butyllithium in pentane (0.6 mL, 1.0 mmol, 10 eq.) over 1 minute. After stirring for an additional 8 minutes at -78 °C, the reaction was treated dropwise with a solution of **2-13** (.050 g, 0.10 mmol, 1.0 eq.) in anhydrous THF (2 mL) over 30 seconds. After 30 more minutes at -78 °C, the reaction was warmed to room temperature and stirred for 2 hours. The reaction was treated with 1.0 M HCl in H₂O (3 mL, 3 mmol, 30 eq.) and heated to 50 °C. After stirring overnight, the reaction was cooled to room temperature and quenched with brine and diluted with 33:67 v/v iPrOH:CH₂Cl₂. The organics were collected, dried over Na₂SO₄, and concentrated. The crude material was purified via flash chromatography on a silica column (10:90 v/v MeOH:CH₂Cl₂). The crude residue was suspended in Et₂O and filtered. The precipitate was dried under vacuum to afford the title compound as a red solid (0.0314 g, 0.0733 mmol, 73.3% yield). ¹H NMR (500 MHz, DMSO-*d*₆) δ 10.50 (s, 1H), 7.87 (d, *J* = 1.6 Hz, 1H), 7.74 (dd, *J* = 8.2, 1.4 Hz, 1H), 7.39 (d, *J* = 7.8 Hz, 1H), 7.19 (s, 1H), 6.83 (s, 1H), 6.69 (d, *J* = 11.9 Hz, 2H), 6.56 (d, *J* = 8.8 Hz, 1H), 6.13 (d, *J* = 8.8 Hz, 1H), 5.53 (t, *J* = 5.7 Hz, 1H), 4.70 (d, *J* = 5.6 Hz, 2H), 0.50 (s, 3H), 0.39 (s, 3H). ¹³C NMR (126 MHz, DMSO-*d*₆) δ 182.83, 159.24, 152.50, 146.66, 143.93, 140.94, 139.98, 136.36, 135.81, 135.54, 131.87, 131.40, 130.15, 127.61, 127.25 (q, *J* = 29.5 Hz), 126.80, 124.01 (q, *J* = 4.6 Hz), 123.99 (q, *J* = 274.6 Hz), 121.81, 116.90, 61.92, -0.84, -

2.47. ^{19}F NMR (471 MHz, $\text{DMSO-}d_6$) δ -57.90. HRMS (ESI^+): m/z calculated for $[\text{M}+\text{H}]^+ = 429.1128$; found = 429.1129.

4-(7-Hydroxy-5,5-dimethyl-3-oxo-3,5-dihydrodibenzo[b,e]silin-10-yl)-3-(trifluoromethyl)benzaldehyde (Probe 4) A round-bottom flask was charged with **A-15** (0.0269 g, 0.063 mmol, 1.0 eq.), 2-iodoxybenzoic acid (0.021 g, 0.075 mmol, 1.2 eq.), and DMSO (3 mL). After stirring 1 hour at room temperature, the reaction was quenched with brine. The resulting mixture was poured through over filter paper. The precipitate was purified via flash chromatography on a silica column (2:98 to 10:90 v/v $\text{MeOH}:\text{CH}_2\text{Cl}_2$ gradient) to afford the title compound as a red solid (0.0083 g, 0.019 mmol, 31.0% yield). ^1H NMR (500 MHz, $\text{DMSO-}d_6$) δ 10.55 (s, 1H), 10.21 (s, 1H), 8.46 (d, $J = 1.4$ Hz, 1H), 8.32 (dd, $J = 7.8, 1.5$ Hz, 1H), 7.72 (d, $J = 7.8$ Hz, 1H), 7.21 (s, 1H), 6.86 (s, 1H), 6.71 (d, $J = 8.0$ Hz, 1H), 6.67 (d, $J = 9.5$ Hz, 1H), 6.52 (d, $J = 8.8$ Hz, 1H), 6.13 (d, $J = 10.2$ Hz, 1H), 0.51 (s, 3H), 0.40 (s, 3H). ^{19}F NMR (471 MHz, $\text{DMSO-}d_6$) δ -58.37. HRMS (ESI^+): m/z calculated for $[\text{M}+\text{H}]^+ = 427.0972$; found = 427.0977.

A.2.3.6 Synthesis of Probe 4-Cl₂



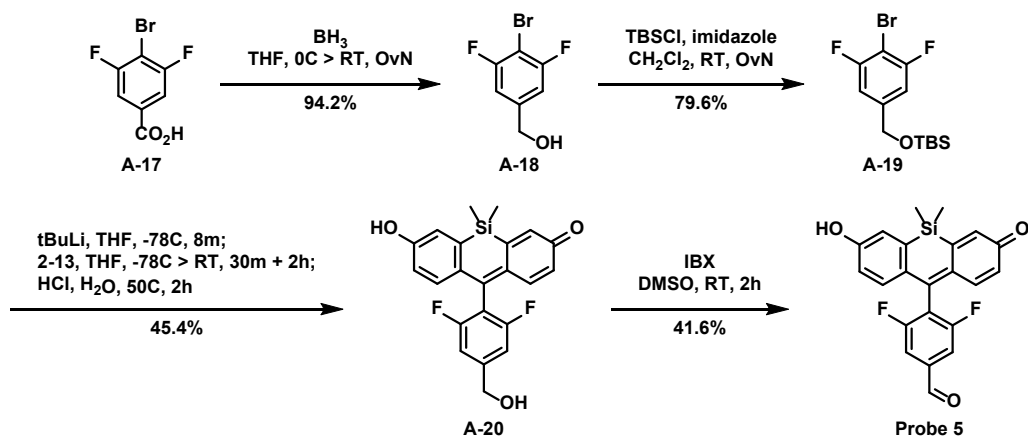
Scheme A.5. Synthesis of Probe 4-Cl₂.

4,6-dichloro-7-hydroxy-10-(4-(hydroxymethyl)-2-(trifluoromethyl)phenyl)-5,5-dimethyldibenzo[b,e]silin-3(5H)-one (A-16). A flame-dried round-bottom flask was charged with **A-14** (.140 g, 0.38 mmol, 10 eq.) and anhydrous THF (5 mL). The reaction was cooled to -78 °C and then treated dropwise with 1.7 M *t*-butyllithium in pentane (0.24 mL, 0.38 mmol, 10 eq.). After stirring for 30 minutes at -78 °C, the reaction was treated dropwise with a solution of **2-13** (.022 g, 0.038 mmol, 1.0 eq.) in anhydrous THF (5 mL). The reaction was warmed to room temperature and stirred for 3 hours. The reaction was treated with 1.0 M HCl in H_2O (2 mL) and heated to 50 °C. After 2 hours, the reaction was cooled to room temperature and quenched with brine and diluted with 33:67 v/v $\text{iPrOH}:\text{CH}_2\text{Cl}_2$. The organics were collected, dried over Na_2SO_4 , and concentrated. The crude material was purified via flash chromatography on a silica column (2:98 v/v $\text{MeOH}:\text{CH}_2\text{Cl}_2$) to afford the title compound (0.0153 g, 0.0308 mmol, 80.5% yield). ^1H

NMR (400 MHz, Methanol-*d*₄) δ 7.91 (d, *J* = 1.6 Hz, 1H), 7.76 (d, *J* = 7.5 Hz, 1H), 7.35 (d, *J* = 7.9 Hz, 1H), 6.77 (d, *J* = 9.4 Hz, 2H), 6.56 (d, *J* = 9.4 Hz, 2H), 4.80 (s, 2H), 0.88 (s, 3H), 0.85 (s, 3H). ¹⁹F NMR (376 MHz, Methanol-*d*₄) δ -60.81.

4-(4,6-dichloro-7-hydroxy-5,5-dimethyl-3-oxo-3,5-dihydrodibenzo[b,e]silin-10-yl)-3-(trifluoromethyl)benzaldehyde (Probe 4-Cl₂). A vial was charged with **A-16** (0.0123 g, 0.024 mmol, 1.0 eq.) and DMSO (2 mL). The solution was cooled in an ice bath until a slurry started to form. At this point, the reaction was treated with IBX (0.0083 g, 0.03 mmol, 1.2 eq.) and warmed back to room temperature. After stirring for 2 hours, the DMSO was blown off with air. The crude material was purified via flash chromatography on a silica column (2:98 v/v iPrOH:CH₂Cl₂) to afford the title compound (0.0016 g, 0.0032 mmol, 13.1% yield).

A.2.3.7 Synthesis of Probe 5



Scheme A.6. Synthesis of Probe 5.

(4-Bromo-3,5-difluorophenyl)methanol (A-18) A round-bottom flask was charged with 4-bromo-3,5-difluorobenzoic acid (0.234 g, 1.0 mmol, 1.0 eq.) and anhydrous THF (10 mL). The solution was cooled to 0 °C and then treated dropwise with 1.0 M BH₃-THF in THF (3.0 mL, 3.0 mmol, 3.0 eq.) over 3 minutes. The reaction was removed from the cold bath. After stirring at room temperature overnight, the reaction was cooled to 0 °C and quenched with H₂O. The THF was removed under reduced pressure. Product was extracted with EtOAc. The organics were collected, washed with brine, dried over Na₂SO₄, and concentrated. The crude material was purified via flash chromatography on a silica column (25:75 to 50:50 v/v EtOAc:hexanes gradient) to afford the title compound as a white solid (0.210 g, 0.942 mmol, 94.2% yield). ¹H NMR (500 MHz, CDCl₃) δ 6.97 (d, *J* = 7.0 Hz, 2H), 4.67 (s, 2H), 1.91 (s, 1H). ¹³C NMR (126 MHz, CDCl₃)

δ 160.13 (dd, J = 249.2, 4.5 Hz), 143.27 (t, J = 8.1 Hz), 111.98 – 108.81 (m), 96.48 (t, J = 24.5 Hz), 63.78 (t, J = 2.0 Hz). ^{19}F NMR (471 MHz, CDCl_3) δ -105.06 (d, J = 7.1 Hz).

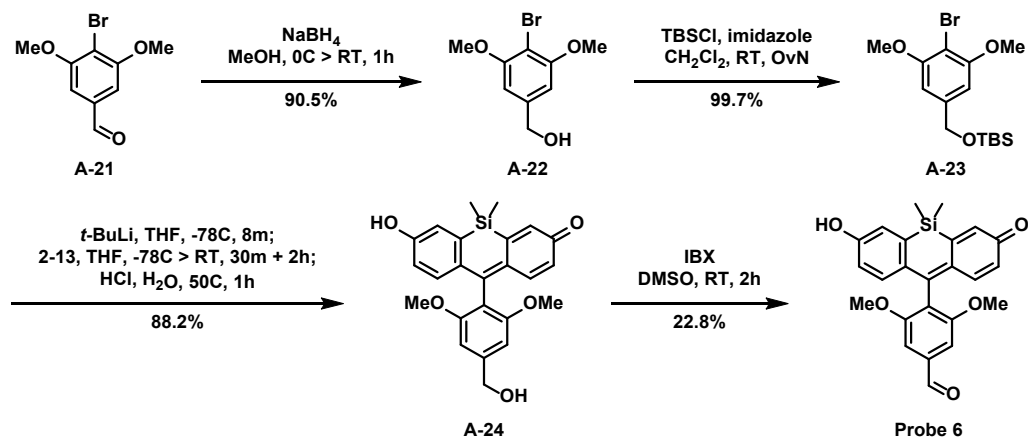
((4-Bromo-3,5-difluorobenzyl)oxy)(tert-butyl)dimethylsilane (A-19) A round-bottom flask was charged with **A-18** (0.492 g, 2.21 mmol, 1.0 eq.) imidazole (0.165 g, 2.4 mmol, 1.1 eq.) and CH_2Cl_2 (10 mL). Once a solution had formed, *tert*-butyldimethylsilyl chloride (0.365 g, 2.4 mmol, 1.1 eq.) was added. After stirring overnight at room temperature, the reaction was filtered. The filtrate was washed with 1.0 M HCl in H_2O , dried over Na_2SO_4 , and concentrated under reduced pressure to afford the title compound as a colorless oil (0.592 g, 1.76 mmol, 79.6% yield). ^1H NMR (500 MHz, CDCl_3) δ 6.93 (d, J = 7.8 Hz, 2H), 4.67 (s, 2H), 0.94 (s, 9H), 0.11 (s, 6H). ^{13}C NMR (126 MHz, CDCl_3) δ 160.01 (dd, J = 248.4, 4.5 Hz), 144.23 (t, J = 8.1 Hz), 109.40 – 108.88 (m), 95.65 (t, J = 24.7 Hz), 63.70 (t, J = 2.1 Hz), 26.00, 18.50, -5.22. ^{19}F NMR (471 MHz, CDCl_3) δ -105.65 (d, J = 7.1 Hz).

10-(2,6-Difluoro-4-(hydroxymethyl)phenyl)-7-hydroxy-5,5-dimethyldibenzo[b,e]silin-3(5H)-one (A-20) A flame-dried round-bottom flask was charged with **A-19** (0.340 g, 1.0 mmol, 10 eq.) and anhydrous THF (5 mL). The reaction was cooled to -78°C and then treated dropwise with 1.7 M *t*-butyllithium in pentane (0.60 mL, 1.0 mmol, 1.0 eq.) over 5 minutes. After stirring for an additional 8 minutes at -78°C , the reaction was treated dropwise with a solution of **2-13** (0.050 g, 0.10 mmol, 1.0 eq.) in anhydrous THF (3 mL) over 4 minutes. After addition, the reaction was warmed to room temperature and stirred for 2 hours. The reaction was treated with 3.0 M HCl (1.0 mL, 3.0 mmol, 30 eq.) and heated to 50°C . After stirring for 2 hours, the reaction was cooled to room temperature and quenched with brine. The organics were collected, dried over Na_2SO_4 , and concentrated. The crude material was purified via flash chromatography on a silica column (5:95 v/v MeOH: CH_2Cl_2 gradient) to afford the title compound as a red solid (0.018 g, 0.0454 mmol, 45.4% yield). ^1H NMR (500 MHz, Methanol- d_4) δ 7.19 (d, J = 8.1 Hz, 2H), 7.05 (s, 2H), 7.03 (d, J = 5.2 Hz, 2H), 6.50 (d, J = 9.4 Hz, 2H), 4.74 (s, 2H), 0.50 (s, 6H). ^{13}C NMR (126 MHz, Methanol- d_4) δ 161.04 (dd, J = 246.8, 7.4 Hz), 148.71 (d, J = 8.6 Hz), 147.83, 131.39, 115.64 (t, J = 22.1 Hz), 111.97 – 106.78 (m), 63.77, -1.50. ^{19}F NMR (471 MHz, Methanol- d_4) δ -114.31 (d, J = 8.1 Hz). HRMS (ESI $^+$): m/z calculated for $[\text{M}+\text{H}]^+ = 397.1066$; found = 397.1070.

3,5-Difluoro-4-(7-hydroxy-5,5-dimethyl-3-oxo-3,5-dihydrodibenzo[b,e]silin-10-yl)benzaldehyde (Probe 5) A round-bottom flask was charged with **A-20** (0.0157 g, 0.040 mmol,

1.0 eq.), 2-iodoxybenzoic acid (0.014 g, 0.048 mmol, 1.2 eq.), and DMSO (1 mL). After stirring 2 hours at room temperature, the reaction was concentrated. The crude material was purified via flash chromatography on a silica column (5:95 v/v iPrOH:CH₂Cl₂) to afford the title compound as a red solid (0.0065 g, 0.0165 mmol, 41.6% yield). ¹H NMR (500 MHz, CDCl₃) δ 10.05 (t, *J* = 1.6 Hz, 1H), 7.61 (d, *J* = 6.0 Hz, 2H), 7.03 (d, *J* = 2.5 Hz, 2H), 6.89 (dt, *J* = 9.4, 1.0 Hz, 2H), 6.55 (dd, *J* = 9.5, 2.4 Hz, 2H), 0.46 (s, 6H). ¹³C NMR (126 MHz, CDCl₃) δ 188.90, 160.41 (dd, *J* = 252.7, 6.3 Hz), 144.37, 142.98, 138.84 (t, *J* = 7.3 Hz), 137.48, 130.61, 129.90, 123.05, 122.75 (t, *J* = 22.1 Hz), 112.98 – 112.28 (m), -1.30. ¹⁹F NMR (471 MHz, CDCl₃) δ -107.90 (d, *J* = 6.1 Hz). HRMS (ESI⁺): *m/z* calculated for [M+H]⁺ = 395.0910; found = 395.0916.

A.2.3.8 Synthesis of Probe 6



Scheme A.7. Synthesis of Probe 6.

(4-bromo-3,5-dimethoxyphenyl)methanol (A-22) A round-bottom flask was charged with 4-bromo-3,5-dimethoxybenzaldehyde (1.23 g, 5.0 mmol, 1.0 eq.) were treated with MeOH (20 mL). After cooling to 0 °C, the solution was treated with NaBH₄ (0.190 g, 5.0 mmol, 1.0 eq.). The reaction was warmed to room temperature. After 1 hour, the reaction was quenched with sequential addition of H₂O (5 mL), 1.0 M NaOH (5 mL), and more H₂O (5 mL). MeOH was removed under reduced pressure and the resulting mixture was filtered. The precipitate was dried under vacuum to afford the title compound as a white crystalline solid (1.118 g, 4.52 mmol, 90.5% yield). ¹H NMR (500 MHz, Chloroform-*d*) δ 6.60 (s, 2H), 4.68 (d, *J* = 5.1 Hz, 2H), 3.91 (s, 6H), 1.75 (t, *J* = 5.7 Hz, 1H). ¹³C NMR (126 MHz, Chloroform-*d*) δ 157.29, 141.81, 103.13, 99.82, 65.34, 56.61.

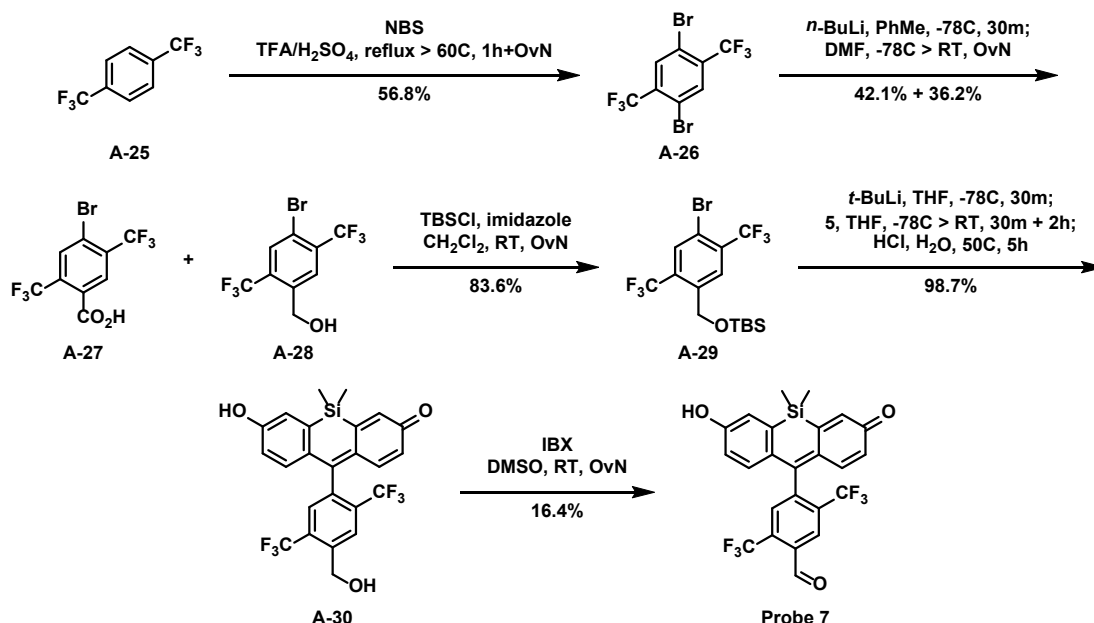
((4-bromo-3,5-dimethoxybenzyl)oxy)(tert-butyl)dimethylsilane (A-23) A round-bottom flask was charged with **A-22** (1.118 g, 4.52 mmol, 1.0 eq.), imidazole (0.75 g, 11 mmol, 2.4 eq.), and CH₂Cl₂ (25 mL). Once a solution had formed, *tert*-butyldimethylsilyl chloride (0.80 g, 5.3 mmol, 1.2 eq.) was added. After stirring overnight at room temperature, the reaction was washed with 1.0 M HCl in H₂O. The organics were collected, dried over Na₂SO₄, and concentrated under reduced pressure. The crude material was purified via flash chromatography on a silica column (5:95 v/v EtOAc:hexanes) to afford the title compound as a colorless oil (1.63 g, 4.51 mmol, 99.7% yield). ¹H NMR (500 MHz, Chloroform-*d*) δ 6.57 (s, 2H), 4.71 (s, 2H), 3.89 (s, 6H), 0.95 (s, 9H), 0.11 (s, 6H). ¹³C NMR (126 MHz, Chloroform-*d*) δ 157.06, 142.62, 102.26, 98.86, 64.80, 56.51, 26.04, 18.53, -5.08.

7-hydroxy-10-(4-(hydroxymethyl)-2,6-dimethoxyphenyl)-5,5-dimethyldibenzo[b,e]silin-3(5H)-one (A-24) A flame-dried round-bottom flask was charged with **A-23** (0.364 g, 1.0 mmol, 10 eq.) and dry THF (5 mL). The reaction was cooled to -78 °C and then treated dropwise with 1.7 M *t*-butyllithium in pentane (0.59 mL, 1.0 mmol, 10 eq.) over 60 seconds. After stirring for an additional 8 minutes at -78 °C, the reaction was treated dropwise with a solution of **2-13** (0.050 g, 0.10 mmol, 1.0 eq.) in dry THF (2 mL) over 90 seconds. 30 minutes after addition, the reaction was warmed to room temperature and stirred for 2 hours. The reaction was treated with 1.0 M HCl (3 mL, 3 mmol, 30 eq.) and heated to 50 °C. After stirring for 1 hour, the reaction was cooled to room temperature and diluted with H₂O. The THF was removed under reduced pressure. Product was extracted from the remaining mixture with 33:67 v/v iPrOH:CH₂Cl₂. The organics were collected, dried over Na₂SO₄, and concentrated. The crude material was purified via flash chromatography on a silica column (2:98 to 5:95 v/v MeOH:CH₂Cl₂ gradient) to afford the title compound as a red solid (0.0371 g, 0.0882 mmol, 88.2% yield). ¹H NMR (500 MHz, DMSO-*d*₆) δ 10.35 (s, 1H), 7.04 (s, 1H), 6.89 (s, 3H), 6.80 (s, 2H), 6.67 (s, 1H), 6.16 (s, 1H), 5.35 (t, *J* = 5.8 Hz, 1H), 4.61 (d, *J* = 4.7 Hz, 2H), 3.62 (s, 6H), 0.43 (s, 6H). ¹³C NMR (126 MHz, DMSO-*d*₆) δ 156.78, 151.87, 145.49, 114.13, 101.97, 63.09, 55.83, -1.50.

4-(7-hydroxy-5,5-dimethyl-3-oxo-3,5-dihydrodibenzo[b,e]silin-10-yl)-3,5-dimethoxybenzaldehyde (Probe 7) A round-bottom flask was charged with **A-24** (0.0145 g, 0.035 mmol, 1.0 eq.), 2-iodoxybenzoic acid (0.0114 g, 0.041 mmol, 1.2 eq.), and DMSO (1 mL). After stirring 2 hours at room temperature, the reaction was quenched with brine. The resulting mixture was poured through over filter paper. The precipitate was purified via flash

chromatography on a silica column (2:98 to 4:96 v/v iPrOH:CH₂Cl₂ gradient) to afford the title compound as a red solid (0.0033 g, 0.0079 mmol, 22.8% yield). ¹H NMR (500 MHz, DMSO-*d*₆) δ 10.41 (s, 1H), 10.08 (s, 1H), 7.40 (s, 2H), 7.16 (s, 1H), 6.88 (d, *J* = 10.1 Hz, 1H), 6.79 (s, 1H), 6.76 (d, *J* = 8.7 Hz, 1H), 6.69 (d, *J* = 8.2 Hz, 1H), 6.13 (d, *J* = 9.7 Hz, 1H), 3.74 (s, 6H), 0.44 (s, 6H). ¹³C NMR (126 MHz, DMSO-*d*₆) δ 192.58, 157.59, 149.76, 138.09, 122.20, 105.17, 56.32, -1.53.

A.2.3.9 Synthesis of Probe 7



Scheme A.8. Synthesis of Probe 7.

1,4-dibromo-2,5-bis(trifluoromethyl)benzene (A-26) A flame-dried round-bottom flask was charged with 1,4-bis(trifluoromethyl)benzene (2.75 mL, 17.8 mmol, 1.0 eq.), trifluoroacetic acid (50 mL), and H₂SO₄ (12 mL). The reaction was heated to reflux. After 10 minutes, the reaction was treated with *N*-bromosuccinimide (9.48 g, 53.2 mmol, 3.0 eq.) portionwise over 3 hours. After the first hour, the heat was decreased to 60 °C. After stirring overnight, the reaction was cooled to 0 °C, diluted with ice, and poured through a fritted funnel. The precipitate was collected and purified by sublimation to afford the title compound as a white solid (3.75 g, 10.1 mmol, 56.8% yield). ¹H NMR (500 MHz, Chloroform-*d*) δ 8.01 (s, 2H). ¹³C NMR (126 MHz, Chloroform-*d*) δ 134.64 (q, *J* = 32.6 Hz), 134.35 (q, *J* = 5.9 Hz), 121.52 (q, *J* = 274.8 Hz), 119.26. ¹⁹F NMR (471 MHz, Chloroform-*d*) δ -63.61.

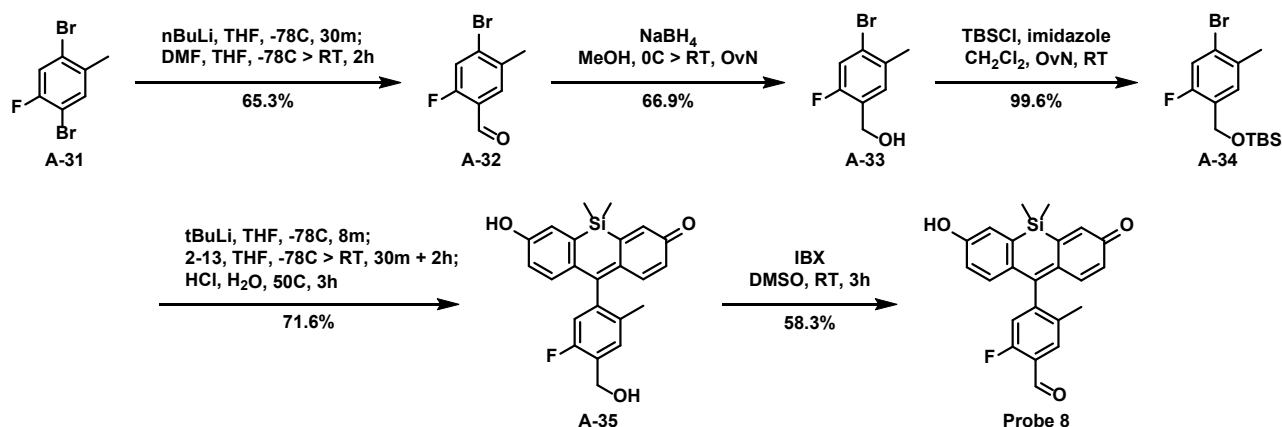
(4-bromo-2,5-bis(trifluoromethyl)phenyl)methanol (A-28) and **4-bromo-2,5-bis(trifluoromethyl)benzoic acid (A-27)** A flame-dried round-bottom flask was charged with **A-26** (0.374 g, 1.0 mmol, 1.0 eq.) and dry toluene (10 mL). The reaction was cooled to -78 °C and then treated dropwise with 2.5 M *n*-butyllithium in hexanes (0.40 mL, 1.0 mmol, 1.0 eq.) over 45 seconds. After stirring for 30 minutes at -78 °C, the reaction was treated with *N,N*-dimethylformamide (0.10 mL, 1.2 mmol, 1.2 eq.). The reaction was warmed to room temperature. After stirring overnight, the reaction was quenched with 0.1 M NaOH and diluted with EtOAc. The organics were collected, dried over Na₂SO₄, and concentrated to afford the title compound **(37)** as a white solid (0.136 g, 0.421 mmol, 42.1% yield). ¹H NMR (500 MHz, Chloroform-*d*) δ 8.14 (s, 1H), 7.97 (s, 1H), 4.90 (d, *J* = 4.1 Hz, 2H), 1.95 (t, *J* = 5.3 Hz, 1H). ¹³C NMR (126 MHz, Chloroform-*d*) δ 139.37, 133.85 (q, *J* = 32.5 Hz), 132.44 (q, *J* = 5.8 Hz), 131.18 (q, *J* = 33.0 Hz), 128.01 (q, *J* = 5.5 Hz), 122.81 (q, *J* = 274.6 Hz), 122.46 (q, *J* = 274.1 Hz), 118.93 (q, *J* = 1.3 Hz), 60.37 (q, *J* = 3.1 Hz). ¹⁹F NMR (471 MHz, Chloroform-*d*) δ -61.25, -63.21. The basic aqueous solution was acidified with 1M HCl and filtered. The precipitate was dried under reduced pressure to afford the title compound **(36)** as a white solid (0.122 g, 0.362 mmol, 36.2% yield). ¹H NMR (500 MHz, DMSO-*d*₆) δ 14.23 (s, 1H), 8.37 (s, 1H), 8.21 (s, 1H). ¹³C NMR (126 MHz, DMSO-*d*₆) δ 165.68, 133.45 (q, *J* = 5.4 Hz), 132.22 (q, *J* = 31.2 Hz), 132.15 (q, *J* = 1.7 Hz), 131.26 (q, *J* = 32.9 Hz), 129.50 (q, *J* = 5.4 Hz), 122.44, 121.97 (q, *J* = 274.1 Hz), 121.83 (q, *J* = 274.5 Hz). ¹⁹F NMR (471 MHz, DMSO-*d*₆) δ -58.86, -62.26.

((4-bromo-2,5-bis(trifluoromethyl)benzyl)oxy)(tert-butyl)dimethylsilane (A-29) A round-bottom flask was charged with **A-28** (0.136 g, 0.42 mmol, 1.0 eq.), imidazole (0.038 g, 0.56 mmol, 1.3 eq.), and CH₂Cl₂ (10 mL). Once a solution had formed, *tert*-butyldimethylsilyl chloride (0.078 g, 0.52 mmol, 1.2 eq.) was added. After stirring overnight at room temperature, the reaction was washed with 1.0 M HCl in H₂O (2x10 mL). The organics were collected, dried over Na₂SO₄, and concentrated under reduced pressure. The crude material was purified via flash chromatography on a silica column (2:98 v/v EtOAc:hexanes) to afford the title compound as a colorless oil (0.154 g, 0.35 mmol, 83.6% yield). ¹H NMR (500 MHz, Chloroform-*d*) δ 8.19 (s, 1H), 7.93 (s, 1H), 4.88 (s, 2H), 0.97 (s, 9H), 0.14 (s, 6H). ¹³C NMR (126 MHz, Chloroform-*d*) δ 140.45, 133.64 (q, *J* = 31.7 Hz), 132.11 (q, *J* = 5.8 Hz), 130.49 (q, *J* = 32.4 Hz), 127.36 (q, *J* = 5.5 Hz), 122.91 (q, *J* = 274.8 Hz), 122.61 (q, *J* = 274.0 Hz), 118.21 (q, *J* = 1.9 Hz), 60.35 (q, *J* = 3.3 Hz), 25.91, 18.43, -5.36. ¹⁹F NMR (471 MHz, Chloroform-*d*) δ -61.84, -63.36.

7-hydroxy-10-(4-(hydroxymethyl)-2,5-bis(trifluoromethyl)phenyl)-5,5-dimethyldibenzo[b,e]silin-3(5H)-one (A-30) A flame-dried round-bottom flask was charged with **A-29** (0.441 g, 1.0 mmol, 10 eq.) and dry THF (5 mL). The reaction was cooled to -78 °C and then treated dropwise with 1.7 M *t*-butyllithium in pentane (0.60 mL, 1.0 mmol, 10 eq.) over 3 minutes. After stirring for an additional 8 minutes at -78 °C, the reaction was treated dropwise with a solution of **2-13** (0.050 g, 0.10 mmol, 1.0 eq.) in dry THF (2 mL) over 1 minute. 30 minutes after addition, the reaction was warmed to room temperature and stirred for 2 hours. The reaction was treated with 1.0 M HCl (3 mL, 3.0 mmol, 30 eq.) and heated to 50 °C. After stirring for 5 hours, the reaction was cooled to room temperature. The THF was removed under reduced pressure. Product was extracted with 33:67 v/v iPrOH:CH₂Cl₂. The organics were collected, dried over Na₂SO₄, and concentrated. The crude material was purified via flash chromatography on a silica column 2:98 to 4:96 v/v MeOH:CH₂Cl₂ gradient) to afford the title compound as a red solid (0.049 g, 0.0987 mmol, 98.7% yield). ¹H NMR (500 MHz, DMSO-*d*₆) δ 10.54 (s, 1H), 8.29 (s, 1H), 7.82 (s, 1H), 7.20 (s, 1H), 6.85 (s, 1H), 6.74 (s, 1H), 6.65 (s, 1H), 6.52 (s, 1H), 6.15 (s, 1H), 5.90 (t, *J* = 5.6 Hz, 1H), 4.85 (d, *J* = 4.8 Hz, 2H), 0.50 (s, 3H), 0.41 (s, 3H). ¹³C NMR (126 MHz, DMSO-*d*₆) δ 182.78, 159.31, 150.24, 146.56, 142.47, 140.61, 140.02, 136.78, 136.59, 135.38, 131.47, 131.18, 130.94, 129.06, 128.77, 128.57, 127.91, 127.09, 126.11, 124.49, 124.35, 122.31, 122.17, 121.95, 117.03, 58.51, -1.00, -2.23. ¹⁹F NMR (471 MHz, DMSO-*d*₆) δ -58.69, -59.77.

4-(7-hydroxy-5,5-dimethyl-3-oxo-3,5-dihydrodibenzo[b,e]silin-10-yl)-2,5-bis(trifluoromethyl)benzaldehyde (Probe 7) A round-bottom flask was charged with **A-30** (0.0102 g, 0.021 mmol, 1.0 eq.), 2-iodoxybenzoic acid (0.0080 g, 0.027 mmol, 1.3 eq.), and DMSO (1 mL). After 2 hours, the reaction was concentrated. The crude material was purified via flash chromatography on a silica column (5:95 v/v iPrOH:CH₂Cl₂) to afford the title compound as a red solid (0.00167 g, 0.00338 mmol, 16.4% yield).

A.2.3.10 Synthesis of Probe 8



Scheme A.9. Synthesis of Probe 8.

4-Bromo-2-fluoro-5-methylbenzaldehyde (A-32) A flame-dried round-bottom flask was charged with 1,4-dibromo-2-fluoro-5-methylbenzene (3.2 g, 12 mmol, 1.0 eq.) and anhydrous THF (30 mL). The reaction was cooled to -78 °C and then treated dropwise with 2.5 M n-butyllithium in hexanes (5.03 mL, 12.6 mmol, 1.05 eq.) over 10 minutes. After stirring an additional 30 minutes at room -78 °C, the reaction was treated dropwise with a solution of DMF (1.67 mL, 21.6 mmol, 1.8 eq.) in anhydrous THF (3 mL) over 5 minutes. The reaction was warmed to room temperature. After 2 hours, the reaction was quenched with brine and diluted with EtOAc. The organics were collected, dried over Na₂SO₄, and concentrated under reduced pressure. The crude material was purified via flash chromatography on a silica column (10:90 v/v CH₂Cl₂:hexanes) to afford the title compound as a white solid (1.70 g, 7.83 mmol, 65.3% yield). ¹H NMR (500 MHz, CDCl₃) δ 10.29 (s, 1H), 7.71 (d, *J* = 7.3 Hz, 1H), 7.42 (d, *J* = 9.6 Hz, 1H), 2.41 (s, 3H). ¹³C NMR (126 MHz, CDCl₃) δ 186.58 (d, *J* = 5.8 Hz), 162.27 (d, *J* = 260.3 Hz), 135.12 (d, *J* = 3.9 Hz), 132.53 (d, *J* = 9.7 Hz), 129.56 (d, *J* = 2.4 Hz), 123.09 (d, *J* = 8.2 Hz), 120.78 (d, *J* = 23.2 Hz), 22.20. ¹⁹F NMR (471 MHz, CDCl₃) δ -125.06 (t, *J* = 8.5 Hz).

(4-Bromo-2-fluoro-5-methylphenyl)methanol (A-33) A round-bottom flask was charged with A-32 (0.508 g, 2.34 mmol, 1.0 eq.) were treated with MeOH (10 mL). After cooling to 0 °C, the solution was treated with NaBH₄ (0.090 g, 2.34 mmol, 1.0 eq.) The reaction was warmed to room temperature. After stirring overnight, the reaction was quenched with sequential addition of H₂O (5 mL), 1.0 M NaOH in H₂O (5 mL), and more H₂O (5 mL). MeOH was removed under reduced pressure. Product was extracted with CH₂Cl₂. The organics were collected, dried over Na₂SO₄, and concentrated to afford the title compound as a colorless oil (0.343 g, 1.57 mmol,

66.9% yield). ^1H NMR (500 MHz, CDCl_3) δ 7.29 (d, $J = 7.8$ Hz, 1H), 7.26 (d, $J = 9.3$ Hz, 1H), 4.69 (s, 2H), 2.36 (s, 3H). ^{13}C NMR (126 MHz, CDCl_3) δ 158.42 (d, $J = 248.1$ Hz), 133.98 (d, $J = 3.7$ Hz), 130.81 (d, $J = 4.8$ Hz), 126.92 (d, $J = 14.7$ Hz), 123.71 (d, $J = 9.6$ Hz), 119.40 (d, $J = 24.5$ Hz), 59.08 (d, $J = 3.8$ Hz), 22.18. ^{19}F NMR (471 MHz, CDCl_3) δ -122.30 (t, $J = 8.7$ Hz).

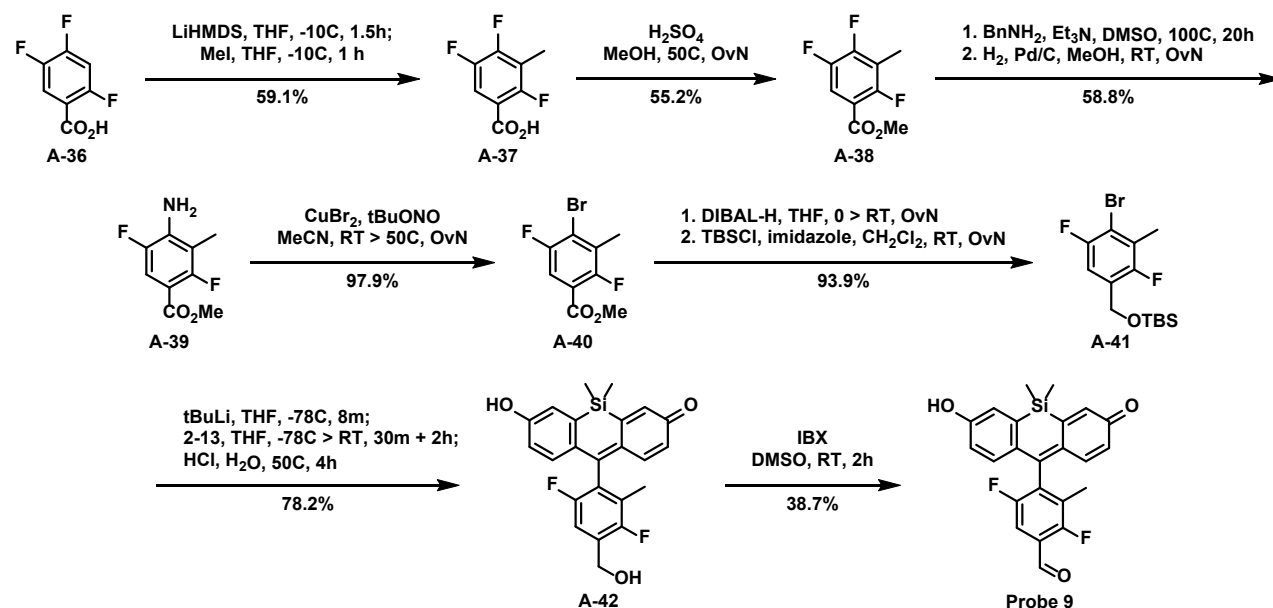
((4-Bromo-2-fluoro-5-methylbenzyl)oxy)(*tert*-butyl)dimethylsilane (A-34) A round-bottom flask was charged with **A-33** (0.219 g, 1.0 mmol, 1.0 eq.), imidazole (0.136 g, 2.0 mmol, 2.0 eq.), and CH_2Cl_2 (10 mL). Once a solution had formed, *tert*-butyldimethylsilyl chloride (0.301 g, 2.0 mmol, 2.0 eq.) was added. After stirring overnight at room temperature, the reaction was washed with 1.0 M HCl in H_2O . The organics were collected, dried over Na_2SO_4 , and concentrated under reduced pressure to afford the title compound as a colorless oil (0.332 g, 0.996 mmol, 99.6% yield). ^1H NMR (500 MHz, CDCl_3) δ 7.32 (d, $J = 7.8$ Hz, 1H), 7.20 (d, $J = 9.3$ Hz, 1H), 4.70 (s, 2H), 2.36 (s, 3H), 0.94 (s, 9H), 0.11 (s, 6H). ^{13}C NMR (126 MHz, CDCl_3) δ 157.66 (d, $J = 247.3$ Hz), 133.59 (d, $J = 3.4$ Hz), 129.98 (d, $J = 5.2$ Hz), 127.66 (d, $J = 14.4$ Hz), 122.65 (d, $J = 9.2$ Hz), 118.88 (d, $J = 24.4$ Hz), 58.76 (d, $J = 4.3$ Hz), 26.06, 22.31, 18.57, -5.21. ^{19}F NMR (471 MHz, CDCl_3) δ -122.56 (t, $J = 8.6$ Hz).

10-(5-Fluoro-4-(hydroxymethyl)-2-methylphenyl)-7-hydroxy-5,5-dimethyldibenzo[b,e]silin-3(5H)-one (A-35) A flame-dried round-bottom flask was charged with **A-34** (0.334 g, 1.0 mmol, 10 eq.) and anhydrous THF (5 mL). The reaction was cooled to -78°C and then treated dropwise with 1.7 M *t*-butyllithium in pentane (0.59 mL, 1.0 mmol, 10 eq.) over 1 minute. After stirring for an additional 8 minutes at -78°C , the reaction was treated dropwise with a solution of **2-13** (0.051 g, 0.10 mmol, 1.0 eq.) in anhydrous THF (2 mL) over 1 minute. After addition, the reaction was warmed to room temperature and stirred for 2 hours. The reaction was treated with 1.0 M HCl in H_2O (3 mL, 3 mmol, 30 eq.) and heated to 50°C . After stirring for 3 hours, the reaction was cooled to room temperature and quenched with brine. The organics were collected, dried over Na_2SO_4 , and concentrated. The crude material was purified via flash chromatography on a silica column (2:98 v/v MeOH: CH_2Cl_2). The crude residue was dissolved in CH_2Cl_2 , triturated with hexanes, and collected by filtration to afford the title compound as a red solid (0.0281 g, 0.0716 mmol, 71.6% yield). ^1H NMR (500 MHz, $\text{DMSO}-d_6$) δ 10.52 (s, 1H), 7.47 (d, $J = 7.4$ Hz, 1H), 7.18 (s, 1H), 7.03 (d, $J = 10.1$ Hz, 1H), 6.77 (s, 4H), 6.19 (s, 1H), 5.35 (t, $J = 5.7$ Hz, 1H), 4.62 (d, $J = 5.3$ Hz, 2H), 1.96 (s, 3H), 0.47 (s, 3H), 0.44 (s, 3H). ^{13}C NMR (126 MHz, $\text{DMSO}-d_6$) δ 157.66 (d, $J = 244.5$ Hz), 139.18 (d, $J = 7.6$ Hz), 131.14 (d, $J = 3.3$ Hz), 130.59 (d, J

= 4.8 Hz), 128.81 (d, J = 15.0 Hz), 115.60 (d, J = 22.2 Hz), 56.62 (d, J = 3.6 Hz), 18.25, -1.33, -1.65. ^{19}F NMR (471 MHz, DMSO- d_6) δ -124.04 (t, J = 8.8 Hz). HRMS (ESI $^+$): m/z calculated for $[\text{M}+\text{H}]^+ = 393.1317$; found = 393.1321.

2-Fluoro-4-(7-hydroxy-5,5-dimethyl-3-oxo-3,5-dihydrodibenzo[b,e]silin-10-yl)-5-methylbenzaldehyde (Probe 8) A round-bottom flask was charged with **A-35** (0.0069 g, 0.018 mmol, 1.0 eq.), 2-iodoxybenzoic acid (0.0060 g, 0.021 mmol, 1.2 eq.), and DMSO (1 mL). After stirring 3 hours at room temperature, the reaction was concentrated. The crude material was purified via flash chromatography on a silica column (5:95 v/v iPrOH:CH₂Cl₂) to afford the title compound as a red solid (0.0040 g, 0.0102 mmol, 58.3% yield). ^1H NMR (500 MHz, DMSO- d_6) δ 10.57 (s, 1H), 10.29 (s, 1H), 7.87 (d, J = 6.8 Hz, 1H), 7.38 (d, J = 10.5 Hz, 1H), 7.22 (d, J = 2.7 Hz, 1H), 6.85 (s, 1H), 6.80 (d, J = 10.4 Hz, 1H), 6.75 (d, J = 7.8 Hz, 1H), 6.67 (d, J = 8.6 Hz, 1H), 6.17 (d, J = 10.1 Hz, 1H), 2.03 (s, 3H), 0.48 (s, 3H), 0.45 (s, 3H). ^{13}C NMR (126 MHz, DMSO- d_6) δ 187.58, 182.82, 161.48 (d, J = 257.5 Hz), 159.62 (d, J = 1.8 Hz), 152.52, 147.70 (d, J = 8.8 Hz), 146.58, 140.54, 140.16, 136.66, 134.78, 132.71 (d, J = 3.2 Hz), 130.57, 130.01, 127.51, 126.48, 123.29 (d, J = 8.0 Hz), 122.30, 117.66 (d, J = 20.7 Hz), 117.29, 18.00, -1.36, -1.64. ^{19}F NMR (471 MHz, DMSO- d_6) δ -124.88 (dd, J = 10.5, 7.1 Hz). HRMS (ESI $^+$): m/z calculated for $[\text{M}+\text{H}]^+ = 391.1160$; found = 391.1163.

A.2.3.11 Synthesis of Probe 9



Scheme A.10. Synthesis of Probe 9.

2,4,5-Trifluoro-3-methylbenzoic acid (A-37) A round-bottom flask was charged with anhydrous THF (6 mL) and 1.0 M LiHMDS in THF (6.5 mL, 6.5 mmol, 2.3 eq.). The solution was cooled to -10 °C and then treated dropwise with a solution of 2,4,5-trifluorobenzoic acid (0.503 g, 2.8 mmol, 1.0 eq.) in anhydrous THF (3 mL) over 4 minutes. After stirring for 1.5 hours, the reaction was treated dropwise with methyl iodide (0.193 mL, 3.1 mmol, 1.1 eq.). After stirring for 1 hour, the reaction was quenched with cold 3 M HCl (2 mL) followed by cold 6 M HCl (2.5 mL) and warmed to room temperature. The THF was removed under reduced pressure. Product was extracted with EtOAc. The organics were collected, dried over Na₂SO₄, and concentrated. The crude residue was recrystallized in H₂O to afford the title compound as a white solid (0.321 g, 1.69 mmol, 59.1% yield). ¹H NMR (500 MHz, CDCl₃) δ 7.70 (td, *J* = 9.5, 6.6 Hz, 1H), 2.29 (t, *J* = 2.3 Hz, 3H). ¹³C NMR (126 MHz, CDCl₃) δ 167.64, 157.44 (ddd, *J* = 259.7, 7.2, 2.4 Hz), 152.89 (ddd, *J* = 256.8, 14.1, 8.6 Hz), 146.54 (ddd, *J* = 246.4, 13.6, 3.5 Hz), 117.38 (dd, *J* = 23.4, 17.5 Hz), 117.00 (dt, *J* = 20.5, 1.9 Hz), 113.05 (ddd, *J* = 11.7, 5.5, 4.0 Hz), 7.77 (dt, *J* = 3.8, 1.9 Hz). ¹⁹F NMR (471 MHz, CDCl₃) δ -112.01 – -112.19 (m), -126.87 – -127.01 (m), -141.35 (ddd, *J* = 21.8, 16.3, 10.3 Hz).

Methyl 2,4,5-trifluoro-3-methylbenzoate (A-38) A round-bottom flask was charged with **A-37** (3.58 g, 18.8 mmol, 1.0 eq.), MeOH (40 mL), and conc. H₂SO₄ (2 mL). The reaction was heated to 50 °C. After stirring overnight, the reaction was neutralized with saturated NaHCO₃ and diluted with EtOAc. The organics were collected, dried over Na₂SO₄, and concentrated. The crude material was purified via flash chromatography on a silica column (5:95 v/v EtOAc:hexanes) to afford the title compound as a colorless oil (2.12 g, 10.4 mmol, 55.2% yield). ¹H NMR (400 MHz, CDCl₃) δ 7.61 (td, *J* = 9.3, 6.6 Hz, 1H), 3.92 (s, 3H), 2.26 (t, *J* = 2.2 Hz, 3H). ¹⁹F NMR (376 MHz, CDCl₃) δ -114.06 – -114.71 (m), -129.48 (dt, *J* = 19.4, 9.3 Hz), -142.34 (ddd, *J* = 22.0, 16.0, 10.1 Hz).

Methyl 4-amino-2,5-difluoro-3-methylbenzoate (A-39) A pressure flask was charged with **A-38** (0.97 g, 5.0 mmol, 1.0 eq.), benzylamine (0.65 mL, 6.0 mmol, 1.2 eq.), triethylamine (1.03 mL, 7.4 mmol, 1.5 eq.), and DMSO (2 mL). The reaction was heated to 100 °C for 20 hours. After cooling to room temperature, the reaction was poured into brine and diluted with EtOAc. The organics were washed with more brine, dried over Na₂SO₄, and concentrated under reduced pressure. To the crude residue was added 10% w/w Pd/C (0.069 g) and MeOH (20 mL). The mixture was stirred vigorously under hydrogen (1 atm) overnight at room temperature. The

reaction filtered through Celite®. The crude material was purified via flash chromatography on a silica column (10:90 v/v EtOAc:hexanes) to afford the title compound as a white solid (0.579 g, 2.88 mmol, 58.8% yield). ¹H NMR (500 MHz, CDCl₃) δ 7.41 (dd, *J* = 11.4, 6.4 Hz, 1H), 4.17 (s, 2H), 3.84 (s, 3H), 2.06 (d, *J* = 2.4 Hz, 3H). ¹³C NMR (126 MHz, CDCl₃) δ 164.63 (dd, *J* = 4.4, 2.4 Hz), 157.46 (dd, *J* = 252.7, 1.2 Hz), 146.09 (dd, *J* = 234.7, 2.1 Hz), 139.30 (dd, *J* = 14.1, 8.3 Hz), 114.57 (dd, *J* = 22.3, 3.1 Hz), 110.90 (dd, *J* = 22.4, 3.4 Hz), 106.06 (dd, *J* = 13.2, 7.0 Hz), 51.97, 8.67 (dd, *J* = 6.8, 2.4 Hz). ¹⁹F NMR (471 MHz, CDCl₃) δ -116.80 (ddd, *J* = 15.5, 6.1, 2.1 Hz), -140.73 (dd, *J* = 16.0, 11.4 Hz).

Methyl 4-bromo-2,5-difluoro-3-methylbenzoate (A-40) A flame-dried round-bottom flask was charged with **A-39** (0.310 g, 1.54 mmol, 1.0 eq.), CuBr₂ (1.72 g, 7.7 mmol, 5.0 eq.), and anhydrous MeCN (10 mL). The reaction was treated with *tert*-butyl nitrite (0.28 mL, 2.3 mmol, 1.5 eq.) and heated to 50 °C. After stirring overnight, the reaction was cooled and diluted with saturated NaHCO₃. Product was extracted with EtOAc. The organics were combined, dried over Na₂SO₄, and concentrated to afford the title compound as a yellow solid (0.40 g, 1.51 mmol, 97.9% yield). ¹H NMR (500 MHz, CDCl₃) δ 7.54 (dd, *J* = 8.3, 6.0 Hz, 1H), 3.93 (s, 3H), 2.41 (d, *J* = 2.9 Hz, 3H). ¹³C NMR (126 MHz, CDCl₃) δ 163.62 (dd, *J* = 4.3, 2.3 Hz), 156.27 (dd, *J* = 123.6, 3.1 Hz), 154.28 (dd, *J* = 109.3, 3.1 Hz), 129.33 (d, *J* = 21.2 Hz), 118.01 (dd, *J* = 22.2, 5.2 Hz), 117.90 (dd, *J* = 13.6, 7.1 Hz), 115.17 (dd, *J* = 26.8, 1.9 Hz), 52.70, 15.08 (dd, *J* = 4.9, 2.2 Hz). ¹⁹F NMR (471 MHz, CDCl₃) δ -109.15 (dd, *J* = 16.9, 8.2 Hz), -113.13 (ddq, *J* = 16.6, 5.9, 2.7 Hz).

((4-Bromo-2,5-difluoro-3-methylbenzyl)oxy)(*tert*-butyl)dimethylsilane (A-41) A flame-dried round-bottom flask was charged with **A-40** (0.525 g, 2.0 mmol, 1.0 eq.) and anhydrous THF (10 mL). The reaction was cooled to 0 °C before treating dropwise with 1.0 M DIBAL-H in CH₂Cl₂ (5.0 mL, 5.0 mmol, 2.5 eq.) over 2 minutes. The reaction was slowly warmed to room temperature with the melting ice bath. After stirring overnight minutes, the reaction was quenched via the sequential addition of H₂O (5 mL), 1.0 M NaOH in H₂O (5 mL), and more H₂O (5 mL). The reaction was diluted with Et₂O. The organics were collected, dried over Na₂SO₄, and concentrated. The crude residue was treated imidazole (0.21 g, 3.0 mmol, 1.5 eq.) and CH₂Cl₂ (20 mL). Once a solution had formed, *tert*-butyldimethylsilyl chloride (0.47 g, 3.0 mmol, 1.5 eq.) was added. After stirring overnight at room temperature, the reaction was purified via flash chromatography on a silica column (2:98 v/v EtOAc:hexanes) to afford the title compound as a colorless oil (0.660 g, 1.88 mmol, 93.9% yield). ¹H NMR (500 MHz, CDCl₃) δ 7.13 (dd, *J* = 8.7,

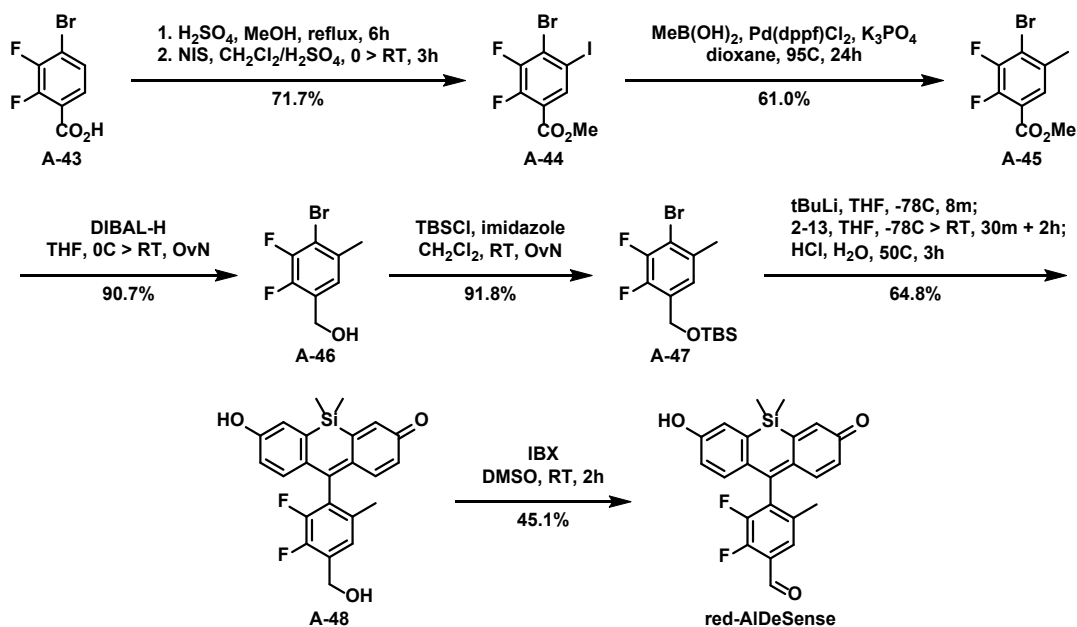
6.2 Hz, 1H), 4.72 (s, 2H), 2.34 (d, $J = 2.6$ Hz, 3H), 0.95 (s, 9H), 0.12 (s, 6H). ^{13}C NMR (126 MHz, CDCl_3) δ 155.71 (dd, $J = 241.8, 2.9$ Hz), 153.43 (dd, $J = 242.4, 2.7$ Hz), 129.15 (dd, $J = 18.2, 7.2$ Hz), 126.55 (d, $J = 20.5$ Hz), 112.00 (dd, $J = 26.3, 5.6$ Hz), 110.20 (dd, $J = 22.8, 5.5$ Hz), 58.68 (d, $J = 5.3$ Hz), 26.03, 18.53, 14.81 (dd, $J = 4.1, 2.2$ Hz), -5.26. ^{19}F NMR (471 MHz, CDCl_3) δ -110.43 (dd, $J = 16.3, 8.8$ Hz), -124.14 (ddd, $J = 15.9, 6.1, 2.7$ Hz).

10-(3,6-Difluoro-4-(hydroxymethyl)-2-methylphenyl)-7-hydroxy-5,5-dimethyldibenzo[b,e]silin-3(5H)-one (A-42) A flame-dried round-bottom flask was charged with **A-41** (0.349 g, 1.0 mmol, 10 eq.) and anhydrous THF (5 mL). The reaction was cooled to -78°C and then treated dropwise with 1.7 M *t*-butyllithium in pentane (0.59 mL, 1.0 mmol, 10 eq.) over 1 minute. After stirring for an additional 8 minutes at -78°C , the reaction was treated dropwise with a solution of **2-13** (0.050 g, 0.10 mmol, 1.0 eq.) in anhydrous THF (2 mL) over 1 minute. After addition, the reaction was warmed to room temperature and stirred for 2 hours. The reaction was treated with 1.0 M HCl in H_2O (3 mL, 3 mmol, 30 eq.) and heated to 50°C . After stirring for 4 hours, the reaction was cooled to room temperature and quenched with brine. The organics were collected, dried over Na_2SO_4 , and concentrated. The crude material was purified via flash chromatography on a silica column (5:95 to 10:90 v/v $\text{iPrOH}:\text{CH}_2\text{Cl}_2$ gradient). The crude residue was suspended in CH_2Cl_2 and collected by filtration to afford the title compound as a red solid (0.0321 g, 0.0782 mmol, 78.2% yield). ^1H NMR (500 MHz, $\text{DMSO}-d_6$) δ 10.58 (s, 1H), 7.29 (dd, $J = 9.2, 5.6$ Hz, 1H), 7.04 (s, 2H), 6.81 (d, $J = 9.4$ Hz, 2H), 6.49 (s, 2H), 5.51 (s, 1H), 4.65 (s, 2H), 1.91 (d, $J = 2.2$ Hz, 3H), 0.47 (s, 3H), 0.45 (s, 3H). ^{13}C NMR (126 MHz, $\text{DMSO}-d_6$) δ 154.67 (d, $J = 237.9$ Hz), 153.80 (d, $J = 241.6$ Hz), 147.20, 131.25 (dd, $J = 18.4, 7.7$ Hz), 128.97, 125.98 (dd, $J = 20.0, 4.4$ Hz), 124.40 (dd, $J = 19.5, 3.1$ Hz), 112.38 (dd, $J = 25.6, 5.4$ Hz), 56.59 (d, $J = 4.1$ Hz), 11.54 (d, $J = 2.2$ Hz), -1.26, -1.84. ^{19}F NMR (471 MHz, $\text{DMSO}-d_6$) δ -119.71 (dd, $J = 18.1, 9.3$ Hz), -126.85 (dd, $J = 18.1, 5.3$ Hz). HRMS (ESI $^+$): m/z calculated for $[\text{M}+\text{H}]^+ = 411.1223$; found = 411.1216.

2,5-Difluoro-4-(7-hydroxy-5,5-dimethyl-3-oxo-3,5-dihydrodibenzo[b,e]silin-10-yl)-3-methylbenzaldehyde (Probe 9) A round-bottom flask was charged with **A-42** (0.0174 g, 0.042 mmol, 1.0 eq.), 2-iodoxybenzoic acid (0.016 g, 0.051 mmol, 1.2 eq.), and DMSO (1 mL). After stirring 4 hours at room temperature, the reaction was concentrated. The crude material was purified via flash chromatography on a silica column (5:95 v/v $\text{iPrOH}:\text{CH}_2\text{Cl}_2$) to afford the title compound as a red solid (0.0067 g, 0.0164 mmol, 38.7% yield). ^1H NMR (500 MHz, $\text{DMSO}-d_6$)

δ 10.62 (s, 1H), 10.29 (d, J = 2.4 Hz, 1H), 7.66 (dd, J = 8.2, 5.1 Hz, 1H), 7.24 (s, 1H), 6.88 (s, 2H), 6.77 (s, 2H), 6.20 (s, 1H), 2.00 (d, J = 2.0 Hz, 3H), 0.48 (s, 3H), 0.46 (s, 3H). ^{19}F NMR (471 MHz, DMSO- d_6) δ -118.07 (dd, J = 18.3, 8.5 Hz), -127.14 (dd, J = 18.5, 4.8 Hz). HRMS (ESI $^+$): m/z calculated for $[\text{M}+\text{H}]^+ = 409.1066$; found = 409.1077.

A.2.3.12 Synthesis of red-AIDeSense



Scheme A.11. Synthesis of red-AIDeSense.

Methyl 4-bromo-2,3-difluoro-5-iodobenzoate (A-44) A round-bottom flask was charged with 4-bromo-2,3-difluorobenzoic acid (1.00 g, 4.22 mmol, 1.0 eq.) and MeOH (5 mL). The reaction was cooled to 0 °C and then treated dropwise with conc. H_2SO_4 (1 mL) over 30 seconds. The reaction was heated to reflux. After 6 hours, the reaction was poured into H_2O and diluted with EtOAc. The organics were collected, washed with 1.0 M NaOH in H_2O , dried over Na_2SO_4 , and concentrated under reduced pressure. The material was dissolved in CH_2Cl_2 (4 mL) and cooled to 0 °C. The reaction was treated dropwise with conc. H_2SO_4 (4 mL) over 2 minutes. While still cold, the reaction was treated portionwise with *N*-iodosuccinimide (1.41 g, 6.3 mmol, 1.5 eq.) over 2 minutes. The reaction was warmed to room temperature. After stirring for 3 hours, the reaction was quenched via addition of ice. The organics were collected, washed with saturated NaHCO_3 , washed with aqueous $\text{Na}_2\text{S}_2\text{O}_3$, dried over Na_2SO_4 , and concentrated. The crude material was purified via flash chromatography on a silica column (10:90 v/v CH_2Cl_2 :hexanes) to afford the title compound as a white solid (1.14 g, 3.02 mmol, 71.7% yield). ^1H NMR (500 MHz, CDCl_3) δ

8.21 (dd, $J = 6.4, 1.3$ Hz, 1H), 3.94 (s, 3H). ^{13}C NMR (126 MHz, CDCl_3) δ 162.38 (t, $J = 3.4$ Hz), 150.25 (dd, $J = 267.8, 15.4$ Hz), 148.70 (dd, $J = 253.4, 15.2$ Hz), 136.20 (d, $J = 4.0$ Hz), 124.04 (d, $J = 18.7$ Hz), 120.69 (d, $J = 8.0$ Hz), 94.51 (dd, $J = 5.1, 2.5$ Hz), 53.12. ^{19}F NMR (471 MHz, CDCl_3) δ -116.92 (d, $J = 21.2$ Hz), -130.87 (dd, $J = 21.1, 6.6$ Hz).

Methyl 4-bromo-2,3-difluoro-5-methylbenzoate (A-45) A pressure flask was charged with **A-44** (0.900 g, 2.39 mmol, 1.0 eq.), methylboronic acid (0.286 g, 4.78 mmol, 2.0 eq.), K_3PO_4 (1.01 g, 4.78 mmol, 2.0 eq.), and anhydrous 1,4-dioxane (10 mL). The mixture was degassed for 15 minutes via concurrent sparging with N_2 and sonication before being treated with $\text{Pd}(\text{dppf})\text{Cl}_2$ (0.053 g, 0.072 mmol, 0.03 eq.). The reaction was sealed and heated to 95 °C. After stirring for 24 hours, the reaction was cooled, poured into H_2O . Product was extracted with Et_2O . The organics were combined, washed with H_2O , dried over Na_2SO_4 , and concentrated. The crude material was purified via flash chromatography on a silica column (10:90 v/v CH_2Cl_2 :hexanes) to afford the title compound as a white solid (0.386 g, 1.46 mmol, 61.0% yield). ^1H NMR (500 MHz, CDCl_3) δ 7.59 (dd, $J = 6.7, 2.1$ Hz, 1H), 3.93 (s, 3H), 2.40 (s, 3H). ^{13}C NMR (126 MHz, CDCl_3) δ 163.80 (t, $J = 3.6$ Hz), 148.63 (dd, $J = 247.9, 14.8$ Hz), 148.51 (dd, $J = 263.8, 15.4$ Hz), 134.65 (d, $J = 4.5$ Hz), 126.62 (d, $J = 3.4$ Hz), 118.52 (d, $J = 7.3$ Hz), 117.99 (d, $J = 17.4$ Hz), 52.77, 22.12 (d, $J = 2.3$ Hz). ^{19}F NMR (471 MHz, CDCl_3) δ -125.94 (dd, $J = 21.7, 2.5$ Hz), -135.08 (dd, $J = 21.4, 6.7$ Hz).

(4-Bromo-2,3-difluoro-5-methylphenyl)methanol (A-46) A flame-dried round-bottom flask was charged with **A-45** (0.386 g, 1.46 mmol, 1.0 eq.) and anhydrous THF (10 mL). The reaction was cooled to 0 °C before treating dropwise with 1.0 M DIBAL-H in hexanes (3.2 g, 3.2 mmol, 2.2 eq.) over 3 minutes. The reaction was slowly warmed to room temperature with the melting ice bath. After stirring overnight, the reaction was concentrated and resuspended in 1.0 M NaOH in H_2O . Product was extracted with Et_2O , dried over Na_2SO_4 , and concentrated to afford the title compound as a white solid (0.313 g, 1.32 mmol, 90.7% yield). ^1H NMR (500 MHz, CDCl_3) δ 7.12 (dd, $J = 6.8, 2.0$ Hz, 1H), 4.73 (d, $J = 4.9$ Hz, 2H), 2.39 (s, 3H), 1.84 (t, $J = 6.1$ Hz, 1H). ^{13}C NMR (126 MHz, CDCl_3) δ 147.74 (dd, $J = 247.0, 14.3$ Hz), 146.70 (dd, $J = 249.0, 14.4$ Hz), 134.76 (d, $J = 4.2$ Hz), 128.30 (d, $J = 11.6$ Hz), 124.23 (t, $J = 3.4$ Hz), 111.74 (d, $J = 17.2$ Hz), 58.78 (dd, $J = 3.7, 2.7$ Hz), 22.26 (d, $J = 2.4$ Hz). ^{19}F NMR (471 MHz, CDCl_3) δ -128.37 (dd, $J = 21.7, 2.5$ Hz), -144.51 (dd, $J = 21.9, 6.7$ Hz).

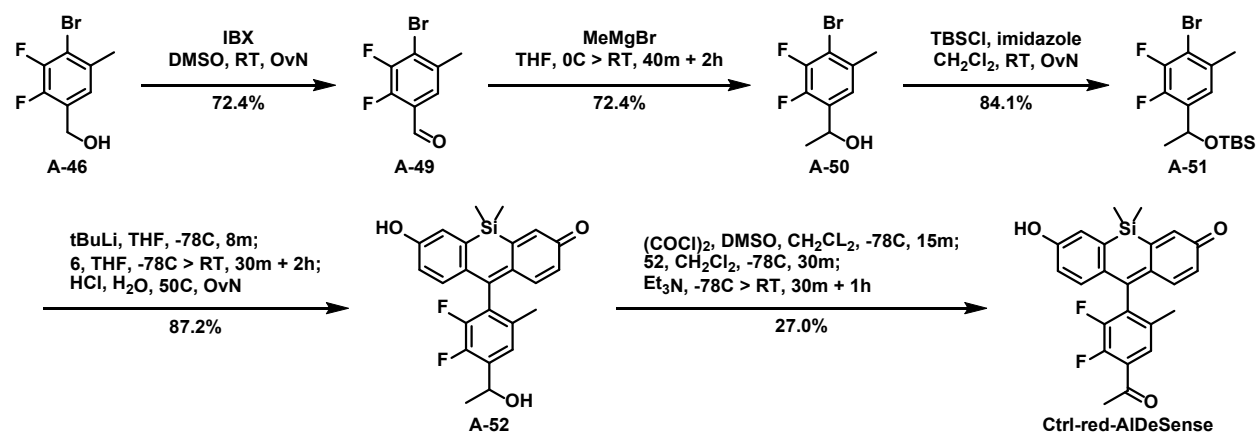
((4-Bromo-2,3-difluoro-5-methylbenzyl)oxy)(tert-butyl)dimethylsilane (A-47) A round-bottom flask was charged with **A-46** (0.313 g, 1.32 mmol, 1.0 eq.), imidazole (0.111 g, 1.6 mmol, 1.2 eq.), and CH₂Cl₂ (10 mL). Once a solution had formed, *tert*-butyldimethylsilyl chloride (0.235 g, 1.6 mmol, 1.2 eq.) was added. After stirring overnight at room temperature, the reaction was washed with 1.0 M HCl in H₂O. The organics were collected, dried over Na₂SO₄, and concentrated under reduced pressure to afford the title compound as a colorless oil (0.426 g, 1.21 mmol, 91.8% yield). ¹H NMR (500 MHz, CDCl₃) δ 7.14 (dd, *J* = 7.1, 2.0 Hz, 1H), 4.74 (s, 2H), 2.39 (s, 3H), 0.95 (s, 9H), 0.13 (s, 6H). ¹³C NMR (126 MHz, CDCl₃) δ 147.48 (dd, *J* = 246.3, 14.2 Hz), 146.02 (dd, *J* = 248.2, 14.4 Hz), 134.29 (d, *J* = 4.1 Hz), 129.08 (d, *J* = 11.4 Hz), 123.51 (t, *J* = 3.5 Hz), 110.73 (d, *J* = 17.1 Hz), 58.64 (dd, *J* = 4.0, 2.9 Hz), 26.01, 22.35 (d, *J* = 2.3 Hz), 18.53, -5.26. ¹⁹F NMR (471 MHz, CDCl₃) δ -129.36 (dd, *J* = 22.0, 2.2 Hz), -144.86 (dd, *J* = 21.8, 6.9 Hz).

10-(3,6-Difluoro-4-(hydroxymethyl)-2-methylphenyl)-7-hydroxy-5,5-dimethyldibenzo[b,e]silin-3(5H)-one (A-48) A flame-dried round-bottom flask was charged with **A-47** (0.352 g, 1.0 mmol, 10 eq.) and anhydrous THF (5 mL). The reaction was cooled to -78 °C and then treated dropwise with 1.7 M *t*-butyllithium in pentane (0.59 mL, 1.0 mmol, 10 eq.) over 1 minute. After stirring for an additional 8 minutes at -78 °C, the reaction was treated dropwise with a solution of **2-13** (0.052 g, 0.10 mmol, 1.0 eq.) in anhydrous THF (2 mL) over 30 seconds. After addition, the reaction was warmed to room temperature and stirred for 2 hours. The reaction was treated with 1.0 M HCl in H₂O (3 mL, 3 mmol, 30 eq.) and heated to 50 °C. After stirring for 3 hours, the reaction was cooled to room temperature and quenched with brine. The organics were collected, dried over Na₂SO₄, and concentrated. The crude material was purified via flash chromatography on a silica column (5:95 to 10:95 v/v MeOH:CH₂Cl₂ gradient). The crude material was further purified via flash chromatography on a silica column (Et₂O) to afford the title compound as a red solid (0.0266 g, 0.0648 mmol, 64.8% yield). ¹H NMR (500 MHz, Methanol-*d*₄) δ 7.33 (d, *J* = 6.1 Hz, 1H), 7.06 (d, *J* = 2.5 Hz, 2H), 6.97 (d, *J* = 9.4 Hz, 2H), 6.51 (d, *J* = 8.7 Hz, 2H), 4.79 (s, 2H), 2.05 (s, 3H), 0.54 (s, 3H), 0.51 (s, 3H). ¹⁹F NMR (471 MHz, Methanol-*d*₄) δ -142.01 (d, *J* = 21.7 Hz), -149.82 (dd, *J* = 21.7, 6.4 Hz). HRMS (ESI⁺): *m/z* calculated for [M+H]⁺ = 411.1223; found = 411.1226.

2,5-Difluoro-4-(7-hydroxy-5,5-dimethyl-3-oxo-3,5-dihydrodibenzo[b,e]silin-10-yl)-3-methylbenzaldehyde (red-AIDeSense) A round-bottom flask was charged with **A-48** (0.0259 g,

0.063 mmol, 1.0 eq.), 2-iodoxybenzoic acid (0.0214 g, 0.076 mmol, 1.2 eq.), and DMSO (1 mL). After stirring 2 hours at room temperature, the reaction was concentrated. The crude material was purified via flash chromatography on a silica column (5:95 v/v iPrOH:CH₂Cl₂) to afford the title compound as a red solid (0.0116 g, 0.0284 mmol, 45.1% yield). ¹H NMR (500 MHz, CDCl₃) δ 10.41 (s, 1H), 7.63 (d, *J* = 5.4 Hz, 1H), 7.05 (d, *J* = 2.5 Hz, 2H), 6.83 (d, *J* = 9.4 Hz, 2H), 6.56 (dd, *J* = 9.5, 2.4 Hz, 2H), 2.09 (s, 3H), 0.47 (s, 3H), 0.45 (s, 3H). ¹³C NMR (126 MHz, CDCl₃) δ 185.76, 171.89, 150.99 (dd, *J* = 261.5, 14.4 Hz), 148.04, 147.71 (dd, *J* = 249.6, 12.5 Hz), 144.72, 137.45, 135.42 (d, *J* = 14.1 Hz), 134.27 (d, *J* = 3.9 Hz), 129.92, 129.68, 125.21 (d, *J* = 5.3 Hz), 124.02 (d, *J* = 3.6 Hz), 123.14, 18.98 (d, *J* = 1.8 Hz), -1.24, -1.44. ¹⁹F NMR (471 MHz, CDCl₃) δ -136.14 (d, *J* = 22.2 Hz), -149.06 (dd, *J* = 22.4, 5.9 Hz). HRMS (ESI⁺): *m/z* calculated for [M+H]⁺ = 409.1066; found = 409.1071.

A.2.3.13 Synthesis of Ctrl-red-AIDeSense



Scheme A.12. Synthesis of Ctrl-red-AIDeSense.

4-Bromo-2,3-difluoro-5-methylbenzaldehyde (A-49) A round-bottom flask was charged with **A-46** (0.460 g, 1.94 mmol, 1.0 eq.), 2-iodoxybenzoic acid (0.81 g, 2.9 mmol, 1.5 eq.), and DMSO (10 mL). After stirring overnight at room temperature, the reaction was poured into brine and diluted with Et₂O. The organics were collected, washed with H₂O, dried over Na₂SO₄, and concentrated under reduced pressure to afford the title compound as a light yellow solid (0.330 g, 1.40 mmol, 72.4% yield). ¹H NMR (500 MHz, CDCl₃) δ 10.27 (s, 1H), 7.52 (d, *J* = 6.3 Hz, 1H), 2.43 (s, 3H). ¹³C NMR (126 MHz, CDCl₃) δ 185.50 (dd, *J* = 6.0, 3.1 Hz), 150.71 (dd, *J* = 261.8, 14.7 Hz), 148.15 (dd, *J* = 249.7, 13.5 Hz), 135.79 (d, *J* = 4.3 Hz), 123.82 (d, *J* = 5.8 Hz), 123.17 (d, *J* = 3.7 Hz), 120.31 (d, *J* = 17.1 Hz), 22.27 (d, *J* = 2.3 Hz). ¹⁹F NMR (471 MHz, CDCl₃) δ -126.06 (d, *J* = 21.8 Hz), -147.66 (dd, *J* = 21.6, 6.2 Hz).

1-(4-Bromo-2,3-difluoro-5-methylphenyl)ethan-1-ol (A-50) A flame-dried round-bottom flask was charged with A-49 (0.388 g, 1.65 mmol, 1.0 eq.) and anhydrous THF (5 mL). The reaction was cooled to 0 °C and then treated dropwise with 3.0 M methylmagnesium bromide in Et₂O (0.66 mL, 1.98 mmol, 1.2 eq.) over 1 minute. After stirring for an additional 40 minutes at 0 °C, the reaction was warmed to room temperature and stirred for 2 hours. The reaction was quenched with brine and diluted with Et₂O and CH₂Cl₂. The organics were collected, dried over Na₂SO₄, and concentrated. The crude material was dissolved in CH₂Cl₂ and treated with imidazole (0.011 g, 0.165 mmol, 0.1 eq.) and *tert*-butyldimethylsilyl chloride (0.024 g, 0.165 mmol, 0.1 eq.). After stirring for 10 minutes, the reaction was quenched with MeOH and concentrated. The crude residue purified via flash chromatography on a silica column (10:90 v/v EtOAc:hexanes) to afford the title compound as a colorless oil (0.300 g, 1.19 mmol, 72.4% yield). ¹H NMR (500 MHz, CDCl₃) δ 7.17 (dd, *J* = 6.8, 2.0 Hz, 1H), 5.16 (q, *J* = 6.5 Hz, 1H), 2.39 (s, 3H), 1.95 (s, 1H), 1.50 (d, *J* = 6.4 Hz, 3H). ¹³C NMR (126 MHz, CDCl₃) δ 147.66 (dd, *J* = 246.7, 14.6 Hz), 145.91 (dd, *J* = 248.2, 14.4 Hz), 134.74 (d, *J* = 4.2 Hz), 133.27 (d, *J* = 10.4 Hz), 121.75 (t, *J* = 3.4 Hz), 111.07 (d, *J* = 17.2 Hz), 64.25 (d, *J* = 2.4 Hz), 24.28, 22.35 (d, *J* = 2.3 Hz). ¹⁹F NMR (471 MHz, CDCl₃) δ -128.62 (dd, *J* = 21.9, 2.2 Hz), -144.99 (dd, *J* = 22.3, 6.8 Hz).

(1-(4-Bromo-2,3-difluoro-5-methylphenyl)ethoxy)(*tert*-butyl)dimethylsilane (A-51) A round-bottom flask was charged with A-50 (0.300 g, 1.19 mmol, 1.0 eq.), imidazole (0.163 g, 2.4 mmol, 2.0 eq.), and CH₂Cl₂ (10 mL). Once a solution had formed, *tert*-butyldimethylsilyl chloride (0.358 g, 2.4 mmol, 2.0 eq.) was added. After stirring overnight at room temperature, the reaction was concentrated under reduced pressure. The crude material was purified via flash chromatography on a silica column (hexanes) to afford the title compound as a colorless oil (0.367 g, 1.00 mmol, 84.1% yield). ¹H NMR (500 MHz, CDCl₃) δ 7.19 (ddd, *J* = 6.7, 2.1, 0.9 Hz, 1H), 5.11 (q, *J* = 6.3 Hz, 1H), 2.38 (s, 3H), 1.39 (d, *J* = 6.3 Hz, 3H), 0.90 (s, 9H), 0.07 (s, 3H), -0.01 (s, 3H). ¹³C NMR (126 MHz, CDCl₃) δ 147.40 (dd, *J* = 246.2, 14.8 Hz), 145.23 (dd, *J* = 247.1, 14.3 Hz), 134.52 (d, *J* = 11.0 Hz), 134.34 (d, *J* = 4.1 Hz), 122.13 (t, *J* = 3.4 Hz), 110.33 (d, *J* = 17.3 Hz), 64.36 (t, *J* = 2.5 Hz), 25.93, 22.42 (d, *J* = 2.3 Hz), 18.35, -4.81, -4.87. ¹⁹F NMR (471 MHz, CDCl₃) δ -129.38 (d, *J* = 22.2 Hz), -145.34 (dd, *J* = 22.4, 6.9 Hz).

10-(3,6-Difluoro-4-(1-hydroxyethyl)-2-methylphenyl)-7-hydroxy-5,5-dimethyldibenzo[b,e]silin-3(5H)-one (A-52) A flame-dried round-bottom flask was charged with A-51 (0.357 g, 1.0 mmol, 5 eq.) and anhydrous THF (10 mL). The reaction was cooled to -78 °C

and then treated dropwise with 1.7 M *t*-butyllithium in pentane (0.59 mL, 1.0 mmol, 5 eq.) over 1 minutes. After stirring for an additional 8 minutes at -78 °C, the reaction was treated dropwise with a solution of **2-13** (0.100 g, 0.20 mmol, 1.0 eq.) in anhydrous THF (5 mL) over 3 minutes. After stirring for 30 minutes, the reaction was warmed to room temperature and stirred for 2 hours. The reaction was treated with 1.0 M HCl in H₂O (6 mL, 6 mmol, 60 eq.) and heated to 50 °C. After stirring overnight, the reaction was cooled to room temperature, quenched with brine, and diluted with Et₂O. The organics were collected, dried over Na₂SO₄, and concentrated. The crude material was purified via flash chromatography on a silica column (5:95 v/v MeOH:CH₂Cl₂). The crude material was further purified via flash chromatography on a silica column (0:100 to 10:90 v/v MeOH:Et₂O gradient) to afford the title compound as a red solid (0.074 g, 0.174 mmol, 87.2% yield). ¹H NMR (500 MHz, Methanol-*d*₄) δ 7.44 – 7.30 (m, 1H), 7.04 (d, *J* = 2.5 Hz, 2H), 6.95 (dd, *J* = 9.5, 0.9 Hz, 1H), 6.93 (dd, *J* = 9.4, 0.9 Hz, 1H), 6.51 (dd, *J* = 9.4, 2.4 Hz, 1H), 6.48 (dd, *J* = 9.4, 2.4 Hz, 1H), 5.21 (q, *J* = 6.5 Hz, 1H), 2.04 (s, 3H), 1.55 (d, *J* = 6.5 Hz, 3H), 0.52 (s, 3H), 0.49 (s, 3H). ¹³C NMR (126 MHz, Methanol-*d*₄) δ 152.40, 146.43, 139.50, 136.99 (d, *J* = 10.6 Hz), 134.10, 130.63, 130.27, 128.30 (d, *J* = 14.2 Hz), 126.12, 123.77, 123.39, 64.42, 24.45, 18.93 (d, *J* = 2.0 Hz), -1.39, -1.67. ¹⁹F NMR (471 MHz, Methanol-*d*₄) δ -142.00 (d, *J* = 21.8 Hz), -150.09 (dd, *J* = 21.7, 6.3 Hz). HRMS (ESI⁺): *m/z* calculated for [M+H]⁺ = 425.1379; found = 425.1376.

10-(4-Acetyl-3,6-difluoro-2-methylphenyl)-7-hydroxy-5,5-dimethyldibenzo[b,e]silin-3(5H)-one (Ctrl-red-AIDeSense) A flame-dried round-bottom flask was charged with anhydrous CH₂Cl₂ (1 mL) and oxalyl chloride (0.10 mL, 1.2 mmol, 20 eq.). The reaction was cooled to -78 °C and then treated dropwise with a solution of DMSO (0.17 mL, 2.4 mmol, 40 eq.) in anhydrous CH₂Cl₂ (1 mL) over 2 minutes. After stirring for an additional 15 minutes at -78 °C, the reaction was treated dropwise with a solution of **A-52** (0.026 g, 0.061 mmol, 1.0 eq.) in anhydrous CH₂Cl₂ (2.5 mL) over 5 minutes. After stirring for 30 minutes, the reaction was treated dropwise with Et₃N (0.34 mL, 2.4 mmol, 40 eq.) over 1 minute. After stirring for 30 minutes, the reaction was warmed to room temperature and stirred for 1 hour. The reaction poured into a dilute HCl solution and diluted with CH₂Cl₂. The organics were collected, dried over Na₂SO₄, and concentrated. The crude material was purified via flash chromatography on a silica column (5:95 v/v iPrOH:CH₂Cl₂). The crude material was further purified via flash chromatography on a silica column (0:100 to 100:0 v/v Et₂O:CH₂Cl₂ gradient) to afford the title compound as a red solid (0.0070 g, 0.0166 mmol, 27.0% yield). ¹H NMR (500 MHz, CDCl₃) δ 7.63 (d, *J* = 6.0 Hz, 1H), 7.03 (d, *J* = 2.5 Hz, 2H),

6.83 (d, $J = 9.5$ Hz, 2H), 6.53 (dd, $J = 9.5, 2.5$ Hz, 2H), 2.73 (d, $J = 4.5$ Hz, 3H), 2.07 (s, 3H), 0.48 (s, 3H), 0.46 (s, 3H). ^{13}C NMR (126 MHz, CDCl_3) δ 194.56, 151.65, 147.13, 144.22, 137.17, 135.91, 133.69 (dd, $J = 8.9, 5.4$ Hz), 130.07, 128.39, 126.80 (d, $J = 9.9$ Hz), 125.66, 123.12, 31.65 (d, $J = 6.8$ Hz), 18.98, -1.22, -1.40. ^{19}F NMR (471 MHz, CDCl_3) δ -136.39 (d, $J = 23.0$ Hz), -137.81 (dq, $J = 21.6, 5.2$ Hz). HRMS (ESI $^+$): m/z calculated for $[\text{M}+\text{H}]^+ = 423.1223$; found = 423.1229.

A.3 Rhodamines and rhodols for ALDH1A3 supporting information

A.3.1 Experimental procedure

Quantum yield assays

Fluorescence quantum yields were determined using rhodamine 6G ($\Phi_{\text{F}}=0.94$ in EtOH at 500 nm excitation and 510-700 nm emission) as a reference standard. The same quartz fluorescence cuvette was used for all samples. A minimum of 5 data points were collected for each fluorophore, each with the absorbance held below 0.1 to avoid the inner filter effect. A line of best fit was found for the sum of the fluorescence over the 510-700 nm range versus the absorbance at 500 nm (the excitation wavelength). Data analysis was completed in Microsoft Excel.

Expression and purification of ALDH isoforms

Plasmids for ALDH1A1 and ALDH1A3 were generously provided by Professor Daria Mochly-Rosen (Stanford). Expression and purification of each isoform was performed as previously described.⁷¹

ALDH isoform selectivity

Each ALDH isoform was added to a 50 mM triethanolamine solution (pH 7.4) containing 2.0 mM NAD^+ and 100 μM propanal at room temperature. ALDH isoform activity was determined by monitoring the rate of NADH production through the increase in absorbance at 340 nm ($\epsilon = 6220 \text{ M}^{-1}\text{cm}^{-1}$). For these assays, 1 unit is defined as the amount of enzyme that catalyzes the conversion of 1 μM substrate per minute. For every combination of dye and enzyme, 2 μM dye was preincubated with 2.0 mM NAD^+ in 50 mM triethanolamine solution (pH 7.4). The reaction was initiated by addition of 1 unit of ALDH. Dyes were excited at their absorbance maximum wavelength, and fluorescence was measured continuously at their fluorescence maximum wavelength.

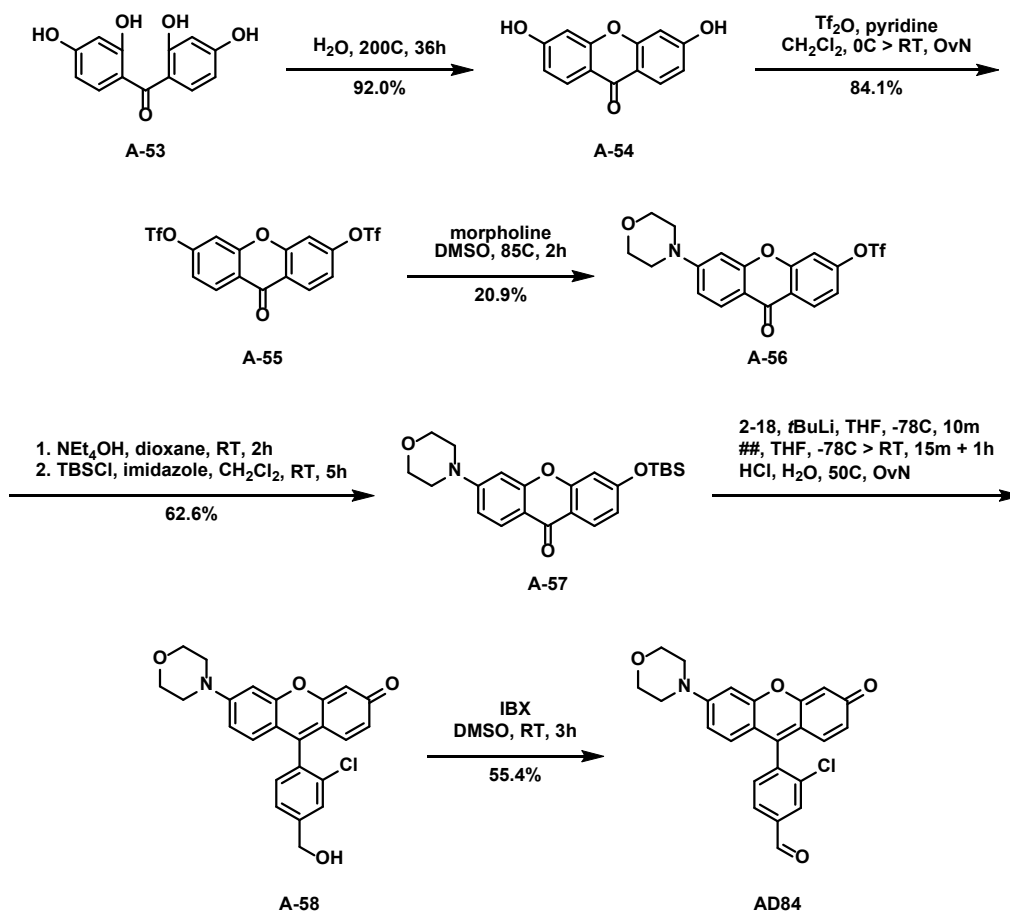
A.3.2 Synthesis and characterization

A.3.2.1 Synthesis of chlorinated benzaldehyde precursor

((4-bromo-3-chlorophenyl)methanol (2-17)). A flame-dried flask was charged with 4-bromo-3-chlorobenzoic acid (1.00 g, 4.25 mmol, 1.0 eq.) and anhydrous THF (10 mL). After cooling to 0 °C, the solution was treated with carbonyl diimidazole (0.75 g, 4.7 mmol, 1.2 eq.) and warmed back to room temperature. After stirring for 1 hour, the reaction was treated dropwise with a solution of NaBH₄ (0.48 g, 12.7 mmol, 3.0 eq.) in H₂O (5 mL) over 1 minute. After stirring for 3 hours, the reaction was diluted with EtOAc and H₂O. The organic layer was washed with 1 M NaOH in H₂O, 1 M HCl in H₂O, dried over Na₂SO₄, and concentrated to afford the title compound as a colorless oil (0.755 g, 3.41 mmol, 80.3% yield). ¹H NMR (400 MHz, Chloroform-*d*) δ 7.59 (d, *J* = 8.2 Hz, 1H), 7.48 (d, *J* = 2.0 Hz, 1H), 7.11 (dd, *J* = 8.2, 2.0 Hz, 1H), 4.65 (s, 2H).

((4-bromo-3-chlorobenzyl)oxy)(tert-butyl)dimethylsilane (2-18). A flask was charged with **2-17** (0.755 g, 3.41 mmol, 1.0 eq.), imidazole (0.25 g, 3.8 mmol, 1.1 eq.) and CH₂Cl₂ (10 mL). While stirring at room temperature, the solution was treated with TBSCl (0.55 g, 3.8 mmol, 1.1 eq.). After stirring overnight, the reaction was washed with dilute HCl, dried over Na₂SO₄, and concentrated under reduced pressure to afford the title compound as a colorless oil (1.112 g, 3.31 mmol, 97.2% yield). ¹H NMR (499 MHz, Chloroform-*d*) δ 7.55 (d, *J* = 8.2 Hz, 1H), 7.42 (d, *J* = 1.9 Hz, 1H), 7.06 (dd, *J* = 8.2, 2.0 Hz, 1H), 4.66 (s, 2H), 0.94 (s, 9H), 0.10 (s, 6H).

A.3.2.2 Synthesis of AD84



Scheme A.13. Synthesis of AD84.

3,6-dihydroxy-9H-xanthen-9-one (A-54). An autoclave chamber was charged with **A-53** (2.00 g, 8.12 mmol, 1.0 eq.) and H_2O (12 mL). The chamber was sealed and heated to 200°C with a sand bath. After heating for 36 hours, the reaction was slowly returned to room temperature. Once cool, the reaction was suspended in Et_2O and H_2O and filtered. The precipitate was washed with H_2O and vacuum dried to afford the title compound as a light brown solid (1.702 g, 7.46 mmol, 92.0% yield). ^1H NMR (500 MHz, $\text{DMSO}-d_6$) δ 10.83 (s, 2H), 7.98 (d, $J = 8.7$ Hz, 2H), 6.86 (dd, $J = 8.7, 2.2$ Hz, 2H), 6.82 (d, $J = 2.3$ Hz, 2H).

9-oxo-9H-xanthene-3,6-diyl bis(trifluoromethanesulfonate) (A-55). A flame-dried flask was charged with **A-54** (4.25 g, 18.5 mmol, 1.0 eq.) and anhydrous CH_2Cl_2 (100 mL). The mixture was cooled to 0°C before treating with anhydrous pyridine (15 mL, 185 mmol, 10 eq.) over 2 minutes. While still at 0°C , the reaction was treated dropwise with triflic anhydride (7.4 mL, 44.3 mmol, 2.4 eq.) over 7 minutes. After slowly coming to room temperature overnight, the

reaction was washed with H₂O (50 mL), 1 M HCl in H₂O (3x50 mL), and brine (50 mL). The organic layer was collected, dried over Na₂SO₄, and concentrated under reduced pressure. The crude solid was dissolved in CH₂Cl₂, triturated with hexanes, and filtered. This was repeated once more on the filtrate. The resulting precipitate was vacuum dried to afford the title compound as an off-white solid (7.68 g, 15.5 mmol, 84.1% yield). ¹H NMR (400 MHz, Chloroform-*d*) δ 8.46 (d, *J* = 8.8 Hz, 2H), 7.50 (d, *J* = 2.3 Hz, 2H), 7.36 (dd, *J* = 8.8, 2.3 Hz, 2H).

6-morpholino-9-oxo-9H-xanthen-3-yl trifluoromethanesulfonate (A-56). A pressure flask was charged with **A-55** (0.600 g, 1.22 mmol, 1.1 eq.), DMSO (6 mL), and morpholine (0.096 mL, 1.11 mmol, 1.0 eq.). After stirring for 2 hours at 85 °C, the reaction was cooled to room temperature, diluted with brine, and extracted from with EtOAc (5x). The organic layers were combined, dried over Na₂SO₄, and concentrated under reduced pressure. The crude yellow solid was purified via flash chromatography on a silica column (25:75 to 40:60 v/v EtOAc:hexanes gradient) to afford the title compound (0.100 g, 0.233 mmol, 20.9% yield). ¹H NMR (400 MHz, Chloroform-*d*) δ 8.36 (d, *J* = 8.8 Hz, 1H), 8.12 (d, *J* = 9.1 Hz, 1H), 7.34 (d, *J* = 2.3 Hz, 1H), 7.29 – 7.16 (m, 1H), 6.89 (dd, *J* = 9.0, 2.4 Hz, 1H), 6.67 (d, *J* = 2.4 Hz, 1H), 3.86 (dd, *J* = 6.0, 3.9 Hz, 4H), 3.38 (dd, *J* = 6.0, 3.1 Hz, 4H). ¹⁹F NMR (376 MHz, Chloroform-*d*) δ -73.06.

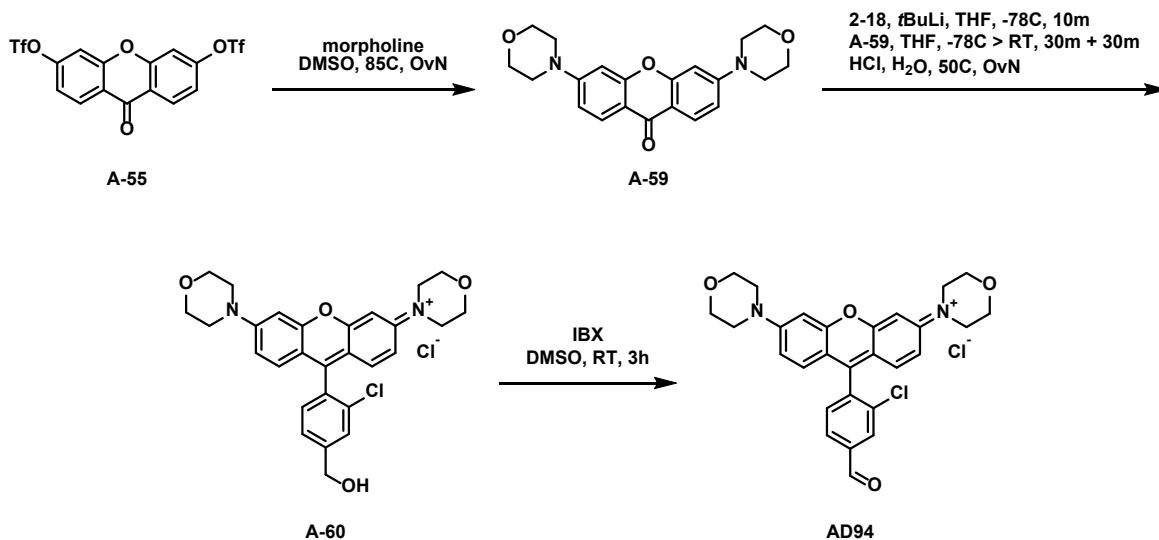
3-((tert-butyldimethylsilyl)oxy)-6-morpholino-9H-xanthen-9-one (A-57). A flask was charged with **A-56** (0.100 g, 0.24 mmol, 1.0 eq.), dioxanes (3 mL), and 1.5 M tetraethylammonium hydroxide in MeOH (0.33 mL, 0.5 mmol, 2.1 eq.). After stirring for 2 hours at room temperature, the volatiles were removed under reduced pressure. The crude yellow solid was dissolved in CH₂Cl₂ (10 mL) and treated with imidazole (0.136 g, 2.0 mmol, 8 eq.) followed by TBSCl (0.155 g, 1.1 mmol, 5 eq.). After stirring for 5 hours, the reaction was concentrated under reduced pressure. The crude material was purified via flash chromatography on a silica column (20:80 to 25:75 v/v EtOAc:hexanes gradient) to afford the title compound (0.060 g, 0.146 mmol, 62.6% yield).

9-(2-chloro-4-(hydroxymethyl)phenyl)-6-morpholino-3H-xanthen-3-one (A-58). A flame-dried flask was charged with **2-18** (0.052 g, 0.15 mmol, 2.0 eq.) and dry THF (2 mL). After cooling to -78 °C, the reaction was charged with 1.7 M *tert*-butyllithium in pentanes (0.09 mL, 0.15 mmol, 2.0 eq.). After 10 minutes, the reaction was treated dropwise with a solution of **A-57** (0.030 g, 0.073 mmol, 1.0 eq.) in dry THF (3 mL). After 15 minutes at -78 °C, the reaction was warmed to room temperature. After stirring for 1 hour, the reaction was treated with 1 M HCl in

H₂O (35 mL) and heated to 50 °C. After stirring overnight, the reaction was cooled to room temperature, neutralized with saturated NaHCO₃ in H₂O and extracted with CH₂Cl₂ (4x). The organic fractions were combined, dried over Na₂SO₄, and concentrated. The crude material was purified via flash chromatography on a silica column (2:98 to 10:90 v/v MeOH:CH₂Cl₂ gradient supplemented with Et₃N) to afford the title compound.

3-chloro-4-(6-morpholino-3-oxo-3H-xanthen-9-yl)benzaldehyde (AD84). A flask was charged with **A-58** (0.0058 g, 0.014 mmol, 1.0 eq.), IBX (0.0044 g, 1.1 eq.), and DMSO (1.5 mL). After stirring at room temperature for 3 hours, the reaction was quenched with brine. Product was extracted with CH₂Cl₂ (4x). The organic fractions were combined, washed with brine, dried over Na₂SO₄, and concentrated under reduced pressure. The crude material was purified via flash chromatography on a silica column (3:97 v/v MeOH:CH₂Cl₂) to afford the title compound (0.0032 g, 0.0076 mmol, 55.4% yield). ¹H NMR (400 MHz, Chloroform-*d*) δ 10.12 (s, 1H), 8.12 (d, *J* = 1.5 Hz, 1H), 7.99 (dd, *J* = 7.8, 1.5 Hz, 1H), 7.51 (d, *J* = 7.7 Hz, 1H), 6.88 – 6.80 (m, 3H), 6.74 (dd, *J* = 9.1, 2.5 Hz, 1H), 6.61 (dd, *J* = 9.6, 1.5 Hz, 1H), 6.54 (s, 1H), 3.87 (t, *J* = 5.9, 3.9 Hz, 4H), 3.43 (t, *J* = 6.0, 4.1 Hz, 4H).

A.3.2.3 Synthesis of AD94



Scheme A.14. Synthesis of AD94.

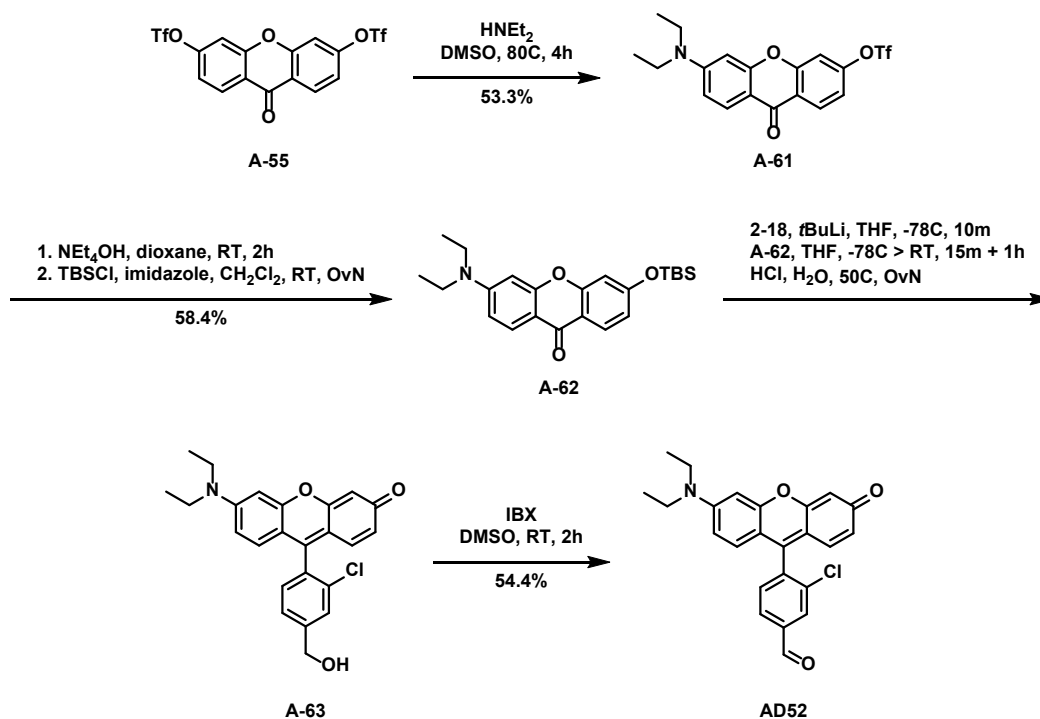
6-morpholino-9-oxo-9H-xanthen-3-yl trifluoromethanesulfonate (A-59). A pressure flask was charged with **A-55** (1.0 g, 2.03 mmol, 1.0 eq.), DMSO (10 mL), and morpholine (0.88 mL, 10.2 mmol, 5.0 eq.). After stirring for overnight at 85 °C, the reaction was cooled to room temperature, triturated with brine, and collected via vacuum filtration. The crude yellow solid was

purified via flash chromatography on a silica column (30:70 to 80:20 v/v EtOAc:hexanes gradient) to afford the title compound. ¹H NMR (400 MHz, Chloroform-*d*) δ 8.17 (d, *J* = 9.0 Hz, 2H), 6.89 (dd, *J* = 9.0, 2.5 Hz, 2H), 6.70 (d, *J* = 2.4 Hz, 2H), 3.88 (dd, *J* = 6.5, 3.3 Hz, 8H), 3.36 (dd, *J* = 6.5, 3.2 Hz, 8H).

4-(9-(2-chloro-4-(hydroxymethyl)phenyl)-6-morpholino-3H-xanthen-3-ylidene)morpholin-4-ium chloride (A-60). A flame-dried flask was charged with **2-18** (0.055 g, 0.16 mmol, 2.0 eq.) and dry THF (2 mL). After cooling to -78 °C, the reaction was charged with 1.7 M *tert*-butyllithium in pentanes (0.095 mL, 0.16 mmol, 2.0 eq.). After 10 minutes, the reaction was treated dropwise with a solution of **A-59** (0.030 g, 0.08 mmol, 1.0 eq.) in dry THF (3 mL). After 30 minutes at -78 °C, the reaction was warmed to room temperature. After stirring for another 30 minutes, the reaction was treated with 1 M HCl in H₂O (35 mL) and heated to 50 °C. After stirring overnight, the reaction was cooled to room temperature, neutralized with saturated NaHCO₃ in H₂O and extracted with CH₂Cl₂ (4x). The organic fractions were combined, dried over Na₂SO₄, and concentrated. The crude material was purified via flash chromatography on a silica column (5:95 to 10:90 v/v MeOH:CH₂Cl₂) to afford the title compound. ¹H NMR (400 MHz, Chloroform-*d*) δ 7.69 (s, 1H), 7.59 (d, *J* = 7.7 Hz, 1H), 7.31 (d, *J* = 9.5 Hz, 2H), 7.27 – 7.19 (m, 3H), 7.16 (d, *J* = 2.5 Hz, 2H), 4.85 (s, 2H), 3.90 (t, *J* = 4.6 Hz, 8H), 3.78 (t, *J* = 4.4 Hz, 8H).

4-(9-(2-chloro-4-formylphenyl)-6-morpholino-3H-xanthen-3-ylidene)morpholin-4-ium chloride (AD94). A flask was charged with **A-60** (0.0022 g, 0.0042 mmol, 1.0 eq.), IBX (0.0018 g, 0.0058, 1.5 eq.), and DMSO (1 mL). After stirring at room temperature for 3 hours, the reaction was quenched with brine. Product was extracted with CH₂Cl₂ (4x). The organic fractions were combined, washed with brine, dried over Na₂SO₄, and concentrated under reduced pressure. The crude material was purified via flash chromatography on a silica column (3:97 to 8:92 v/v MeOH:CH₂Cl₂ gradient) to afford the title compound. ¹H NMR (400 MHz, Chloroform-*d*) δ 10.15 (s, 1H), 8.16 (d, *J* = 1.4 Hz, 1H), 8.08 (dd, *J* = 7.7, 1.3 Hz, 1H), 7.63 (d, *J* = 7.7 Hz, 1H), 7.34 (s, 2H), 7.26 (s, 2H), 7.15 (d, *J* = 9.4 Hz, 2H), 3.92 (t, *J* = 4.7 Hz, 8H), 3.83 (t, *J* = 4.7 Hz, 8H).

A.3.2.4 Synthesis of AD52



Scheme A.15. Synthesis of AD52.

6-morpholino-9-oxo-9H-xanthene-3-yl trifluoromethanesulfonate (A-61). A pressure flask was charged with **A-55** (1.00 g, 2.03 mmol, 1.0 eq.), DMSO (10 mL), and diethylamine (0.50 mL, 4.83 mmol, 2.4 eq.). After stirring for 4 hours at 80°C , the reaction was cooled to room temperature, diluted with brine, and extracted from with Et_2O (6x). The organic layers were combined, washed with brine, dried over Na_2SO_4 , and concentrated under reduced pressure. The crude yellow solid was purified via flash chromatography on a silica column (0:100 to 1:99 v/v $\text{MeOH}:\text{CH}_2\text{Cl}_2$ gradient) to afford the title compound (0.450 g, 1.08 mmol, 53.3% yield).

3-((tert-butyldimethylsilyl)oxy)-6-morpholino-9H-xanthene-9-one (A-62). A flask was charged with **A-61** (0.450 g, 1.08 mmol, 1.0 eq.), dioxanes (6 mL), and 1.5 M tetraethylammonium hydroxide in MeOH (2.5 mL, 3.2 mmol, 3.0 eq.). After stirring for 2 hours at room temperature, the volatiles were removed under reduced pressure. The crude yellow solid was dissolved in CH_2Cl_2 (10 mL) and treated with imidazole (0.144 g, 2.0 mmol, 2.0 eq.) followed by TBSCl (0.148 g, 0.98 mmol, 0.9 eq.). After stirring for 5 hours, the reaction was concentrated under reduced pressure. The crude material was purified via flash chromatography on a silica column (5:95 to 15:85 v/v $\text{EtOAc}:\text{hexanes}$ gradient) to afford the title compound (0.250 g, 0.629 mmol, 58.4% yield).

yield). ¹H NMR (400 MHz, Chloroform-*d*) δ 8.16 (d, *J* = 9.4 Hz, 1H), 8.08 (d, *J* = 9.1 Hz, 1H), 6.82 – 6.75 (m, 2H), 6.62 (dd, *J* = 9.1, 2.2 Hz, 1H), 6.42 (d, *J* = 2.2 Hz, 1H), 3.40 (q, *J* = 7.1 Hz, 4H), 1.19 (t, *J* = 7.1 Hz, 6H), 0.98 (s, 9H), 0.25 (s, 6H).

9-(2-chloro-4-(hydroxymethyl)phenyl)-6-morpholino-3H-xanthen-3-one (A-63). A flame-dried flask was charged with **2-18** (0.053 g, 0.16 mmol, 2.1 eq.) and dry THF (2 mL). After cooling to -78 °C, the reaction was charged with 1.7 M *tert*-butyllithium in pentanes (0.10 mL, 0.17 mmol, 2.2 eq.). After 10 minutes, the reaction was treated dropwise with a solution of **A-62** (0.030 g, 0.075 mmol, 1.0 eq.) in dry THF (3 mL). After 15 minutes at -78 °C, the reaction was warmed to room temperature. After stirring for 2 hour, the reaction was treated with 1 M HCl in H₂O (35 mL) and heated to 50 °C. After stirring overnight, the reaction was cooled to room temperature, neutralized with saturated NaHCO₃ in H₂O and extracted with CH₂Cl₂ (4x). The organic fractions were combined, dried over Na₂SO₄, and concentrated. The crude material was purified via flash chromatography on a silica column (1:99 to 8:92 v/v MeOH:CH₂Cl₂ gradient) to afford the title compound. ¹H NMR (400 MHz, Chloroform-*d*) δ 7.63 (s, 1H), 7.46 (d, *J* = 7.7 Hz, 1H), 7.33 (d, *J* = 7.8 Hz, 1H), 6.93 (d, *J* = 9.2 Hz, 1H), 6.89 (d, *J* = 9.4 Hz, 1H), 6.64 (d, *J* = 2.5 Hz, 1H), 6.61 (d, *J* = 2.4 Hz, 1H), 6.62 – 6.52 (m, 2H), 4.84 (s, 2H), 3.50 (q, *J* = 7.2 Hz, 4H), 1.40 – 1.12 (m, 6H).

3-chloro-4-(6-morpholino-3-oxo-3H-xanthen-9-yl)benzaldehyde (AD54). A flask was charged with **A-63** (0.0024 g, 0.0059 mmol, 1.0 eq.), IBX (0.0016 g, 0.0058 mmol, 1.0 eq.), and DMSO (0.4 mL). After stirring at room temperature for 2 hours, the reaction was quenched with brine. Product was extracted with CH₂Cl₂ (4x). The organic fractions were combined, washed with brine, dried over Na₂SO₄, and concentrated under reduced pressure. The crude material was purified via flash chromatography on a silica column (3:97 v/v MeOH:CH₂Cl₂) to afford the title compound (0.0013 g, 0.0059 mmol, 54.4% yield).

Appendix B. Self-immolative ALDH probe

B.1 Introduction

As discussed in chapter 2, members of the ALDH family are very important for detoxifying endogenous and xenobiotic aldehydes, among other roles. In the interest of continuing to improve our ability to detect these important enzymes in complex biological settings, we set out to develop ratiometric/turn-on probes for that relied on ALDH's unique mechanism.

Generalizable, self-immolative triggers are advantageous over integrated triggers (e.g. d-PeT quenching aldehyde groups) because they can be much more readily switched between readout platforms. This could be range from switching to another wavelength to facilitate multicolor imaging, to switching to another modality entirely (^{19}F MRI, photoacoustic imaging, etc.) To accomplish this, we considered a number of designs which would have a stable "aldehyde" that could be oxidized to an unstable "carboxylic acid." The quotations are meant to emphasize that we did not limit ourselves to the traditional definitions of aldehyde and carboxylic acid. Doing so is extremely challenging because the aldehyde is generally more reactive; it is a better electrophile and more likely to undergo E1_{cb} type eliminations. The carboxylate feature that might be used would be feature nucleophilicity absent from the aldehyde. However, the aldehyde hydrate formed in equilibrium in aqueous environments is a better nucleophile.

For these reasons we expanded our potential substrate scope to formyl groups. Depending on the stability on enzyme bound intermediates, we proposed such formyl groups could undergo nucleophilic attack by the active site cysteine. (Figure B.1) Hydride transfer from the tetrahedral intermediate to the NAD(P)^+ cofactor would proceed as usual. Hydrolysis of the thioester bioisostere would release the unstable acid (carbonic acid, carbamic acid, etc.) which would spontaneously decompose to CO_2 and an uncapped self-immolative linker. Finally the uncapped linker would self-immolate to release the free dye. Thus, the probe would rely on the oxidative capabilities of the ALDH enzyme to achieve selectivity over other enzymes (i.e. esterases). Isoform selectivity would be pursued through careful modifications of the trigger's linker.

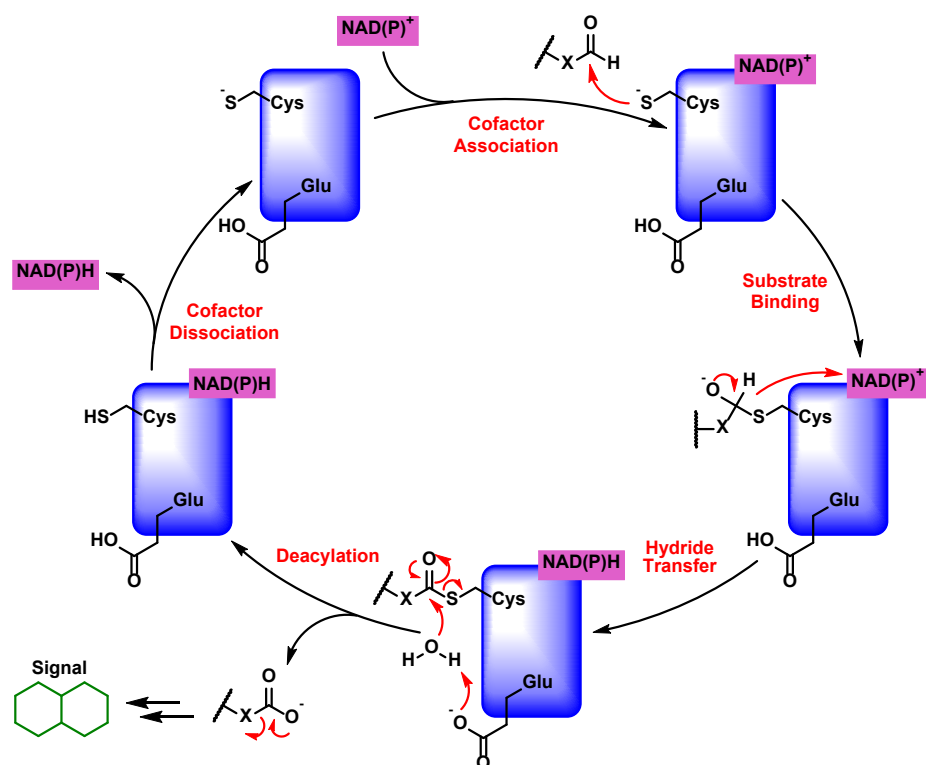


Figure B.1. Proposed mechanism for ALDH-catalyzed oxidation of formyl group.

B.2 Chemistry

The two designs we pursued involved an alkyl *S*-formyl group and an alkyl *N*-formyl group. (Figure B.2) These would undergo ALDH-catalyzed oxidation to the carbonothioic acid and carmabic acid, respectively. Decarboxylation would uncap the nucleophilic alkyl heteroatom to cyclize and form the γ - or δ -thiolactone and -lactam, respectively.

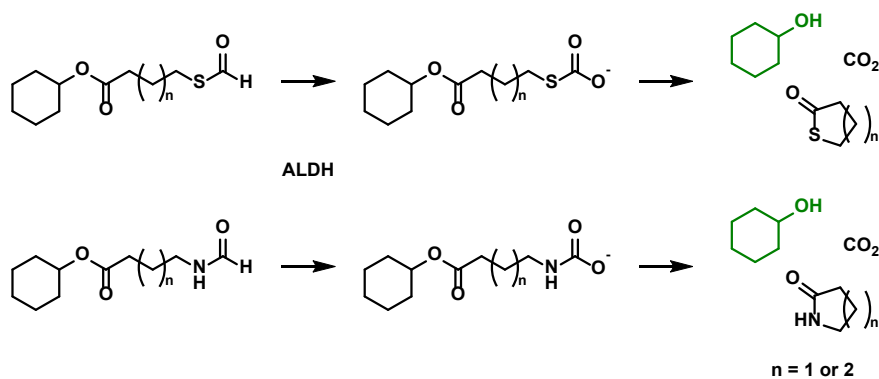
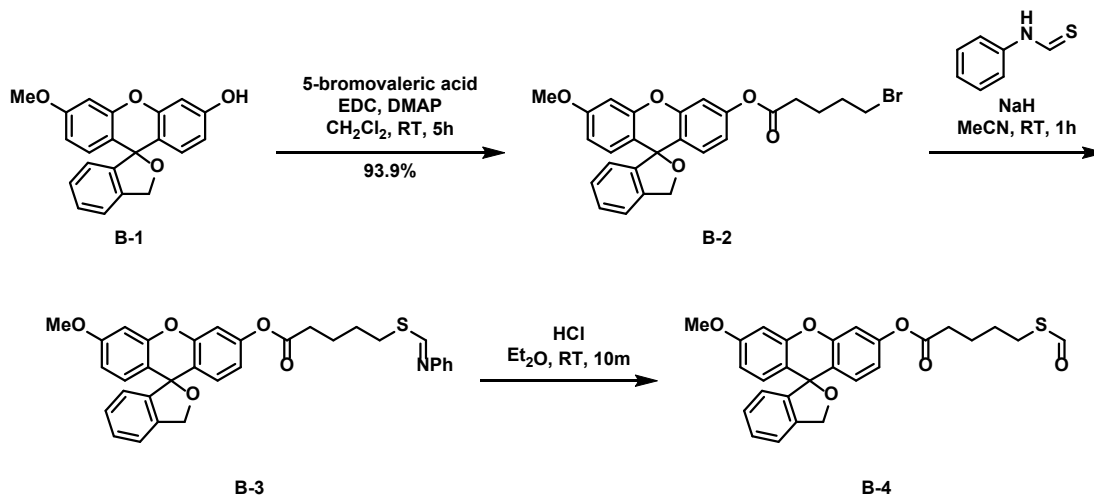


Figure B.2. Mechanism of dye release from *S*-formyl and *N*-formyl generalizable trigger-capped probes.

B.2.1 *S*-formyl trigger

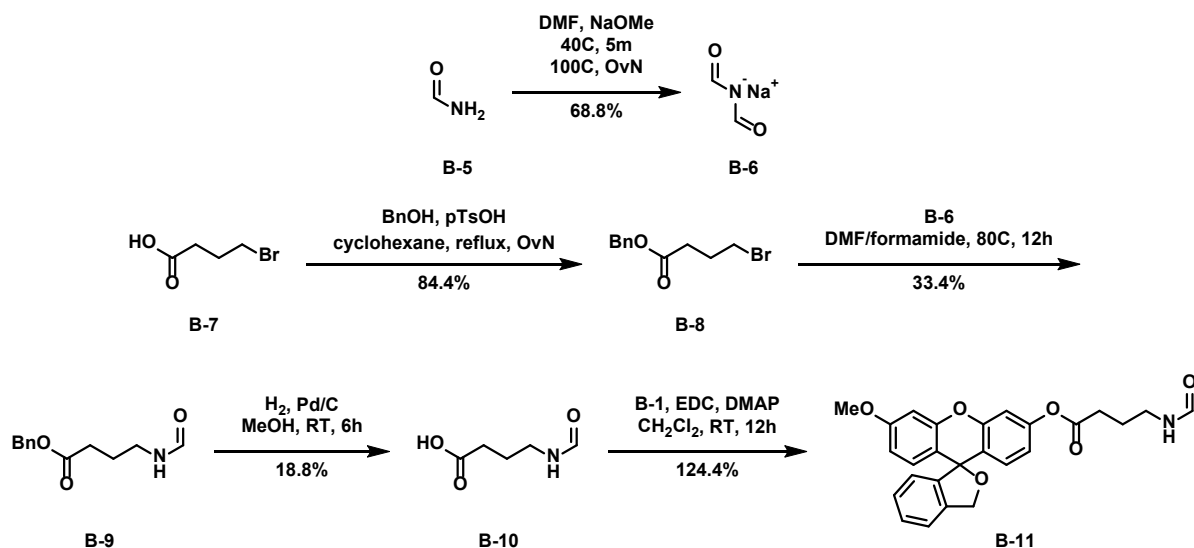
Synthesis of a probe bearing the *S*-formyl trigger was successful when constructing the trigger on the probe. (Scheme B.1) Briefly, a fluorescein analogue was esterified with 5-bromovaleric acid under conventional EDC coupling conditions to afford ester **B-2**. The bromine was displaced by deprotonated *N*-phenylthioformamide to form thioamide **B-3**. (Notably, the same conditions resulted in cyclopropanation of the 4-bromobutyric acid analogue.) The resulting *S*-alkylated product was chemoselectively hydrolyzed to the desired *S*-formyl probe in **B-4**.



Scheme B.1. Synthesis of *S*-formyl probe.

B.2.2 *N*-formyl trigger

The elevated temperatures required for alkylating with formamide derivatives proved too high for the pre-esterified dye above, precluding a synthesis analogous to that taken for the *S*-formyl probe above. Instead, 4-formamidobutyric acid was synthesized and then coupled onto a fluorescein analogue for testing. (Scheme B.2) To achieve this, diformylimide sodium salt **B-6** was prepared from formamide and DMF. Concurrently, benzyl protected 4-bromobutyric acid **B-8** was prepared using Fisher esterification conditions. These two were coupled via substitution of the bromine. Conveniently, performing the reaction with formamide as a cosolvent led to *in situ* deformylation of the diformylimide to the desired mono-alkylated formamide **B-9**. Palladium-catalyzed hydrogenation removed the benzyl protecting group to produce carboxylic acid **B-10**. The resulting free acid was coupled with the fluorescein derivative under standard EDC conditions to afford the desired *N*-formyl probe **B-11**.



Scheme B.2. Synthesis of *N*-formyl probe.

B.3 In vitro testing

To test our hypothesis that oxidation was required for successful turnover of the probe, the *S*-formyl probe was treated with just NAD^+ , with purified ALDH, or cotreated with both enzyme and cofactor. The probe was a substrate against all 6 tested ALDH isoforms, though a poor substrate for ALDH1A3, 3A1, and 5A1. (Figure B.3) The screens against ALDH1A1 and 1A2 seemed to confirm our hypothesis. In both, esterase activity (tested in the absence of NAD^+) turned the *S*-formyl probe over just slightly faster than background hydrolysis. Dehydrogenase activity (tested in the presence of NAD^+) was significantly higher by comparison indicating hydride transfer was required for rapid turnover. This trend was contradicted by the data showing turnover of the probe by ALDH2 was faster in the absence of NAD^+ .

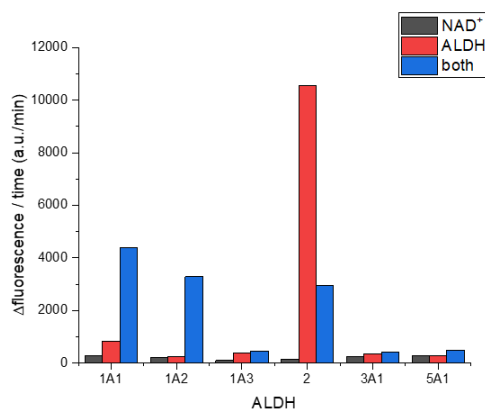


Figure B.3. Initial rates of the *S*-formyl probe turnover in the presence of ALDH, NAD^+ , or both.

This suggests that NAD^+ acts as an inhibitor to ALDH2 esterase activity. These findings are inconsistent with earlier reports that NAD^+ enhances ALDH2 esterase activity, nearly doubling the rate at the 100 μM concentrations used in our assay.⁸⁷ The major difference is previous reports were looking at a substrate that could only undergo esterase cleavage. Here, the enzyme has three possible paths: (1) esterase cleavage without NAD^+ bound, (2) esterase cleavage with NAD^+ bound, and (3) hydride transfer. Our data suggests that NAD^+ binding proceeds faster than substrate binding, but once bound the enzyme commits to hydride transfer rather than esterase cleavage. This is the first reported observation of such a phenomenon.

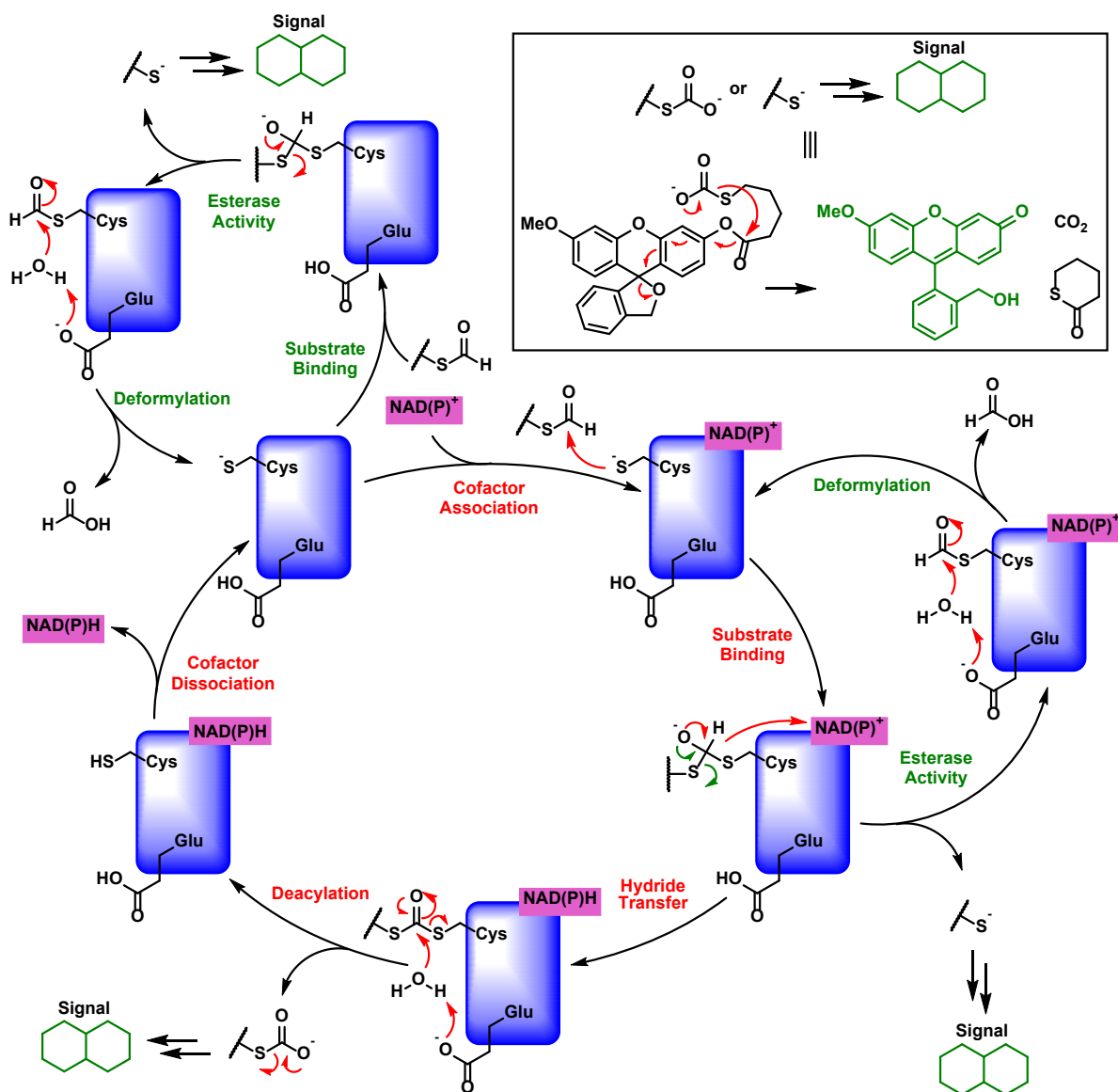


Figure B.4. Updated mechanism of ALDH2 esterase and dehydrogenase activity on the *S*-formyl probe.

Soon after screening the *S*-formyl probe against ALDH isoforms, it was screened for stability in the presence of biologically relevant ROS/RNS/RSS. The first reactive species it was tested against was glutathione. In principle, the electrophilic thioformate could be attacked by the nucleophilic sulfur of glutathione. The resulting tetrahedral intermediate could then expel either glutathione or the deformedylated probe. This is exactly what was seen. (Figure B.5) When incubated with physiological levels of glutathione (1 mM), the probe was entirely turned over with 30 minutes.

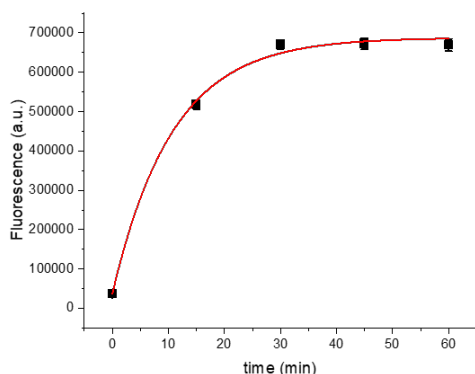


Figure B.5. Response of the *S*-formyl probe to 1 mM glutathione at 37 °C.

The instability observed when testing the *S*-formyl probe prevented its application in any cell-based system. However, the dehydrogenase activity observed motivated us to explore similar options. We hypothesized an analogous *N*-formyl probe would improve stability to free biological thiols while still maintaining reactivity with ALDH isoforms. We also synthesized a control dye, **B-15**, featuring the fluorescein analogue capped as the caproate ester. The control was intended to determine whether any failure to an undesired analyte was due to reactivity at the formyl group or at the phenyl ester.

The *N*-formyl probe and the control probe were both incubated with 1 mM glutathione, and change in fluorescence was monitored using the plate reader. (Figure B.6). Negligible turn on was observed with the control. This indicated that the ester bond was stable to glutathione. On the other hand, a steady turn on was observed with the *N*-formyl probe. Since aryl ester was previously measured to be stable, this suggested a formyl transfer from the probe to glutathione. The newly formed amine then underwent the gamma-lactam formation to release the dye.

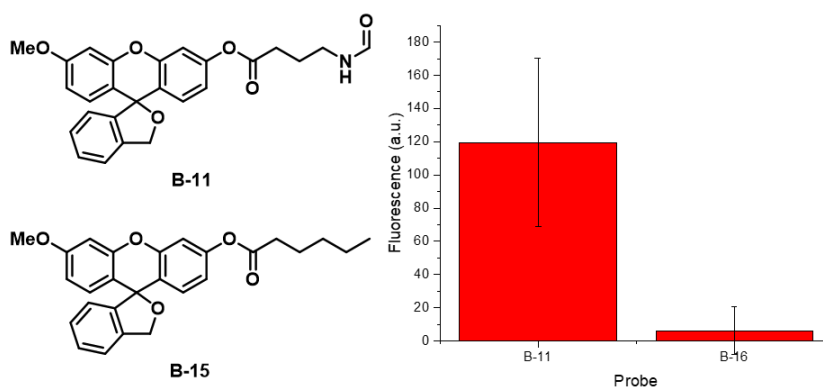


Figure B.6. The *N*-formyl probe and control probes response to 1 mM glutathione.

B.4 Future directions and outlook

While there is the possibility of continuing to improve either the *S*-formyl or *N*-formyl probes for use in purified enzyme assays or other highly simplified environments for applications such as high throughput screening, neither is likely ever to be useful native cells. Continuing along the proposed mechanism would require a more stable formate equivalent. One possibility would be a formyl hydrazine that is incapable of self-immolation until deformylation.

In reality, a self-immolative linker may not be feasible in the development of novel ALDH probes with varying isoform selectivity. Likely new probes will require changes in the electronics leading to changes in the photophysical properties without any deprotection event.

B.5 Supporting information

B.5.1 Materials and methods

Expression and purification of ALDH isoforms

Plasmids for ALDH1A1, ALDH1A2, ALDH1A3, ALDH2, ALDH3A1, ALDH4A1, and ALDH4A1 were generously provided by Professor Daria Mochly-Rosen (Stanford). Expression and purification of each isoform was performed as previously described.⁷¹

ALDH isoform and chemical selectivity

Each ALDH isoform was added to a 50 mM triethanolamine solution (pH 7.4) containing 2.0 mM NAD⁺ and 100 μ M substrate at room temperature. Benzaldehyde was the substrate for ALDH3A1. Propanal was the substrate for all other isoforms. ALDH isoform activity was determined by monitoring the rate of NADH production through the increase in absorbance at 340 nm ($\epsilon = 6220 \text{ M}^{-1}\text{cm}^{-1}$). For these assays, 1 unit is defined as the amount of enzyme that catalyzes

the conversion of 1 μM substrate per minute. For every combination of dye and enzyme or glutathione, 2 μM dye was preincubated with 2.0 mM NAD^+ in 50 mM triethanolamine solution (pH 7.4). The reaction was initiated by addition of 1 unit of ALDH or 1 mM glutathione. All measurements were performed in triplicate using in 96-well plates using a plate reader.

B.5.2 Synthesis and characterization

B.5.2.1 Synthesis of *S*-formyl probe

3'-methoxy-3H-spiro[isobenzofuran-1,9'-xanthen]-6'-yl 5-bromopentanoate (B-2) A flask was charged with **B-1** (0.22 g, 0.66 mmol, 1.0 eq.), 5-bromovaleric acid (0.133 g, 0.73 mmol, 1.1 eq.), EDC-HCl (1.02 g, 5.3 mmol, 8.0 eq.), DMAP (0.054 g, 0.33 mmol, 0.5 eq.), and CH_2Cl_2 (10 mL). After stirring at room temperature for 5 hours, the reaction was washed with sat. NH_4Cl . The organic layer was purified via flash chromatography on a silica column (CH_2Cl_2) to afford the title compound (0.308 g, 0.62 mmol, 93.9%). ^1H NMR (500 MHz, Chloroform-*d*) δ 7.41 – 7.35 (m, 2H), 7.27 (dt, J = 8.4, 4.3 Hz, 1H), 7.01 (d, J = 2.3 Hz, 1H), 6.99 (d, J = 8.6 Hz, 1H), 6.91 (d, J = 7.8 Hz, 1H), 6.90 (d, J = 8.6 Hz, 1H), 6.78 (dd, J = 8.6, 2.3 Hz, 1H), 6.74 (d, J = 2.5 Hz, 1H), 6.64 (dd, J = 8.7, 2.5 Hz, 1H), 5.32 (s, 2H), 3.81 (s, 3H), 3.45 (t, J = 6.4 Hz, 2H), 2.61 (t, J = 7.2 Hz, 2H), 1.99 (p, J = 6.5 Hz, 2H), 1.91 (p, J = 6.8 Hz, 2H). ^{13}C NMR (126 MHz, Chloroform-*d*) δ 171.30, 160.44, 151.32, 150.99, 150.82, 144.72, 139.00, 129.88, 129.82, 128.48, 128.28, 123.94, 122.48, 120.78, 116.89, 116.79, 111.44, 109.69, 100.47, 83.36, 72.30, 55.55, 33.38, 33.04, 31.91, 23.44.

3'-methoxy-3H-spiro[isobenzofuran-1,9'-xanthen]-6'-yl (E)-5-(((phenylimino)methyl)thio)pentanoate (B-3) A flame-dried flask was charged with thioformanilide (0.095 g, 0.070 mmol, 1.0 eq.), 60% by weight NaH (0.028 g, 0.070 mmol, 1.0 eq.) and anhydrous MeCN (1 mL). A separate flame-dried flask was charged with **B-2** (0.348 g, 0.070 mmol, 1.0 eq.) and anhydrous MeCN (1 mL). The solution of **B-2** was added dropwise to the mixture of thioformanilide over 1 minute. After stirring at room temperature for 1 hour, the reaction was concentrated under reduced pressure. The crude residue was suspended in Et_2O and poured through filter paper. The filtrate was collected and concentrated to a yellow-orange solid.

3'-methoxy-3H-spiro[isobenzofuran-1,9'-xanthen]-6'-yl 5-(formylthio)pentanoate (B-4) A flask was charged with **B-3** and Et_2O (10 mL). The solution was treated with dropwise conc. HCl (0.060 mL, 0.70 mmol, 1.0 mmol). After stirring for 10 minutes, the reaction was poured through filter paper and washed with CH_2Cl_2 . The filtrate was concentrated under reduced

pressure. The resulting crude residue was purified via flash chromatography on silica gel (30:70 v/v EtOAc:hexanes) to afford the title compound. ¹H NMR (500 MHz, Chloroform-*d*) δ 10.14 (s, 1H), 7.39 – 7.34 (m, 2H), 7.30 – 7.23 (m, 1H), 6.99 (d, *J* = 2.4 Hz, 1H), 6.97 (d, *J* = 8.5 Hz, 1H), 6.90 (d, *J* = 7.6 Hz, 1H), 6.88 (d, *J* = 8.7 Hz, 1H), 6.76 (dd, *J* = 8.6, 2.3 Hz, 1H), 6.73 (d, *J* = 2.5 Hz, 1H), 6.63 (dd, *J* = 8.7, 2.6 Hz, 1H), 5.31 (s, 2H), 3.82 (s, 3H), 3.03 (t, *J* = 7.1 Hz, 2H), 2.60 (t, *J* = 7.2 Hz, 2H), 1.84 (dtd, *J* = 8.9, 7.7, 7.1, 5.6 Hz, 2H), 1.75 (dtd, *J* = 9.8, 7.3, 5.0 Hz, 2H). ¹³C NMR (126 MHz, Chloroform-*d*) δ 187.55, 171.37, 160.52, 151.42, 151.08, 150.91, 144.80, 139.09, 129.93, 129.87, 128.54, 128.33, 124.05, 122.54, 120.81, 116.94, 116.89, 111.51, 109.75, 100.56, 83.45, 72.36, 55.61, 33.78, 29.01, 26.24, 23.91.

B.5.2.2 Synthesis of *N*-formyl probe

diformylimide sodium salt (B-6) A flask was charged with DMF (100 mL, 1290 mmol, 3.5 eq.) and NaOMe (20.0 g, 370 mmol, 1.0 eq.). The reaction was heated to 40 °C and then treated with formamide (35 mL, 880 mmol, 2.4 eq.). The flask was attached to a short path distillation column and heated to 100 °C. After stirring overnight, the reaction was concentrated under reduced pressure while still hot. The slurry was cooled to room temperature, poured over filter paper, washed with DMF (100 mL), and vacuum dried. The precipitate was collected and further dried under reduced pressure at 75 °C to afford the title compound as an off-white solid (24.2 g, 255 mmol, 68.8%). ¹H NMR (500 MHz, DMSO-*d*₆) δ 8.96 (s, 2H). ¹³C NMR (126 MHz, DMSO-*d*₆) δ 180.75.

benzyl 4-bromobutyrate (B-8) A flask was charged with 4-bromobutyric acid (1.68 g, 10 mmol, 1.0 eq.), cyclohexane (30 mL), pTsOH-H₂O (0.22 g, 1.0 mmol, 0.1 eq.), and lastly benzyl alcohol (1.35 mL, 13 mmol, 1.3 eq.). The flask was fitted with a Dean-Stark apparatus and heated to 110 °C. After stirring overnight, the reaction was cooled to room temperature. The reaction was washed with sat. NaHCO₃ followed by brine, dried over Na₂SO₄, and concentrated under reduced pressure to afford the title compound as a colorless oil (2.17 g, 8.44 mmol, 84.4%). ¹H NMR (500 MHz, Chloroform-*d*) δ 7.41 – 7.29 (m, 5H), 5.13 (s, 2H), 3.46 (t, *J* = 6.4 Hz, 2H), 2.56 (t, *J* = 7.2 Hz, 2H), 2.28 – 2.10 (m, 2H).

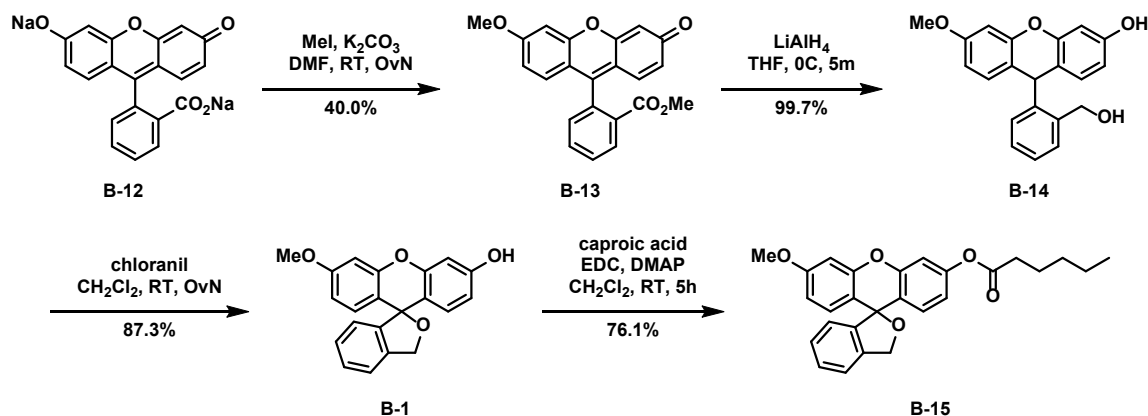
benzyl 4-formamidobutyrate (B-9) A flask was charged with **B-8** (0.50 g, 1.94 mmol, 1.0 eq.), DMF, (5 mL) and formamide (5 mL). The solution was treated with **A-6** (0.186 g, 1.94 mmol, 1.0 eq.). The reaction was heated to 80 °C for 12 hours. Once cool, the reaction was concentrated. The crude material was purified via flash chromatography on silica gel (0:100 to

70:30 v/v EtOAc:hexanes gradient) to afford the title compound (0.162 g, 0.732 mmol, 37.7%). ¹H NMR (500 MHz, Chloroform-*d*) δ 7.96 (s, 1H), 7.38 – 7.26 (m, 5H), 5.11 (s, 2H), 4.17 (td, *J* = 6.3, 0.9 Hz, 2H), 2.44 (t, *J* = 7.4 Hz, 2H), 1.99 (p, *J* = 6.8 Hz, 2H). ¹³C NMR (126 MHz, Chloroform-*d*) δ 172.33, 160.77, 135.77, 128.46, 128.16, 128.15, 66.23, 62.68, 30.48, 23.77.

4-formamidobutyric acid (B-10) A flask was charged with **A-9** (0.162 g, 0.73 mmol, 1.0 eq.), MeOH (5 mL), and 10% w/w palladium on carbon (0.030 g). The reaction was performed under H₂ gas at 1 atm. After stirring vigorously for 6 hours, the reaction was filtered through Celite®. The crude material was purified via flash chromatography on silica gel (50:50 to 70:30 v/v EtOAc:hexanes gradient followed by 10:90 v/v MeOH/CH₂Cl₂) to afford the title compound (0.018 g, 0.137 mmol, 18.8%). ¹H NMR (500 MHz, Chloroform-*d*) δ 8.06 (s, 1H), 4.23 (t, *J* = 6.3 Hz, 2H), 2.49 (t, *J* = 7.3 Hz, 2H), 2.02 (p, *J* = 6.8 Hz, 2H).

3'-methoxy-3H-spiro[isobenzofuran-1,9'-xanthen]-6'-yl 4-formamidobutyrate (B-11)
A flask was charged with **A-10** (0.018 g, 0.137 mmol, 1.0 eq.), **A-1** (0.057 g, 0.17 mmol, 1.25 eq.), EDC-HCl (0.215 g, 1.10 mmol, 8.0 eq.), DMAP (0.010 g, 0.08 mmol, 0.6 eq.), and CH₂Cl₂ (3 mL). After stirring for 12 hours at room temperature, the reaction was washed with sat. NH₄Cl. The organic layer was purified via flash chromatography on silica gel (50:50 v/v EtOAc:hexanes) to afford the title compound. ¹H NMR (500 MHz, Chloroform-*d*) δ 8.08 (s, 1H), 7.36 (q, *J* = 4.9, 3.7 Hz, 2H), 7.27 (tt, *J* = 5.6, 3.0 Hz, 1H), 6.99 (d, *J* = 2.4 Hz, 1H), 6.97 (d, *J* = 8.6 Hz, 1H), 6.90 (d, *J* = 7.5 Hz, 1H), 6.88 (d, *J* = 8.7 Hz, 1H), 6.77 (dd, *J* = 8.6, 2.3 Hz, 1H), 6.72 (d, *J* = 2.6 Hz, 1H), 6.63 (dd, *J* = 8.8, 2.6 Hz, 1H), 5.31 (s, 2H), 4.29 (t, *J* = 6.2 Hz, 2H), 3.82 (s, 3H), 2.69 (t, *J* = 7.3 Hz, 2H), 2.12 (p, *J* = 6.8 Hz, 2H). ¹³C NMR (126 MHz, Chloroform-*d*) δ 171.00, 161.01, 160.51, 151.40, 151.08, 150.81, 144.74, 139.08, 129.98, 129.88, 128.55, 128.34, 124.04, 122.59, 120.82, 116.88, 116.82, 111.53, 109.72, 100.53, 83.44, 72.35, 62.80, 55.61, 30.88, 23.94.

B.5.2.3 Synthesis of control probe



Scheme B.3. Synthesis of control-formyl probe.

methyl 2-(6-methoxy-3-oxo-3H-xanthen-9-yl)benzoate (B-13) A flame-dried flask was charged with fluorescein sodium salt (3.76 g, 10 mmol, 1.0 eq.), K₂CO₃ (4.15 g, 30 mmol, 3.0 eq.), and anhydrous DMF (30 mL). While stirring at room temperature, the reaction was treated dropwise with MeI (2.5 mL, 40 mmol, 4.0 mL). After stirring overnight, the reaction was poured into brine. The mixture was extracted from CH₂Cl₂. The organic layer was washed with sat. NaHCO₃, dried over Na₂SO₄, and concentrated. The crude residue was purified via flash chromatography (10:90 v/v MeOH:CH₂Cl₂) to afford the title compound as an orange solid (1.442 g, 4.00 mmol, 40.0%). ¹H NMR (500 MHz, Chloroform-*d*) δ 8.24 (dd, *J* = 7.9, 1.4 Hz, 1H), 7.73 (td, *J* = 7.5, 1.4 Hz, 1H), 7.67 (td, *J* = 7.7, 1.4 Hz, 1H), 7.31 (dd, *J* = 7.6, 1.3 Hz, 1H), 6.96 (d, *J* = 2.4 Hz, 1H), 6.88 (d, *J* = 8.9 Hz, 1H), 6.84 (d, *J* = 9.7 Hz, 1H), 6.73 (dd, *J* = 8.9, 2.4 Hz, 1H), 6.53 (dd, *J* = 9.7, 1.9 Hz, 1H), 6.45 (d, *J* = 1.9 Hz, 1H), 3.91 (s, 3H), 3.63 (s, 3H). ¹³C NMR (126 MHz, Chloroform-*d*) δ 185.80, 165.73, 164.15, 159.06, 154.41, 134.77, 132.82, 131.25, 130.70, 130.43, 130.32, 130.05, 129.78, 128.95, 121.40, 117.72, 114.95, 113.55, 105.92, 100.44, 56.11, 52.55.

9-(2-(hydroxymethyl)phenyl)-6-methoxy-9H-xanthen-3-ol (B-14) A flame-dried flask was charged with **B-13** (0.362 g, 1.0 mmol, 1.0 eq.) and anhydrous THF (10 mL). The orange mixture was cooled to 0 °C before being treated portionwise with LiAlH₄ (0.57 g, 1.5 mmol, 1.5 eq.) over 3 minutes. After stirring for 5 minutes, the reaction was quenched via the slow addition of 1M HCl (5 mL) and diluted with H₂O. The THF was removed under reduced pressure. The remaining aqueous layer was extracted from with CH₂Cl₂ (3x15 mL). The organic layers were combined, dried over Na₂SO₄, and concentrated to afford the title compound as a light yellow powder (0.335 g, 1.00 mmol, 99.7%). ¹H NMR (500 MHz, Chloroform-*d*) δ 7.43 (dd, *J* = 5.3,

3.7 Hz, 1H), 7.29 – 7.24 (m, 2H), 7.22 (t, $J = 5.2, 3.7$ Hz, 1H), 6.81 (d, $J = 8.6$ Hz, 1H), 6.78 (d, $J = 8.6$ Hz, 1H), 6.66 (d, $J = 2.6$ Hz, 1H), 6.60 (d, $J = 2.5$ Hz, 1H), 6.53 (dd, $J = 8.6, 2.6$ Hz, 1H), 6.43 (dd, $J = 8.3, 2.5$ Hz, 1H), 5.49 (s, 1H), 5.01 (s, 1H), 4.64 (s, 2H), 3.81 (s, 3H).

6'-methoxy-3H-spiro[isobenzofuran-1,9'-xanthen]-3'-ol (B-1) A flask was charged with **B-14** (0.231 g, 0.69 mmol, 1.0 eq.) and CH₂Cl₂ (3 mL). Once a solution had formed, chloranil (0.189 g, 0.76 mmol, 1.1 eq.) was added. After stirring overnight, the reaction was purified via flash chromatography on silica gel (0:100 to 5:95 v/v MeOH:CH₂Cl₂ gradient) to afford the title compound as an orange solid (0.200 g, 0.602 mmol, 87.3%). ¹H NMR (500 MHz, Methanol-*d*₄) δ 7.42 (d, $J = 7.6$ Hz, 1H), 7.38 (t, $J = 7.5$ Hz, 1H), 7.28 (t, $J = 7.3$ Hz, 1H), 6.82 (d, $J = 8.7$ Hz, 1H), 6.81 (d, $J = 7.9$ Hz, 1H), 6.75 (d, $J = 8.6$ Hz, 1H), 6.74 (d, $J = 2.6$ Hz, 1H), 6.63 (dd, $J = 8.8, 2.6$ Hz, 1H), 6.60 (d, $J = 2.5$ Hz, 1H), 6.51 (dd, $J = 8.6, 2.5$ Hz, 1H), 5.25 (s, 2H), 3.81 (s, 3H).

3'-methoxy-3H-spiro[isobenzofuran-1,9'-xanthen]-6'-yl caproate (B-15) A flask was charged with **B-1** (0.332 g, 1.0 mmol, 1.0 eq.), caproic acid (0.14 mL, 1.1 mmol, 1.1 eq.), EDC-HCl (1.53 g, 8.0 mmol, 8.0 eq.), DMAP (0.06 g, 0.5 mmol, 0.5 eq.), and CH₂Cl₂ (10 mL). After stirring for 5 hours at room temperature, the reaction was washed with sat. NH₄Cl. The organic layer was purified via flash chromatography on silica gel (10:90 to 30:70 v/v EtOAc:hexanes gradient) to afford the title compound (0.3272 g, 0.761 mmol, 76.1%). ¹H NMR (500 MHz, Chloroform-*d*) δ 7.41 – 7.34 (m, 2H), 7.32 – 7.22 (m, 1H), 7.00 (d, $J = 2.3$ Hz, 1H), 6.98 (d, $J = 8.6$ Hz, 1H), 6.91 (d, $J = 7.5$ Hz, 1H), 6.89 (d, $J = 8.8$ Hz, 1H), 6.78 (dd, $J = 8.6, 2.3$ Hz, 1H), 6.73 (d, $J = 2.5$ Hz, 1H), 6.64 (dd, $J = 8.7, 2.5$ Hz, 1H), 5.32 (s, 2H), 3.82 (s, 3H), 2.56 (t, $J = 7.5$ Hz, 2H), 1.76 (p, $J = 7.4$ Hz, 2H), 1.43 – 1.36 (m, 4H), 0.94 (t, $J = 7.1$ Hz, 3H).

Appendix C. Acoustogenic probe for calcium

C.1 Introduction

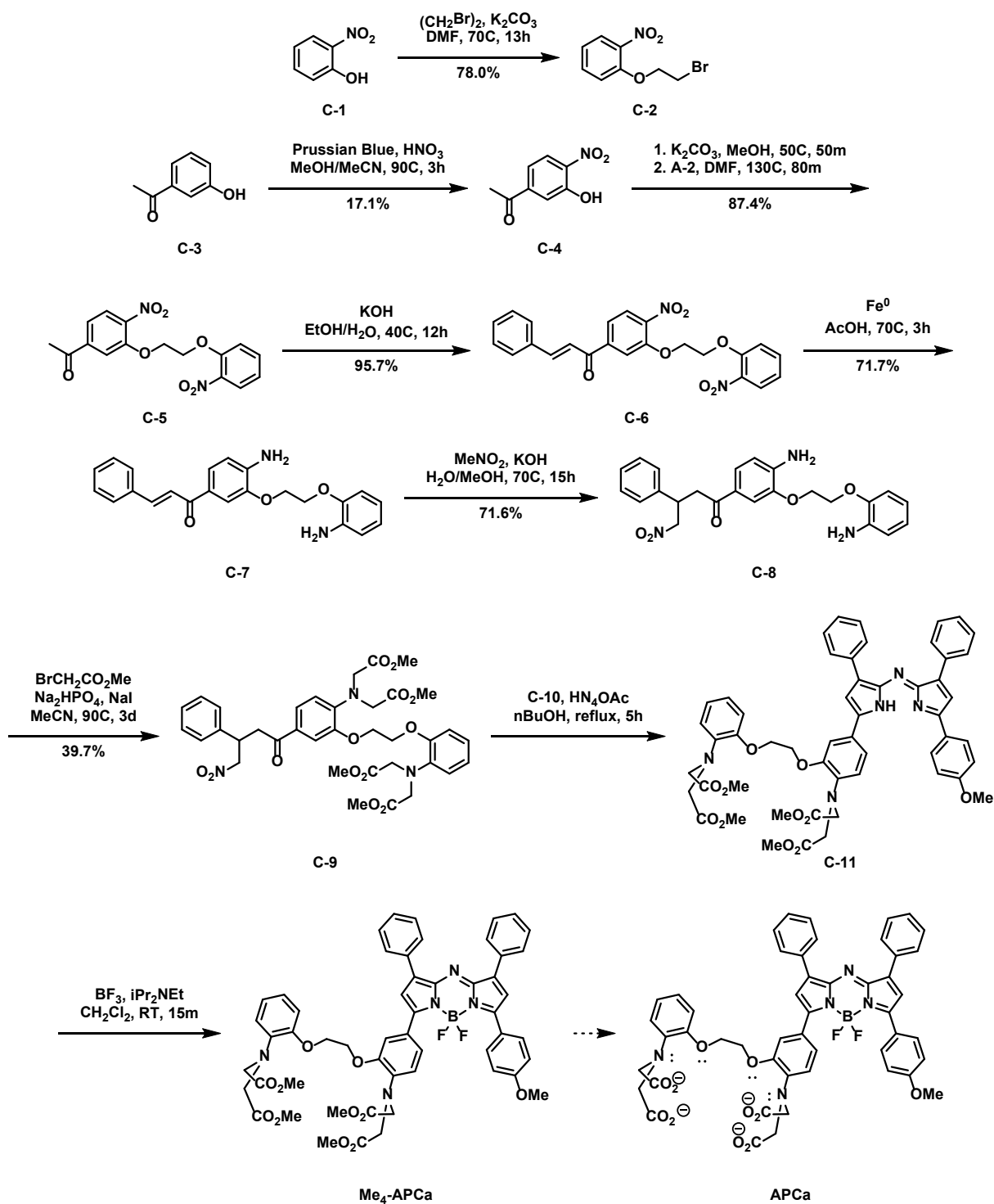
Calcium (Ca^{2+}) is one of the most important metal ions necessary for normal brain function.⁸⁸ Specifically, it is an integral component of signal transduction, where it acts as a second messenger to exert control over membrane excitability, synaptogenesis, and neurotransmission. To achieve control over such a diverse range of cellular functions, the concentration of cytosolic Ca^{2+} is tightly regulated to maintain a resting-state concentration 20,000-fold more dilute than extracellular Ca^{2+} concentrations. However, upon stimulation, extracellular Ca^{2+} , as well as Ca^{2+} in the mitochondrial and endoplasmic reticulum stores are rapidly released down this gradient into the cytoplasm. This change triggers downstream signaling events such as activation of the Ca^{2+} -dependent transcription factor, NFAT, to initiate transcription.⁸⁹ While this bulk phenomenon has been appreciated for decades,¹⁴ the relative contributions of calcium oscillation frequency, amplitude, and duty cycle to transcriptional activity remain unclear. In order to understand this fundamental biological process with both high resolution cellular imaging and deep tissue imaging, we aim to design a multimodal (fluorescent and photoacoustic) reversible probe for Ca^{2+} .

C.2 Design and synthesis of APCa

With the goal of developing a ratiometric photoacoustic probe for Ca^{2+} , we set out to synthesize acoustogenic probe for calcium (APCa) based on the azo-BODIPY platform. The term “acoustogenic” was coined by the Chan lab in 2015 to stipulate a turn-on, analyte-responsive photoacoustic probe. The design was based on the well-established BAPTA moiety first developed by Roger Tsien. In the unbound state (low Ca^{2+}), the aniline lone pair would be free to conjugate into the BODIPY core. In the Ca^{2+} -bound state (high Ca^{2+}), the aniline lone pair would be involved in Ca^{2+} coordination, precluding conjugation and hypsochromically shifting the absorbance spectrum.

Many synthetic routes were pursued; only the synthesis which yielded the tetramethylated precursor will be described (Scheme C.1). Synthesis began with the Prussian Blue-catalyzed nitration of 3-hydroxyacetophenone to 3-hydroxy-4-nitroacetophenone **C-4**. The excellent regioselectivity reported in literature⁹⁰ was not reproducible, but the desired isomer was easily isolable with improved isomeric yields over the uncatalyzed reaction. The phenol was then converted to the potassium phenoxide with K_2CO_3 , isolated, and then alkylated with separately synthesized 1-(2-bromoethoxy)-2-nitrobenzene **C-2** to form the diaryl **C-5**. An aldol condensation

was then performed with benzaldehyde to afford chalcone **C-6**. The two aryl nitro groups were chemoselectively reduced to their corresponding anilines in **C-7** using the Bechamp reduction in AcOH. A Michael addition was then performed using nitromethane to prepare the azo-BODIPY precursor **C-8**. Before dimerization, **C-9** was formed via tetraalkylation with methyl bromoacetate at elevated temperatures in MeCN. Significant quantities of trialkylated product were also isolated which could be resubjected to reaction conditions. This tetramethyl-BAPTA-functionalized aza-BODIPY precursor **C-9** was dimerized with methoxy precursor **C-10** (synthesized by Christopher Reinhardt), requiring temperatures >110 °C for solubility and efficient coupling. Incorporation of BF₂ with BF₃-Et₂O occurred rapidly to produce the tetramethylated APCa (Me₄-APCa). Chemoselective deprotection of the Me₄-APCa to afford APCa was unsuccessful under all tested conditions.



Scheme C.1. Synthesis towards APCa.

An analogous synthesis was also attempted using allyl bromoacetate (synthesized by Effie Zhou) towards tetraallylated APCa (Allyl₄-APCa). The alkylation, dimerization, and BF₂

incorporation were equally successful to the methyl analogues in the synthesis of Allyl₄-APCa. However, removal of the allyl protecting groups was unsuccessful under all tested conditions.

C.3 Preliminary results

Without free carboxylate moieties, Me₄-APCa does not have a strong affinity for Ca²⁺. No colorimetric changes were observed upon washing with aqueous CaCO₃. However, some preliminary testing could proceed through protonation studies. This strategy is commonly used to screen a probe's response in which the mechanism involves modulating the nitrogen's lone pair electrons.⁸ Protonation of the aniline under acidic conditions can effectively simulate APCa binding of Ca²⁺ since, in both cases, the nitrogen lone pairs are prevented from delocalizing into the azo-BODIPY dye.

Using this strategy, unbound dye was found to have a maximum absorbance around 725 nm in CHCl₃. (Figure C.1.A) Simulating Ca²⁺-binding by protonation with TFA, the absorbance blue-shifted to 670 nm. An similar change was seen in the emission spectra of Me₄-APCa, blue-shifting from 779 nm to 712 nm upon cation binding. (Figure C.1.B) Analogous spectra were not obtained in an aqueous buffer since Me₄-APCa aggregated in standard PBS buffer, confounding photophysical spectra. The polyanionic nature of APCa is expected to prevent similar aggregation as the active probe.

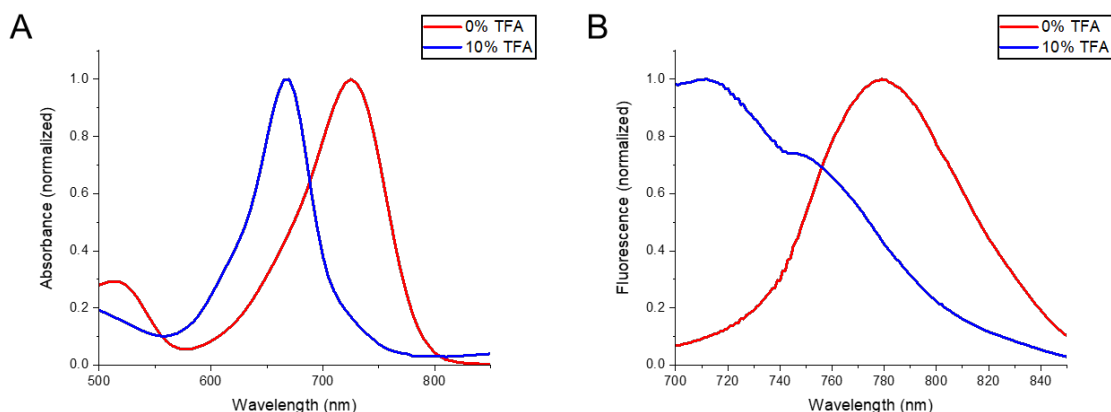


Figure C.1. Spectra of Me₄-APCa with cation binding. (A) Absorbance and (B) emission spectra of 2 μM Me₄-APCa in both 0% and 10% TFA in CHCl₃. Emission spectra acquired using 680 nm excitation.

An important quality for the azo-BODIPY dye platform is it is often multimodal; it can be used for both fluorescence and photoacoustic imaging. This ability to use one probe for both high-resolution, limited-depth confocal microscopy and lower-resolution, deep-tissue photoacoustic

imaging improves translatability in experiments from *in vitro* to *in vivo* settings. For this reason, we were able to use the fluorescence properties of Me₄-APCa to show that the probe is cell permeable. (Figure C.2) This provides strong evidence that a cell-permeable APCa can be synthesized – likely one protected by AM esters.

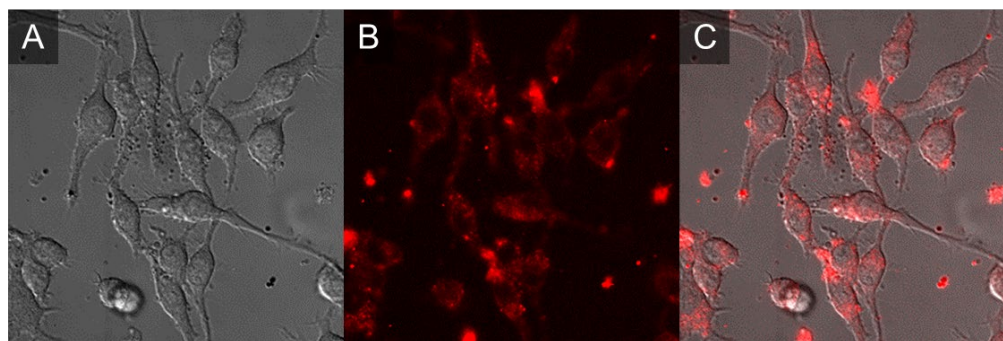


Figure C.2. Fluorescence imaging of Me₄-APCa-stained mammalian cells. (A) Brightfield, (B) Cy7-filter, and (C) overlay images acquired after staining with Me₄-APCa. Images were acquired using the Cy7 filter set on an epifluorescence microscope.

C.4 Future directions and outlook

Currently this project is limited by lack of a synthetically accessible probe. More rigorous screening of deprotection conditions for Me₄-APCa and Allyl₄-APCa would be a logical first step. Previous attempts were limited by the quantity of protected APCa. On the way towards producing more protected APCa, a viable alternative may be deprotection before BF₂ incorporation. In every deprotection attempt wherein a reaction occurred, deborylation was observed. Thus, so long as BF₂ incorporation is possible in the presence of the BAPTA moiety, this could provide APCa in an equal number of steps. A more involved alternative would be incorporation of an alternative protecting group (e.g. *p*-methoxybenzyl ester or *tert*-butyl ester). In any case, APCa will need to be protected with AM ester groups for cell permeability.

C.5 Supporting information

C.5.1 Materials and methods

3-hydroxyacetophenone and NH₄OAc were purchased from AK Scientific. EtOH was purchased from Decon Labs. AcOH, CH₂Cl₂, DMF, MeCN, MeOH, and nBuOH were purchased from Fisher Scientific. 1,2-dibromoethane, 2-nitrophenol, DIPEA, K₂CO₃, KOH, MeNO₂, Na₂HPO₄, and NaI were purchased from Oakwood Chemical. Anhydrous DMF, anhydrous MeCN, benzaldehyde, BF₃-Et₂O, and Fe⁰ were purchased from Sigma Aldrich. Dry CH₂Cl₂ and dry DMF

were each prepared by drying commercial DMF over freshly activated 4 Å molecular sieves for a minimum of 24 hours. All other chemicals were used as commercially supplied without further purification.

C.5.2 Synthesis and characterization

1-(2-bromoethoxy)-2-nitrobenzene (C-2) A flame-dried flask was charged with 2-nitrophenol (14.4 g, 100 mmol, 1.0 eq.), K₂CO₃ (15.3 g, 100 mmol, 1.0 eq.), and dry DMF (40 mL). The mixture was rapidly treated with 1,2-dibromoethane (35 mL, 400 mmol, 4.0 eq.) and heated to 70 °C for 13 hours. Once cool, the reaction was diluted with brine and extracted with EtOAc. The organic layer was collected, washed with brine, sat. NH₄Cl, and brine, then dried over Na₂SO₄ and concentrated under reduced pressure to afford the title compound as a yellow oil (19.2 g, 78.0 mmol, 78.0%). ¹H NMR (400 MHz, Chloroform-*d*) δ 7.84 (dd, *J* = 8.3, 1.7 Hz, 1H), 7.54 (ddd, *J* = 8.4, 7.4, 1.7 Hz, 1H), 7.13 – 7.04 (m, 2H), 4.42 (t, *J* = 6.5 Hz, 2H), 3.67 (t, *J* = 6.5 Hz, 2H).

3-hydroxy-4-nitroacetophenone (C-4) A pressure flask was charged with 3-hydroxyacetophenone (3.19 g, 23.3 mmol, 1.0 eq.), Prussian Blue (2.00 g, 2.33 mmol, 0.10 eq.), MeOH (20 mL), and MeCN (20 mL). The mixture was treated with conc. HNO₃ (2.3 mL, 35 mmol, 1.5 eq.). The pressure flask was sealed and heated to 90 °C for 3 hours. After cooling, the mixture was poured over filter paper. After concentration under reduced pressure, the crude filtrate was purified via flash chromatography on a silica column (10:90 v/v EtOAc:hexanes) to afford the title compound as a yellow solid (0.72 g, 4.0 mmol, 17.1%). ¹H NMR (500 MHz, Chloroform-*d*) δ 10.52 (s, 1H), 8.19 (d, *J* = 8.8 Hz, 1H), 7.69 (d, *J* = 1.9 Hz, 1H), 7.52 (dd, *J* = 8.8, 1.9 Hz, 1H), 2.63 (s, 3H). ¹³C NMR (126 MHz, Chloroform-*d*) δ 196.24, 155.09, 143.81, 135.76, 125.73, 120.43, 119.24, 27.12.

1-(4-nitro-3-(2-(2-nitrophenoxy)ethoxy)phenyl)ethan-1-one (C-5) A flask was charged with **C-4** (1.202 g, 6.64 mmol, 1.0 eq.) and MeOH (20 mL). The solution was treated with K₂CO₃ (0.467 g, 3.38g, 0.51 eq.). After 30 minutes at room temperature, the reaction was concentrated under reduced pressure. The resulting dark red solid was dissolved in anhydrous DMF (20 mL) and treated with **C-2** (1.65 g, 6.64 mmol, 1.0 eq.). The reaction was heated to 130 °C for 80 minutes. After cooling to room temperature, the reaction was treated with H₂O (80 mL) and further cooled to 4 °C. The mixture was filtered, and the precipitate was vacuum dried to afford the title compound as a light brown solid (2.01 g, 5.80 mmol, 87.4%). ¹H NMR (500 MHz, Chloroform-*d*)

δ 7.86 (d, J = 8.3 Hz, 1H), 7.81 (dd, J = 8.0, 1.7 Hz, 1H), 7.75 (d, J = 1.6 Hz, 1H), 7.62 (dd, J = 8.3, 1.6 Hz, 1H), 7.57 (ddd, J = 8.4, 7.4, 1.7 Hz, 1H), 7.20 (dd, J = 8.4, 1.1 Hz, 1H), 7.09 (ddd, J = 8.4, 7.4, 1.1 Hz, 1H), 4.60 (dd, J = 5.6, 3.4 Hz, 2H), 4.54 (dd, J = 5.8, 3.4 Hz, 2H), 2.67 (s, 3H).

(E)-1-(4-nitro-3-(2-(2-nitrophenoxy)ethoxy)phenyl)-3-phenylprop-2-en-1-one (C-6) A flask was charged with **C-5** (1.505 g, 4.35 mmol, 1.0 eq.), EtOH (50 mL), 10 M KOH (1.3 mL, 13 mmol, 3.0 eq.), and lastly benzaldehyde (0.66 mL, 6.5 mmol, 1.5 eq.). The reaction was heated to 40 °C for 12 hours. After cooling to room temperature, the reaction was treated with sat. NH_4Cl (50 mL) and further cooled to 4 °C. The mixture was filtered, and the precipitate was vacuum dried to afford the title compound as a light brown solid (1.808 g, 4.16 mmol, 95.8%). ^1H NMR (500 MHz, Chloroform- d) δ 7.91 (d, J = 8.3 Hz, 1H), 7.87 (d, J = 15.7 Hz, 1H), 7.83 (dd, J = 8.1, 1.7 Hz, 1H), 7.80 (d, J = 1.5 Hz, 1H), 7.72 – 7.65 (m, 3H), 7.61 – 7.54 (m, 1H), 7.49 (d, J = 15.7 Hz, 1H), 7.47 – 7.44 (m, 3H), 7.23 (d, J = 8.6 Hz, 1H), 7.09 (t, J = 7.7 Hz, 1H), 4.63 (dd, J = 5.6, 3.5 Hz, 2H), 4.57 (dd, J = 5.8, 3.5 Hz, 2H).

(E)-1-(4-amino-3-(2-(2-aminophenoxy)ethoxy)phenyl)-3-phenylprop-2-en-1-one (C-7) A flask was charged with **C-6** (0.221 g, 0.50 mmol, 1.0 eq.), Fe^0 (0.280g, 5.0 mmol, 10 eq.), and AcOH (5 mL). The reaction was heated to 70 °C for 3 hours, and then the solvent was removed under reduced pressure. The crude residue suspended in EtOAc, CH_2Cl_2 , sat. NaHCO_3 , and brine. After concentration of the organic layer under reduced pressure, the crude filtrate was purified via flash chromatography on a silica column (40:60 v/v EtOAc:hexanes) to afford the title compound as a yellow solid (0.134 g, 0.36 mmol, 71.6%). ^1H NMR (500 MHz, DMSO- d_6) δ 7.90 (d, J = 15.6 Hz, 1H), 7.85 (dd, J = 7.8, 1.8 Hz, 2H), 7.75 (dd, J = 8.4, 1.8 Hz, 1H), 7.63 (d, J = 15.5 Hz, 1H), 7.61 (d, J = 1.9 Hz, 1H), 7.49 – 7.38 (m, 3H), 6.88 (dd, J = 8.0, 1.3 Hz, 1H), 6.71 (d, J = 8.3 Hz, 1H), 6.69 (td, J = 7.5, 1.3 Hz, 1H), 6.64 (dd, J = 7.7, 1.8 Hz, 1H), 6.52 (td, J = 7.6, 1.8 Hz, 1H), 5.84 (s, 2H), 4.72 (s, 2H), 4.42 (dd, J = 6.1, 2.9 Hz, 2H), 4.33 (dd, J = 6.1, 2.9 Hz, 2H).

1-(4-amino-3-(2-(2-aminophenoxy)ethoxy)phenyl)-4-nitro-3-phenylbutan-1-one (C-8) A flask was charged with **C-7** (1.02 g, 2.72 mmol, 1.0 eq.) and MeOH (30 mL). While stirring, the reaction was treated with 10 M KOH in H_2O (0.82 mL, 8.2 mmol, 3.0 eq.) followed by MeNO_2 (0.44 mL, 8.2 mmol, 3.0 eq.). The reaction was heated to 70 °C. After 15 hours, the reaction was concentrated and then resuspended in CH_2Cl_2 and sat. NH_4Cl . The aqueous layer was extracted from with more CH_2Cl_2 . The organic fractions were combined and concentrated. The crude residue was purified via flash chromatography on a silica column (40:60 v/v EtOAc:hexanes) to afford the

title compound as a light brown solid (0.852 g, 1.96 mmol, 71.8%). ¹H NMR (499 MHz, Chloroform-*d*) δ 7.47 (d, *J* = 1.8 Hz, 1H), 7.44 (dd, *J* = 8.2, 1.8 Hz, 1H), 7.33 (t, *J* = 7.3 Hz, 2H), 7.31 – 7.23 (m, 3H), 6.85 (d, *J* = 7.5 Hz, 1H), 6.82 (dd, *J* = 7.6, 1.4 Hz, 1H), 6.72 (ddd, *J* = 7.3, 4.1, 2.5 Hz, 2H), 6.63 (d, *J* = 8.2 Hz, 1H), 4.83 (dd, *J* = 12.5, 6.4 Hz, 1H), 4.67 (dd, *J* = 12.5, 8.3 Hz, 1H), 4.47 – 4.32 (m, 6H), 4.20 (p, *J* = 7.2 Hz, 1H), 3.83 (s, 2H), 3.37 (dd, *J* = 17.1, 6.3 Hz, 1H), 3.30 (dd, *J* = 17.1, 7.8 Hz, 1H).

dimethyl 2,2'-((2-(2-(2-(bis(2-methoxy-2-oxoethyl)amino)-5-(4-nitro-3-phenylbutanoyl)phenoxy)ethoxy)phenyl)azanediyl)diacetate (C-9) A pressure flask was charged with **C-8** (0.369 g, 0.82 mmol, 1.0 eq.), NaI (0.127 g, 0.82 mmol, 1.0 eq.), Na₂HPO₄ (1.17 g, 8.2 mmol, 10 eq.), and anhydrous MeCN (8 mL). The mixture was treated methyl bromoacetate (0.78 mL, 8.2 mmol, 10 eq.) and heated to 90 °C. After stirring for 3 days, the reaction was concentrated. The crude residue was purified via flash chromatography on a silica column (30:70 to 50:50 v/v EtOAc:hexanes gradient) to afford the title compound as a light brown solid (0.237 g, 0.33 mmol, 39.7%). ¹H NMR (500 MHz, Chloroform-*d*) δ 7.46 (dd, *J* = 8.4, 1.9 Hz, 1H), 7.43 (d, *J* = 1.9 Hz, 1H), 7.32 (dd, *J* = 8.1, 6.9 Hz, 2H), 7.29 – 7.23 (m, 3H), 6.93 – 6.86 (m, 2H), 6.83 (td, *J* = 7.7, 7.3, 1.9 Hz, 2H), 6.66 (d, *J* = 8.3 Hz, 1H), 4.82 (dd, *J* = 12.5, 6.6 Hz, 1H), 4.67 (dd, *J* = 12.5, 8.1 Hz, 1H), 4.28 (dd, *J* = 6.0, 3.0 Hz, 2H), 4.24 (dd, *J* = 5.9, 2.9 Hz, 2H), 4.20 (s, 4H), 4.23 – 4.14 (m, 1H), 4.14 (s, 4H), 3.56 (s, 6H), 3.56 (s, 6H), 3.38 (dd, *J* = 17.2, 6.6 Hz, 1H), 3.32 (dd, *J* = 17.2, 7.6 Hz, 1H).

1-(4-methoxyphenyl)-4-nitro-3-phenylbutan-1-one (C-10) The title compound was prepared in two steps by Christopher Reinhardt from 4-methoxyacetophenone and benzaldehyde according to literature procedure.⁷

dimethyl 2,2'-((2-(2-(2-(bis(2-methoxy-2-oxoethyl)amino)-5-(5-((5-(4-methoxyphenyl)-3-phenyl-2H-pyrrol-2-ylidene)amino)-4-phenyl-1H-pyrrol-2-yl)phenoxy)ethoxy)phenyl)azanediyl)(Z)-diacetate (C-11) A flask was charged with **C-9** (0.167 g, 0.23 mmol, 1.0 eq.), **C-10** (0.276 g, 0.92 mmol, 4.0 eq.), and nBuOH (5 mL). The mixture was heated to ~110 °C to form a solution, then treated with NH₄OAc (0.26 g, 3.5 mmol, 15 eq.), and further heated to 125 °C. After 5 hours, the reaction was cooled, and the solvent was removed under reduced pressure. The crude mixture was diluted with CH₂Cl₂, washed with H₂O, dried over Na₂SO₄, and concentrated. The crude residue was purified via flash chromatography on a silica column (10:90 v/v EtOAc:CH₂Cl₂) to afford the title compound as a dark turquoise solid.

dimethyl 2,2'-((2-(2-(2-(bis(2-methoxy-2-oxoethyl)amino)-5-(5,5-difluoro-7-(4-methoxyphenyl)-1,9-diphenyl-5H-5l4,6l4-dipyrrolo[1,2-c:2',1'-f][1,3,5,2]triazaborinin-3-yl)phenoxy)ethoxy)phenyl)azanediyldiacetate (Me₄-APCa) A flask was charged with **C-11** (0.005 g, 0.005 mmol, 1.0 eq.) and dry CH₂Cl₂ (2 mL). While stirring, the solution was treated with DIPEA (0.05 mL, 0.25 mmol, 50 eq.) and BF₃-Et₂O (0.02 mL, 0.16 mmol, 30 eq.). After stirring for 15 minutes at room temperature, the reaction was quenched with saturated NaHCO₃ in H₂O and diluted with more CH₂Cl₂. The aqueous layer was extracted from with CH₂Cl₂ until colorless. The organic fractions were combined and dried over Na₂SO₄. The crude residue was purified via flash chromatography on a silica column (5:95 to 20:80 v/v EtOAc:CH₂Cl₂ gradient) to afford the title compound as a dark turquoise solid (0.013 g, 0.013 mmol, 260% yield). ¹H NMR (500 MHz, Acetone-*d*₆) δ 8.25 (d, *J* = 9.0 Hz, 2H), 8.23 – 8.15 (m, 4H), 8.12 (s, 1H), 7.84 (dd, *J* = 8.7, 2.1 Hz, 1H), 7.61 (s, 1H), 7.49 (q, *J* = 7.0 Hz, 4H), 7.48 – 7.43 (m, 1H), 7.46 – 7.41 (m, 1H), 7.41 (d, *J* = 5.1 Hz, 2H), 7.11 (d, *J* = 9.0 Hz, 2H), 6.98 (dd, *J* = 7.7, 1.8 Hz, 1H), 6.90 – 6.78 (m, 5H), 4.41 (dd, *J* = 6.3, 2.1 Hz, 2H), 4.37 (s, 4H), 4.33 (dd, *J* = 5.4, 2.6 Hz, 2H), 4.19 (s, 4H), 3.85 (s, 3H), 3.54 (s, 6H), 3.54 (s, 6H). ¹⁹F NMR (470 MHz, Acetone-*d*₆) δ -131.57 (q, *J* = 32.3 Hz).

Appendix D. β -galactosidase

D.1 Introduction

β -galactosidase is an enzyme that catalyzes the hydrolysis of the glycosidic bond of β -galactosides. Its natural functions include the catabolism of lactose to galactose and glucose and modulation of glycans. Given the abnormal glycan profiles of many cancers, it is expected that modified activity of some glycotransferases and glycosidases would be observed in cancer cells.⁹¹ Among others changes, abnormally high β -galactosidase activity was observed in 50% of primary ovarian cancer samples.⁹¹ Many immortalized ovarian cancer cell lines also show increased β -galactosidase activity.⁹² Numerous fluorescent probes for β -galactosidase have been developed for studying these cancerous cells.^{92,93}

Our interest is in pairing the β -galactosidase activity with ALDH1A1 activity to produce a probe selective for ovarian CSCs. The two-trigger system would facilitate more precise marking of these cells as, individually, these markers are sometimes upregulated in other parts of the body (e.g. senescent cells upregulate β -galactosidase⁹⁴ while hematopoietic stem cells upregulate ALDH1A1).³⁴ The proposed probe, GaldeSense, would be based on the ALDH1A1 selective probe AlDeSense, but the acidic phenol would be capped with β -galactoside trigger. This probe should enable to continued pursuit of ovarian CSCs.⁹⁵

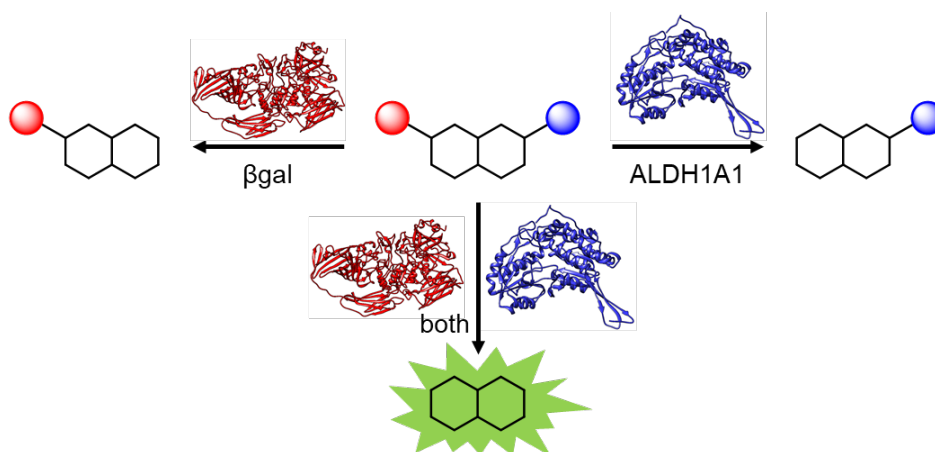
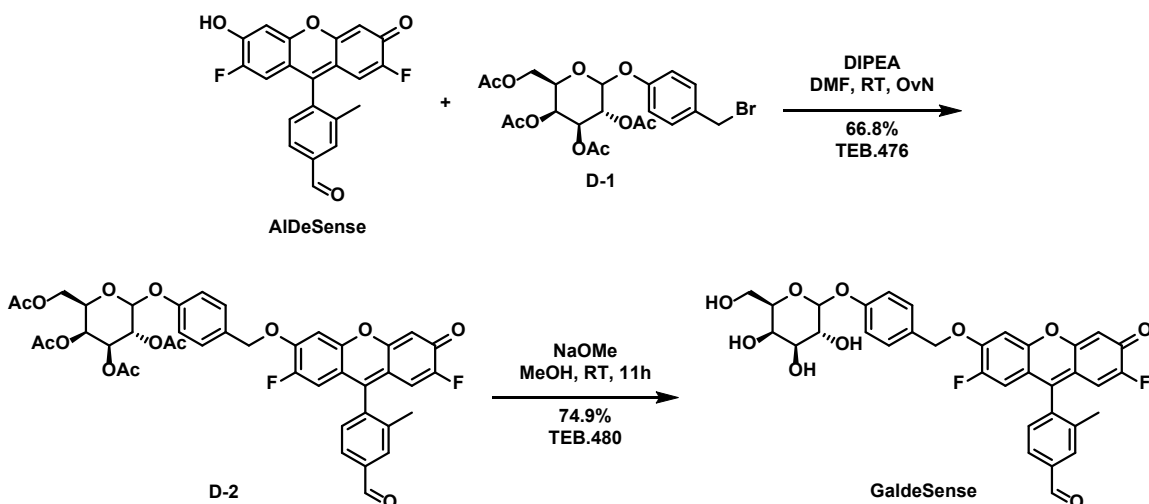


Figure D.1. Fluorescence turn on mechanism of two trigger system for β -galactosidase and ALDH1A1.

D.2 Synthesis

The synthesis of GaldeSense involved the convergent synthesis of AlDeSense and the peracylated galactoside trigger followed by coupling and deprotection. () The synthesis of AlDeSense is described above. The trigger was synthesized by Gina Partipilo according to the

procedure described by Zheng et al.⁹⁶ The phenol of AlDeSense was readily benzylated by the trigger under basic conditions. The peracetylated galactoside was then deprotected using NaOMe to afford GaldeSense.



Scheme D.1. Synthesis of GaldeSense.

D.3 Testing

GaldeSense was first tested against purified β -galactosidase to confirm it was still a substrate. In pH 7.4 triethanolamine buffer, GaldeSense was successfully hydrolyzed to AlDeSense as was evidenced by the change in the absorbance spectrum. (Figure D.2.A) This included a drop in absorbance at 459 nm, a peak consistent with the ether capped AlDeSense AM. It was accompanied by an increase in absorbance at 494 nm coinciding with AlDeSense. Surprisingly, the increase in absorbance at the irradiation wavelength (490 nm) inversely correlated with the fluorescence intensity. (Figure D.2.B) GaldeSense had about half the absorbance but double the fluorescence of equimolar AlDeSense; this suggests GaldeSense has a quantum yield approximately 4 times higher than AlDeSense. This suggested that d-PeT quenching is not effective with the benzyl capped xanthene. This decreased the theoretical turn on achieved when acted on by both β -galactosidase and ALDH1A1, but this may be mitigated by strategic modifications to the self-immolative linker.

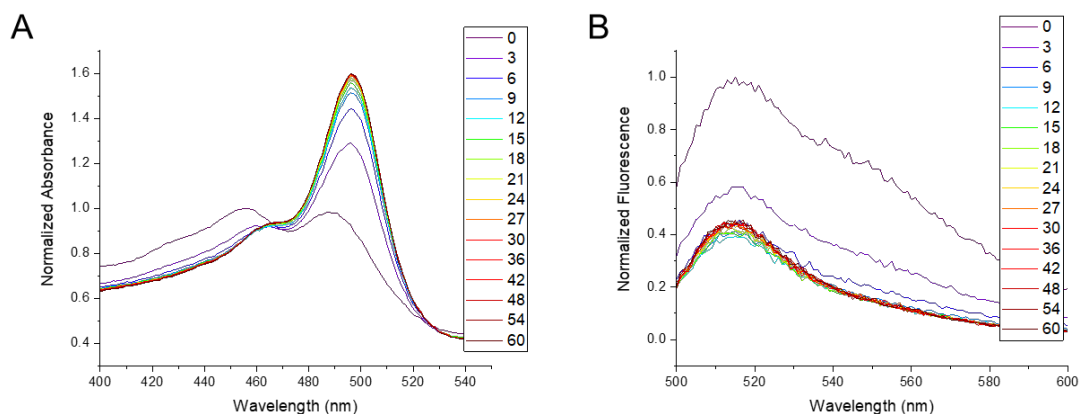


Figure D.2. (A) Absorbance and (B) Fluorescence spectra of GaldeSense in the presence of β -galactosidase.

To delineate whether GaldeSense would be a substrate for ALDH1A1 in cells in the absence of β -galactosidase, GaldeSense was incubated with purified ALDH1A1. There was no change observed in the absorbance spectrum; this was expected since there is no direct change to the chromophore. (Figure D.3.A) On the other hand, a 1.2-fold increase was observed in the fluorescence spectrum. (Figure D.3.B) This indicates that the benzaldehyde moiety still causes some d-PeT quenching in the capped system. More importantly, the change in fluorescence shows GaldeSense is a substrate for ALDH1A1 before and after being acted upon by β -galactosidase.

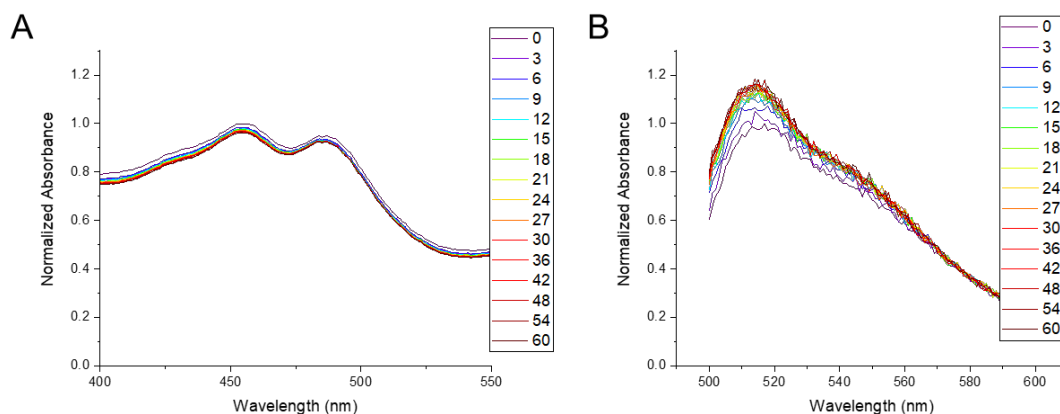


Figure D.3. (A) Absorbance and (B) Fluorescence spectra of GaldeSense in the presence of ALDH1A1.

We now knew that GaldeSense will react with β -galactosidase and ALDH1A1 to produce AlDeSense and an oxidized version of GaldeSense (ox-GaldeSense), respectively. We also knew from previous studies that ALDH1A1 will readily react with the AlDeSense released by β -galactosidase activity on GaldeSense. It remained to be shown that the product of GaldeSense and ALDH1A1, ox-GaldeSense, would be a competent substrate for β -galactosidase. To test this,

GaldeSense was incubated with ALDH1A1 for an hour, long enough to where no additional changes were observed in the fluorescence spectrum. At this time, β -galactosidase was added, and the change in absorbance and fluorescence was monitored. As before, the absorbance at 455 nm decreased while the absorbance at 459 nm increased. Additionally, an increase in fluorescence was observed consistent with uncapping of the fluorophore. Together, these indicated ox-GaldeSense was a competent substrate for β -galactosidase. More importantly, the order of enzymatic reactions from GaldeSense to the bright, oxidized AlDeSense was unimportant to achieve the desired, final readout.

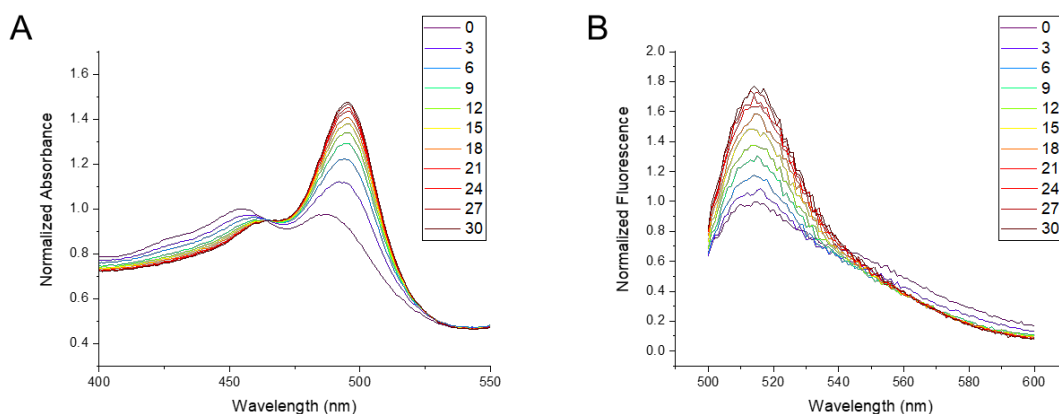


Figure D.4. (A) Absorbance and (B) Fluorescence spectra of ox-GaldeSense in the presence of β -galactosidase.

The next thing to do was test GaldeSense for selectivity, both against glycosyltransferases/glycosidases and against other ALDH isoforms. The first enzyme we explored for selectivity was ALDH1A3. We knew from crystal structures that this was the most similar to ALDH1A1, and we had hypothesized that the phenoxide of AlDeSense was important for selectivity. Therefore, this was the enzyme most likely to cause selectivity issues. When screened against purified ALDH1A3, a slower but steady rise in fluorescence was observed. (Figure D.5.A) This suggested that GaldeSense might be a substrate for ALDH1A3 if not first acted upon by β -galactosidase to form AlDeSense. In a follow up assay, equally active ALDH1A1 or ALDH1A3 was combined with β -galactosidase to directly compare the activity in the mixture. Though GaldeSense turned on faster in the ALDH1A1 solution, a notable turn on was also observed in the ALDH1A3 cuvette. (Figure D.5.B) The poor selectivity for ALDH1A1 over ALDH1A3, along with the poor turn on, precluded the further pursuit of GaldeSense.

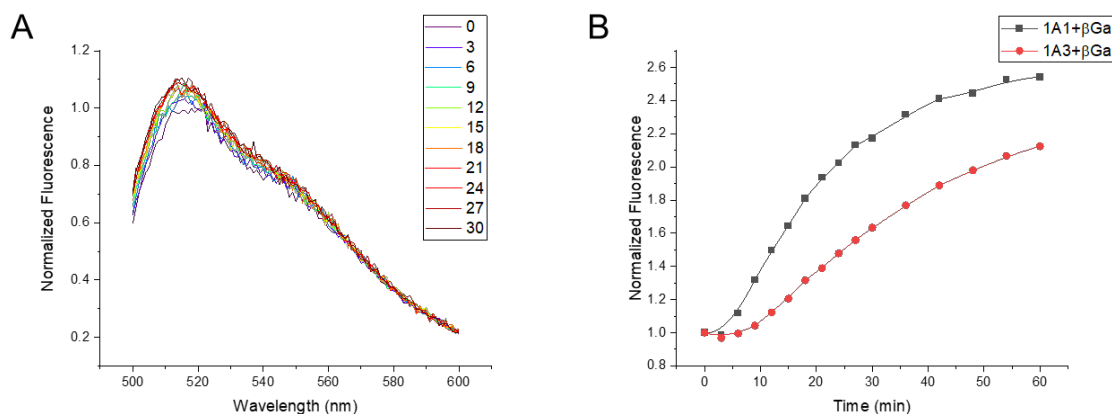


Figure D.5. (A) Fluorescence spectra of GaldeSense in the presence of ALDH1A3. (B) Maximum fluorescence of GaldeSense in the presence of β -galactosidase and either ALDH1A1 or ALDH1A3.

D.4 Future directions and outlook

In order to successfully combine a β -galactosidase probe and an ALDH1A1 probe, two improvements must happen. First, the probe must be selective for ALDH1A1. Red-AIDeSense was selective for ALDH1A1 over ALDH1A3 without the requiring the anionic xanthene moiety of AIDeSense. Drawing on knowledge gained while developing red-AIDeSense, specifically incorporating the 2,3-difluoro-5-methylbenzaldehyde moiety as the ALDH1A1 responsive handle, should afford the required isoform selectivity. Second, the probe should have minimal change in fluorescence between the unreacted and singly reacted states but a large increase in fluorescent signal after reaction with both β -galactosidase and ALDH1A1. To do so, better quenching is needed of the β -galactoside-capped probe. This may be as simple as capping with a self-immolative ester group rather than alkyl or benzyl ether. Or, it may require addition of more complete d-PeT quenching moieties (i.e. NO_2 group) on the β -galactosidase reactive portion of the molecule.

Once a successful probe is synthesized, it can be applied to studying ovarian CSCs in living systems with minimal off target effects. For instance, Urano and coworkers successfully imaged peritoneal metastases originating from ovarian cancers.⁹² It is not clear whether these are caused by ALDH1A1-upregulating CSCs. Comparing the signal of a second generation GaldeSense in primary tumor versus secondary metastases would provide information as to whether ALDH1A1 was upregulated in the metastatic legions.

D.5 Supporting information

D.5.1 Materials and methods

Expression and purification of ALDH isoforms

Plasmids for ALDH1A1 and ALDH1A3 were generously provided by Professor Daria Mochly-Rosen (Stanford). Expression and purification of each isoform was performed as previously described.⁷¹

Enzyme assays

Each ALDH isoform was added to a 50 mM triethanolamine solution (pH 7.4) containing 2.0 mM NAD⁺ and 100 μ M propanal at room temperature. ALDH isoform activity was determined by monitoring the rate of NADH production through the increase in absorbance at 340 nm ($\epsilon = 6220 \text{ M}^{-1}\text{cm}^{-1}$). For these assays, 1 unit is defined as the amount of enzyme that catalyzes the conversion of 1 μ M substrate per minute. β -Galactosidase from *Escherichia coli* was purchased from Sigma Aldrich and resuspended in 100 mM phosphate buffer (pH = 7.03).

For every combination of dye and enzyme, 2 μ M dye was preincubated with 2.0 mM NAD⁺ in 50 mM triethanolamine solution (pH 7.4). The reaction was initiated by addition of 0.5 units of ALDH or 5 μ L Galactosidase (activity unconfirmed). Dyes were excited at their absorbance maximum wavelength, and fluorescence was measured continuously at their fluorescence maximum wavelength. All assays were performed using the Cary UV/vis spectrophotometer and Horiba fluorimeter.

D.5.2 Synthesis and characterization

(2R,3S,4S,5R)-2-(acetoxymethyl)-6-(4-(bromomethyl)phenoxy)tetrahydro-2H-pyran-3,4,5-triyl triacetate (D-1) The title compound was prepared in five steps by Gina Partipilo from galactose and 4-hydroxybenzaldehyde according to literature procedure.⁹⁶

(2R,3S,4S,5R)-2-(acetoxymethyl)-6-(4-(((2,7-difluoro-9-(4-formyl-2-methylphenyl)-3-oxo-3H-xanthen-6-yl)oxy)methyl)phenoxy)tetrahydro-2H-pyran-3,4,5-triyl triacetate (D-2) A flask was charged with **AlDeSense** (0.018 g, 0.050 mmol, 1.0 eq.), **D-1** (0.032 g, 0.6 mmol, 1.2 eq.), anhydrous DMF (1.0 mL), and DIPEA (0.011 mL, 0.06 mmol, 1.2 eq.). After stirring at room temperature overnight, the reaction was concentrated under a stream of air. The crude residue was purified via flash chromatography on a silica column (2:98 v/v MeOH:CH₂Cl₂) to afford the title compound as a red solid (0.0268 g, 0.0334 mmol, 66.8%). ¹H NMR (500 MHz, Chloroform-*d*) δ 10.13 (s, 1H), 7.95 (d, *J* = 1.2 Hz, 1H), 7.92 (dd, *J* = 7.4, 1.2 Hz, 1H), 7.41 (d, *J* = 8.7 Hz,

2H), 7.36 (d, $J = 7.7$ Hz, 1H), 7.17 (d, $J = 6.7$ Hz, 1H), 7.05 (d, $J = 8.7$ Hz, 2H), 6.68 (d, $J = 10.7$ Hz, 1H), 6.59 (d, $J = 6.9$ Hz, 1H), 6.52 (d, $J = 10.4$ Hz, 1H), 5.48 (dd, $J = 10.4, 7.9$ Hz, 1H), 5.45 (dd, $J = 3.4, 1.1$ Hz, 1H), 5.22 (s, 2H), 5.11 (dd, $J = 10.4, 3.4$ Hz, 1H), 5.07 (d, $J = 7.9$ Hz, 1H), 4.23 (dd, $J = 11.3, 6.7$ Hz, 1H), 4.14 (dd, $J = 11.3, 6.5$ Hz, 1H), 4.07 (td, $J = 6.6, 1.2$ Hz, 1H), 2.17 (s, 3H), 2.16 (s, 3H), 2.06 (s, 3H), 2.05 (s, 3H), 2.01 (s, 3H). ^{13}C NMR (126 MHz, Chloroform- d) δ 191.49, 176.16 (d, $J = 20.6$ Hz), 170.43, 170.29, 170.21, 169.45, 167.86, 157.32, 157.24 (d, $J = 1.8$ Hz), 156.83 (d, $J = 268.6$ Hz), 152.18 (d, $J = 13.1$ Hz), 149.95, 149.94 (d, $J = 248.6$ Hz), 147.34 (dd, $J = 9.8, 2.8$ Hz), 138.09, 137.62 (d, $J = 7.2$ Hz), 131.93, 129.96, 129.49, 129.41, 127.88, 118.09 (d, $J = 8.2$ Hz), 117.38, 112.89 (d, $J = 7.4$ Hz), 112.69 (d, $J = 21.4$ Hz), 109.36 (d, $J = 22.2$ Hz), 107.02 (d, $J = 4.9$ Hz), 102.75, 99.52 (d, $J = 1.8$ Hz), 71.38, 71.20, 70.87, 68.70, 66.91, 61.39, 20.85, 20.78, 20.78, 20.70, 19.69. ^{19}F NMR (471 MHz, Chloroform- d) δ -121.87 (dd, $J = 10.4, 6.9$ Hz), -134.63 (dd, $J = 10.9, 6.9$ Hz).

4-(2,7-difluoro-3-oxo-6-((4-(((3R,4S,5R,6R)-3,4,5-trihydroxy-6-(hydroxymethyl)tetrahydro-2H-pyran-2-yl)oxy)benzyl)oxy)-3H-xanthen-9-yl)-3-methylbenzaldehyde (GaldeSense) A flask was charged with **D-2** (0.0268 g, 0.033 mmol, 1.0 eq.), MeOH (2.0 mL), and 2 M NaOMe in MeOH (0.33 mL, 0.066 mmol, 2.0 eq.). After stirring at room temperature for 11 hours, the reaction was quenched with sat. NH_4Cl and concentrated under reduced pressure. The crude residue was purified via flash chromatography on a silica column (10:90 v/v MeOH: CH_2Cl_2) to afford the title compound as an orange solid (0.01587 g, 0.0250 mmol, 74.9%). ^1H NMR (500 MHz, DMSO- d_6) δ 10.14 (s, 1H), 8.03 (s, 1H), 7.97 (dd, $J = 7.7, 1.6$ Hz, 1H), 7.73 (d, $J = 7.0$ Hz, 1H), 7.54 (d, $J = 7.8$ Hz, 1H), 7.44 (d, $J = 8.7$ Hz, 2H), 7.07 (d, $J = 8.7$ Hz, 2H), 6.76 (d, $J = 11.1$ Hz, 1H), 6.61 (d, $J = 11.1$ Hz, 1H), 6.53 (d, $J = 7.1$ Hz, 1H), 5.34 (s, 2H), 5.19 (d, $J = 5.1$ Hz, 1H), 4.89 (s, 1H), 4.84 (d, $J = 7.7$ Hz, 1H), 4.65 (t, $J = 5.3$ Hz, 1H), 4.52 (d, $J = 4.6$ Hz, 1H), 3.69 (t, $J = 3.7$ Hz, 1H), 3.60 – 3.51 (m, 3H), 3.50 – 3.44 (m, 1H), 3.43 – 3.38 (m, 1H), 2.12 (s, 3H). ^{19}F NMR (470 MHz, DMSO- d_6) δ -124.76 (t, $J = 10.2, 6.4$ Hz), -136.38 (dd, $J = 9.8, 7.2$ Hz).

References

- (1) Huang, B.; Babcock, H.; Zhuang, X. (2010) Breaking the Diffraction Barrier: Super-Resolution Imaging of Cells. *Cell* **143**, 1047–1058.
- (2) Wang, L. V.; Hu, S. (2012) Photoacoustic Tomography: In Vivo Imaging from Organelles to Organs. *Science* (80-.). **335**, 1458–1462.
- (3) Levi, J.; Kothapalli, S. R.; Ma, T.-J.; Hartman, K.; Khuri-Yakub, B. T.; Gambhir, S. S. (2010) Design, Synthesis, and Imaging of an Activatable Photoacoustic Probe. *J. Am. Chem. Soc.* **132**, 11264–11269.
- (4) Morgan, T. (2010) Endra Life Sciences Launches First Ever Commercial Photoacoustic 3-D Tomographic Imaging System. 2010.
- (5) Li, H.; Zhang, P.; Smaga, L. P.; Hoffman, R. A.; Chan, J. (2015) Photoacoustic Probes for Ratiometric Imaging of Copper(II). *J. Am. Chem. Soc.* **137**, 15628–15631.
- (6) Knox, H. J.; Hedhli, J.; Kim, T. W.; Khalili, K.; Dobrucki, L. W.; Chan, J. (2017) A Bio reducible N-Oxide-Based Probe for Photoacoustic Imaging of Hypoxia. *Nat. Commun.* **8**, 1794.
- (7) Reinhardt, C. J.; Zhou, E. Y.; Jorgensen, M. D.; Partipilo, G.; Chan, J. (2018) A Ratiometric Acoustogenic Probe for in Vivo Imaging of Endogenous Nitric Oxide. *J. Am. Chem. Soc.* **140**, 1011–1018.
- (8) Zhou, E. Y.; Knox, H. J.; Liu, C.; Zhao, W.; Chan, J. (2019) A Conformationally Restricted Aza-BODIPY Platform for Stimulus-Responsive Probes with Enhanced Photoacoustic Properties. *J. Am. Chem. Soc.* **141**, 17601–17609.
- (9) Fuenzalida Werner, J. P.; Huang, Y.; Mishra, K.; Chmyrov, A.; Ntziachristos, V.; Stiel, A. C. (2020) Challenging a Preconception: Optoacoustic Spectrum Differs from the Absorption Spectrum of Proteins and Dyes for Molecular Imaging. *BioRxiv* 2020.02.01.930230.
- (10) Chen, M.; Knox, H. J.; Tang, Y.; Liu, W.; Nie, L.; Chan, J.; Yao, J. (2019) Simultaneous Photoacoustic Imaging of Intravascular and Tissue Oxygenation. *Opt. Lett.* **44**, 3773.
- (11) Yao, J.; Wang, L. V. (2014) Sensitivity of Photoacoustic Microscopy. *Photoacoustics* **2**, 87–101.
- (12) Carril, M. (2017) Activatable Probes for Diagnosis and Biomarker Detection by MRI. *J. Mater. Chem. B* **5**, 4332–4347.

- (13) Green, O.; Eilon, T.; Hananya, N.; Gutkin, S.; Bauer, C. R.; Shabat, D. (2017) Opening a Gateway for Chemiluminescence Cell Imaging: Distinctive Methodology for Design of Bright Chemiluminescent Dioxetane Probes. *ACS Cent. Sci.* 3, 349–358.
- (14) Tsien, R. Y. (1980) New Calcium Indicators and Buffers with High Selectivity against Magnesium and Protons: Design, Synthesis, and Properties of Prototype Structures. *Biochemistry* 19, 2396–2404.
- (15) Schwarze, T.; Mertens, M.; Müller, P.; Riemer, J.; Wessig, P.; Holdt, H.-J. (2017) Highly K⁺-Selective Fluorescent Probes for Lifetime Sensing of K⁺ in Living Cells. *Chem. - A Eur. J.* 23, 17186–17190.
- (16) Cheng, Z.; Zheng, L.; Xu, H.; Pang, L.; He, H. (2019) A Rhodamine-Based Fluorescent Probe for Fe³⁺: Synthesis, Theoretical Calculation and Bioimaging Application. *Anal. Methods* 11, 2565–2570.
- (17) Jiang, P.; Guo, Z. (2004) Fluorescent Detection of Zinc in Biological Systems: Recent Development on the Design of Chemosensors and Biosensors. *Coord. Chem. Rev.* 248, 205–229.
- (18) Lee, H.; Liu, W.; Brown, A. S.; Landgraf, R.; Wilson, J. N. (2016) Fluorescent Kinase Probes Enabling Identification and Dynamic Imaging of HER2(+) Cells. *Anal. Chem.* 88, 11310–11313.
- (19) Gardner, S. H.; Reinhardt, C. J.; Chan, J. (2020) Advances in Activity-Based Sensing Probes for Isoform-Selective Imaging of Enzymatic Activity. *Angew. Chemie Int. Ed.*
- (20) Hu, M.; Li, L.; Wu, H.; Su, Y.; Yang, P.-Y.; Uttamchandani, M.; Xu, Q.-H.; Yao, S. Q. (2011) Multicolor, One- and Two-Photon Imaging of Enzymatic Activities in Live Cells with Fluorescently Quenched Activity-Based Probes (QABPs). *J. Am. Chem. Soc.* 133, 12009–12020.
- (21) Doura, T.; Kamiya, M.; Obata, F.; Yamaguchi, Y.; Hiyama, T. Y.; Matsuda, T.; Fukamizu, A.; Noda, M.; Miura, M.; Urano, Y. (2016) Detection of LacZ-Positive Cells in Living Tissue with Single-Cell Resolution. *Angew. Chemie - Int. Ed.* 55, 9620–9624.
- (22) Mao, W.; Xia, L.; Wang, Y.; Xie, H. (2016) A Self-Immobilizing and Fluorogenic Probe for β -Lactamase Detection. *Chem. - An Asian J.* 11, 3493–3497.
- (23) Ge, J.; Li, L.; Yao, S. Q. (2011) A Self-Immobilizing and Fluorogenic Unnatural Amino Acid That Mimics Phosphotyrosine. *Chem. Commun.* 47, 10939.

- (24) Tai, C. H.; Lu, C. P.; Wu, S. H.; Lo, L. C. (2014) Synthesis and Evaluation of Turn-on Fluorescent Probes for Imaging Steroid Sulfatase Activities in Cells. *Chem. Commun.* 50, 6116–6119.
- (25) Chan, J.; Dodani, S. C.; Chang, C. J. (2012) Reaction-Based Small-Molecule Fluorescent Probes for Chemoselective Bioimaging. *Nat. Chem.* 4, 973–984.
- (26) Pino, N. W.; Davis, J.; Yu, Z.; Chan, J. (2017) NitroxylFluor: A Thiol-Based Fluorescent Probe for Live-Cell Imaging of Nitroxyl. *J. Am. Chem. Soc.* 139, 18476–18479.
- (27) Umezawa, K.; Yoshida, M.; Kamiya, M.; Yamasoba, T.; Urano, Y. (2017) Rational Design of Reversible Fluorescent Probes for Live-Cell Imaging and Quantification of Fast Glutathione Dynamics. *Nat. Chem.* 9, 279–286.
- (28) Steiger, A. K.; Pardue, S.; Kevil, C. G.; Pluth, M. D. (2016) Self-Immolative Thiocarbamates Provide Access to Triggered H₂S Donors and Analyte Replacement Fluorescent Probes. *J. Am. Chem. Soc.* 138, 7256–7259.
- (29) Xu, H.; Xu, H.; Ma, S.; Chen, X.; Huang, L.; Chen, J.; Gao, F.; Wang, R.; Lou, K.; Wang, W. (2018) Analyte Regeneration Fluorescent Probes for Formaldehyde Enabled by Regiospecific Formaldehyde-Induced Intramolecularity. *J. Am. Chem. Soc.* 140, 16408–16412.
- (30) Yoshida, A.; Rzhetsky, A.; Hsu, L. C.; Chang, C. (1998) Human Aldehyde Dehydrogenase Gene Family. *Eur. J. Biochem.* 251, 549–557.
- (31) Veech, R. L.; Eggleston, L. V.; Krebs, H. A. (1969) The Redox State of Free Nicotinamide–Adenine Dinucleotide Phosphate in the Cytoplasm of Rat Liver. *Biochem. J.* 115, 609–619.
- (32) Morgan, C. A.; Parajuli, B.; Buchman, C. D.; Dria, K.; Hurley, T. D. (2015) N,N-Diethylaminobenzaldehyde (DEAB) as a Substrate and Mechanism-Based Inhibitor for Human ALDH Isoenzymes. *Chem. Biol. Interact.* 234, 18–28.
- (33) Weiner, H.; Ho, K. K. (2007) Can We Change the Rate-Limiting Step of an Aldehyde Dehydrogenase? In *Enzymology and Molecular Bioogy of Carbonyl Metabolism* 133–8; pp 3–8.
- (34) Tomita, H.; Tanaka, K.; Tanaka, T.; Hara, A. (2016) Aldehyde Dehydrogenase 1A1 in Stem Cells and Cancer. *Oncotarget* 7, 11018–11032.
- (35) Yelamanchi, S. D.; Jayaram, S.; Thomas, J. K.; Gundimeda, S.; Khan, A. A.; Singhal, A.; Keshava Prasad, T. S.; Pandey, A.; Somani, B. L.; Gowda, H. (2016) A Pathway Map of

Glutamate Metabolism. *J. Cell Commun. Signal.* 10, 69–75.

- (36) Marcato, P.; Dean, C. A.; Giacomantonio, C. A.; Lee, P. W. K. (2011) Aldehyde Dehydrogenase: Its Role as a Cancer Stem Cell Marker Comes down to the Specific Isoform. *Cell Cycle* 10, 1378–1384.
- (37) M., A.; Bagirova, M.; Nehir, O.; Yaman, S.; Sefik, E.; Cakir, R.; Canim, S.; Elcicek, S.; Yesilkir, S. (2012) Aldehyde Dehydrogenase: Cancer and Stem Cells. In *Dehydrogenases* 3–28; InTech; pp 3–28.
- (38) Suzuki, E.; Chiba, T.; Zen, Y.; Miyagi, S.; Tada, M.; Kanai, F.; Imazeki, F.; Miyazaki, M.; Iwama, A.; Yokosuka, O. (2012) Aldehyde Dehydrogenase 1 Is Associated with Recurrence-Free Survival but Not Stem Cell-like Properties in Hepatocellular Carcinoma. *Hepatol. Res.* 42, 1100–1111.
- (39) Meng, E.; Mitra, A.; Tripathi, K.; Finan, M. A.; Scalici, J.; McClellan, S.; da Silva, L. M.; Reed, E.; Shevde, L. A.; Palle, K.; et al. (2014) ALDH1A1 Maintains Ovarian Cancer Stem Cell-Like Properties by Altered Regulation of Cell Cycle Checkpoint and DNA Repair Network Signaling. *PLoS One* 9, e107142.
- (40) Wang, Y. C.; Yo, Y. Te; Lee, H. Y.; Liao, Y. P.; Chao, T. K.; Su, P. H.; Lai, H. C. (2012) ALDH1-Bright Epithelial Ovarian Cancer Cells Are Associated with CD44 Expression, Drug Resistance, and Poor Clinical Outcome. *Am. J. Pathol.* 180, 1159–1169.
- (41) Prager, B. C.; Xie, Q.; Bao, S.; Rich, J. N. (2019) Cancer Stem Cells: The Architects of the Tumor Ecosystem. *Cell Stem Cell* 24, 41–53.
- (42) Ginestier, C.; Hur, M. H.; Charafe-Jauffret, E.; Monville, F.; Dutcher, J.; Brown, M.; Jacquemier, J.; Viens, P.; Kleer, C. G.; Liu, S.; et al. (2007) ALDH1 Is a Marker of Normal and Malignant Human Mammary Stem Cells and a Predictor of Poor Clinical Outcome. *Cell Stem Cell* 1, 555–567.
- (43) Huang, E. H.; Hynes, M. J.; Zhang, T.; Ginestier, C.; Dontu, G.; Appelman, H.; Fields, J. Z.; Wicha, M. S.; Boman, B. M. (2009) Aldehyde Dehydrogenase 1 Is a Marker for Normal and Malignant Human Colonic Stem Cells (SC) and Tracks SC Overpopulation during Colon Tumorigenesis. *Cancer Res.* 69, 3382–3389.
- (44) Yang, L.; Ren, Y.; Yu, X.; Qian, F.; Bian, B.-S.-J.; Xiao, H.; Wang, W.; Xu, S.; Yang, J.; Cui, W.; et al. (2014) ALDH1A1 Defines Invasive Cancer Stem-like Cells and Predicts Poor Prognosis in Patients with Esophageal Squamous Cell Carcinoma. *Mod. Pathol.* 27,

775–783.

- (45) Zhou, L.; Sheng, D.; Wang, D.; Ma, W.; Deng, Q.; Deng, L.; Liu, S. (2018) Identification of Cancer-Type Specific Expression Patterns for Active Aldehyde Dehydrogenase (ALDH) Isoforms in ALDEFLUOR Assay. *Cell Biol. Toxicol.*
- (46) Marcato, P.; Dean, C. A.; Pan, D.; Araslanova, R.; Gillis, M.; Joshi, M.; Helyer, L.; Pan, L.; Leidal, A.; Gujar, S.; et al. (2011) Aldehyde Dehydrogenase Activity of Breast Cancer Stem Cells Is Primarily Due To Isoform ALDH1A3 and Its Expression Is Predictive of Metastasis. *Stem Cells* 29, 32–45.
- (47) Feng, H.; Liu, Y.; Bian, X.; Zhou, F.; Liu, Y. (2018) ALDH1A3 Affects Colon Cancer in Vitro Proliferation and Invasion Depending on CXCR4 Status. *Br. J. Cancer* 118, 224–232.
- (48) Shao, C.; Sullivan, J. P.; Girard, L.; Augustyn, A.; Yenerall, P.; Rodriguez-Canales, J.; Liu, H.; Behrens, C.; Shay, J. W.; Wistuba, I. I.; et al. (2014) Essential Role of Aldehyde Dehydrogenase 1A3 for the Maintenance of Non-Small Cell Lung Cancer Stem Cells Is Associated with the STAT3 Pathway. *Clin. Cancer Res.* 20, 4154–4166.
- (49) Jones, R. J.; Barber, J. P.; Vala, M. S.; Collector, M. I.; Kaufmann, S. H.; Ludeman, S. M.; Colvin, O. M.; Hilton, J. (1995) Assessment of Aldehyde Dehydrogenase in Viable Cells. *Blood* 85, 2742–2746.
- (50) Storms, R. W.; Trujillo, A. P.; Springer, J. B.; Shah, L.; Colvin, O. M.; Ludeman, S. M.; Smith, C. (1999) Isolation of Primitive Human Hematopoietic Progenitors on the Basis of Aldehyde Dehydrogenase Activity. *Proc. Natl. Acad. Sci.* 96, 9118–9123.
- (51) Minn, I.; Wang, H.; Mease, R. C.; Byun, Y.; Yang, X.; Wang, J.; Leach, S. D.; Pomper, M. G. (2014) A Red-Shifted Fluorescent Substrate for Aldehyde Dehydrogenase. *Nat. Commun.* 5, 3662.
- (52) Pereira, R.; Gendron, T.; Sanghera, C.; Greenwood, H. E.; Newcombe, J.; McCormick, P. N.; Sander, K.; Topf, M.; Årstad, E.; Witney, T. H. (2019) Mapping Aldehyde Dehydrogenase 1A1 Activity Using an [18 F]Substrate-Based Approach. *Chem. - A Eur. J.* 25, 2345–2351.
- (53) Eisinger, K. B. (1983) Intermolecular and Intramolecular Excited State Charge Transfer. *Laser Chem.* 3, 145–162.
- (54) Guido, C. A.; Mennucci, B.; Jacquemin, D.; Adamo, C. (2010) Planar vs. Twisted Intramolecular Charge Transfer Mechanism in Nile Red: New Hints from Theory. *Phys.*

Chem. Chem. Phys. **12**, 8016.

- (55) Maity, S.; Sadlowski, C. M.; George Lin, J.-M.; Chen, C.-H.; Peng, L.-H.; Lee, E.-S.; Vegesna, G. K.; Lee, C.; Kim, S.-H.; Mochly-Rosen, D.; et al. (2017) Thiophene Bridged Aldehydes (TBAs) Image ALDH Activity in Cells via Modulation of Intramolecular Charge Transfer. *Chem. Sci.* **8**, 7143–7151.
- (56) Okda, H. E.; El Sayed, S.; Ferreira, R. C. M.; Gonçalves, R. C. R.; Costa, S. P. G.; M. Raposo, M. M.; Martínez-Máñez, R.; Sancenón, F. (2019) N, N'-Diphenylanilino-Heterocyclic Aldehyde-Based Chemosensors for UV-Vis/NIR and Fluorescence Cu(II) Detection. *New J. Chem.* **43**, 7393–7402.
- (57) Terai, T.; Tomiyasu, R.; Ota, T.; Ueno, T.; Komatsu, T.; Hanaoka, K.; Urano, Y.; Nagano, T. (2013) TokyoGreen Derivatives as Specific and Practical Fluorescent Probes for UDP-Glucuronosyltransferase (UGT) 1A1. *Chem. Commun.* **49**, 3101.
- (58) Ueno, T.; Urano, Y.; Setsukinai, K. I.; Takakusa, H.; Kojima, H.; Kikuchi, K.; Ohkubo, K.; Fukuzumi, S.; Nagano, T. (2004) Rational Principles for Modulating Fluorescence Properties of Fluorescein. *J. Am. Chem. Soc.* **126**, 14079–14085.
- (59) Roth, H.; Romero, N.; Nicewicz, D. (2015) Experimental and Calculated Electrochemical Potentials of Common Organic Molecules for Applications to Single-Electron Redox Chemistry. *Synlett* **27**, 714–723.
- (60) Woydziak, Z.; Fu, L.; Peterson, B. (2013) Efficient and Scalable Synthesis of 4-Carboxy-Pennsylvania Green Methyl Ester: A Hydrophobic Building Block for Fluorescent Molecular Probes. *Synthesis (Stuttg.)* **46**, 158–164.
- (61) Koppaka, V.; Thompson, D. C.; Chen, Y.; Ellermann, M.; Nicolaou, K. C.; Juvonen, R. O.; Petersen, D.; Deitrich, R. A.; Hurley, T. D.; Vasiliou, V. (2012) Aldehyde Dehydrogenase Inhibitors: A Comprehensive Review of the Pharmacology, Mechanism of Action, Substrate Specificity, and Clinical Application. *Pharmacol. Rev.* **64**, 520–539.
- (62) Smaga, L. P.; Pino, N. W.; Ibarra, G. E.; Krishnamurthy, V.; Chan, J. (2020) A Photoactivatable Formaldehyde Donor with Fluorescence Monitoring Reveals Threshold To Arrest Cell Migration. *J. Am. Chem. Soc.* **142**, 680–684.
- (63) Heo, S.-K.; Noh, E.-K.; Ju, L. J.; Sung, J. Y.; Jeong, Y. K.; Cheon, J.; Koh, S. J.; Min, Y. J.; Choi, Y.; Jo, J.-C. (2020) CD45^{dim}CD34⁺CD38[–]CD133⁺ Cells Have the Potential as Leukemic Stem Cells in Acute Myeloid Leukemia. *BMC Cancer* **20**, 285.

- (64) Lee, J.; Abdeen, A. A.; Hedhli, J.; Wycislo, K. L.; Dobrucka, I. T.; Fan, T. M.; Dobrucki, L. W.; Kilian, K. A. (2017) Melanoma Topology Reveals a Stem-like Phenotype That Promotes Angiogenesis. *Sci. Adv.* 3, e1701350.
- (65) Egawa, T.; Koide, Y.; Hanaoka, K.; Komatsu, T.; Terai, T.; Nagano, T. (2011) Development of a Fluorescein Analogue, TokyoMagenta, as a Novel Scaffold for Fluorescence Probes in Red Region. *Chem. Commun.* 47, 4162–4164.
- (66) Grimm, J. B.; Brown, T. A.; Tkachuk, A. N.; Lavis, L. D. (2017) General Synthetic Method for Si-Fluoresceins and Si-Rhodamines. *ACS Cent. Sci.* acscentsci.7b00247.
- (67) Butkevich, A. N.; Belov, V. N.; Kolmakov, K.; Sokolov, V. V.; Shojaei, H.; Sidenstein, S. C.; Kamin, D.; Matthias, J.; Vlijm, R.; Engelhardt, J.; et al. (2017) Hydroxylated Fluorescent Dyes for Live-Cell Labeling: Synthesis, Spectra and Super-Resolution STED. *Chem. - A Eur. J.* 23, 12114–12119.
- (68) Hirabayashi, K.; Hanaoka, K.; Takayanagi, T.; Toki, Y.; Egawa, T.; Kamiya, M.; Komatsu, T.; Ueno, T.; Terai, T.; Yoshida, K.; et al. (2015) Analysis of Chemical Equilibrium of Silicon-Substituted Fluorescein and Its Application to Develop a Scaffold for Red Fluorescent Probes. *Anal. Chem.* 87, 9061–9069.
- (69) ALDH1A1 <https://www.proteinatlas.org/ENSG00000165092-ALDH1A1/cell#human> (accessed Oct 21, 2019).
- (70) Boesch, M.; Sopper, S.; Zeimet, A. G.; Reimer, D.; Gastl, G.; Ludewig, B.; Wolf, D. (2016) Heterogeneity of Cancer Stem Cells: Rationale for Targeting the Stem Cell Niche. *Biochim. Biophys. Acta - Rev. Cancer* 1866, 276–289.
- (71) Anorma, C.; Hedhli, J.; Bearrood, T. E. T. E. T. E.; Pino, N. W. N. W.; Gardner, S. H. S. H.; Inaba, H.; Zhang, P.; Li, Y.; Feng, D.; Dibrell, S. E. S. E.; et al. (2018) Surveillance of Cancer Stem Cell Plasticity Using an Isoform-Selective Fluorescent Probe for Aldehyde Dehydrogenase 1A1. *ACS Cent. Sci.* 4, 1045–1055.
- (72) Miyata, T.; Oyama, T.; Yoshimatsu, T.; Higa, H.; Kawano, D.; Sekimura, A.; Yamashita, N.; So, T.; Gotoh, A. (2017) The Clinical Significance of Cancer Stem Cell Markers ALDH1A1 and CD133 in Lung Adenocarcinoma. *Anticancer Res.* 37, 2541–2547.
- (73) Azuma, E.; Nakamura, N.; Kuramochi, K.; Sasamori, T.; Tokitoh, N.; Sagami, I.; Tsubaki, K. (2012) Exhaustive Syntheses of Naphthofluoresceins and Their Functions. *J. Org. Chem.* 77, 3492–3500.

- (74) Esterbauer, H.; Schaur, R. J.; Zollner, H. (1991) Chemistry and Biochemistry of 4-Hydroxynonenal, Malonaldehyde and Related Aldehydes. *Free Radic. Biol. Med.* *11*, 81–128.
- (75) Benedetti, A.; Comporti, M.; Esterbauer, H. (1980) Identification of 4-Hydroxynonenal as a Cytotoxic Product Originating from the Peroxidation of Liver Microsomal Lipids. *Biochim. Biophys. Acta - Lipids Lipid Metab.* *620*, 281–296.
- (76) Guéraud, F. (2017) 4-Hydroxynonenal Metabolites and Adducts in Pre-Carcinogenic Conditions and Cancer. *Free Radic. Biol. Med.* *111*, 196–208.
- (77) Castro, J. P.; Jung, T.; Grune, T.; Siems, W. (2017) 4-Hydroxynonenal (HNE) Modified Proteins in Metabolic Diseases. *Free Radic. Biol. Med.* *111*, 309–315.
- (78) Barrera, G.; Pizzimenti, S.; Daga, M.; Dianzani, C.; Arcaro, A.; Cetrangolo, G. P.; Giordano, G.; Cucci, M. A.; Graf, M.; Gentile, F. (2018) Lipid Peroxidation-Derived Aldehydes, 4-Hydroxynonenal and Malondialdehyde in Aging-Related Disorders. *Antioxidants* *7*, 102.
- (79) Tamura, H.; Shibamoto, T. (1991) Gas Chromatographic Analysis of Malonaldehyde and 4-Hydroxy-2-(E)-Nonenal Produced from Arachidonic Acid and Linoleic Acid in a Lipid Peroxidation Model System. *Lipids* *26*, 170–173.
- (80) Rotman, B.; Papermaster, B. W. (1966) Membrane Properties of Living Mammalian Cells as Studied by Enzymatic Hydrolysis of Fluorogenic Esters. *Proc. Natl. Acad. Sci.* *55*, 134–141.
- (81) Chyan, W.; Kilgore, H. R.; Gold, B.; Raines, R. T. (2017) Electronic and Steric Optimization of Fluorogenic Probes for Biomolecular Imaging. *J. Org. Chem.* *82*, 4297–4304.
- (82) Tong, Z.; Han, C.; Luo, W.; Li, H.; Luo, H.; Qiang, M.; Su, T.; Wu, B.; Liu, Y.; Yang, X.; et al. (2013) Aging-Associated Excess Formaldehyde Leads to Spatial Memory Deficits. *Sci. Rep.* *3*, 1807.
- (83) Fox, C. H.; Johnson, F. B.; Whiting, J.; Roller, P. P. (1985) Formaldehyde Fixation. *J. Histochem. Cytochem.* *33*, 845–853.
- (84) Roth, A.; Li, H.; Anorma, C.; Chan, J. (2015) A Reaction-Based Fluorescent Probe for Imaging of Formaldehyde in Living Cells. *J. Am. Chem. Soc.* *137*, 10890–10893.
- (85) Bearrood, T. E.; Aguirre-Figueroa, G.; Chan, J. (2020) Rational Design of a Red

- Fluorescent Sensor for ALDH1A1 Displaying Enhanced Cellular Uptake and Reactivity. *Bioconjug. Chem.* *31*, 224–228.
- (86) Schindelin, J.; Arganda-Carreras, I.; Frise, E.; Kaynig, V.; Longair, M.; Pietzsch, T.; Preibisch, S.; Rueden, C.; Saalfeld, S.; Schmid, B.; et al. (2012) Fiji: An Open-Source Platform for Biological-Image Analysis. *Nat. Methods* *9*, 676–682.
- (87) Mann, C. J.; Weiner, H. (1999) Differences in the Roles of Conserved Glutamic Acid Residues in the Active Site of Human Class 3 and Class 2 Aldehyde Dehydrogenases. *Protein Sci.* *8*, 1922–1929.
- (88) Clapham, D. E. (2007) Calcium Signaling. *Cell* *131*, 1047–1058.
- (89) Hogan, P. G.; Chen, L.; Nardone, J.; Rao, A. (2003) Transcriptional Regulation by Calcium, Calcineurin, and NFAT. *Genes Dev.* *17*, 2205–2232.
- (90) Pasnoori, S.; Kamatala, C. R.; Mukka, S. K.; Kancharla, R. R. (2014) Prussian Blue as an Eco-Friendly Catalyst for Selective Nitration of Organic Compounds Under Conventional and Nonconventional Conditions. *Synth. React. Inorganic, Met. Nano-Metal Chem.* *44*, 364–370.
- (91) Chatterjee, S. K.; Bhattacharya, M.; Barlow, J. J. (1979) Glycosyltransferase and Glycosidase Activities in Ovarian Cancer Patients. *Cancer Res.* *39*, 1943–1951.
- (92) Asanuma, D.; Sakabe, M.; Kamiya, M.; Yamamoto, K.; Hiratake, J.; Ogawa, M.; Kosaka, N.; Choyke, P. L.; Nagano, T.; Kobayashi, H.; et al. (2015) Sensitive β -Galactosidase-Targeting Fluorescence Probe for Visualizing Small Peritoneal Metastatic Tumours in Vivo. *Nat. Commun.* *6*, 6463.
- (93) Kamiya, M.; Asanuma, D.; Kuranaga, E.; Takeishi, A.; Sakabe, M.; Miura, M.; Nagano, T.; Urano, Y. (2011) B-Galactosidase Fluorescence Probe With Improved Cellular Accumulation Based on a Spirocyclized Rhodol Scaffold. *J. Am. Chem. Soc.* *133*, 12960–12963.
- (94) Debacq-Chainiaux, F.; Erusalimsky, J. D.; Campisi, J.; Toussaint, O. (2009) Protocols to Detect Senescence-Associated Beta-Galactosidase (SA-Bgal) Activity, a Biomarker of Senescent Cells in Culture and in Vivo. *Nat. Protoc.* *4*, 1798–1806.
- (95) Lupia, M.; Cavallaro, U. (2017) Ovarian Cancer Stem Cells: Still an Elusive Entity? *Mol. Cancer* *16*, 64.
- (96) Zheng, Y.; Li, Q. (2010) Synthesis and Antitumor Activities of 5-Carbohydrate Modified

Cyclophosphamide Derivates. *J. Chinese Pharm. Sci.* No. 20732001, 327–340.